
**UNIVERSITÀ DEGLI STUDI DI MILANO**

***Scuola di Dottorato in Scienze Biologiche e Molecolari***

***Corso di Dottorato in Biologia Cellulare e molecolare***

**XXIV Ciclo**

# Studying the Ras-ERK pathway through single-cell analysis in acute striatal slices

**Ilaria Maria Morella**

PhD Thesis

**Scientific tutors: Prof.ssa Laura Popolo**

**Dott. Riccardo Brambilla**

Anno accademico: 2012-2013

SSD: BIO/10, Biochimica

Thesis performed at:

Dipartimento di Scienze biomolecolari e biotecnologie, Università degli studi di Milano, Via Celoria 26 20133 Milano, Italy

Institute of Experimental Neurology, Division of Neuroscience, San Raffaele Scientific Institute and University, Via Olgettina 58 20132 Milano, Italy

# Contents

*This thesis is dedicated to*
*the memory of Prof. Renata Zippel*
*(1948-2011)*

# PART I

## Abstract

In the central nervous system, the Ras-ERK signaling module, triggered by the small GTPases of the Ras family, plays a key role in different forms of behavioural plasticity, including learning and consolidation of long-term memory. In particular, in the striatum the combined engagement of dopaminergic and glutamatergic pathways leads to a sustained activation of the Ras-ERK pathway, necessary for the normal striatal functions, including learning of procedural actions and habit formation, but also for the behavioural responses to the rewarding properties of drugs of abuse. In addition, an aberrant ERK hyperactivation is implicated in the development of L-DOPA- induced dyskinesia (LID), a severe and disabling pathology characterized by involuntary movements that develop as consequence of L-DOPA treatment in parkinsonian patients.

In this work, I showed the development of a new experimental approach in which striatal slices acutely prepared from adult mice can be incubated in a perfusing chamber and challenged with appropriate agonists and antagonists. First, I validated our system by Western blot analysis performed on striatal slices stimulated for 10 min with glutamate and I confirmed a significant ERK1/2 activation. Next, I developed a system to study ERK activation at a single cell definition monitoring by immunofluorescence analysis the phosphorylation state of two proteins downstream of ERK1/2: S6 ribosomal protein (cytoplasmic target) and histone H3 (nuclear target). I demonstrated that both these proteins are robustly activated upon the application of glutamate, the D1Rs agonist SKF38393 or the neurotrophin BDNF 100 μM and that this event is specifically regulated by the ERK cascade, thus demonstrating that these two proteins are reliable indicators of ERK induction.

Having validated this experimental setting, I next investigated the integration between dopaminergic and glutamatergic signaling specifically in the D1Rs-expressing neurons (direct pathway) and in the D2Rs-expressing neurons (indirect pathway) in adult striatal slices obtained from M4-EGFP mice, expressing EGFP in the direct pathway. My results indicate that an additive integration between glutamate and SKF38393 is necessary to elicit S6, but not histone H3 phosphorylation, and this event is restricted to the direct pathway. Unexpectedly, the application of the D1Rs agonist activates S6 ribosomal protein also in the indirect pathway in a D1Rs-dependent manner. Further experiments will be necessary to clarify the exact mechanism, either direct or indirect, through which D1Rs stimulation mediates S6 activation in the indirect pathway. In addition, I demonstrated that, whereas D1Rs-mediated signalling depends on glutamatergic activity,

glutamatergic activity does not entirely depend on dopaminergic signalling since glutamate-mediated S6 phosphorylation is only partially inhibited (48% of inhibition) following D1Rs blockade. In addition, in the direct pathway, S6 activation seems to be more inhibited (55%) by D1Rs antagonist with respect to the indirect pathway (41%). Further experiments will be performed also in A2A-EGFP mice, expressing EGFP in the indirect pathway, in order to confirm the results concerning the indirect pathway.

In the last part of the project, I used the technique I developed to investigate the role of the Ras-ERK signalling in LID. In particular, I demonstrated that the antidyskinetic property of the recent discovered NOP receptor agonist (N/OFQ) correlates with a negative modulation of D1Rs-mediated signalling in striatal slices obtained from naïve mice, highlighting NOP receptor as a possible drug target. Successively, since recent evidence has demostrated that ERK hyperactivation in dyskinetic mice is reduced by the loss of Ras-GRF1, a neuronal specific Ras exchange factor, ameliorating the dyskinetic symptoms, I wanted to further investigate the effect of Ras-GRF1 ablation on either S6 and histone H3 activation in dyskinetic mice; my results have demonstrated that histone H3 phosphorylation as well as ERK phosphorylation are reduced in dyskinetic Ras-GRF1 KO mice, whereas the level of S6 phosphorylation does not change in comparison to wild-type mice. These findings may indicate that the chronic treatment with L-DOPA produces some adaptive processes that bypass Ras-GRF1 and possibly ERK requirement. For instance, lack of Ras-GRF1 may be compensated by other calcium-sensitive Ras-GEFs, including the striatal-enriched members of Ras-GRP/CalDAG GEFs family, although I cannot exclude that other pathways, including mTOR, converge to activate S6 in dyskinetic mice effectively bypassing ERK. In order to test our hypothesis, further experiments will be performed, for instance by treating dyskinetic wild-type and Ras-GRF1 KO mice or striatal slices obtained from these animals with a MEK inhibitor, to investigate the effect of ERK blockade on L-DOPA induced S6 hyperactivation.

# Aim of the project

The aim of the project is to characterize Ras-ERK pathway in the striatum by developing a new experimental approach based on single-cell analysis in mature striatal slices. This system will be composed by a chamber for pharmacological stimulation in which brain slices are acutely prepared from adult mice, challenged with the appropriate agonists and antagonists and then the induction of ERK cascade can be monitored by using specific antibodies against the phosphorylated form of ERK1/2 or target proteins downstream of the ERK signaling pathway.

In an initial phase, I will validate our ex-vivo system : *i*) by Western blot analysis performed on striatal slices stimulated with glutamate to detect ERK activation; *ii*) by immunofluorescence analysis to target specific neuronal population, for instance in a mouse transgenic line available in our laboratory expressing EGFP specifically in the striatonigral pathway.

Having validating the ex-vivo system, I will set out to further investigate the role of ERK cascade in the integration of glutamatergic and dopaminergic inputs, comparing the striatonigral and the striatopallidal neurons.

In the last part of my thesis, I plan to use the ex-vivo technique I developed to further elucidate the role of Ras-ERK pathway in L-DOPA induced dyskinesia (LID).

# State of the art

## The GTPases superfamily

The GTPases superfamily includes a number of proteins with regulatory functions in cellular proliferation, differentiation, apoptosis and vesicular trafficking. The GTPases are composed by three distinct classes of proteins: i) the heterotrimeric G proteins; ii) the small GTPases Ras-like group, including the products of H(arvey)-Ras, N(euroblastoma)-Ras, K(irsten)-Ras genes: Ras/Rap, Rho/Rac, Rab, Sar1/Arf, Ran; iii) the inititiation and elongation factors.

The scientific interest on Ras biology rose at the beginning of the 1980s, when it was demonstrated that almost 30% of all solid tumors in humans are associated to specific mutations in the Ras gene (Bos et al., 1998). These mutations produce oncogenic forms of Ras that become constitutively active and transduce signals leading to cellular proliferation, transformation and tumorigenesis.

However, it is now known that Ras is implicated in many others cellular events; in particular, it has been shown that: i) Ras and Rho/Rac are involved in gene expression: ii) Rho is a key element for cytoskeletal reorganization; iii) Rab and Sar1/Arf control vesicular trafficking; iv) Ran is involved in the nucleocytoplasmatic transport during G1, S and G2 phases and microtubular organization during mitosis (Wennerberg et al., 2005).

Ras proteins are molecular switches for intracellular signal transduction receiving, modulating and propagating extracellular signals downstream. They are mainly located at the inner face of the plasma membrane in close proximity to different types of receptors, including tyrosine kinase receptors (i.e. the Epidermal Growth Factor Receptor, EGFR, the Platelet Derived Growth Factor Receptor, PDGF or the Nerve Growth Factor Receptor, NGFR), G-protein Coupled Receptors (GPCRs), cytokines receptors, Voltage Gated Calcium Channels (VGCCs), and importantly, in the central nervous system, ionotropic glutamate receptors. Once activated, these receptors transmit the signals through the cell membrane to the monomeric GTPases that can interact with a number of effectors able to propagate the downstream signal, leading to a biological response (Barbacid, 1987; Campbell et al., 1998).

Upon activation, GTPases cycle from an inactive state, GDP-bound, to an active state, GTP-bound. The conversion from the inactive to the active state is catalyzed by the Guanine Nucleotide Exchange Factors(GEFs) and the GTP binding is facilitated by the higher intracellular concentration of GTP with respect to GDP.

Another class of proteins, named Guanine Dissociation Inhibitors (GDIs), stabilizes the binding between Ras and GDP. In addition, given the poor intrinsic GTPase activity of Ras proteins, the conversion from the active to the inactive state is catalyzed by GTPase Activating Proteins (GAPs ), that increase the rate of GTP hydrolysis (Barbacid, 1987; Bourne et al., 1990).

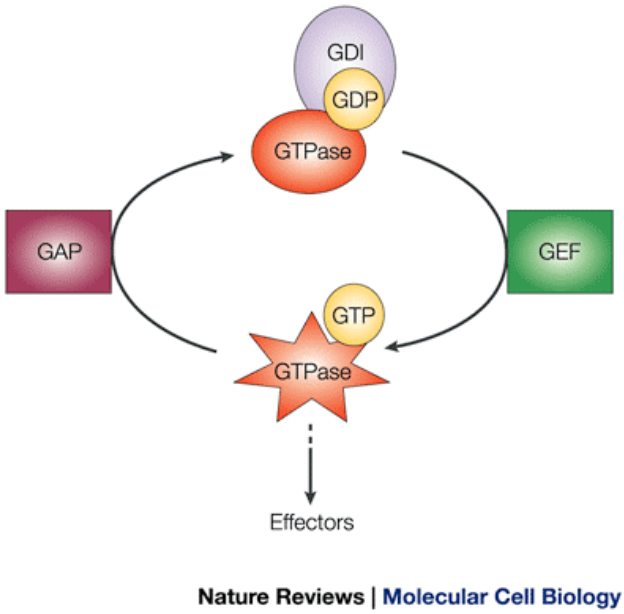


**Fig. 1. Ras activation cycle (**From Coleman M. L. et al., 2004)

***Ras-mediated signalling pathways***

Upon activation, Ras proteins act as key molecular switches for multiple signaling pathways, by recruiting specific effector molecules. Figure 2 summarizes the most studied Ras effectors, i.e. Raf-1/B-Raf and A-Raf pathway, the phosphatidylinositol 3-kinase (PI3K) and RalGDS cascades.

Raf-1, also called MAPKKK, is the first serine/threonine kinase of the Mitogen Activated Protein Kinases (MAPKs) cascade. Once activated Raf-1 phosphorylates MEK (MAPKK) that in turn phosphorylates ERKs (MAPKs). Extracellular signal-Regulated Kinases (ERKs) produce both short-term effects, by phosphorylating several cytoplasmatic substrates, and long-term effects, by activating transcriptional regulators that modulate the expression of the Immediate Early Genes (IEGs).

The phosphatidylinositol 3-kinase (PI3K) pathway is triggered by the direct interaction between Ras and the p110α subunit of PI3K (Rodriguez-Viciana et al.,1996). Activated PI3K catalalyzes the phosphorylation of phosphatidylinositol-4,5-bisphosphate ($PIP_2$) by generating the phosphatidylinositol-3,4.5-triphosphate ($PIP_3$), that acts as second messenger involved in cell survival and in the regulation of gene expression and cellular metabolism. The activation of PI3K and the consequent release of $PIP_3$ lead to the activation of several proteins such as Akt. This protein kinase promotes cell survival by phosphorylating and inactivating glycogen synthase 3 (GSK-3) and BAD. Furthermore, activated PI3K provides a link between Ras and Rho/Rac GTPases signalling, by recruiting the guanine nucleotide exchangers of Rac, that activate the SAP kinase pathway, another member of the MAPK kinase family. Another effector of Ras is RalGDS

that activates RalBP1, a member of the Guanine activating proteins of Rac, Cdc42 and phospholipase D. In addition, it has been demonstrated that also phospholipase Cε (PLCε) directly interacts with Ras; the consequent activation of PLCε generates the second messengers inositol (1,4,5)trisphosphate (Ins$P_3$) and diacylglycerol (DAG), that trigger calcium release from the intracellular stores and the activation of protein kinase C (PKC) (Citro S. et al., 2007).

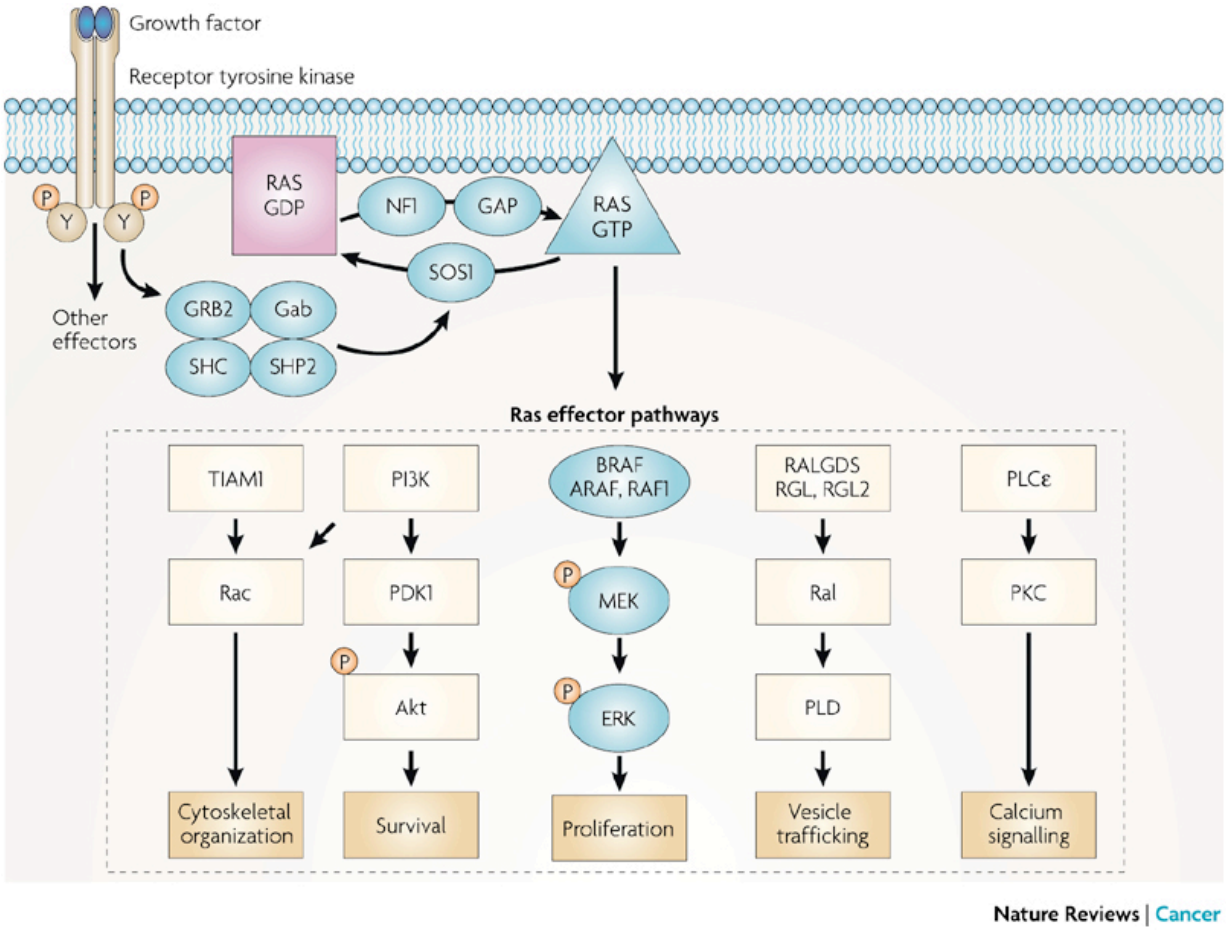


**Fig. 2. Ras-mediated signalling pathways** (From Schubbert S. et al., 2007)

## The MAPKs pathway

The extracellular signal regulated kinase (ERK) pathway belongs to the mitogen-activated protein kinase (MAPK) superfamily, a class of serine/threonine kinases that are highly conserved among the eukaryotes, from yeast to mammals. In the recent years, considerable attention was pointed to this signaling module that has been shown to be a key element regulating a series of biological processes including not only cell proliferation and differentiation, but also neuronal plasticity, survival and apoptosis. On the other hand, a dysregulation of this pathway has been shown to be involved in various pathologies, including neurodegenerative diseases, developmental disorders, diabetes and cancer.

The MAPK cascade is triggered by a wide variety of extracellular signals, including growth factors, cytokines and neurotransmitters, through many intracellular signaling molecules, such as calcium, protein kinase C, PI3-kinase or cAMP, depending on cellular context. This pathway is composed by three enzymes that act in a cascade of sequential phosphorylations; upon activation, the small GTPase Ras recruits Raf to the plasma membrane, inducing its activation; activated Raf is able to phosphorylate MEK which in turn phosphorylates ERK1/2. Once activated, ERKs translocate into the nucleus where they mediate genes transcription by activating specific transcription factors, such as CREB, c-Myc and Elk-1.

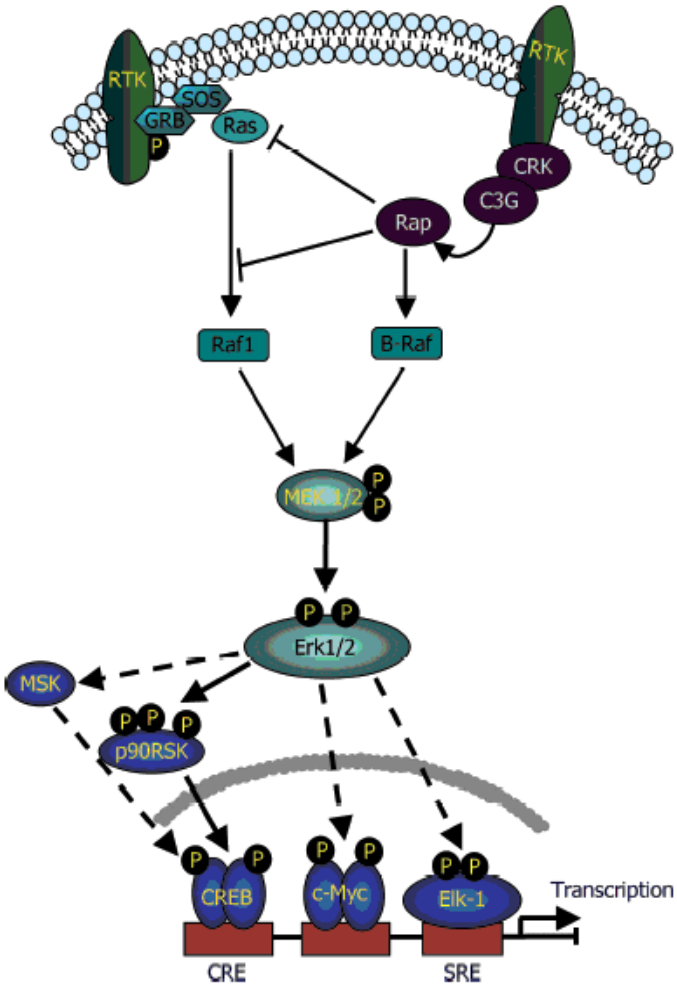


**Fig. 3. The Ras-ERK pathway (**From Davis and Laroche, 2006)

***Raf***

The Raf family is composed by the Ser/Thr kinases A-Raf, B-Raf e Raf1. While A-Raf is mainly expressed in the urogenital apparatus, B-Raf expression is restricted to the central nervous system and testicles (Pearson et al., 2001). Raf proteins contain three conserved regions: CR1, CR2, localized in the regulatory domain at the N-terminus and CR3, localized in the ATP binding region at the C-terminus. Once activated, Raf phosphorylates MEK on Ser218 and Ser222. The exact mechanism of Raf activation has not been completely understood yet, but it might involve both homo- or hetero-dimerization and phosphorylation. Although the kinases involved in Raf phosphorylation are still under investigation, experimental evidence has shown that the activation of Raf-1 might be mediated by Ras via protein kinase C (PKC), while B-Raf is activated by Rap1 via protein kinase A (PKA). In addition, Rap-1 seems to have opposite effects on the two isoforms of Raf, by activating B-Raf and inhibiting Raf-1 (York et al., 1998). It has also been suggested that Ras and Rap might be involved in the modulation of ERK cascade activation; in fact, Rap-1 induces

a sustained phosphorylation of ERK, that is associated with cell differentiation; on the contrary, activation of Ras induces only transient activation of ERK that underlies cell proliferation (York et al., 1998, Marshall et al., 1996).

Interestingly, in the central nervous system, it has been demonstrated that Ras and Rap1 pathways converge to activate the MAPKs via NMDA receptors with different kinetics. In fact, depolarization in cortical neurons induces a rapid and sustained Ras activation but at the same time a much weaker and delayed Rap1 response. This evidence suggests that Ras might act as a fast molecular switch involved in transient responses; on the contrary, Rap1 might be involved in the long-term modulation of the signal (Baldassa et al., 2003).

***MEK***

MEK kinases are dual specificity protein kinases that phosphorylate ERK1/2 on Thr183 e Tyr185, two residues located within the activation loop of ERK1/2. In mammalian cells, MEK kinases are present in two isoforms: MEK1 and MEK2 that share 80% of homology and are ubiquitously expressed.

***ERK1 and ERK2***

ERK1 and ERK2, also known as p44 and p42 MAPK, respectively, are highly homologous isoforms coded by two genes, erk1 (MAPK3) and erk2 (MAPK1). They share 85% sequence identity with much greater identity in the core kinase regions and are ubiquitously expressed, even if ERK2 is the predominant isoform in brain and hematopoietic cells (English and Sweatt, 1996). Phosphorylation by MEK in their activation loop (Tyr185 e Thr183) leads to a conformational change allowing their activation in the cytoplasm and subsequently their translocation into the nucleus, where they can activate transcription factors, either directly or indirectly, in order to induce the expression of several immediate early genes.

In the cytosol, ERK1/2 phosphorylates a wide range of substrates including membrane proteins, such as phospholipase A2, cytoskeletal proteins and several protein kinases such as p90 $^{rsk}$ (90 KDa ribosomal S6 Kinase). p90 $^{rsk}$ kinases (there are three isoforms, Rsk 1,2 and 3) activate cAMP response element (CRE) binding factor (CREB), a member of leucine-zipper transcription factors that binds a specific sequence of DNA, called CRE, that can be found in the promoter of many genes, including c-Fos, FosB and Zif268.

In addition, in the nucleus, ERK1 and 2 can bind and activate serum response element (SRE) binding proteins, such as Elk-1, thus contributing more directly to transcriptional regulation. Finally, ERK1/2 can also regulate gene transcription more globally at the level of chromatin remodelling by phosphorylating histone H3 on Ser10 via the kinase MSK-1 (and MSK2).

The ERK cascade also controls protein translation by activating the p70 S6 kinase-1 (S6K-1), which is phosphorylated by mTOR. S6K1 can directly activate S6 ribosomal protein, that is located near the mRNA and tRNA binding sites on the 40S ribosomal subunit. Although the exact mechanism through which the phosphorylated S6K1 and S6 ribosomal protein are involved in translational regulation is not completely clear, it has been shown that S6 phosphorylation correlates with an increased translation rate. In addition, the ERK-dependent phosphorylation of MAPK-interacting serine/threonine kinase 1 (Mnk1), which can phosphorylate eIF4E, is associated with an enhanced translation initiation (Klann and Dever, 2004).

Since ERK1 and ERK2 are activated by the same stimuli and they have identical substrate specificity, for a long time they have been considered as interchangeable. However, recent experiments conducted on ERK1 and ERK2 knock-out mice highlighted important functional differences between the two isoforms. At the level of the whole organism, clear differences have been shown between ERK isoforms. Precisely, erk2 gene ablation results in early embryonic lethality, showing that ERK1 cannot compensate ERK2 (Saba-El-Leil et al., 2003; Pages et al.,1999), whereas genetic inactivation of ERK1 is fully compatible with adult life (Satoh et al., 2007; Mazzucchelli et al., 2002). In addition, experiments conducted on mouse embryonic fibroblasts (MEFs) from ERK-1 KO mice and RNA interference approaches have given insight into the individual contribution of ERK1 and ERK2 in cell proliferation. In particular, ERK-1 knock out cells isolated from ERK-1 knock-out mice showed that the stimulus-dependent activation of ERK-2 was enhanced without any increase in ERK2 protein (Vantaggiato et al., 2006; Mazzucchelli et al., 2002).

Other studies demonstrated that ERK1 knock-down in culture cells leads to increased cell growth; importantly, the resulting enhancement of ERK2 activation is similar to what observed when constitutive active form of MEK1 is overexpressed via lentiviral vectors into MEFs. On the contrary, the ERK2 knock-down phenotype is similar to what observed with a dominant negative form of MEK1 (Vantaggiato et al., 2006; Indrigo et al., 2010). These results suggested a differential role of ERK1 and ERK2 in transducing intracellular signals; in particular, ERK2 is supposed to interact with MEK more efficiently and ERK1 is likely to act as partial agonist, providing a fine tuning of ERK2 activity (Vantaggiato et al., 2006).

Despite these observations, other studies still claim that ERK isoforms contribute to ERK signalling according to the ratio of their expression levels and not to their specific properties. For instance, in 2008 Lefloch and collaborators have reported that silencing of ERK2 expression slows the proliferation of NIH 3T3 fibroblasts, whereas reduction of ERK1 has no effect. Moreover, silencing of ERK1 further reduces cell proliferation in cells with a limiting level of ERK2 (Lefloch et al.,

2008). More recently, another work have supported the idea that both ERK1 and ERK2 act as redundant and positive-regulators of cell proliferation, since MEFs genetically deficient for erk1 or erk2 show a slower proliferation rate to an extent reflecting the expression level of the kinase (Voisin et al., 2010).

## The role of the MAPKs in learning and memory formation

In the central nervous systems, the ERK signaling cascade connects the stimuli deriving from ionotropic, metabotropic and neurotrophin receptors with cytosolic and nuclear events, leading to gene transcription and de novo protein synthesis. Recent evidence suggested the involvement of the Ras-ERK signaling module with many neuronal functions, such as different forms of plasticity including structural modifications at the synapses, learning and consolidation of long-term memory. Indeed, several components of the Ras-ERK pathway, including Ras and ERK1/2 themselves, but also Ras-GRF1, SynGAP and NF-1 are abundantly expressed in the central nervous system, in particular in brain regions involved in learning and memory (hippocampus, neocortex and cerebellum) (Kim et al., 2003; Zippel et al., 1997; )
In addition, the Ras-ERK cascade is coupled to diverse receptors (NMDARs, AMPARs, VGCCs) and it is potently activated by intracellular increase of calcium and cAMP (Kennedy et al., 2005; Farnsworth et al., 1995).

Long term potentiation (LTP) is the classical cellular model of neuronal plasticity that underlies the formation and the storage of memory and involves both rapid and persistent remodelling of the synapses. Rapid synaptic changes rely on the insertion of AMPA receptors in the plasma membrane and the remodelling of actin cytoskeleton and they are regulated by local calcium, whereas the long lasting modifications require synthesis of new proteins that are involved in the loss or pruning of dendritic spines and the formation or elimination of synapses. LTP can be dependent or independent on NMDA receptors and it consists in two distinct temporal phases: the early LTP, which lasts up to 30-60 minutes and depends on second messengers and kinases activity, and the late LTP, which lasts up to weeks and requires gene transcription and de-novo protein synthesis (Kennedy et al., 2005; Martin et al., 2000).
The molecular mechanisms underlying LTP induction and maintenance can be summarized in figure 4. First of all, glutamate is released as neurotransmitter from the presynaptic neurons and it specifically stimulates AMPA receptors. This event allows the post synaptic membrane to depolarise and $Mg^{++}$ is removed from NMDA receptors, with the consequent channel opening. Following NMDARs activation, calcium enters the post-synaptic neuron and it can mediate the

activation of different protein kinases, including Calcium-calmodulin Kinase II (CamKII), thus contributing to the LTP onset. Interestingly, calcium-calmodulin can also activate Ras-GRF1, a Ras exchange factor specifically expressed in neurons of the adult brain, leading to the activation of the Ras-ERK pathway. Upon a prolonged activation of the post-synaptic neuron, the ERKs are phosphorylated and they translocate into the nucleus where they activate specific transcription factors, such as CREB and Elk-1, and immediate early genes, including zif268, which are necessary for the consolidation of memory (Sheng and Kim, 2002).

In addition, the ERKs have many other substrates, including cytoskeletal proteins (MAP-2 and Tau), which are necessary for synaptic remodelling, and mTOR, a protein associated with the translation machinery (Vaillant et al., 2002; Kelleher et al., 2004).

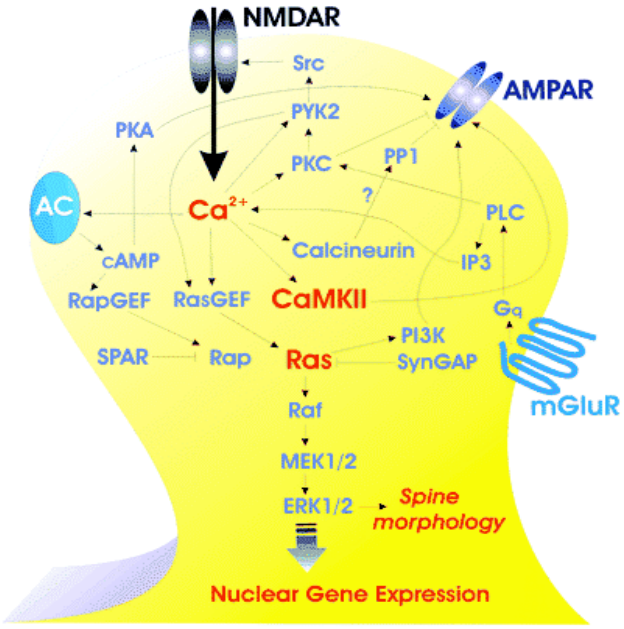


**Fig. 4. The MAPKs activation during long term potentiation (LTP)** (From Sheng M. and Kim M. J., 2002)

In recent years, several studies have extensively documented that a normal-functioning ERK cascade is required in different forms of neuronal plasticity, such as learning and memory formation and consolidation. In particular, the use of the MEK inhibitors UO126 and SL327 provided the first evidence that ERK signalling is required for the brain functions. The initial studies focused on NMDA-dependent long-term potentiation (LTP) in the CA1 and in the dentate gyrus using hippocamapal slices in vitro and demonstrated that three distinct MEK inhibitors completely block late LTP and attenuate early LTP. Consistently, it was shown that the induction of LTP in the dentate gyrus results in a rapid and transient increase of activated ERK (Sweatt, 2001).

Furthermore, it was demonstrated that ERK activation is a key step that regulates AMPARs activity and structural plasticity, thus contributing to increase the synaptic transmission. In particular, MEK inhibitors or the expression of Ras dominant negative forms prevent AMPARs insertion in the post-synaptic neurons and the formation of new dendritic spines (Zhu et al., 2002).

Subsequent studies in vivo highlighted the evidence that the activation of ERK is necessary for the consolidation of long-term memories associated to different types of learning, including fear associated learning (Atkins et al., 1998; Schafe et al., 2000; Selcher et al., 1999; Walz et al., 1999), conditioned taste aversion (Berman et al., 2000; Swank, 2000), object recognition (Kelly et al., 2003) and spatial learning (Blum et al., 1999; Selcher et al., 1999; Hebert and Dash, 2002). These studies have also shown that ERK is hyperphosphorylated after the learning phase and that MEK inhibition results in an impaired consolidation of long-term memory, without affecting short-term memory and learning (Miyamoto, 2006; Davis and Laroche, 2006; Thomas and Huganir, 2004).

It should be noted that all these studies relied on the use of MEK inhibitors that do not allow to dissect any functional difference between ERK1 and ERK2. However, recent studies based on the use of knock-out mice have provided a strong evidence that ERK1 and ERK2 play specific and distinct roles in synaptic plasticity. Although the ERK1 KO mice do not show any compensatory changes in basal ERK2 expression, they manifest a robust increase of ERK2 phosphorylation following exposure to glutamate or dopamine receptor D1 agonist compared with wild type mice. This result correlate with the evidence that synaptic plasticity in the striatum is enhanced in ERK1-KO mice, correlating with an improved memory formation in striatum-dependent learning tasks and an enhanced behavioural response to reward properties of morphine and cocaine (Mazzucchelli et al., 2002; Ferguson et al., 2006).

***Ras-related syndromes***

Mutations within genes of ERKs signalling pathway have been associated to several diseases that often includes neurological and cognitive deficits. A group of syndromes are characterized by cardiac and craniofacial abnormalities and includes Costello, Noonan, LEOPARD, Legius and cardio-facio-cutaneous (CFC) syndromes. A related disorder is also Neurofibromatosis Type 1 disease, mainly characterized by cutaneous abnormalities (café au lait spots), and neurofibromas. All these disorders show a certainly degree of cognitive impairments (from mild to severe) (Aoki et al., 2009; Samuels et al., 2009; Fasano and Brambilla, 2011).

Costello syndrome is associated to a gain of function mutation of H-Ras and has clinical features similar to CFC; in particular, in Costello syndrome 40% of the patients exhibits frontal lobe atrophy, 26% of the patients shows cerebellar abnormalities and all these patients are affected by significant mental retardation.Instead, CFC results from mutations in K-Ras, B-Raf and MEK and

almost 80% of the patients are affected by mental retardation associated with severe CNS abnormalities. Noonan syndrome (NS) has been associated to point mutations in distinct genes coding for upstream proteins in the ERK cascade, such as SHP2, K-Ras, Sos-1 and Raf. All these mutations lead to the upregulation of the ERK pathway and the classical clinical manifestations include pulmonic stenosis, short stature, and facial dysmorphia. In this case, mental retardation has been reported only in 25% of the patients. Neurofibromatosis type 1 (NF1) arises from mutation or deletion of the NF1 gene encoding neurofibromin, a RasGTPase activating protein that acts as a negative regulator of ERK activation. Over half of individuals with NF1 mutations have intellectual impairment. In addition, individuals with deletions encompassing the NF1 gene exhibit a more severe intellectual impairment. LEOPARD syndrome (lentigines, EKG abnormalities, ocular hypertelorism, pulmonic stenosis, abnormal genitalia, retardation of growth, and deafness) arises from loss-of-function mutations in PTPN11 and K-RAS that are distinct from those associated with NS, though there is clinical overlap between the two disorders (Bentires-Alj et al., 2006). Two recent reports of gain-of-function mutations in RAF1 were shown to cause Noonan and LEOPARD syndromes, and were associated with increased ERK activation (Pandit et al., 2007; Razzaque et al., 2007). Recently a new syndrome has been described, termed NF1-like or Legius syndrome, which results from loss-of-function mutations in the SPRED1 gene. The SPRED1 gene product normally acts to suppress ERK activation, as does NF1 (Brems et al., 2007). Thus, loss-of-function mutations in NF1 or SPRED1 result in elevation of ERK pathway activation. These patients are also cognitively impaired and macrocephalic and exhibit facial dysmorphism similar to other NCFC syndromes (Brems et al., 2012).

Among the diseases associated to the ERK pathway, also a X-linked syndrome has been identified: the Coffin-Lowry Syndrome, resulting from mutations at Xp22.2, that causes a loss of function of the kinase RSK-2 (Ribosomal S6 kinase-2), associated to a severe mental retardation (Samuels et al., 2009; Stornetta and Zhu, 2010).

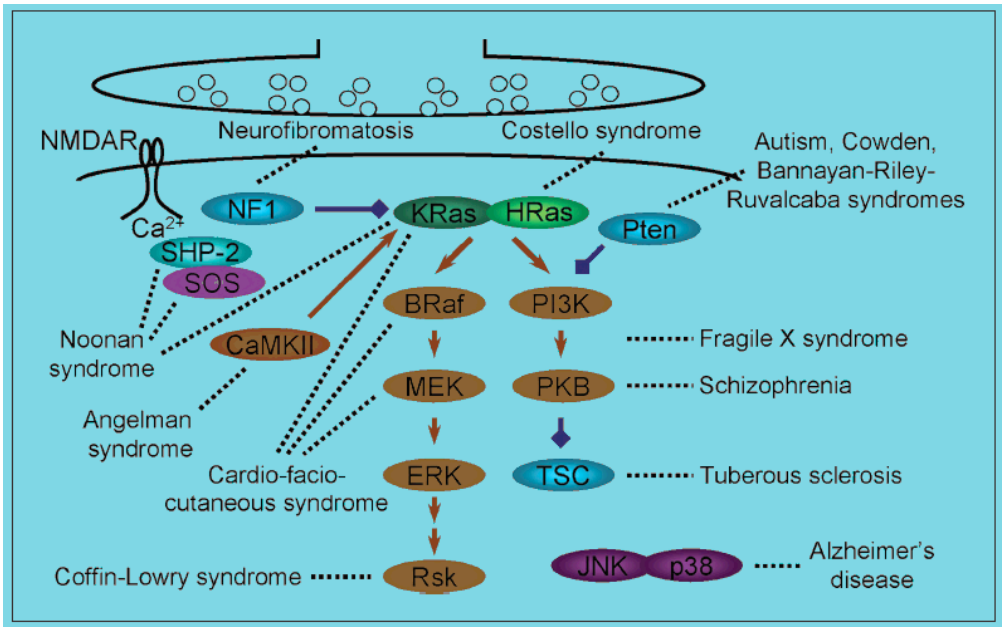


**Fig.5. Mutations of genes in ERK pathway and associated syndromes** (From Stornetta and Zhu, 2010)

***Ras-GRF1***

Ras-GRF1 is a Ras exchange factor exclusively expressed in the central nervous system, in particular in the hippocampus, thalamus, cortex and cerebellum, whereas it is not expressed in the peripheral neuronal cells, and in non-neuronal cells. Subcellular fractionation of the mouse brain has shown that it is localized in synaptosomes and enriched in post-synaptic densities. In the rodents, the expression of Ras-GRF1 is regulated during the development; in fact, this protein has not been found in the embryos but its expression increases in the first few days after birth, a timing that correlates with the maturation of the synapses (Zippel et al., 1997).

Ras-GRF1 can be regulated both by calcium and heterotrimeric G proteins (Shou et al., 1995; Zippel et al., 1996; Mattingly et al., 1999) and more recent studies demonstrated that the N-terminal region of Ras-GRF1 can interact with HIKE domain of the tyrosine kinase receptor TrkA (Robinson et al., 2005). In addition, Ras-GRF1 can be activated by calcium influx through NMDARs; in fact, it has been shown that Ras-GRF1 binds directly the NR2B subunit of NMDA receptor and therefore mediates a large fraction of NMDAR-dependent ERK activation in cultured hippocampal neurons (Krapivinsky et al., 2003).

Experiments conducted on Ras-GRF1 knock-out animals contributed to define the role of the Ras-ERK pathway in the neuronal signalling. In fact, although these animals are viable, fertile and they do not have any phenotypic difference compared to wild-type mice besides a small reduction in body weight, they show learning and memory impairments. In particular, behavioural studies conducted on Ras-GRF1 knock out mice put in evidence that Ras-GRF1 ablation does not affect hippocampal learning and spatial memory, but significantly impairs fear conditioning and

procedural learning (Brambilla et al., 1997; D'Isa et al., 2011). Furthermore, the use of Ras-GRF1 knock out mice has also suggested the implication of Ras-ERK pathway in drug-dependent behavioural changes ("drug addiction"). For instance, Ras-GRF1 knock our mice do not develop tolerance to analgesic and hypolocomotor effects induced by the chronic treatment with cannabinoids (Rubino et al., 2004). More recently, it has been shown that these animals manifest a reduced response to cocaine, measured as locomotor sensitization and conditioned place preference (Fasano et al., 2009).

## Signal transduction in the striatum

The striatum, composed by the caudate putamen and the nucleus accumbens, is the input nucleus of the basal ganglia, a group of interconnected subcortical nuclei sustaining diverse functions as motor control, learning, planning, working memory and emotions.
The basal ganglia also include:
-the globus pallidus pars externa (GPe) and pars interna (GPi),
-the subthalamic nucleus (STN),
-the substantia nigra pars compacta (SNc) and pars reticulata (SNr)

The GABAergic medium spiny neurons (MSNs) are the main neuronal type in the striatum and they receive excitatory glutamatergic inputs from the cortex, thalamus and limbic areas and modulatory dopaminergic inputs from midbrain neurons located in the SNc and in the ventral tegmental area. In addition, MSNs receive inhibitory synapses originating from other MSNs and GABAergic interneurons, and many others afferents such as cholinergic and serotoninergic inputs.
The putamen efferent neurons connect the striatum to the output nuclei of the basal ganglia, such as GPi and SNr, via two distinct projection systems: the "direct striatonigral pathway", that projects directly to these nuclei, and the "indirect striatopallidal pathway", which projects via a circuit including the GPe and the STN. The MSNs of the direct pathway express preferentially the D1 subtype of dopamine receptors (D1Rs) and they produce the neuropeptide cotransmitters dynorphin and the substance P, whereas the MSNs of the indirect pathway are enriched in D2 subtype of dopamine receptors type 2 (D2Rs) and adenosine A2A receptors and they produce the neuropeptide enkephaline.
According to the general model of basal ganglia transmission, the direct pathway disinhibits the thalamo-cortical neurons thus promoting the motor activity, whereas the indirect pathway reduces motor activity by inhibiting the thalamo-cortical neurons. In addition, dopamine promotes motor

activity by exerting opposite actions on the two pathways; in particular, it activates the striatonigral MSNs and, in the same time, inhibits the striatopallidal MSNs.

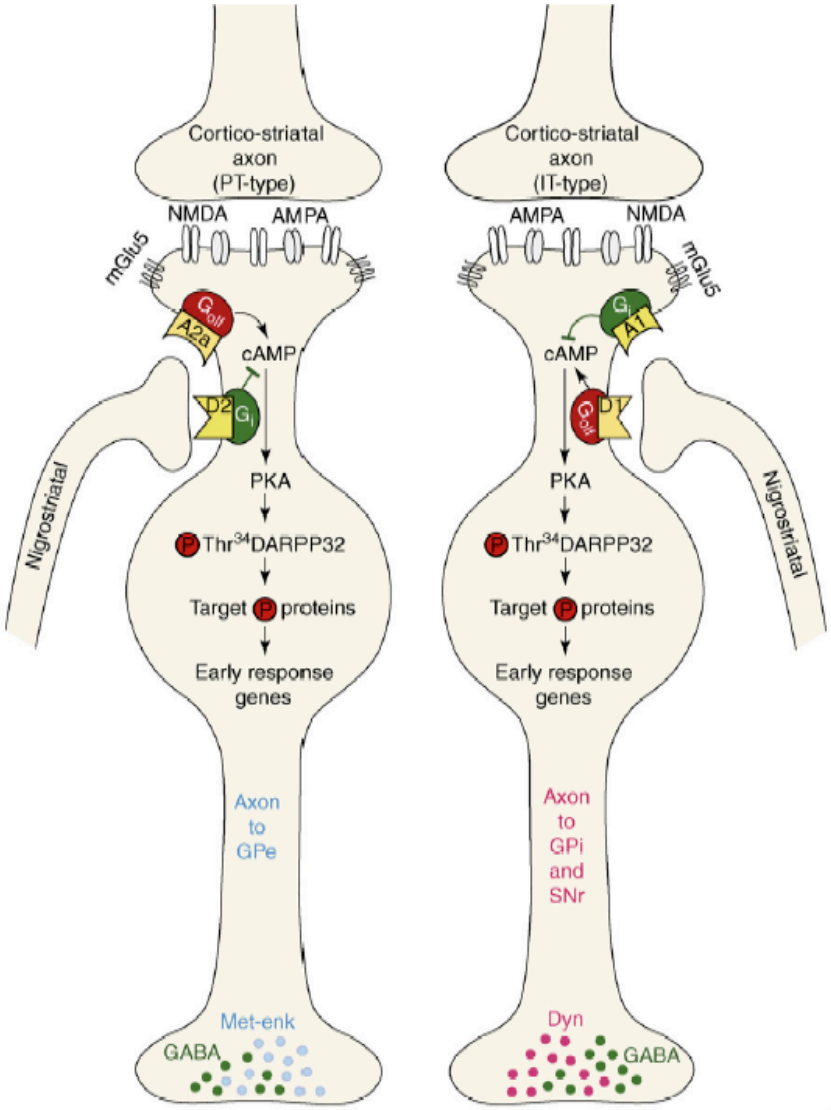


**Fig. 6. The two distinct classes of striatal MSNs.** Representation of a striatopallidal MSN (left) and a striatonigral MSN (right)(From Cenci, 2007).

***Dopaminergic and glutamatergic signalling in the striatum and their synergism***

Dopaminergic signalling in the striatum is mediated by the two classes of dopamine receptors, D1Rs and D2Rs, that are coupled respectively to the Gαolf and Gαi/o, thereby exerting opposite effects on the production of cAMP. Once stimulated by burst firing of dopaminergic neurons, the D1Rs promote the Gαolf-mediated stimulation of adenyl-cyclase, thus increasing intracellular cAMP level and leading to the enhancement of motor activity. The increase in cytosolic cAMP levels results in the activation of various intracellular targets, such as cAMP-regulated phosphoprotein of 32 kDa (DARPP-32), that mediates the activation of several downstream factors

involved in the control of the excitability of the MSNs. Once activated, DARPP-32 acts as a strong inhibitor of the phosphatase PP1 and thus prevents the dephosphorylation of different downstream targets of PKA, thereby amplifying the cAMP-mediated responses. PP-1 acts at the level of NMDARs, by dephosphorylating the NR1 subunit, and also activates the striatal-enriched tyrosine phosphatase (STEP) that dephosphorylates the regulatory tyrosine of ERK.

A series of studies have shown that D1Rs-mediated PKA activation promotes surface expression of both AMPARs and NMDARs, even though the precise mechanism is still unknown. It has been suggested that PKA may be involved in receptor trafficking through DARPP-32-mediated inhibiton of PP-1 and through the inhibition of STEP (Braithwaite et al., 2006). Another mechanism underlying the surface expression of glutamate receptors may be mediated by an independent pathway involving Src-family tyrosine kinases (Pascoli et al., 2010).

The D2Rs have higher affinity for dopamine and therefore they are activated by low basal levels of dopamine; upon stimulation, the D2Rs mediate a tonic inhibition on adenyl-cyclase and membrane potential, thereby opposing the action of D1Rs but also A2A receptors. In addition, released Gβγ subunits stimulate phospholipase Cβ, leading to the activation of PKC and calcium release from the intracellular stores. Several studies have highlighted the evidence that the activation of D2Rs reduce the excitability of striatopallidal neurons by decreasing AMPARs currents of MSNs recorded in brain slices and also promoting the trafficking of AMPARs out of the synaptic membrane (Cepeda et al.,1993; Hakansson et al., 2006). In addition, D2Rs are able to modulate in a coordinate manner the activity of different ion channels, thus reducing the responsiveness of MSNs to glutamatergic inputs (Hernandez-Lopez et al., 2000).

***The ERK cascade in the striatum***

Different types of ionotropic and metabotropic glutamate receptors are stimulated by glutamate released from corticostriatal and corticothalamic neurons.

As summarized in figure 6, NMDARs activation allows calcium influx that stimulates various proteins, such as Ras-GRF1, thereby triggering the ERK cascade. This event is amplified by D1Rs stimulation through a cAMP-independent pathway involving the Src-family tyrosine kinases (SFK) and through the DARPP-32-mediated inhibition of PP-1, thus blocking the dephosphorylation of NR1 subunit of NMDARs and the activation of STEP (Pascoli et al., 2010; Valjent et al., 2005). In this manner, the ERK cascade is likely to act as coincident detector between the dopamine and the glutamate pathways.

A large part of calcium-dependent activation of ERK seems to be mediated by Ras-GRF1 (Fasano et al, 2009), but also two other GEFs, CalDAG GEFI and CalDAG GEFII, stimulated by calcium and diacyl glycerol, are involved in the triggering of ERK pathway (Toki et al., 2001).

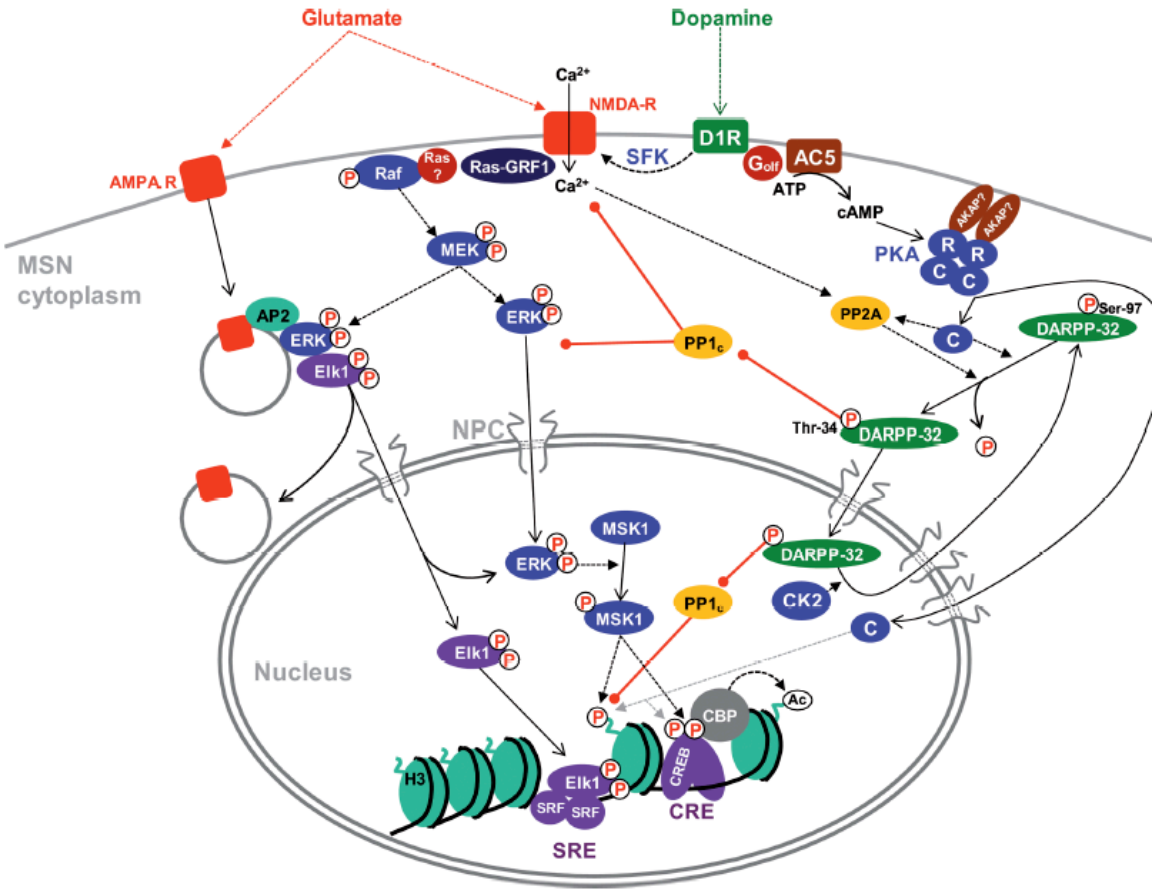


**Fig. 7. Glutamatergic and dopaminergic signalling pathways in striatonigral MSNs** (From Matamales and Girault, 2011). Glutamate-induced ERK activation involves calcium influx from NMDARs that stimulates RasGRF1, triggering Raf/MEK/ERK cascade. Active ERK, together with Elk1, is able to associate with endocytosed AMPARs through the adaptor protein AP2; this complex mediates the nuclear import of active ERK and Elk1. ERK activation is strongly potentiated by dopamine-induced D1Rs activation through two different mechanisms: i) cAMP-independent pathway involving Src family tyrosine kinases (SFK); ii) cAMP/PKA pathway that inhibits protein phosphatase 1 (PP1) through phospho-DARPP-32. D1Rs stimulation promotes the Gαolf-mediated stimulation of adenyl-cyclase 5 (AC5), thus increasing intracellular cAMP level. The inactive PKA heterotetramer is anchored through AKAPs; cAMP binds the regulatory subunits (R) of PKA and releases the catalytic subunits (C). C subunits phosphorylate several substrates in the cytoplasm and also diffuse into the nucleus where they mediate the activation of CREB and histone H3.

### *ERK effectors in MSNs*

The activation of PKA and ERK mediates gene transcription through the phosphorylation of several downstream proteins, including other kinases and transcription factors. Among the effectors of ERK, it should be mentioned RSK family composed by RSK1-3 that are able to phosphorylate CREB on Ser133. This factor is one of the most studied targets of the ERK pathway and it is also the substrate of PKA and many other kinases, including CamKII/IV and PKC (Johannensen and Moens, 2007). CREB binds constitutively the CRE sites located in the promoters of a series of

genes in its inactive form; once phosphorylated on Ser133, CREB is activated and binds the co-activator CREB binding protein (CBP) that interacts with the translational machinery. Another important partner of CREB is the transducer of regulated CREB (ToRC), that is activated by cAMP and calcium and promotes the nuclear localization of CREB.

Another target of the ERK cascade is the transcription factor Elk1, a member of the Ets family that forms the ternary complex following the association with serum response factor (SRF), a MADS box protein that binds DNA at the $CC(A/T)_6GG$ consensus sequence, known as a CArG box or serum response element (SRE). SRE has been found in the promoters of actin cytoskeleton genes and immediate-early genes, including c-fos, Arc and Egr1 (Miano et al., 2007, Besnard et al., 2010). In MSNs, Elk-1 is located in part in the cytoplasm and it accumulates into the nucleus following ERK-dipendent phosphorylation (Vanhoutte et al., 1999). In addition , ERK and Elk1 are recruited from neuritis to cell bodies and nucleus in response to glutamate stimulation and they undergo retrograde trafficking with AMPARs (Trifilieff et al., 2009).

The ERK cascade not only controls transcription by activating a series of transcription factors, but also by regulating chromatin remodelling. In the nucleus, DNA is packaged into chromatin, a DNA-protein complex, that regulates the transcriptional rate of different genes depending on the degree of its condensation. In particular, condensed or relaxed chromatin respectively represses or promotes transcription. Distinct post-translational modifications can occur at histones tails, the major protein component of chromatin, thereby contributing to the dynamic process of chromatin remodelling. It has been shown that Lys9/Lys14 acetylation and Ser10 phosphorylation of histone H3 are involved in transcriptional regulation; in particular, a rapid but transient phosphorylation on Ser10 of histone H3 has been associated with transcriptional activation of immediate-early transcriptional genes (IEGs), including c-fos and c-jun, upon mitogenic or stress stimuli (Mahadevan et al., 1991; Chadee et al., 1999). In addition, Lys9 methylation promotes gene silencing, whereas Lys9 acetylation correlates with transcriptional activation. In hippocampal neurons , H3-Ser10 phosphorylation in combination with Lys14 methylation mirrors the increase of c-fos transcription, in response to the stimulation of different receptors such as D1Rs (Crosio et al., 2003). In addition, H3-Ser10 phosphorylation is increased following cocaine treatment and this event depends on MSK-1 (Brami-Cherrier et al., 2005) and occurs selectively in the striatonigral pathway (Bertran-Gonzalez et al., 2008). Importantly, the use of MSK-1 knock out mice treated with cocaine have demonstrated the critical role of MSK-1 in cocaine–induced transcriptional events leading to drug addiction. In particular, MSK-1 knock-out mice have shown decreased locomotor sensitization and many nuclear responses induced by cocaine, such as histone H3 phosphorylation, are blocked; on the contrary, zif268 expression and conditioned place preference are not impaired. (Brami-Cherrier et al, 2005).

Conversely, recent evidence supports the idea that H3-Ser10 phosphorylation in striatopallidal neurons, triggered by D2Rs blockade, is not mediated by MSK-1, but it might depend on A2Rs-mediated activation of cAMP/PKA/DARPP-32 signalling pathway (Bertran-Gonzalez et al., 2008).

## L-DOPA-induced dyskinesia

Recent studies have demonstrated that the Ras-ERK pathway in the striatum plays a pivotal role not only in the normal striatal functions, but it is also involved in neurological diseases such as L-DOPA-induced dyskinesia (LID).

Parkinson's disease (PD) is a frequent neurodegenerative disorder that affects about 1-2% of the population over 60 years. PD is caused by the progressive death of dopaminergic neurons in the substantia nigra pars compacta and leads to a deficit in dopamine transmission to the striatum. The depletion of dopamine in the posterior putamen, which is the motor region of the striatum, causes the four symptoms of PD: bradykinesia/akinesia, rigidity, tremor and postural instability (Fahn, 2003).

The pharmacological treatments currently available for PD are based on dopamine replacement, through the administration of the dopamine precursor L-DOPA, which is converted into dopamine in the Parkinsonian brain providing a partial restoration of dopamine levels. Although L-DOPA represents an efficient therapy at the initial phase of the disease, after few years its therapeutic effect is shortened to the intake of a single dose. This phenomenon, called "wearing-off effect", imposes an escalation in the dosage of the drug, thus inducing the appearance of abnormal involuntary movements or dyskinesia (Obeso et al., 2000).

It has been estimated that up to 90% of the patients develop dyskinesia within 10 years from the beginning of the therapy and, for this reason, LID currently represents one of the major challenges in the treatment of PD. LID is a severe motor complication characterized by a mixture of chorea (abrupt movements that seem to flow from one body part to another) and dystonia (slow twisting movements) (Cenci, 2007). Dyskinesia is usually most severe during the two-three hours that follow a drug dose, when plasma and brain levels of exogenous L-DOPA reach their peak (Fahn, 2000). However, dyskinesia can also be present when brain L-DOPA concentration is low. Dyskinesia is also frequent at the beginning or at the end of L-DOPA action cycle, when L-DOPA levels are rising or falling.

Currently, three strategies are used to prevent or reduce LID. The first is based on the administration of long-acting agonists instead of L-DOPA, in order to avoid the pulsatile dopamine receptor stimulation that is induced by the common L-DOPA therapy and it is also the main risk

factor for developing LID. Unfortunately, dopamine agonists have also side effects and they are not as effective as L-DOPA in treating PD.

The second strategy consists in giving non-dopaminergic drugs during L-DOPA treatment, in order to reduce dyskinesia. In particular, several drugs, such as serotonin reuptake inhibitors, adrenergic antagonists and NMDA receptors antagonist have shown antidyskinetic properties. However, the efficacy of these drugs is quite modest; the most effective agent and the only one currently marketed for LID treatment, amantadine, is able to reduce dyskinesia in the range of 40-60% in the best responding patients.

A final strategy is the neurosurgical intervention targeting specific nuclei within the basal ganglia (Deep Brain Stimulation, DBS), developed in 1987 by Benabid and collaborators as treatment for PD. This strategy is based on high-frequency stimulation (HFS) of the STN or GPi through chronically implanted macroelectrodes. After setting the electrode placement, the stimulation voltage is progressively increased while checking both the clinical efficiency and the induction threshold for side effects, such as dyskinesia, muscle contractions, or eye deviation (Benabid et al., 2009). At present, in the overall PD patient population, the GPi is less frequently chosen than the STN as a target for DBS surgery because pallidal stimulation is commonly regarded as having a weaker antiparkinsonian effect, although it provides a direct and pronounced antidyskinetic effect (Toda et al., 2004; Follett, 2004; Guridi et al., 2008). Conversely, STN-HFS does not have an antidyskinetic effect per se, but effectively improves tremor, rigidity and bradykinesia allowing for L-DOPA dosage to be reduced by an average of 60% (Limousin et al., 1998), thus indirectly improving dyskinesia too (Benabid et al., 2000; Toda et al., 2004). However, although many successful cases have been reported in literature, it has to be considered that this strategy, in addition to being expensive and invasive, can be offered only to restricted groups of patients, responding to specific criteria (Benabid et al., 2006).

In recent years the study of the molecular changes occurring in the striatum during the development of LID and the role of the specific components of the signalling machinery has revealed potential new therapeutic targets. For this purpose, different experimental PD models have been used; before describing the alterations occurring in the intracellular signalling during LID, it is useful to describe briefly the two major animal models that have been used: the 1-methyl 4-phenyl 1,2,3,6-tetrahydropyridine (MPTP)-treated primate and mice and the 6-hydroxydopamine (6-OHDA) lesioned rodents.

The neurotoxin MPTP was discovered in the 1980s when it was found to produce striking parkinsonian features in humans (Langston et al., 1983). Subsequently it contributed to the

improvement of PD research, by providing a symptomatic model of the disease. MPTP is uptaken by astrocytes where it is converted to MPDP+ through the action of monoamine oxidase type B (MAO-B). MPDP+ is then metabolized to MPP+, which is taken up by DA transporters (DAT) through dopamine uptake sites on dopamine nerve terminals and concentrated in mitochondria. Here MPP+ inhibits complex I of the mitochondrial respiratory chain, decreasing tissue ATP and stimulating the production of reactive oxygen species (ROS) (Nicklas et al., 1985; Przedborski and Jackson-Lewis, 1998). The resulting disturbance of mitochondrial function can lead to oxidative stress and neuronal death. MPTP is generally administered by intracarotid injection or subcutaneously and the behavioural evaluations are usually performed at least 3 months after MPTP administration in order to have stable motor deficits.

The 6-OHDA model consists in an intracerebral infusion, typically unilaterally, of the neurotoxin 6-OHDA. Specifically, 6-OHDA is directly injected into the medial forebrain bundle (MFB) or the dorsal striatum, leading to retrograde dopaminergic cell loss in the SN, the area predominantly affected in PD.

***Changes in cAMP -mediated signalling in the onset and development of LID***

It is currently known that dopamine depletion determines an hyper-responsiveness of D1Rs to L-DOPA, that cannot be attributed to increased levels of D1Rs since a number of studies did not find significant changes in the number or affinity of D1Rs (Turjanski et al., 1997; Hurley et al., 2001; Aubert et al., 2005).

Chronic administration of L-DOPA promotes also the release of BDNF from corticostriatal neurons, leading to the activation of TrkB receptors and increased expression of D3Rs in striatonigral MSNs. Direct interaction with D3Rs is likely to increase the levels of membrane-bound D1Rs, thereby exacerbating D1R sensitization and dyskinetic behaviour.

Consistent evidence now indicates that cAMP-mediated signalling plays a pivotal role in the development of dyskinesia. In fact, the enhanced responsiveness of D1Rs results in an increased coupling to Golf, thus leading to an increase in cAMP production and PKA activation (Herve et al., 2001, Santini et al., 2007). Importantly, the abnormal enhancement of cAMP signalling that occurs during LID is also linked to an hyperactivation of downstream effectors, such as GluR1 subunit of AMPAR (Santini et al., 2007). PKA-mediated phosphorylation of Ser845 of GluR1 promotes glutamatergic transmission by maintaining the AMPARs in an open state and by increasing their surface expression; this event correlates with LID since in MPTP-lesioned monkeys, that represent an experimental model of PD, LID is increased by administration of AMPARs agonist and reduced by AMPARs antagonist (Konitsiotis et al., 2000).

Recent evidence has also suggested that the administration of L-DOPA to 6-OHDA lesioned mice increases the phosphorylation of DARPP-32. This event leads to the inhibition of PP-1, thereby suppressing the dephosphorylation of downstream target proteins. In addition, DARPP-32 knock mice chronically treated with L-DOPA show a significant attenuation of LID symptoms. Phosphorylation of DARPP-32 in LID is also involved in the activation of GluR1 via inhibition of PP-1-mediated dephosphorylation (Santini et al., 2007) and it is implicated in the increase of expression of immediate early genes, such as c-fos, arc and zif268 (Svenningsson et al., 2000).

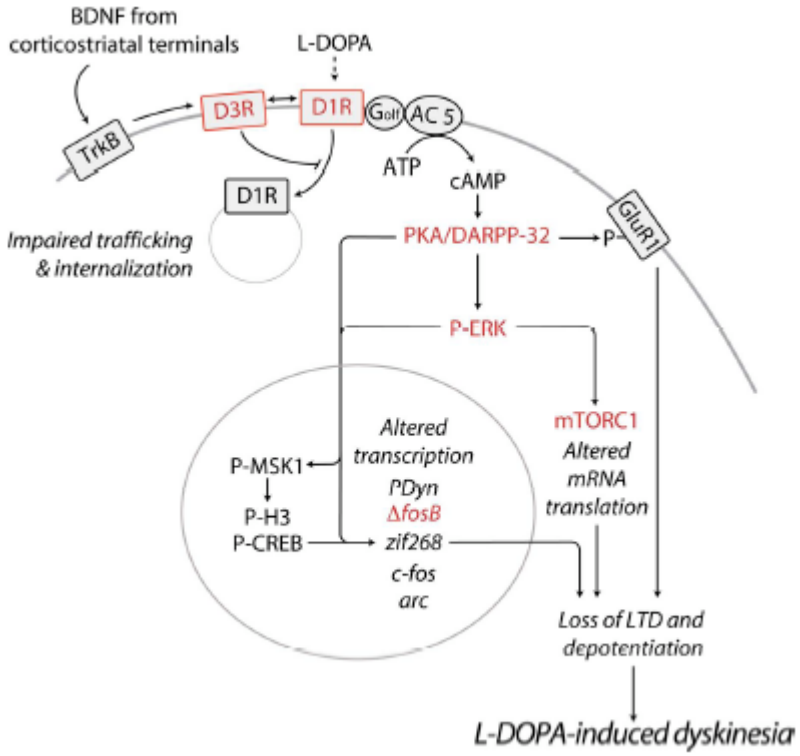


**Fig.8. The signalling pathways activated by L-DOPA and involved in LID** (From Feyder et al., 2011). Supersensitization of D1Rs in LID may be mediated by different mechanisms. First, chronic L-DOPA treatment promote the release of BDNF from corticostriatal neurons, leading to TrkB receptors activation and increased expression of D3Rs in the striatonigral MSNs. The interaction between D3Rs and D1Rs may lead to increased D1Rs expression on MSNs surface. Another possible mechanism underlying D1Rs sensitization in LID is mediated by cAMP/PKA/DARPP-32 pathway.; in fact, increased D1Rs responsivity results in PKA and DARPP-32 hyperactivation, leading to an augmented ERK signalling. This aberrant ERK activation leads to increased MSK-1, CREB and histone H3 phosphorylation, causing an altered gene transcription; in addition, ERK promotes mTORC signalling thereby enhancing protein synthesis.

***Alterations of ERK activity in LID***

A number of experimental evidence indicate that ERK hyperactivation is a major additional consequence associated to D1Rs supersensitization and that ERK activity correlates well with the

LID symptoms in animal models (Gerfen et al., 2003; Pavon et al., 2006; Santini et al., 2007; Westin et al., 2007; Fasano et al., 2010; Santini et al., 2010).

Increase of ERK activity can be achieved through several mechanisms. First of all, activated DARPP-32 may control ERK 1/2 phosphorylation through the inhibition of the protein phosphatase STEP which normally negatively controls MEK1/2 (Valjent et al., 2005). This idea is also supported by the observation that in 6-OHDA lesioned DARPP-32 knock out mice the hyperactivation of ERK does not occur upon L-DOPA treatment (Santini et al., 2007). In addition, the relevance of abnormal activation of ERK in LID is also supported by the observation that Ras-GRF1 ablation can prevent the development of LID and reduce ERK activity. Importantly, the combined administration of MEK inhibitors (such as SL237) enhances the antidyskinetic effect observed in Ras-GRF1 deficient mice. In addition, striatal inhibition of Ras-GRF1 and ERK signalling using viral vectors ameliorates already established dyskinetic symptoms in the non human primates (NHP), thus opening the way for a possible therapy of LID based on targeting Ras-GRF1 (Fasano et al., 2010; Fasano and Brambilla, 2011).

In the nucleus, ERK activates MSK-1, that directly phosphorylates histone H3, thereby regulating transcription of several genes c-fos, dynorphin and zif268, which are hyperactivated in 6-OHDA lesioned rodents treated with L-DOPA (Santini et al., 2009; Andersson et al., 1999).

Recent studies conducted on transgenic mice expressing EGFP in the striatonigral (Drd1 mice) or in the striatopallidal (Drd2 mice) pathway demonstrated that L-DOPA-induced ERK-MSK1-H3 activation is restricted to the striatonigral pathway without affecting the striatopallidal MSNs. Moreover, ERK-MSK1-H3 upregulation depends on D1R activation since it is prevented by the administration of the specific antagonist of D1Rs, but not by blocking D2Rs (Santini et al., 2009).

Finally, the involvement of ERK in LID may depend not only on the regulation of transcription but also on the modulation of local protein synthesis in the cytoplasm. In this regard, ERK1/2 have been proposed to activate mTOR complex 1 (mTORC1), a component of mTOR involved in the control of protein synthesis and autophagy (Costa-Mattioli et al., 2009). In particular, ERK phosphorylates, directly or via RSK, the tuberous sclerosis complex 1 (TSC1) that consequently is inhibited, leading to the activation of mTORC1. It has been recently shown that LID is associated with an increased phosphorylation of S6 ribosomal protein and two targets of mTORC1, the S6 kinase and the initiation factor 4E-binding protein (4EBP), in the striatonigral pathway. Collectively these events are likely to be involved in the enhancement of protein translation observed in LID (Richter and Sonenberg, 2005; Ruvinsky and Meyuhas, 2006; Roux et al.,2007). Importantly, the blockade of mTORC1 by the specific inhibitor rapamycin has been found to attenuate LID in

dyskinetic mice, thus suggesting that an aberrant enhancement of protein synthesis may be implicated in the development of LID (Santini et al., 2009).

# Materials and methods

**Experimental animals.** Experiments were conducted in 2 months old mice C57/BL6 purchased from Charles River Laboratories, in BAC transgenic mice expressing EGFP under the control of muscarinic receptor M4 promoter selectively in the direct pathway (M4-EGFP mice, Dobrossy et al, 2011) and in Ras-GRF1 knock out mice (Brambilla et al., 1997).
Animals were housed in a 12h light-dark cycle, in stable conditions of temperature, with food and water ad libitum. All experimental procedures were performed in accordance with protocols approved by the Institutional Animal Care and Use Committee (IACUC) and communicated to the local authorities.

**Genotyping.** Mouse tails biopsy were digested in 500 µl of tail buffer with 1 mg/ml Proteinase K (Roche) overnight at 55°C. Genomic DNA was purified throughout two successive steps, in which the samples were mixed with an equal volume of phenol/chloroform solution, vortexed for 30 sec and the aqueous phase was recovered centrifuging for 5 min at room temperature. The DNA was then precipitated adding 2.5 volumes of absolute ethanol and centrifuging for 5 min. The resulting pellet was washed with 70% ethanol, let dry and resuspended in 150 µl of sterile water.
The hot-start PCR for M4-EGFP mice was performed as follows:

95°C for 5 min
94°C for 30 sec
60°C for 30 sec } for 30 cycles
72°C for 30 sec
72°C for 10 min

Forward primer: 5'-CACATGAAGCAGCACGACTT-3'
Reverse primer: 5'-TGCTCAGGTAGTGGTTGTCG-3'.

The hot-start PCR for Ras-GRF1 KO mice was performed as follows:

95°C for 5 min
94°C for 1 min
68°C for 2 min } for 35 cycles
72°C for 2 min
72°C for 10 min

Ras-GRF1 mutant forward primer: CTGCTAAAGCGCATGCTCCAGACTGCC
Ras-GRF1 mutant reverse primer: CGTGACTCCTCAGGATGAGGTGCTGTGG
Ras-GRF1 wild-type forward primer: AACAGATCACCCTGTATTTGAGCGTATCGTCGG
Ras-GRF1 wild-type reverse primer: CAGTAAGTGATAGCAGACAGTGGGTCAACAGG

DNA was then loaded onto 1% agarose gel and separated by electrophoresis at constant voltage in order to visualize the transgene.

**Preparation of acute striatal slices.** Mice were anesthetized, killed by decapitation and the brain was rapidly removed in ice-cold carboxygenated sucrose-based dissecting solution. 200 μm-thick slices were cut using a vibratome (VT1000S, LeicaMicrosystems) keeping the brain submerged in ice-cold carboxigenated sucrose-based dissecting solution. The slices were then transferred to the brain slice chamber-BSC1 (Scientific System design Inc., Mississauga, ON, Canada), placing them upon a lens paper (up to 4 slices in every chamber). The slices were then incubated for 1h at 32°C and constantly perfused with carboxygenated artificial cerebrospinal fluid. After the recovery period, the slices were stimulated with the appropriate agonists for 10 min. In the experiments with the inhibitors, the slices were pre-treated with U0126 for 1 hour during the recovery period, whereas SCH23390, CNQX and AP5 were applied 30 min before the stimulation.

**Western blot analysis.** Following stimulation, the slices were rapidly frozen in dry ice, homogenized in ice-cold SDS lysis buffer and boiled for 5 min. Following dosage with Biorad DC protein Assay (Biorad), the desired amount of protein was added to an equal volume of sample buffer 1X and boiled for 5 min. The samples were then separated by SDS-PAGE onto 10% polyacrylamide gels (acrylamide/bysacrylamide 40:1, Merck) at constant amperage (35 mA/gel) in a Biorad electrophoresis apparatus filled with running buffer 1X. The proteins were transferred to nitrocellulose membranes (Schechter and Schuell) for 2 h at constant amperage (250 mA) using an immersion apparatus (Biorad) filled with transfer buffer 1X. After Ponceau staining (Sigma Aldrich), the membranes were washed in TBS 1X and blocked in TBS-Tween 0.1% with 5% BSA for 1 h at room temperature. The membranes were then incubated with anti-phospho-p44/p42 MAP kinase (1:1000, Cell signaling) overnight at 4°C and anti-GAPDH (1:1000, Sigma Aldrich) for 2 hours at room temperature. Following three washes in TBS-Tween 0.1%, the membranes were incubated with the secondary antibodies: anti-mouse or anti-rabbit IgG, horseradish peroxidase linked whole antibody (from sheep, GE Healthcare).

Following three washes in TBS-Tween 0.1%, the membranes were developed using ECL PLUS kit (GE Healthcare) according to the manufacturer's instructions. Different exposures were taken using Amersham Hyperfilm ECL high performance chemiluminescence film (GE Healthcare) with automatic developer apparatus (Kodak).

The immunoblots were then analyzed using ImageJ software to measure the optical density of the bands, using anti-GAPDH as loading control.

**Immunofluorescence.** Following stimulation, the slices were fixed in 4% paraformaldehylde for 15 min at room temperature and rinsed three times for 10 min in 0.1M sodium phosphate buffer pH 7.4. The slices were then cryoprotected overnight in 30 % sucrose in 0.1M sodium phosphate buffer pH 7.4 overnight at 4°C. 18 μm cryosections were cut and washed three times for 10 min with Dulbecco's phosphate buffered saline (D-PBS, Invitrogen). After blocking in D-PBS containing 5% normal goat serum and 0.1% Triton X-100 for 1 hour at room temperature, the sections were incubated overnight at 4°C with the primary antibodies: anti-phospho-S6 ribosomal protein (Ser 235/236) 1:200 (Cell signaling Technology), anti-phospho (Ser10)-acetylated (Lys14) histone H3 1:1000 (Upstate), anti-NeuN 1:1000 (CHEMICON).

The sections were then washed three times for 10 min with D-PBS and incubated for 1h at room temperature with the secondary antibodies: Alexa Fluor 546 goat anti-mouse (1:200) or goat anti-mouse Pacific blue (1:200) or Alexa Fluor 488 goat anti-mouse (1:500, Invitrogen) and Alexa Fluor 488 goat anti-rabbit (1:500, Invitrogen) or Cy3-conjugated goat anti-rabbit (1:200, Jackson Immunoresearch).

Following the incubation with the secondary antibodies the sections were washed three times for 10 min with D-PBS and the coverslips were mounted using the fluorescent mounting medium (Dako).

In the experiments conducted on M4-EGFP mice, following the incubation with the secondary antibodies the sections were washed three times for 10 min with D-PBS and incubated with anti-GFP rabbit polyclonal antibody Alexa Fluor 488-conjugated (Invitrogen) for 5 h at 4°C. The sections were then washed three times for 10 min with D-PBS and the coverslips were mounted using the fluorescent mounting medium (Dako).

Images were obtained using a laser scanning confocal microscopy (Leica SP2), equipped with the corresponding lasers and the appropriate filters sets to avoid the cross-talk between the fluorophores. Neuronal quantification was performed with ImageJ software on images taken at 40X magnification by counting phospho-S6 or phospho-H3 immunoreactive neurons among NeuN positive neurons in each slice, in 2 cryosections per slice. In the experiments with M4-EGFP mice, also the number of phospho-S6 or phospho-H3 positive neurons among EGFP-positive cells and among EGFP-negative cells was counted. Statistical analysis were performed using GraphPad Prism 5.

**Immunohistochemistry.** Following transcardiac perfusion with with 4% paraformaldehyde (PFA)

in PBS, postfixation, cryopreservation, and storage in anti-freeze solution at -20° C, 35 µm-thick free-floating sections were rinsed three times with KPBS, incubated for 15 min in quenching solution and rinsed again three times in KPBS-Triton 0.1% (KPBS-T). The sections were then incubated overnight at 4 °C with the primary antibody: anti-TH (1:1000, Pel-Freez Biologicals) or anti-phospho-p44/42 MAP kinase (1:200, Cell signalling) in 5% normal goat serum in KPBS-T. Sections were then rinsed three times in KPBS-T and incubated with the biotinylated anti-rabbit secondary antibody 1:200 (Vector Labs) for 2 h. Tissue sections were processed further using Avidine Biotin Elite (ABC kit, Vector Labs) following the manufacturer's instructions. Following 1 h incubation in ABC solution, the sections were rinsed three times in KPBS-T and incubated with 1 ml of 0.05% DAB in KPBS. After 2-3 min, 13 µl of 3% $H_2O_2$ were added to the sections for 30-60 sec. Following three washes, the sections were mounted onto Superfrost slides, let dry overnight and dehydrated throughout successive immersions, each one lasting two min and repeated 2 times, in 50%, 75%, 95% and 100% ethanol solutions. The sections were coverslipped with d-N-butyl-phthalate in xylene (DPX) and images were acquired using a Quantification of p-ERK positive neurons was performed from dorsolateral striatum, in 4 sections per mouse, bilaterally, using the Image J software. All visible positive nuclei or cell bodies within a field were counted and expressed as number of cells per square millimeter.

**Drugs.** Glutamate, BDNF SCH-23390 were purchased from Sigma Aldrich, SKF-38393, UO126, CNQX and AP5 were purchased from Tocris; N/OFQ was synthetized in the Department of experimental and Clinical Medicine, Section of Pharmacology, University of Ferrara, Italy.
Stocks of glutamate, BDNF, SCH-23390, SKF-38393 and AP5 were easily dissolved in $H_20$, N/OFQ was dissolved in saline and stocks of UO126 and CNQX were dissolved in DMSO

## *Buffers and solutions*

Tail buffer
50 mM Tris HCl pH 8
100 mM EDTA pH 8
100 mM NaCl
0.5% (w/v) SDS
Up to volume with sterile water and filter.

Phenol Chloroform solution

25:24:1 (v : v : v) phenol: chloroform: 3-methyl-1-butanol (Sigma Aldrich)

DNA loading buffer 6X

50 mM bromophenol blue

1mM EDTA

50% (w/v) glycerol

TBE 10X pH 8

980 mM Trizma base

980 mM Boric Acid

10 mM EDTA

Dissolve in deionized water and adjust pH

Agarose gel

1% agarose dissolved in TBE 1X with 1mg/ml ethidium bromide

Sucrose-based dissecting solution 10X

87 mM NaCl

2.5 mM KCl

7 mM $MgCl_2\,6H_2O$

1 mM $NaH_2PO_4\,H_2O$

75 mM sucrose

25mM $NaHCO_3$

10mM D-glucose

0.5 mM $CaCl_2$ (1M stock)

2 mM kynurenic acid

Artificial cerebrospinal fluid 10X

124mM NaCl

5mM KCl

1.3 mM $MgSO_4$ $7H_2O$

1.2 mM $NaH_2PO_4$ $H_2O$

25mM $NaHCO_3$

10mM D-glucose

2.4mM $CaCl_2$ (1M stock)

Lysis buffer pH 6.8

125 mM Trizma base

2.5% SDS

Sample buffer 5X

10% (w/v) SDS

250 mM Tris HCl pH 6.8

50% glycerol

0.02% bromophenol blue

111 mM dithiothreitol (DTT)

up to volume with glycerol

Stacking gel 4.5%

4.5% acrylamide/bis-acrylamide (40:1, Merck)

125 mM Tris HCl pH 6.8

0.1% SDS

0.05% ammonium persulfate

0.005% N,N,N',N'-tetramethylethylenediamine (TEMED)

Running gel 10%

10% acrylamide/bis-acrylamide (40:1)

375 mM Tris HCl pH 8.8

0.1% SDS

0.05% ammonium persulfate

0.005% N,N,N',N'-tetramethylethylenediamine (TEMED)

Running buffer 10X

250 mM Trizma base

1.92 M glycine

Transfer buffer 1X

25 mM Trizma base

190 mM glycine

20% methanol

TBS 10X pH 7.4

200 mM Trizma base

1.5 M NaCl

0.2 M phosphate buffer pH 7.4

4.32 g $Na_2HPO_4$ $2H_2O$

0.78 g $NaH_2PO_4$ $H_2O$

An equal volume of deionized water was added to obtain 0.1M phosphate buffer.

Anti-freeze solution

320 ml PBS 1X pH 7.4

240 ml ethylene glycol

240 ml glycerol

KPBS 10X

1.4 M NaCl

26 mM KCl

64 mM $Na_2HPO_4$

15 mM $KH_2PO_4$

Quenching solution

3% $H_2O_2$

10% methanol

in KPBS 1X

# Results

## Glutamate and SKF38393 induce S6 ribosomal protein and histone H3 phosphorylation in an ex-vivo model of striatal slices

In order to investigate the regulation of Ras-ERK signalling in the striatum, we set up an ex-vivo system in which striatal slices can be acutely prepared from adult mice, incubated in a perfusing chamber and then stimulated with appropriate agonists and antagonists.

In order to validate this experimental model, we first stimulated slices with glutamate, with the D1R agonist SKF38393 or with the brain derived neurotrophic factor (BDNF), three stimuli able to activate the ERK cascade (Sgambato et al., 1998; Vanhoutte et al., 1999; Kaplan and Miller, 2000; Pascoli et al., 2010).

In the initial phase, we decided to test the ability of glutamate to phosphorylate ERK1/2 using Western blot analysis, that gives an initial measure of the global striatal activation of this signalling pathway. As shown in figure 9, 200 μm-thick slices stimulated with 100 μM glutamate for 10 min show a significant increase of phospho-ERK1/2.

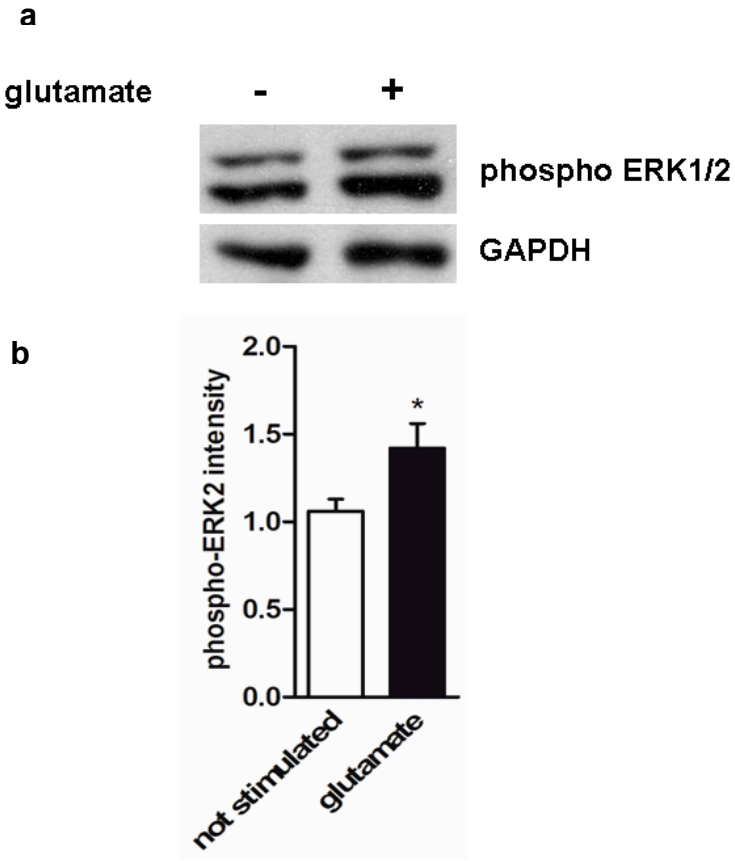


**Fig.9. Adult striatal slices show an increase in ERK2 phosphorylation following the stimulation with glutamate 100 μM.** a) Representative immunoblots of striatal slices obtained from adult wild-type mice and stimulated or not with glutamate 100 μM for 10 min. Following stimulation, the slices were lysed and equal amounts of proteins (20 μg) for each sample were separated onto SDS-PAGE electrophoresis. After Western blot, the nitrocellulose membranes were probed against phospho-ERK1/2 and GAPDH as loading control. b) The histogram represents the mean±SEM of phospho-ERK2 induction expressed as the ratio normalized to not stimulated slices. Unpaired Student's t test has revealed a significant increase in ERK2 phosphorylation upon glutamate stimulation in comparison to the not-stimulated condition (* $p<0.05$, n=39 for stimulated and not stimulated groups).

Next, in order to develop a system to study ERK activation at a single cell definition, and to have the possibility to discriminate between different cell populations in the striatum, for instance using the available BAC transgenic mice expressing EGFP, we decided to test several antibodies against the phosphorylated form of ERK1/2. Unfortunately, none of the antibodies tested showed a significant signal in immunofluorescence (data not shown). Therefore, we decided to test two specific phospho-antibodies against two proteins that have been previously shown to be downstream of ERK1/2: S6 ribosomal protein (cytoplasmic target) and histone H3 (nuclear target).
Brains were rapidly dissected from 2 months-old wild-type mice and 200 μM striatal slices were cut using a vibratome. Slices were then transferred in the perfusing chamber for 1 hour at 32°C. After the recovery period, slices were stimulated for 10 min with glutamate (100 μM), SKF38393 (100 μM) or BDNF (100 μM), fixed and cryoprotected overnight at 4°C. 18 μm cryosections were then co-labeled with anti-phospho (Ser235/236) S6 ribosomal protein (in green, fig. 10 and fig. 12 panel a) or anti-phospho (Ser10)-acetyl (Lys14) histone H3 (in green, fig. 11 panel a and fig.12 panel c) and with the antibody against the specific neuronal marker NeuN (in red, fig. 10, 11, panel a and fig. 12, panel a,c). The percentage of activation was calculated by counting phospho-S6 or phospho-H3 positive neurons among NeuN positive neurons. As shown in the graphs (fig. 10, 11, panel b and c and fig. 12, panel b and d), the application of either glutamate, SKF38393 or BDNF elicits a strong activation of both S6 ribosomal protein and histone H3.

**The MEK inhibitor U0126 completely blocks the phosphorylation of S6 ribosomal protein and histone H3**

We next assessed whether the phosphorylation of S6 ribosomal protein and histone H3 on those specific sites was indeed ERK-dependent.
In order to do this, striatal slices were pre-treated with 5 μM U0126, a specific MEK inhibitor, for 1 hour before the stimulation with 100 μM glutamate. As shown in the figure 13 and 14, the phosphorylation of both S6 ribosomal protein and histone H3 was completely abolished by the treatment with 5 μM U0126.
This result demonstrates that the activation of these two proteins is specifically regulated by the ERK cascade.

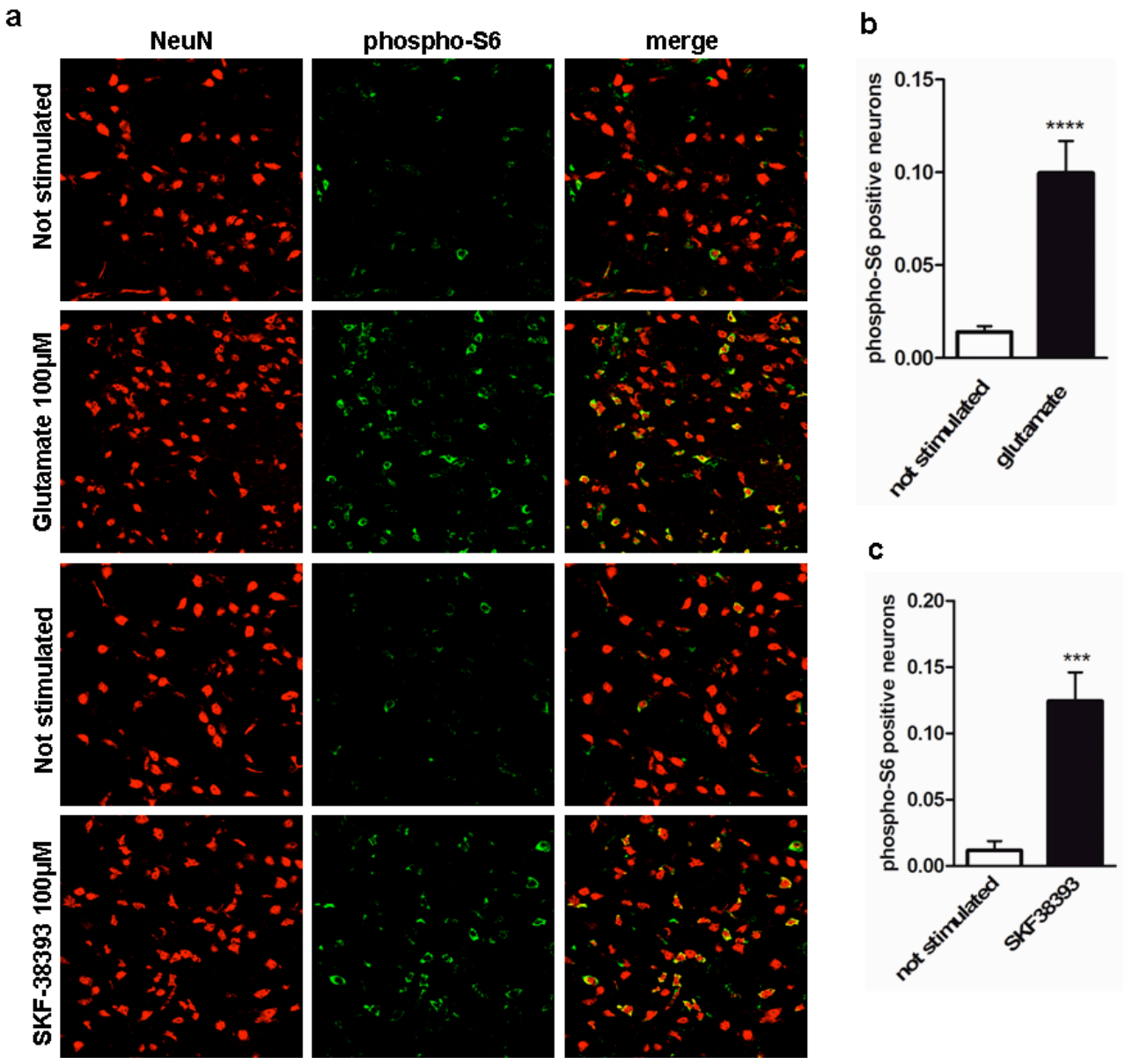


**Fig.10. Glutamate and SKF-38393 activate S6 ribosomal protein in a model of adult striatal slices.** a) Double immunolabeling of phospho S6 ribosomal protein (Ser235/236) (green) and NeuN (red) in striatal slices obtained from adult wild-type mice stimulated or not with glutamate 100 µM or SKF-38393 100 µM for 10 min. b) The data from the quantification are represented in the graphs as mean±SEM (n=13 and n=14 for the groups respectively stimulated or not with glutamate, n=7 for the groups stimulated or not with SKF-38393). Phospho-S6 levels were significantly increased in striatal neurons stimulated with glutamate (stimulated *vs* not stimulated, **** $p<0.0001$, unpaired Student's t-test) and SKF38393 (stimulated *vs* not stimulated *** $p<0.001$, unpaired Student's t-test).

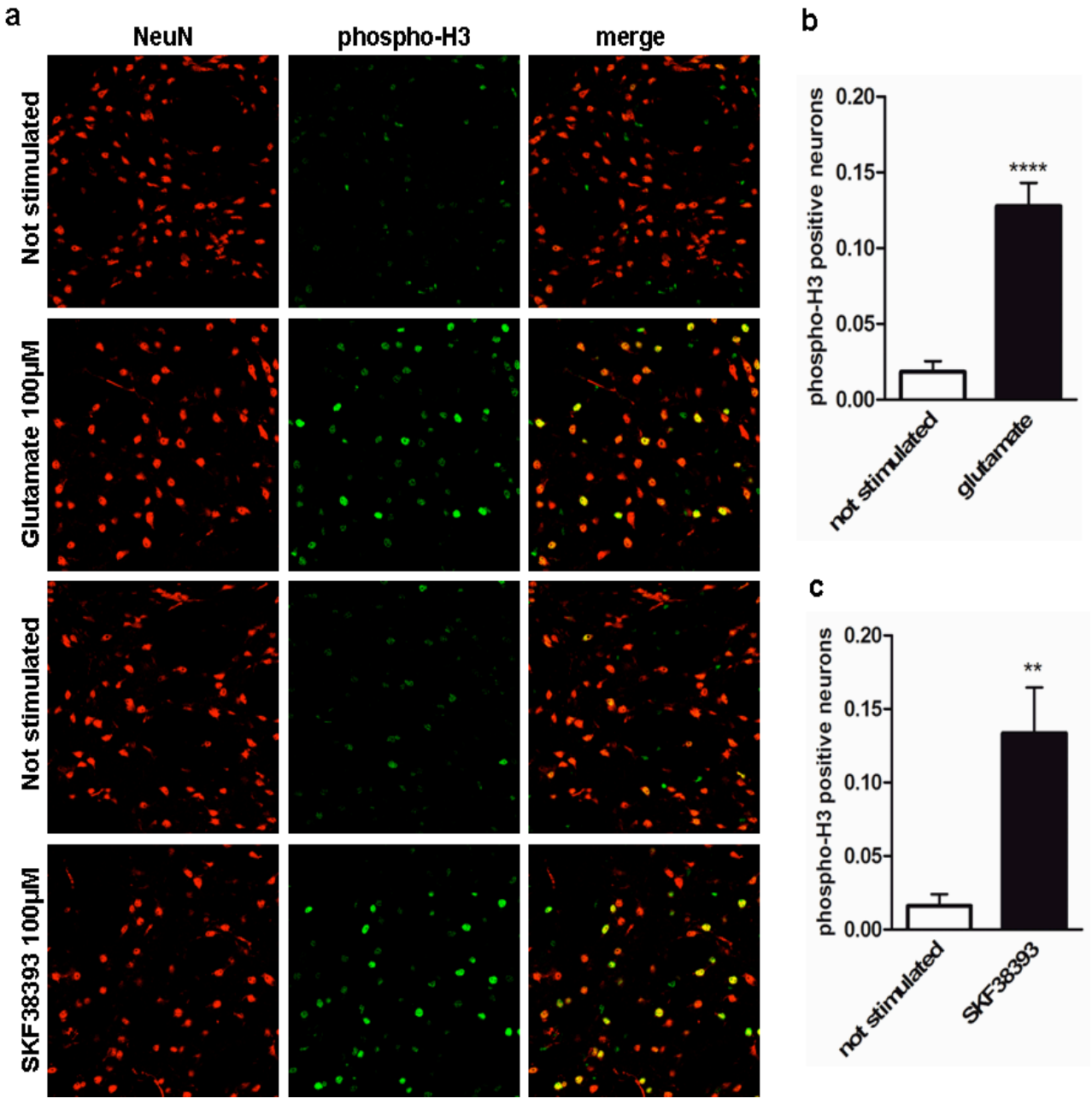


**Fig.11. Glutamate and SKF-38393 activate histone H3 in a model of adult striatal slices.** a) Double immunolabeling of phospho (Ser10)-acetyl (Lys14) histone H3 (in green) and NeuN (in red) in striatal slices obtained from adult wild-type mice stimulated or not with glutamate 100 µM or SKF-38393 100 µM for 10 min. b) The data from the quantification are represented in the graphs as mean±SEM (n=7 and n=9 for the groups respectively stimulated or not with glutamate, n=11 for the groups stimulated or not with SKF-38393). The unpaired Student's t-test indicated a significant difference between the groups (stimulated *vs* not stimulated, **** $p<0.0001$, ** $p<0.01$).

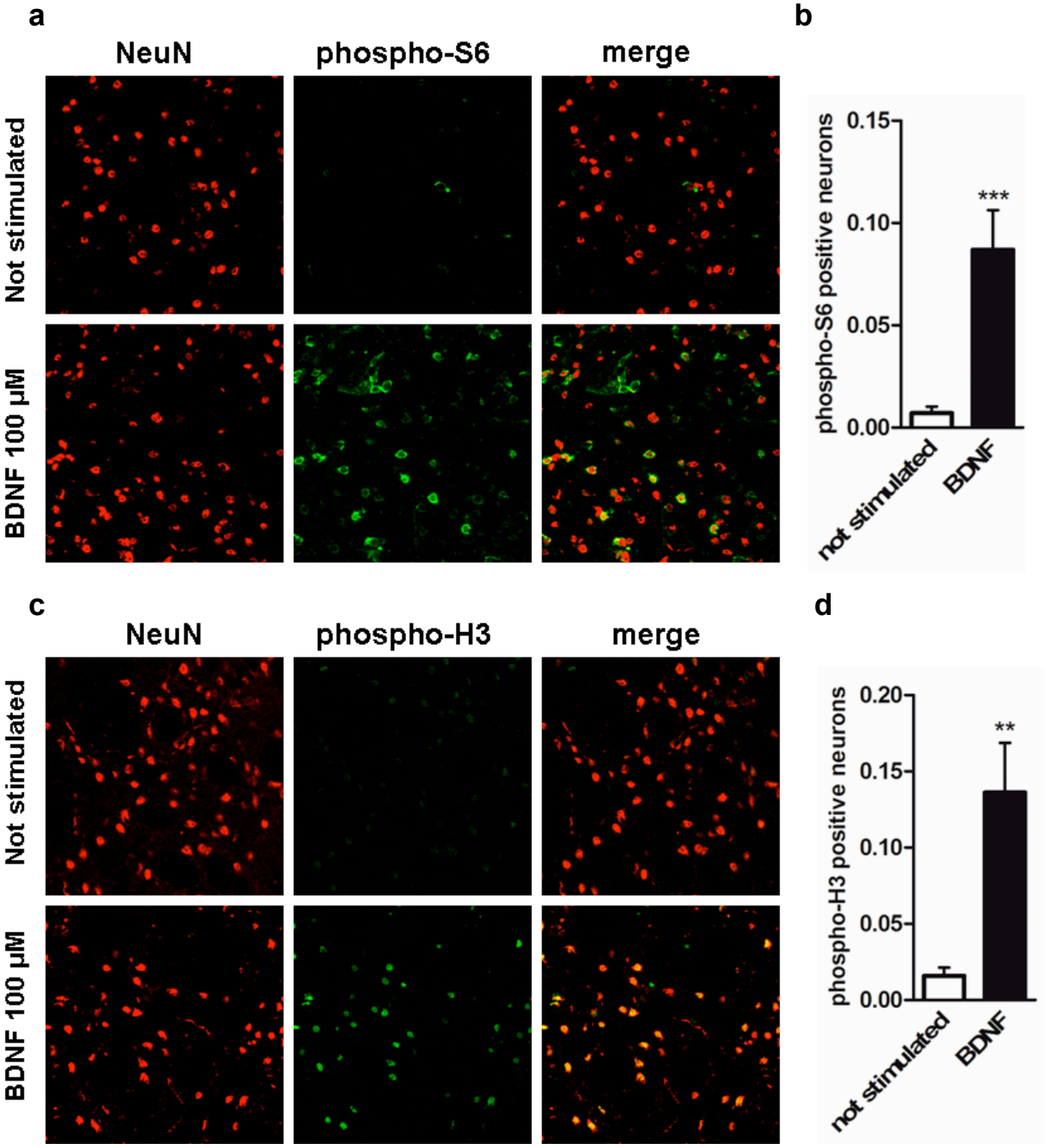


**Fig.12. BDNF induces S6 and histone H3 phosphorylation in adult striatal slices.** Striatal slices obtained from wild type mice were incubated for 1h at 32°C and then stimulated with BDNF 100 µM for 10 min. The slices were then processed for immunofluorescence. a) Double immunolabeling of phospho-S6 (green) and NeuN (red). The data from the quantification are represented in the graph (panel b) as mean±SEM (n=10). c) Double immunolabeling of phospho-H3 (green) and NeuN (red). The data from the quantification are represented in the graph (panel d) as mean±SEM (n=8 for not stimulated group; n=7 for BDNF stimulated group. Statistical analysis were performed using unpaired Student's t test (stimulated *vs* not stimulated, ** $p<0.01$, *** $p<0.001$)

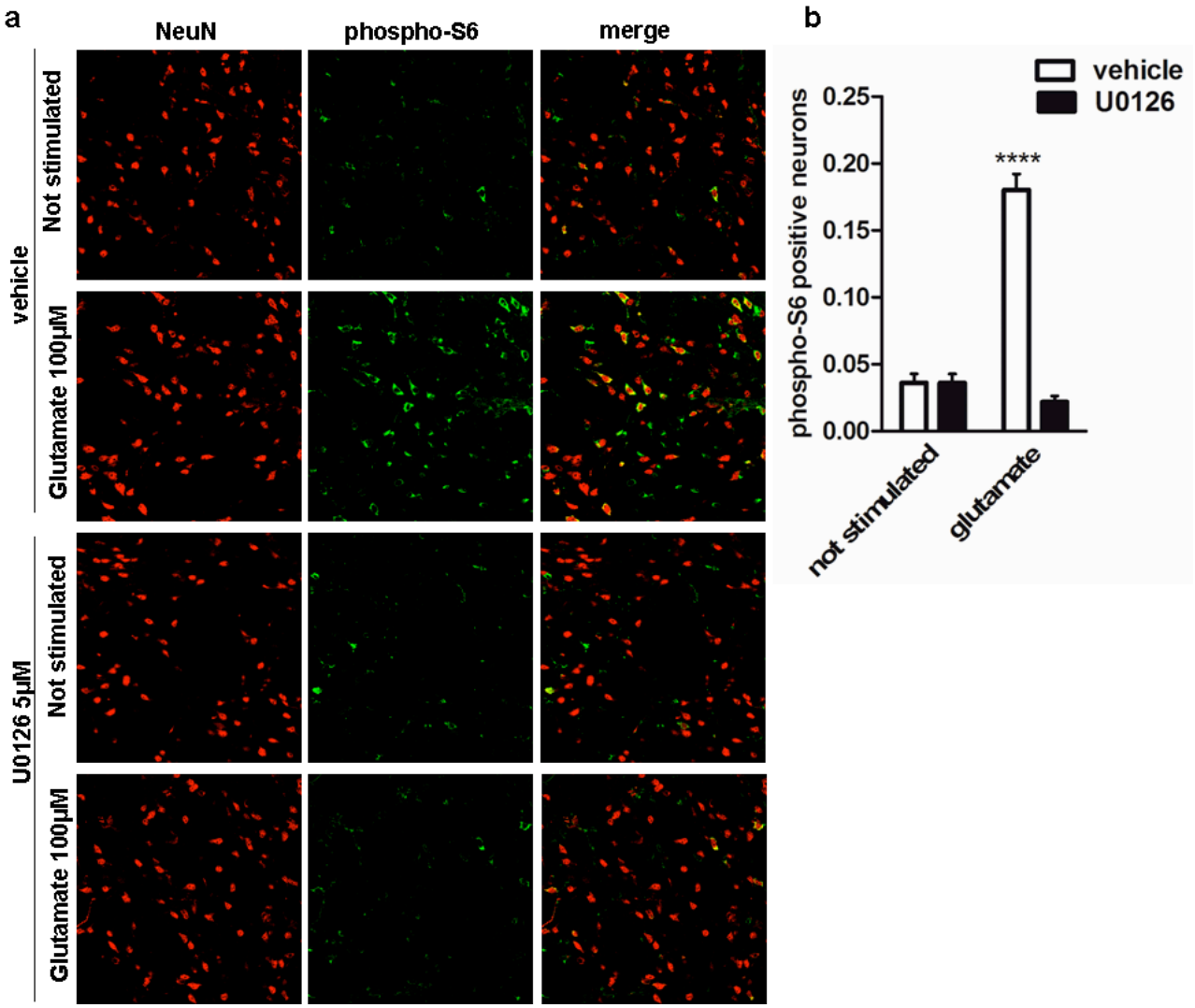


**Fig. 13. S6 ribosomal protein phosphorylation is prevented by MEK inhibitor U0126 in striatal slices.** a) Striatal slices were pre-treated with 5µM U0126 or vehicle for 1 h before the stimulation with glutamate 100 µM for 10 min. The slices were then immunolabeled with anti-phospho S6 ribosomal protein (Ser235/236) (green) and anti-NeuN (red) antibodies. b) The data from the quantification are represented in the graph as mean±SEM (n=14 for the groups treated with the vehicle, n=10 and n=8 for the groups treated with U0126 and respectively stimulated or not with glutamate ). Statistical analysis were performed using two-way ANOVA followed by Bonferroni's post-hoc test (glutamate *vs* not stimulated , **** $p<0.0001$).

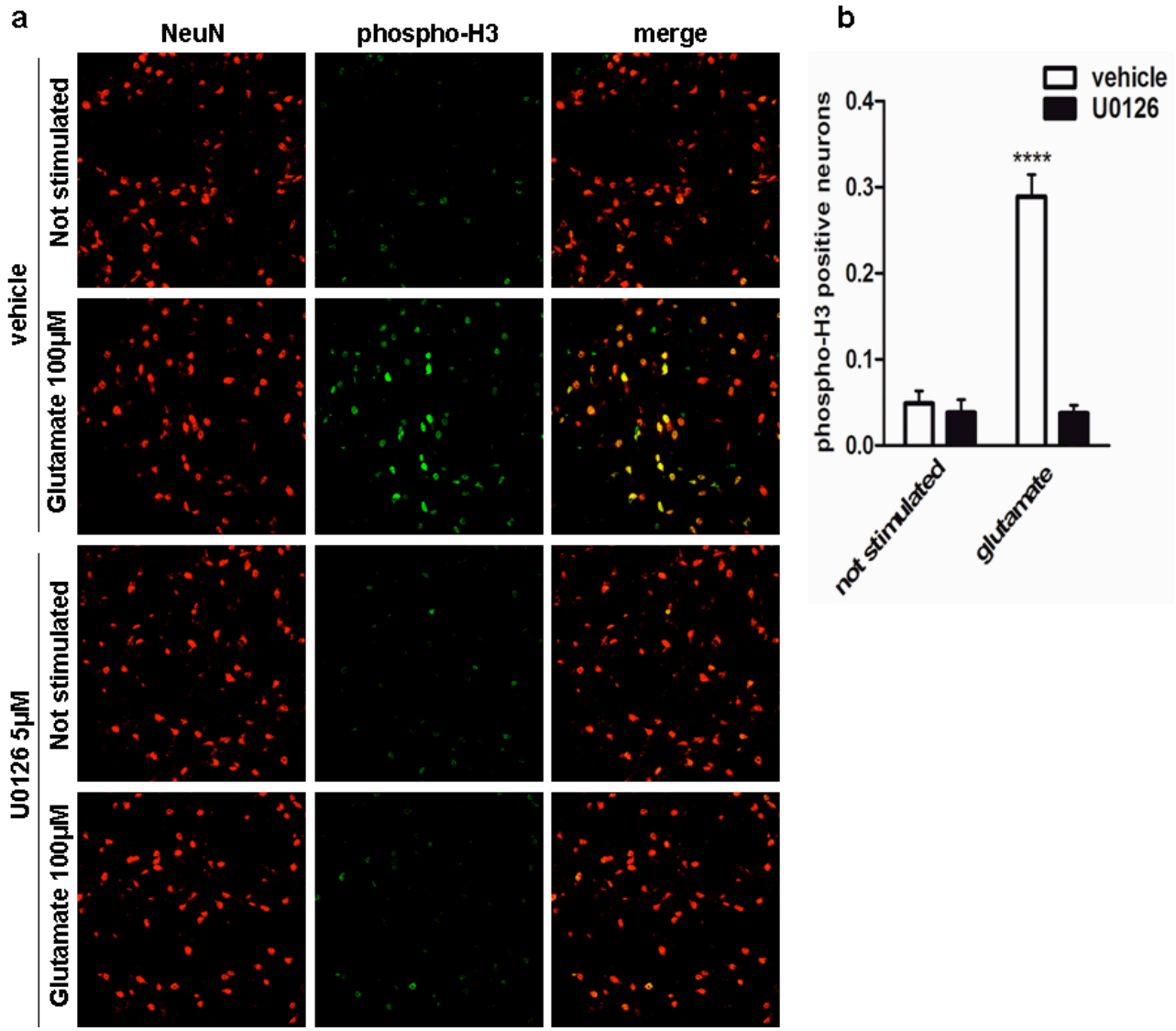


**Fig.14. Histone H3 phosphorylation is prevented by MEK inhibitor U0126 in striatal slices.** a) Adult striatal slices were pre-treated with U0126 5µM or vehicle for 1 hour before the stimulation with glutamate 100 µM for 10 min. The slices were processed for immunofluorescence against phospho- histone H3 (green) and NeuN (red). b) The data from the quantification are represented in the graph as mean±SEM (n=4 and n=3 for the groups treated with vehicle and respectively stimulated or not with glutamate, n=6 and n=5 for the groups treated with U0126 and respectively stimulated or not with glutamate). Statistical analysis were performed using two-way ANOVA and post-hoc comparisons between groups using Bonferroni's post-hoc test (glutamate *vs* not stimulated , **** $p<0.0001$).

**Co-stimulation with glutamate and SKF38393 causes an additive effect on the activation of S6 ribosomal protein in the striatonigral MSNs, but not in the striatopallidal MSNs**

An important open question is the integration between glutamatergic and dopaminergic signals within the striatum. Previous experiments conducted on organotypic slices analysed by western blot demonstrated that the co-stimulation with glutamate and SKF38393 caused a clear additive effect on the phosphorylation of ERK2 in comparison with that observed upon single stimulations (Fasano et al., 2009).

To further elucidate this point, we took advantage of our ex-vivo system applied on M4-EGFP transgenic mice that express EGFP specifically in the striatonigral pathway, to compare the changes in S6 activation between the two major neuronal population in the striatum (Fasano et al, 2010).

Firstly, we wanted to confirm that in this EGFP expressing transgenic the percentage of neurons expressing or not EGFP were similar, as expected from the known ratio of MSN belonging to the direct and indirect pathway. Our results, obtained from 21 M4-EGFP mice and co-labeled against NeuN and EGFP (fig. 15) demonstrate that the percentage of striatonigral MSNs (47%) is similar to the percentage of striatopallidal MSNs (52%), thus validating M4-EGFP mice as a model to compare the striatal signalling in the two pathways.

**a**

| mice | % of striatonigral MSNs | % of striatopallidal MSNs |
|---|---|---|
| 1 | 47,1 | 52,9 |
| 2 | 46,9 | 53,1 |
| 3 | 50,7 | 49,3 |
| 4 | 49,6 | 50,4 |
| 5 | 45,7 | 54,3 |
| 6 | 45,6 | 54,4 |
| 7 | 47,3 | 52,7 |
| 8 | 44,1 | 55,9 |
| 9 | 45,6 | 54,4 |
| 10 | 49 | 51 |
| 11 | 43,6 | 56,4 |
| 12 | 46,9 | 53,1 |
| 13 | 44,6 | 55,4 |
| 14 | 48,7 | 51,3 |
| 15 | 47 | 53 |
| 16 | 50 | 50 |
| 17 | 49,7 | 50,3 |
| 18 | 50,4 | 49,6 |
| 19 | 49,4 | 50,6 |
| 20 | 49,2 | 50,8 |
| 21 | 48,1 | 51,9 |

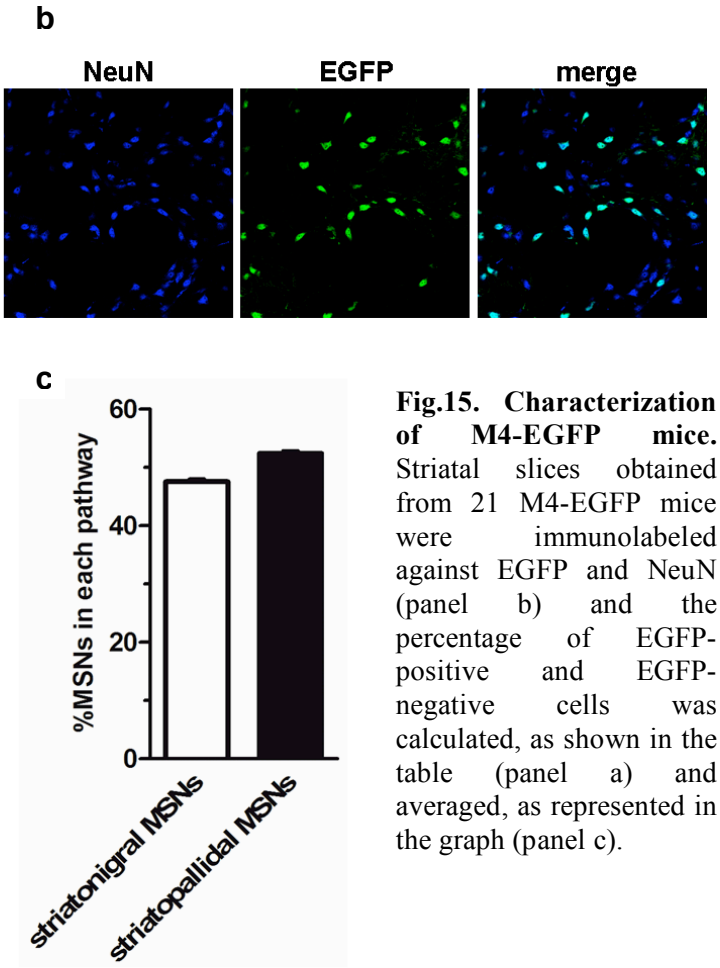


**Fig.15. Characterization of M4-EGFP mice.** Striatal slices obtained from 21 M4-EGFP mice were immunolabeled against EGFP and NeuN (panel b) and the percentage of EGFP-positive and EGFP-negative cells was calculated, as shown in the table (panel a) and averaged, as represented in the graph (panel c).

However, before using the M4-EGFP animals, we also determined the lowest concentration of both glutamate and SKF38393 able to elicit S6 and histone H3 phosphorylation after a 10 min stimulation. The treatment with different doses of glutamate or SKF-38393 indicates that 20 µM of glutamate and SKF-38393 is sufficient to induce a maximal S6 (fig. 16,18) and H3 phosphorylation (fig.17,19), whereas slices challenged with lower doses of glutamate and SKF-38393 (5 µM, 2 µM, and 1 µM) failed to show a significant activation of both S6 and histone H3.

Therefore, we investigated the phosphorylation of both S6 and histone H3 in EGFP-positive cells and EGFP-negative cells in striatal slices obtained from M4-EGFP mice and we stimulated them with either glutamate 20 µM, SKF38393 20 µM or co-stimulated them for 10 min. We found that glutamate activates S6 ribosomal protein ( in red, fig. 20, panel a ) preferentially in the striatopallidal neurons ( in blue and EGFP-negative cells). Unexpectedly, we also found that SKF-38393 activates S6 ribosomal protein not only in the direct pathway but also in the indirect

pathway. In addition, S6 phosphorylation is enhanced by the combined treatment with glutamate and SKF38393; interestingly, this additive effect seems to be restricted to the striatonigral MSNs (in green), whereas in the striatopallidal MSNs the phosphorylation of S6 ribosomal protein upon co-stimulation is not significantly different to that observed upon single stimulations.

To further elucidate the SKF38393-induced activation of S6 in the indirect pathway, we pre-treated the slices with SCH-23390 50 μM, the selective antagonist of D1Rs, for 30 min before the stimulation with SKF-38393 20 μM. Interestingly, upon D1Rs blockade, S6 phosphorylation is completely prevented both in the striatonigral and striatopallidal MSNs, as shown in fig. 21.

This result suggests that the SKF-38393-dependent S6 activation in the indirect pathway might be mediated by D1Rs, either directly or indirectly.

Our data also clearly indicate that the basal phosphorylation of S6, completely abolished by MEK inhibition with U0126 in both neuronal populations (fig. 22), is about two times higher in the indirect pathway in comparison with the direct pathway. This asymmetry is probably attributable to the increased excitability of the striatopallidal MSNs with respect to the striatonigral MSNs (Cepeda et al., 2008; Day et al., 2008).

We next examined the activation of histone H3 following stimulation with glutamate, SKF38393 or co-stimulation. Differently from what observed for S6 activation, the co-application of glutamate and SKF38393 does not further increase the level of histone H3 phosphorylation in each pathway in comparison with the single stimulations, suggesting that at the doses used of glutamate and SKF38393 H3 is maximally activated (fig. 23).

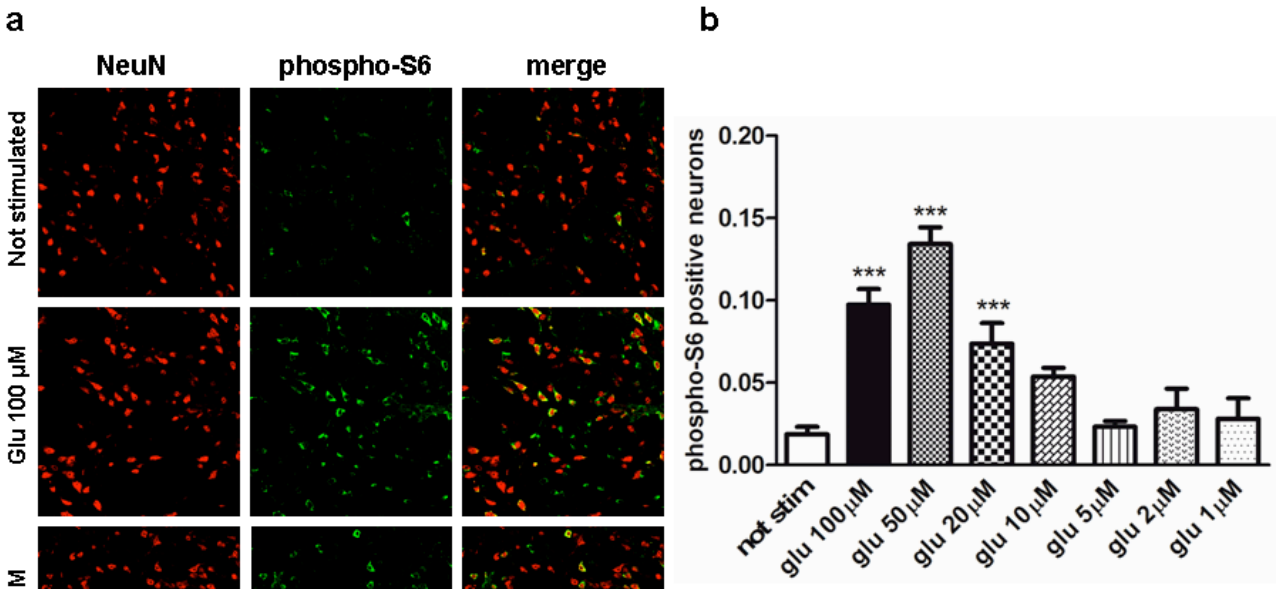


**Fig.16. Glutamate induces S6 phosphorylation in a dose dependent manner in adult striatal slices.** Striatal slices obtained from wild type mice were incubated for 1h at 32°C and then stimulated with different doses of glutamate (100, 50, 20, 10, 5, 2, 1 µM) for 10 min. The slices were then processed for immunofluorescence. a) Double immunolabeling of phospho-S6 (green) and NeuN (red). b) The data from the quantification are represented in the graph as mean±SEM (n=23 for not stimulated, n=13 for glu 100 µM, n=9 for glu 50 µM, n=7 for glu 20 µM, n=8 for glu 10 µM, 2µM and 1µM and n=6 for glu 5µM). Statistical analysis were performed using one-way ANOVA and post-hoc comparisons between groups using Bonferroni test (stimulated *vs* not stimulated, *** $p<0.001$)

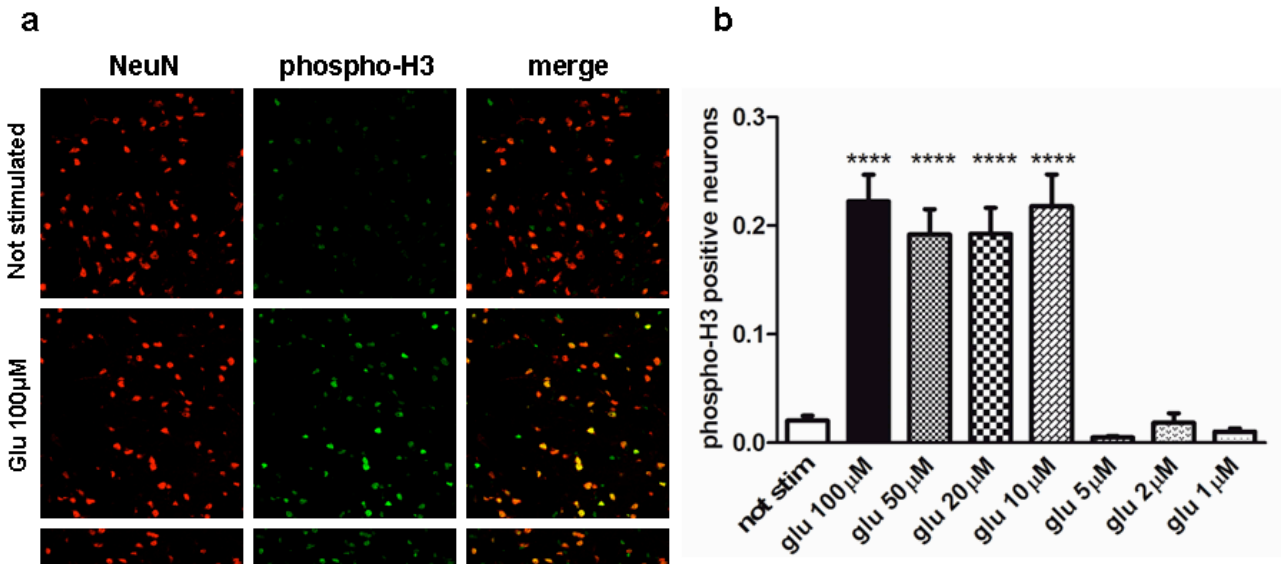


**Fig.17. Glutamate induces histone H3 phosphorylation in a dose dependent manner in adult striatal slices.** Striatal slices obtained from wild type mice were incubated for 1h at 32°C and then stimulated with different doses of glutamate (100, 50, 20, 10, 5, 2, 1 µM) for 10 min. The slices were then processed for immunofluorescence. a) Double immunolabeling of phospho-H3 (green) and NeuN (red). b) The data from the quantification are represented in the graph as mean±SEM (n=26 for not stimulated, n=13 for glu 100 µM, n=8 for glu 50 µM, n=7 for glu 20 µM, 2 µM and 1µM, n=9 for glu 10 µM and n=12 for glu 5 µM). Statistical analysis were performed using one-way ANOVA and post-hoc comparisons between groups using Bonferroni test (stimulated *vs* not stimulated, **** $p<0.0001$)

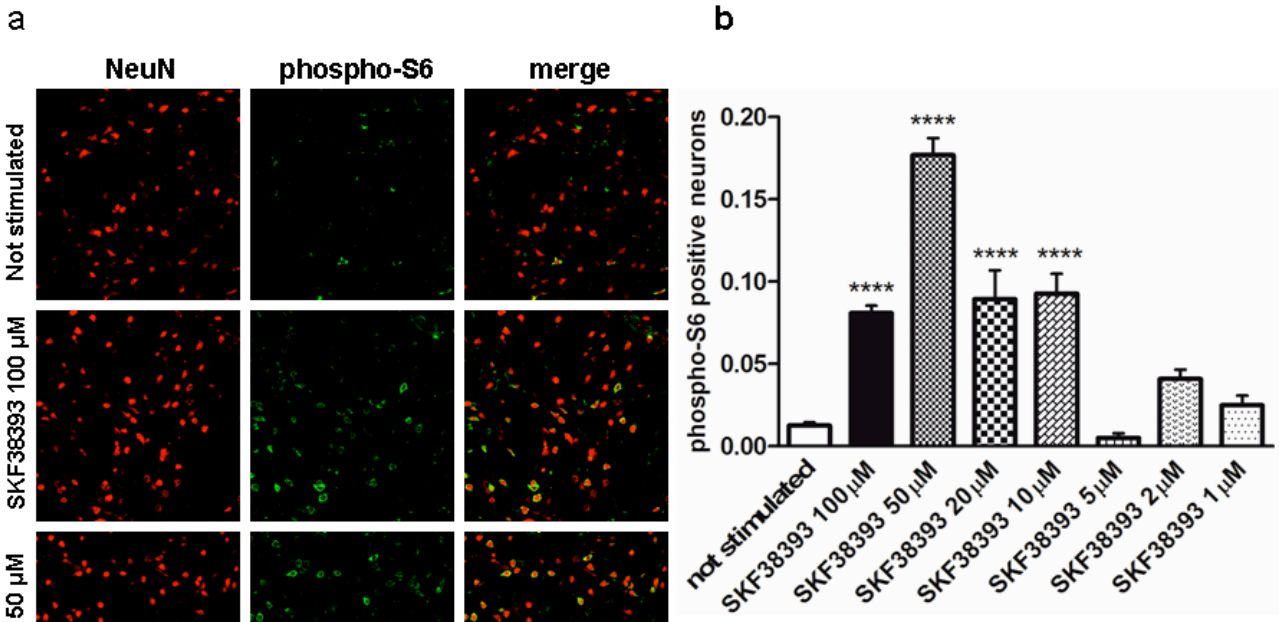


**Fig.18. SKF38383 induces S6 ribosomal protein phosphorylation in a dose dependent manner in adult striatal slices.** Striatal slices obtained from wild type mice were incubated for 1h at 32°C and then stimulated with different doses of SKF38393 (100, 50, 20, 10, 5, 2, 1 µM) for 10 min. The slices were then processed for immunofluorescence. a) Double immunolabeling of phospho-S6 (green) and NeuN (red). b) The data from the quantification are represented in the graph as mean±SEM (n=27 for not stimulated, n=9 for SKF 100 µM and 20 µM, n=15 for SKF 50 µM, n=7 for SKF 10 µM and
1 µM, n=6 for SKF 5 µM and n=8 for SKF 2 µM). Statistical analysis were performed using one-way ANOVA and post-hoc comparisons between groups using Bonferroni test (stimulated *vs* not stimulated,**** $p<0.0001$)

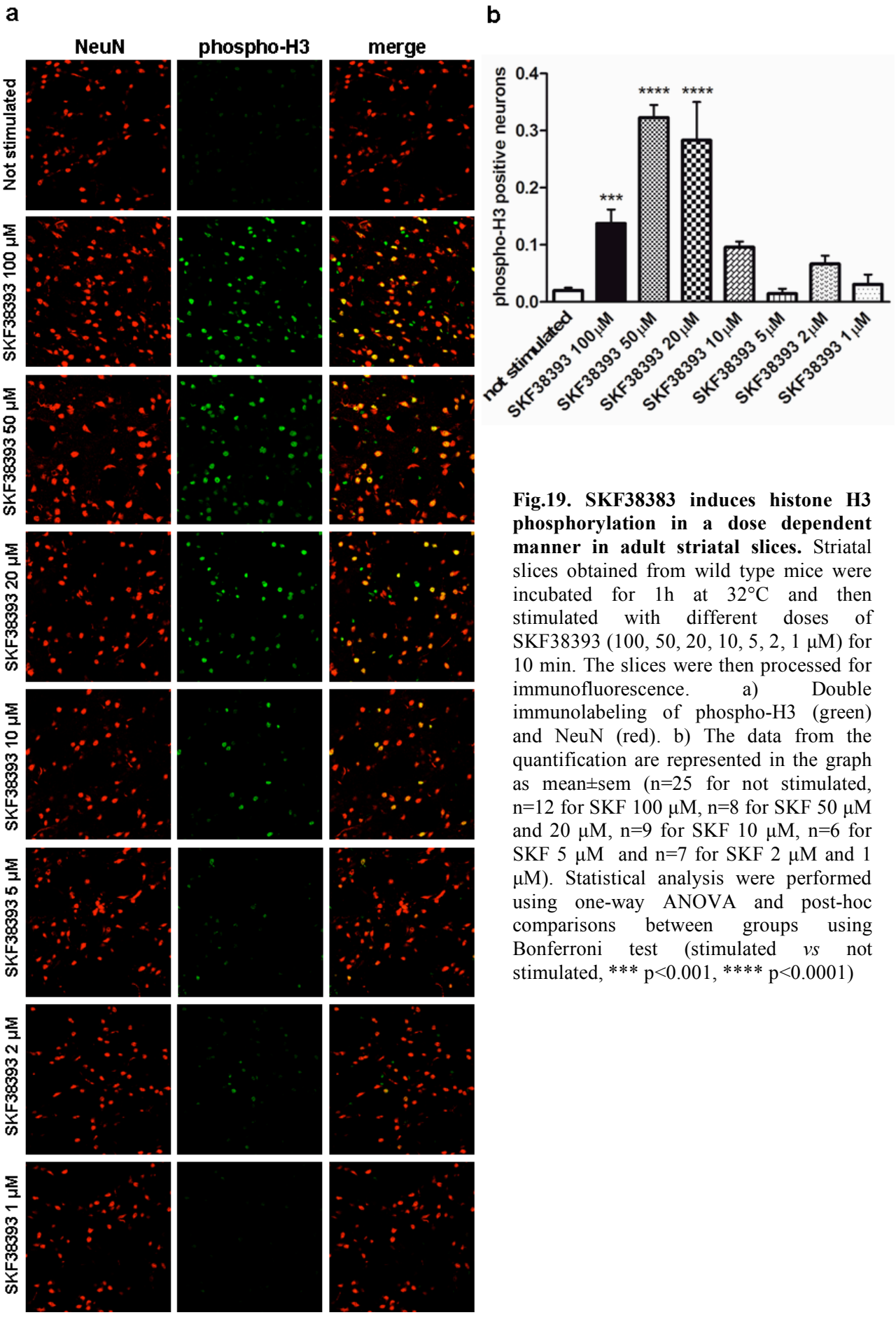


**Fig.19. SKF38383 induces histone H3 phosphorylation in a dose dependent manner in adult striatal slices.** Striatal slices obtained from wild type mice were incubated for 1h at 32°C and then stimulated with different doses of SKF38393 (100, 50, 20, 10, 5, 2, 1 µM) for 10 min. The slices were then processed for immunofluorescence. a) Double immunolabeling of phospho-H3 (green) and NeuN (red). b) The data from the quantification are represented in the graph as mean±sem (n=25 for not stimulated, n=12 for SKF 100 µM, n=8 for SKF 50 µM and 20 µM, n=9 for SKF 10 µM, n=6 for SKF 5 µM and n=7 for SKF 2 µM and 1 µM). Statistical analysis were performed using one-way ANOVA and post-hoc comparisons between groups using Bonferroni test (stimulated *vs* not stimulated, *** $p<0.001$, **** $p<0.0001$)

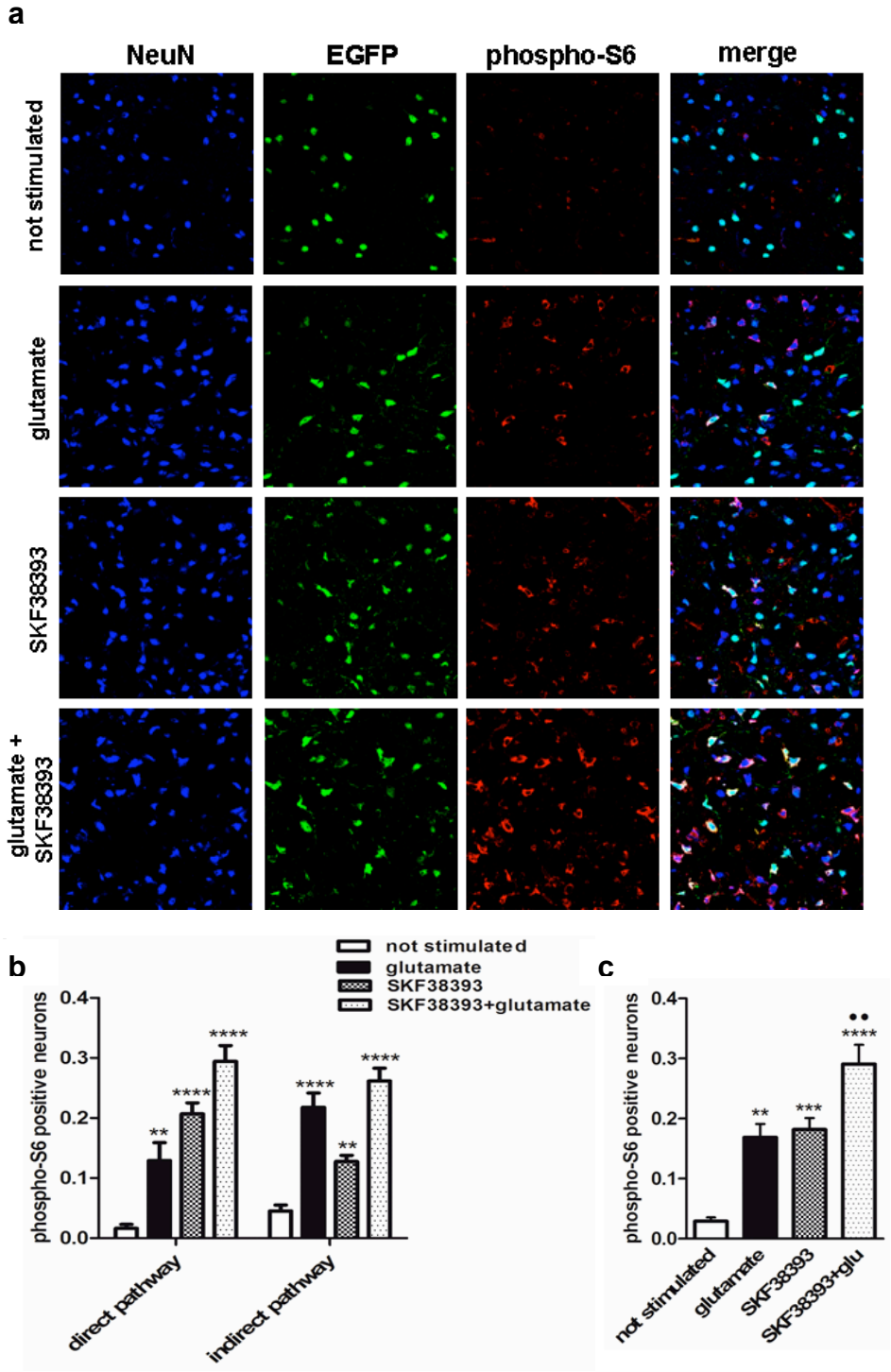


**Fig.20. The co-application of glutamate and SKF38383 has an additive effect on S6 activation in the direct pathway.** Striatal slices obtained from M4-EGFP mice were stimulated with glutamate 20 µM, SKF38393 20 µM or their combination for 10 min. a) Immunofluorescence against phospho-S6 ribosomal protein (red), NeuN (blue) and EGFP (green). b) S6 positive cells among EGFP positive cells (direct pathway) and EGFP negative cells (indirect pathway) were counted. The data are expressed as mean±SEM (n=10 for not stimulated, n=9 for glutamate, n=11 for SKF38393 and for glutamate+ SKF-38393). One-way ANOVA and post-hoc comparisons between groups using Bonferroni test were performed (stimulated *vs* not stimulated, ** $p<0.01$, **** $p<0.0001$). c) The graph represents the number of S6 positive neurons among NeuN positive neurons. One way ANOVA followed by Bonferroni post-hoc test revealed a significant effect of treatment (stimulated *vs* not stimulated ** $p<0.01$, *** $p<0.001$, **** $p<0.0001$, skf+glu *vs* glutamate and skf+glu *vs* SKF-38393, •• $p<0.01$).

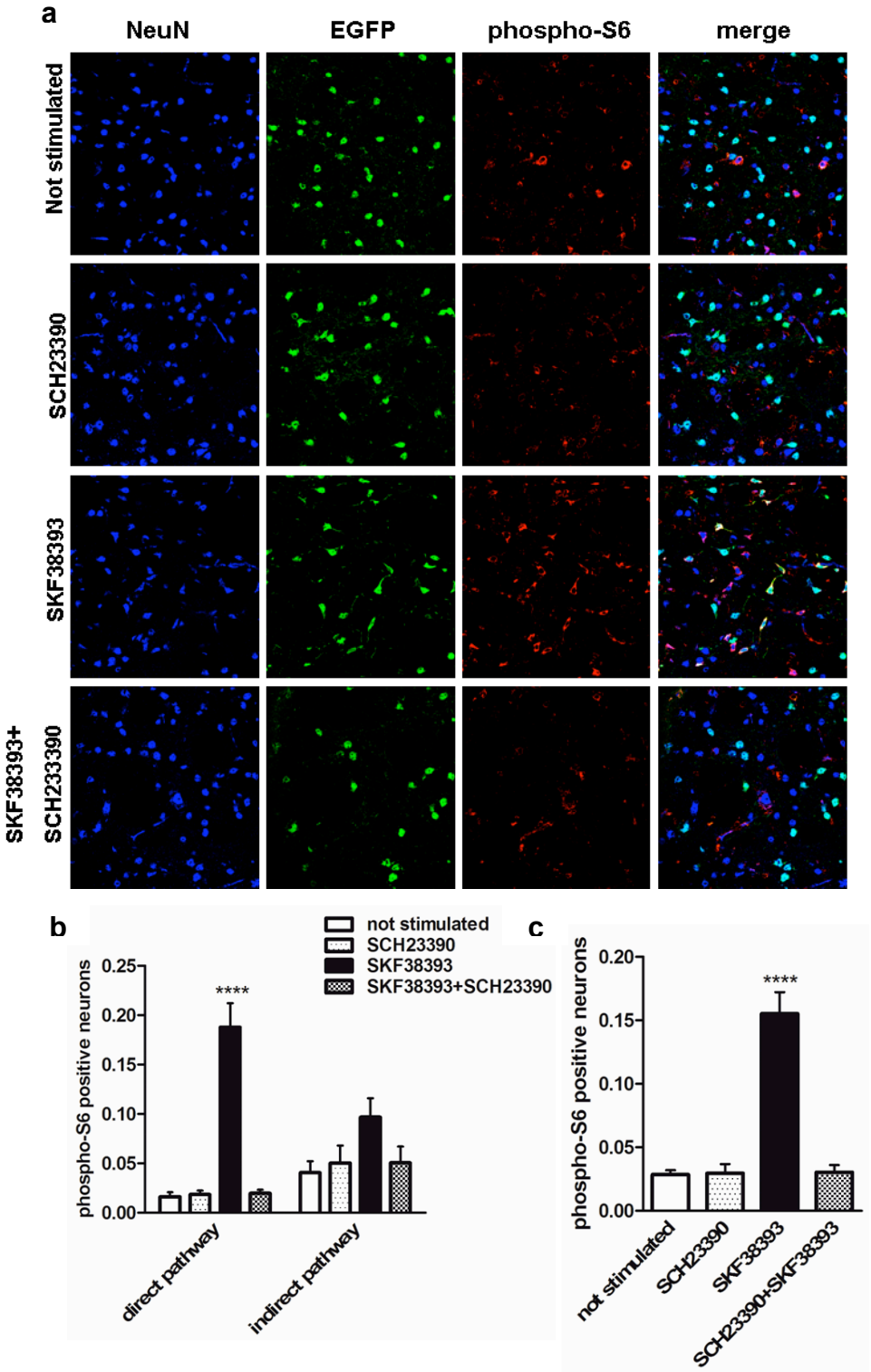


**Fig.21. The blockade of D1Rs completely prevents S6 activation in both direct and indirect pathways.** Striatal slices obtained from M4-EGFP mice were pretreated or not with SCH23390 for 30 min and then stimulated with SKF38393 20 μM for 10 min. a) Immunofluorescence against phospho-S6 ribosomal protein (red), NeuN (blue) and GFP (green). b) The graph represents the number of S6 positive neurons in the direct and in the indirect pathway in the different conditions. The data are expressed as mean±SEM (n=8 for for SKF38393 and n=7 for the other conditions. One-way ANOVA and post-hoc Bonferroni test showed a significant difference between stimulated and not stimulated groups (**** $p<0.0001$). c) The graph represents the number of S6 positive neurons among NeuN positive neurons. One way ANOVA followed by Bonferroni post-hoc test revealed a significant effect of treatment (stimulated *vs* not stimulated, **** $p<0.0001$).

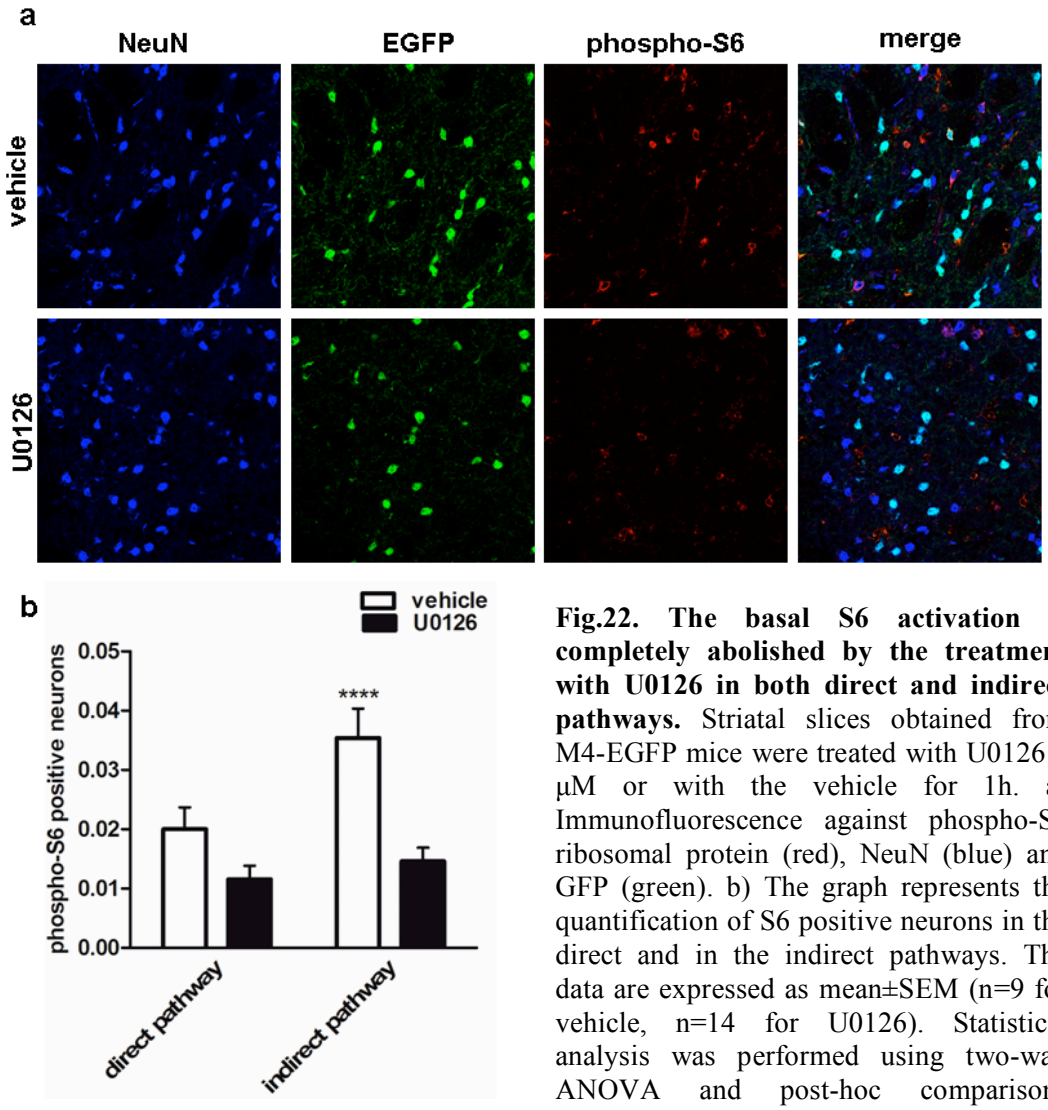


**Fig.22. The basal S6 activation is completely abolished by the treatment with U0126 in both direct and indirect pathways.** Striatal slices obtained from M4-EGFP mice were treated with U0126 5 µM or with the vehicle for 1h. a) Immunofluorescence against phospho-S6 ribosomal protein (red), NeuN (blue) and GFP (green). b) The graph represents the quantification of S6 positive neurons in the direct and in the indirect pathways. The data are expressed as mean±SEM (n=9 for vehicle, n=14 for U0126). Statistical analysis was performed using two-way ANOVA and post-hoc comparisons between groups using Bonferroni test (vehicle *vs* U0126, **** $p<0.0001$).

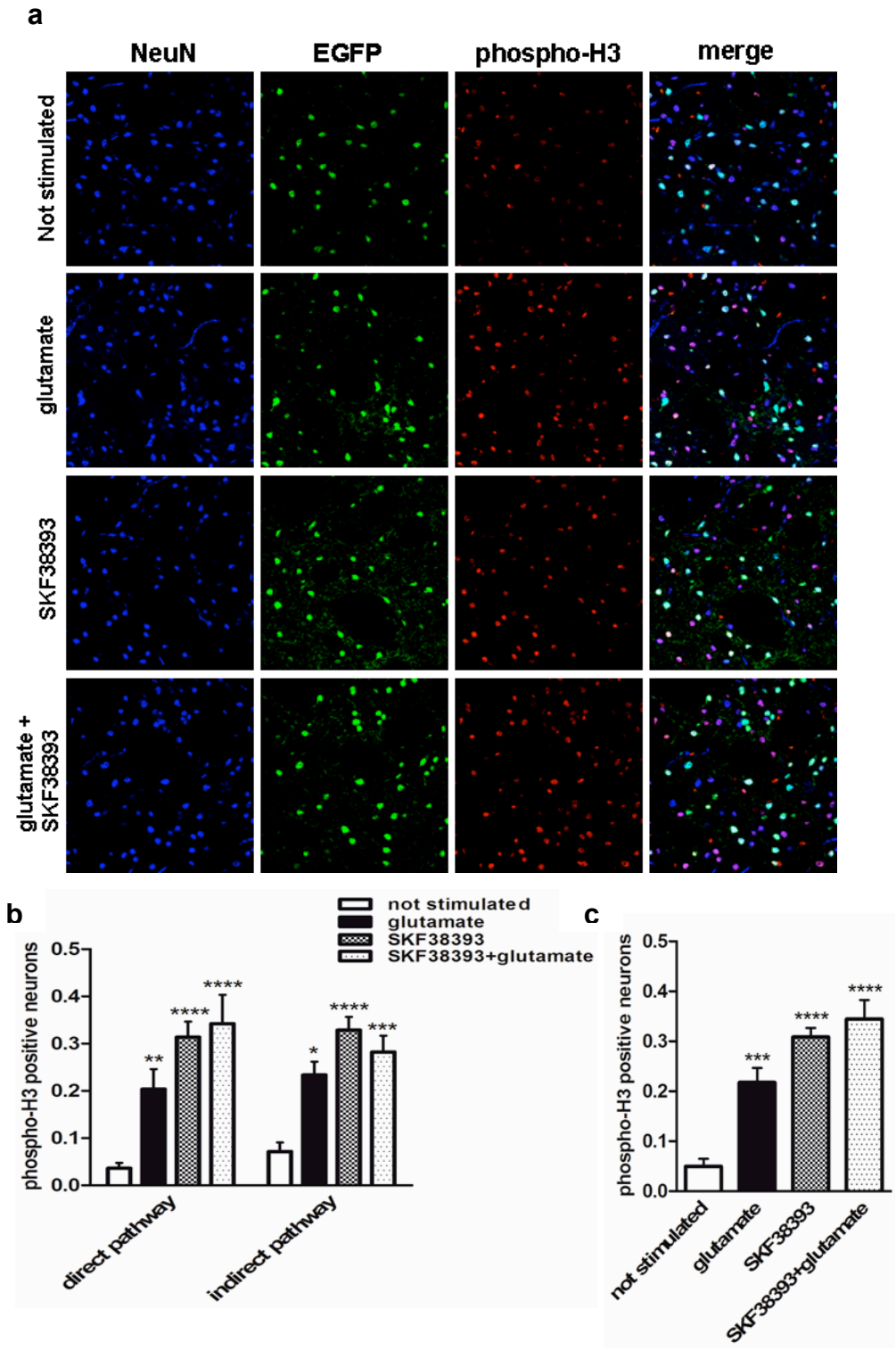


**Fig.23. The co-application of glutamate and SKF-38383 does not increase the level of histone H3 phosphorylation in adult striatal slices.** Striatal slices obtained from M4-EGFP mice were stimulated with glutamate 20 µM, SKF-38393 20 µM or their combination for 10 min. a) Immunofluorescence against phospho-H3 (red), NeuN (blue) and GFP (green). b) The graph represents the quantification of H3 positive neurons in the striatonigral and in the striatopallidal pathways in the different conditions. The data are expressed as mean±SEM (n=8 for not stimulated, n=9 for glutamate, n=8 for SKF38393 and n=7 for glutamate+ SKF-38393). Statistical analysis was performed using one-way ANOVA and post-hoc comparisons between groups using Bonferroni test (stimulated *vs* not stimulated, * $p<0.05$, ** $p<0.01$, **** $p<0.0001$). c) The graph represents the number of S6 positive neurons among NeuN positive neurons. One-way ANOVA and Bonferroni post-hoc test revealed a significant effect of treatments (stimulated *vs* not stimulated, *** $p<0.001$, **** $p<0.0001$).

**SKF38393-mediated S6 activation is completely abolished by the treatment with the NMDARs antagonist and glutamate–mediated S6 phosphorylation is decreased following the application of the D1Rs antagonist**

Another important point is the potential crosstalk in the MSN circuitry between D1Rs and NMDARs; an early evidence showed that cocaine-induced ERK activation in vivo in the striatum requires the concomitant stimulation of D1Rs and NMDARs (Valjent et al., 2005). In addition, previous experiments performed in our laboratory have suggested that a crosstalk between NMDARs and D1Rs, possibly via Ras-GRF1, is necessary to activate ERK in organotypic slices (Fasano et al., 2009).

To elucidate in detail the crosstalk between D1Rs and glutamate receptors in both striatonigral and striatopallidal MSNs, we took advantage of our ex-vivo system by treating striatal slices from M4-EGFP mice with glutamate and SKF38393 in the presence of specific antagonists of NMDARs and D1Rs. Firstly, we found that S6 phosphorylation is completely prevented by the specific antagonists of either AMPARs and NMDARs (fig. 24). We next found that SKF38393-dependent S6 activation is totally abolished either in the direct and indirect pathway not only by the treatment with the corresponding antagonist SCH23390 but also when SKF38393 is applied in combination with the NMDAR antagonist AP5. Conversely, glutamate-mediated S6 activation is totally prevented by the treatment with AP5 but it is only partially blocked (48% of inhibition) when glutamate is applied in combination with SCH23390 (fig. 25). In addition, in the direct pathway S6 activation seems to be more inhibited (55 % of inhibition) by SCH23390 with respect to the indirect pathway (41% of inhibition).

These results suggest that a crosstalk between NMDARs and D1Rs is required to trigger ERK cascade either in the striatonigral and striatopallidal pathways.

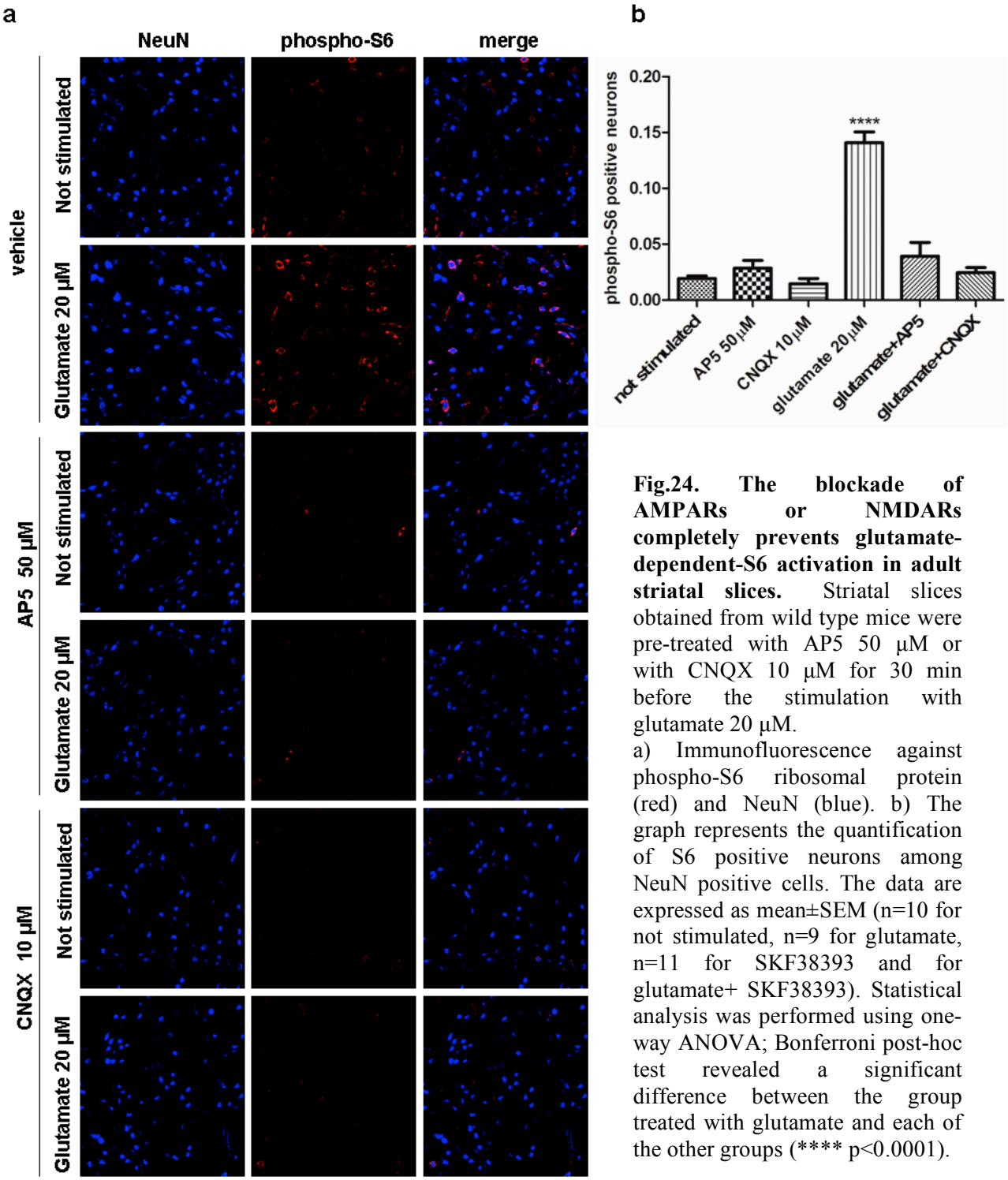


**Fig.24. The blockade of AMPARs or NMDARs completely prevents glutamate-dependent-S6 activation in adult striatal slices.** Striatal slices obtained from wild type mice were pre-treated with AP5 50 µM or with CNQX 10 µM for 30 min before the stimulation with glutamate 20 µM.
a) Immunofluorescence against phospho-S6 ribosomal protein (red) and NeuN (blue). b) The graph represents the quantification of S6 positive neurons among NeuN positive cells. The data are expressed as mean±SEM (n=10 for not stimulated, n=9 for glutamate, n=11 for SKF38393 and for glutamate+ SKF38393). Statistical analysis was performed using one-way ANOVA; Bonferroni post-hoc test revealed a significant difference between the group treated with glutamate and each of the other groups (**** $p<0.0001$).

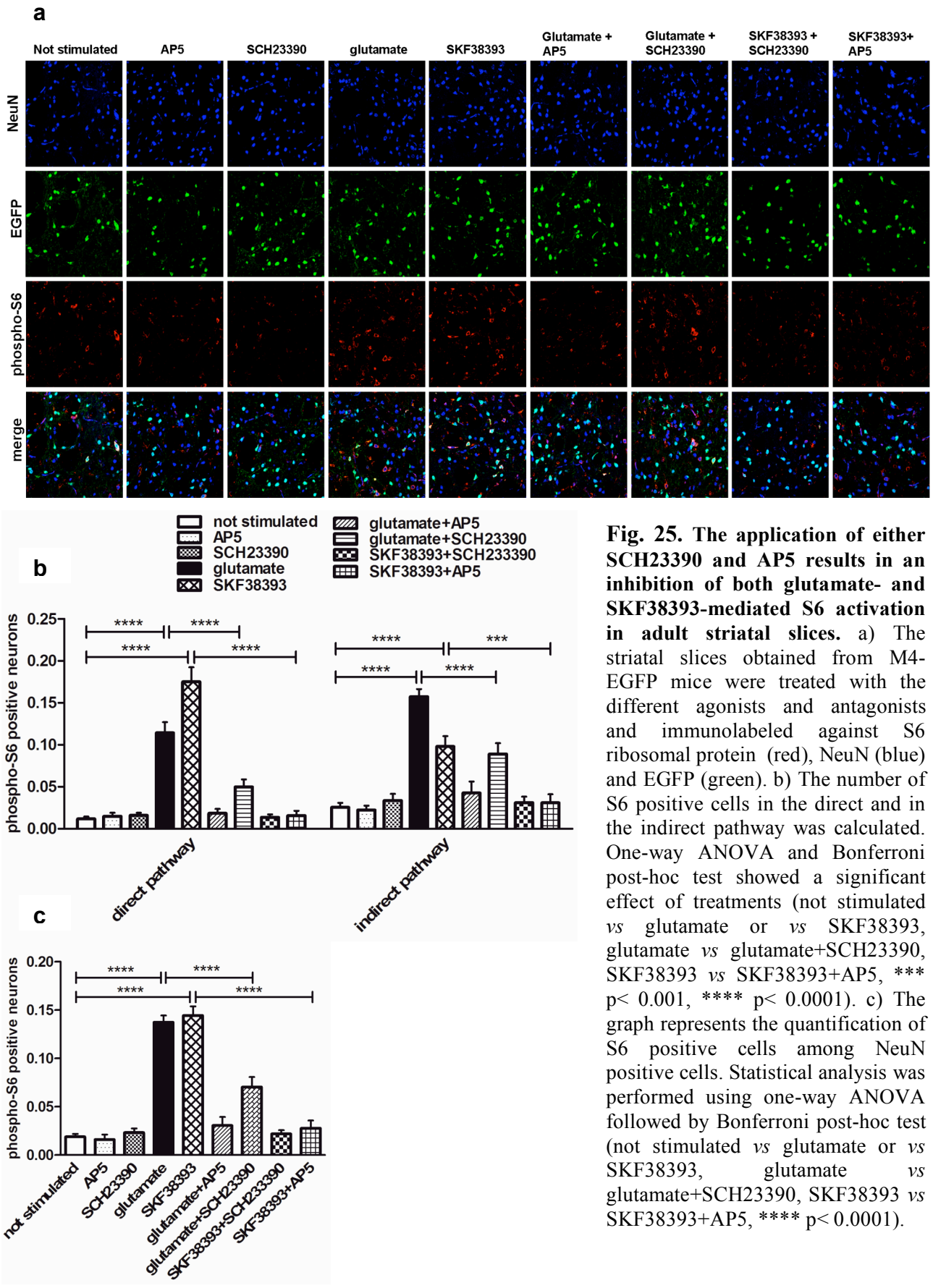


**Fig. 25. The application of either SCH23390 and AP5 results in an inhibition of both glutamate- and SKF38393-mediated S6 activation in adult striatal slices.** a) The striatal slices obtained from M4-EGFP mice were treated with the different agonists and antagonists and immunolabeled against S6 ribosomal protein (red), NeuN (blue) and EGFP (green). b) The number of S6 positive cells in the direct and in the indirect pathway was calculated. One-way ANOVA and Bonferroni post-hoc test showed a significant effect of treatments (not stimulated *vs* glutamate or *vs* SKF38393, glutamate *vs* glutamate+SCH23390, SKF38393 *vs* SKF38393+AP5, *** $p < 0.001$, **** $p < 0.0001$). c) The graph represents the quantification of S6 positive cells among NeuN positive cells. Statistical analysis was performed using one-way ANOVA followed by Bonferroni post-hoc test (not stimulated *vs* glutamate or *vs* SKF38393, glutamate *vs* glutamate+SCH23390, SKF38393 *vs* SKF38393+AP5, **** $p < 0.0001$).

**D1Rs-mediated ERK activation is prevented by the neuropeptide nociceptin/orphanin FQ (N/OFQ)**

In the last part of this project, we have decided to use the ex-vivo technique we developed to investigate the role of Ras-ERK signalling in pathological conditions in the striatum, including L-DOPA induced diskynesia (LID) (Berthet and Bezard, 2009; Jenner, 2008). It is well known that this neurological condition is associated with hyperesponsiveness of D1 receptors on striatonigral MSNs leading to an increased activity of the Ras-ERK pathway

Recently, several studies have been conducted to elucidate the molecular mechanisms underlying LID. For instance, the nociceptin opioid (NOP) receptor has been suggested as a new potential therapeutic target (Marti et al., 2012). The endogenous agonist of NOP receptor is nociceptin (N/OFQ) that is able to trigger a series of intracellular events mediated by G-proteins, including the inhibition of adenylyl cyclase and $Ca^{++}$ channels, and the activation of phospholipase C (PLC), $K^{+}$ channels and MAPKs. In the central nervous system, the main effect of N/OFQ is the inhibition of the release of neurotransmitters, including acetylcholine, catecholamines, GABA and glutamate. Recent studies have provided a link between N/OFQ and Parkinson's Disease; in particular, an increase of N/OFQ expression was found in parkinsonian patients. Consistently, NOP receptor antagonists reversed experimental parkinsonism. In addition, recent evidences have shown that N/OFQ counteracts striatal D1 signalling postsynaptically , pointing to a possible beneficial effect of NOP receptor agonists in LID. In vivo studies conducted by Morari's group and collaborators have suggested that N/OFQ reduces dyskinesia in 6-OHDA lesioned rats and also in MPTP-treated macaques without impairing the antiparkinsonian effect of L-DOPA (Marti et al., 2012).

Thus, we investigated whether the antidyskinetic property of N/OFQ could be ascribed to the inhibition of D1Rs-mediated signalling. In particular, we used our ex-vivo system to monitor the effect of N/OFQ alone or given with SKF-38393 on S6 phophorylation in striatal slices obtained from naïve mice. As shown in figure 26, the application of N/OFQ 1 μM is ineffective alone but totally prevents the D1Rs-mediated ERK signalling activation.

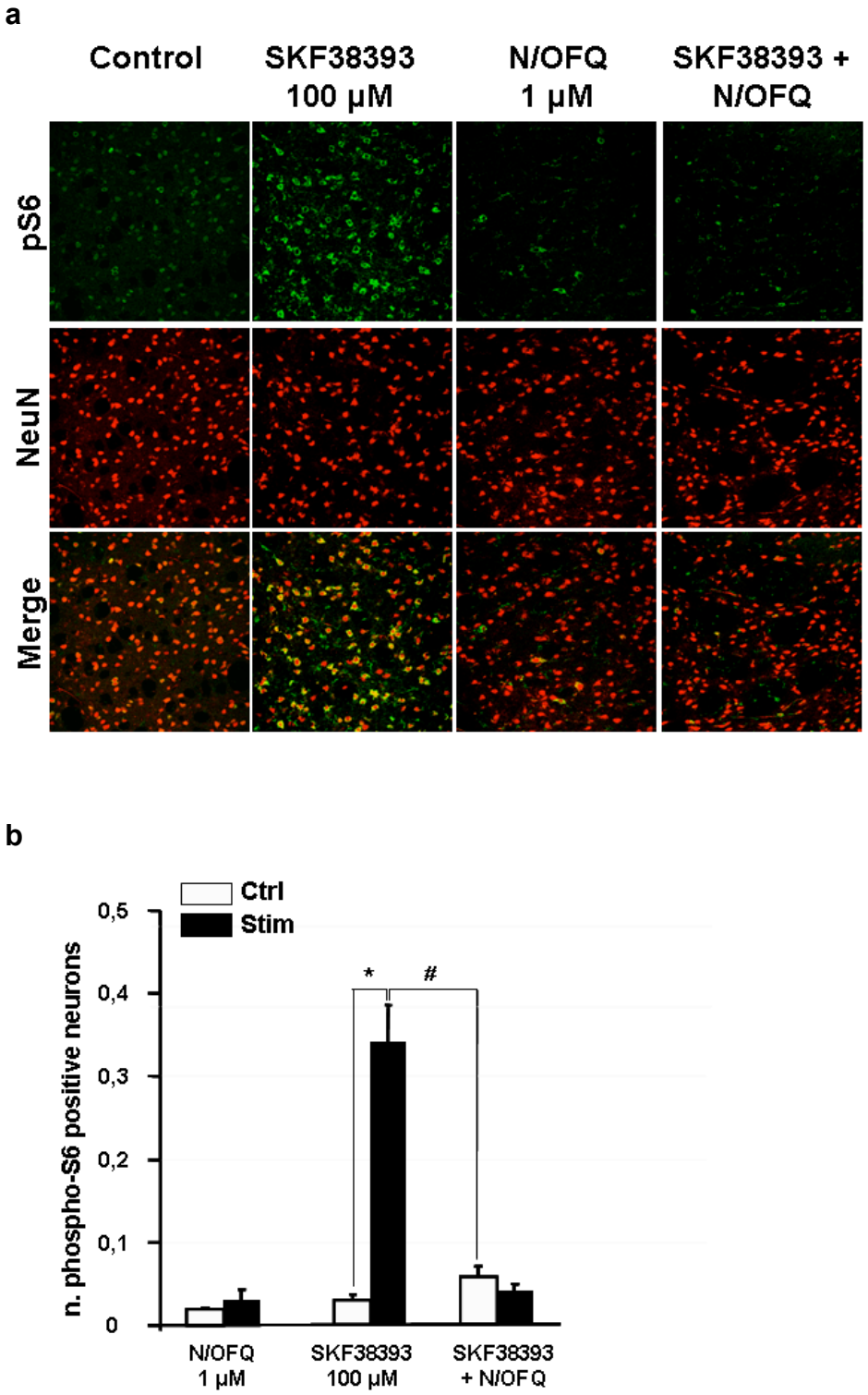


**Fig. 26. N/OFQ inhibits D1 receptor-mediated activation of ERK signalling in mouse striatal slices.** a) Representative photomicrographs showing ERK-dependent S6 phosphorylation (pS6 Ser235/236) (green) and NeuN (red) immunofluorescence in mouse striatal slices in response to SKF38393 (100 µM), N/OFQ (1 µM), or their combination. b) Phospho-S6 levels were significantly increased in striatal neurons stimulated with SKF38393 (Student's *t* test, Control vs SKF38393, $t(10)6.452$, $*p=0.0006$). N/OFQ, ineffective by itself, prevented the effect of SKF38393 (Student's *t* test, Control vs SKF38393N/OFQ, $t(12)0.947$, $p=0.363$). One-way ANOVA revealed a significant effect of treatment $F(5,31)27.235$, $p>0.0001$. Bonferroni's *post hoc*, SKF38393 vs SKF38393N/OFQ, $\#p<0.0001$. Data are expressed as number ± SEM of pS6 positive cells with respect to NeuN positive cells.

**Ras-GRF1 ablation prevents histone H3 hyperactivation but not S6 phosphorylation, in dyskinetic mice**

Previous work from my laboratory has demonstrated that the absence of Ras-GRF1 attenuates LID in 6-OHDA lesioned mice and this effect correlates with a significant decrease of ERK1/2 phosphorylation in the dorsolateral lesioned striatum (Fasano et al, 2010). In addition, S6 ribosomal protein and histone H3 have been found to be hyperactivated in dyskinetic mice specifically in the striatonigral pathway (Santini et al., 2009).

Therefore, we set out to investigate the effect of Ras-GRF1 ablation in LID by monitoring the changes in S6 and histone H3 phosphorylation. In collaboration with Milica Cerovic (Cardiff University), Ras-GRF1 KO mice and wt littermates were stereotactically injected with one microliter of 6-hydroxydopamine (6-OHDA)-HCl (3 μg/μL) into the right ascending medial forebrain bundle. Mice were then evaluated in the open field 2 weeks after lesion to estimate the success rate of lesioning. Starting from day 18, mice were treated twice a day, for 9 consecutive days with an escalating L-dopa dosing regimen (1.5, 3, and 6 mg/kg) plus benserazide (12 mg/kg) to induce LID. We next confirmed the entity of the neurotoxic damage induced by 6-OHDA by immunohistochemistry using antibodies against tyrosine hydroxylase (TH), the enzyme responsible for catalyzing the conversion of L-tyrosine into L-DOPA. As shown in fig. 27 (panel a, b), both wild-type and RasGRF1 KO mice show a positive TH staining in the intact side, whereas the lesioned side shows a profound loss of dopaminergic fibers. Consistently with previous results, we also found an hyperactivation of ERK1/2 in the dorsolateral lesioned striatum of wt mice, whereas lower levels of ERK1/2 phosphorylation were observed in Ras-GRF1 KO mice (fig.27, panel c, d).

Interestingly, immunofluorescence analysis (fig. 28) has demonstrated that Ras-GRF1 ablation while reduces histone H3 phosphorylation in Ras-GRF1 KO dyskinetic mice (fig. 28, panel c, d), does not alter the level of S6 phosphorylation in comparison to wild type mice (fig. 28, panel a, b), suggesting that pS6 in dyskinetic animals may be independent from Ras-GRF1 activity, while it is likely to be still ERK dependent.

Altogether, these in vivo data confirm the validity of the analysis of the Ras-ERK pathway using pS6 and pH3 antibodies also in pathological conditions of the the striatum, such as LID.

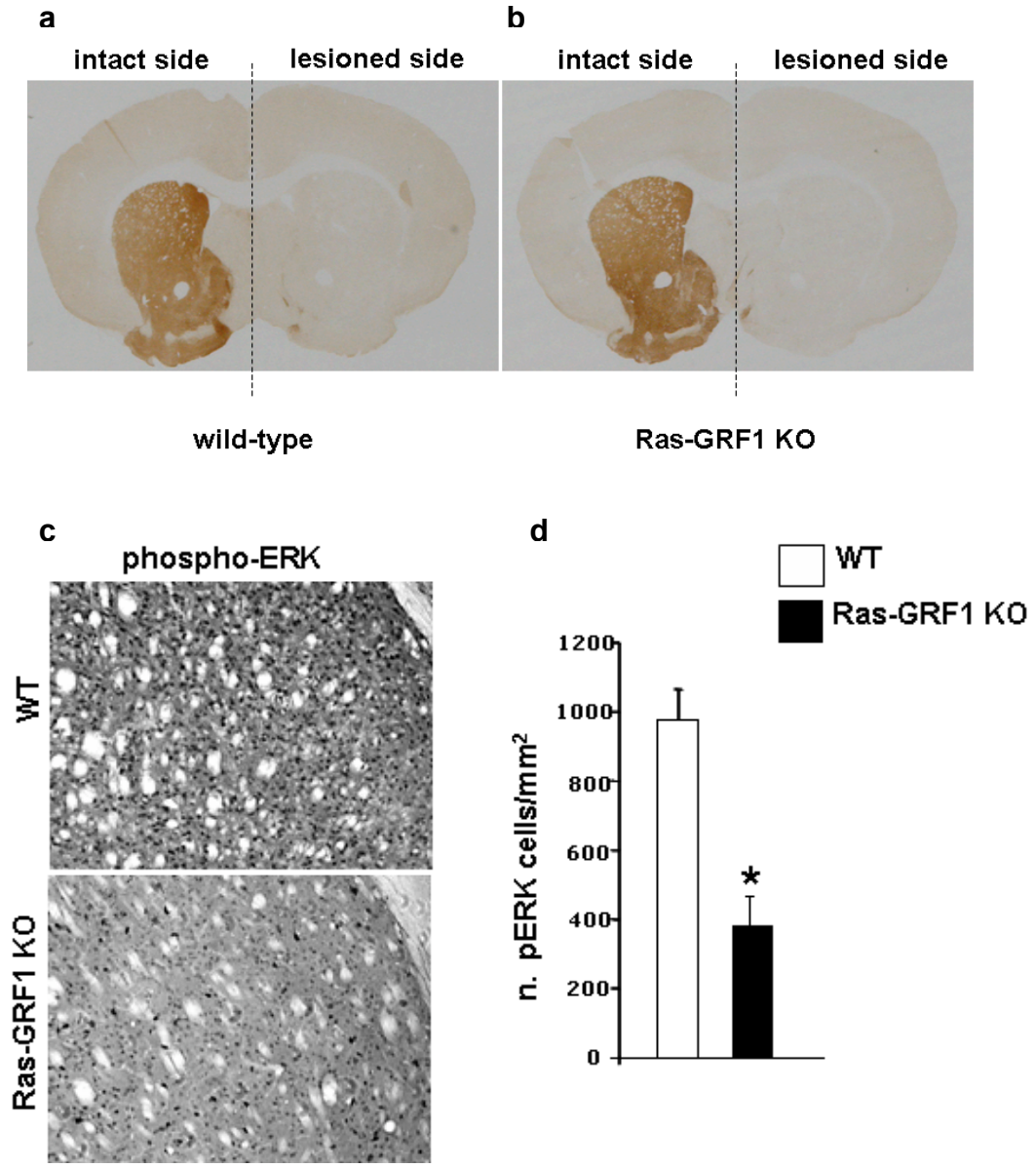


**Fig. 27. Dyskinetic Ras-GRF1 KO mice show a reduction in ERK phosphorylation.** a,b) Representative images of TH positive staining in the intact striatum (left part of the slice) in wild-type (a) and Ras-GRF1 KO (b) mice. Following 6-OHDA lesion a profound loss of dopamine fibers in the striatum was observed (right part of the slice). c) Representative photomicrographs of phospho-ERK1/2 immunoreactive cells in the dorsolateral part of the striatum after 9 days of L-dopa treatment. An aberrant phospho-ERK activation was observed in dyskinetic WT animals while a reduction was seen in Ras-GRF1 KO animals. c) Quantification of p-ERK1/2 positive cells (mean±sem) in the striatum of Ras-GRF1 mutants and control animals. Two–way ANOVA revealed a significant reduction in the number of pERK positive cells in lesioned striatum of Ras-GRF1 mutants (n=8) in comparison to littermate controls (n=8) (Tukey's HSD test, *p<.001 genotype effect).

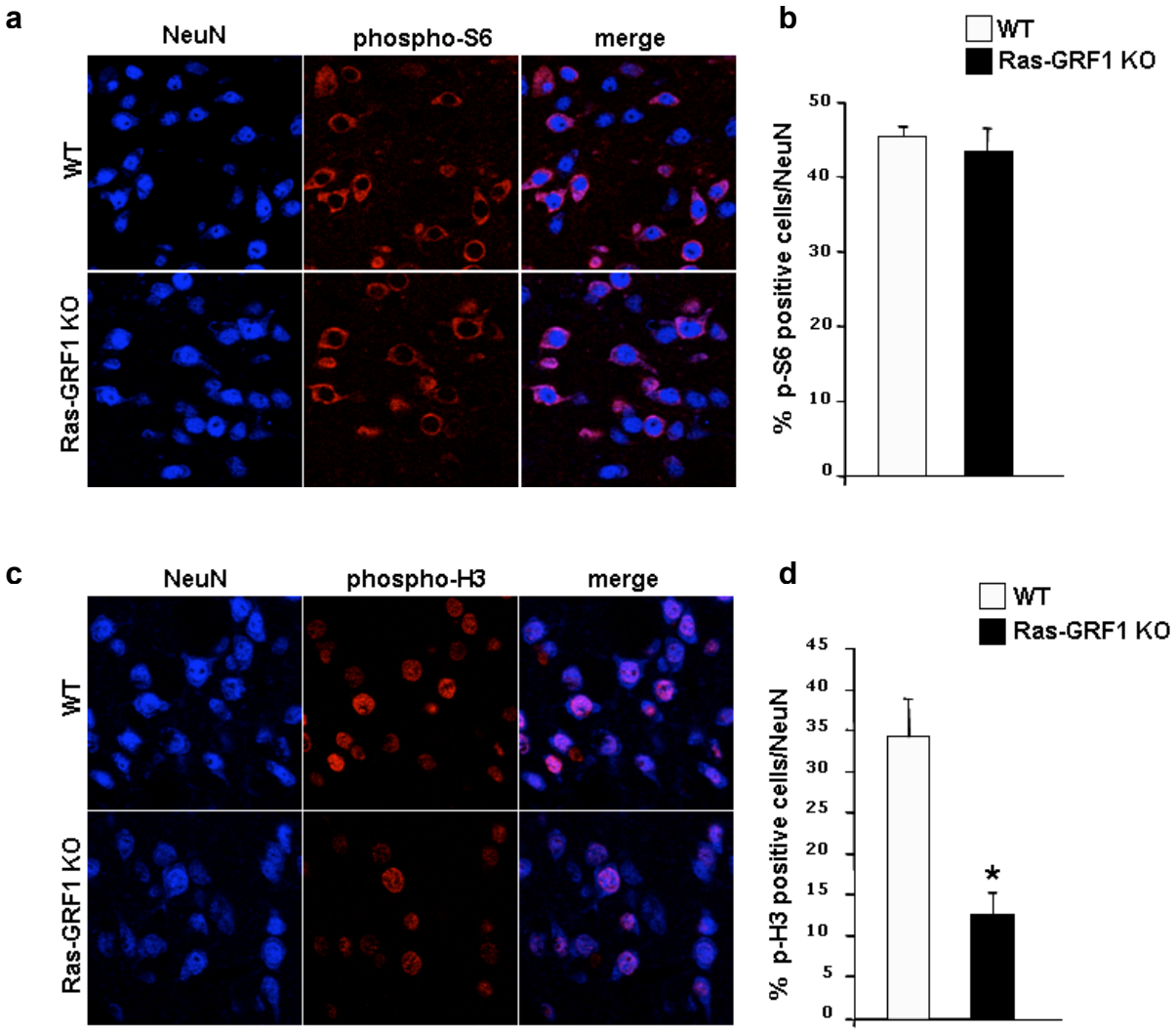


**Fig. 28. Dyskinetic Ras-GRF1 KO mice show a reduction in histone H3, but not in S6 activation.** a,c) Immunofluorescence of phospho-S6 or phospho-H3 (red), and NeuN (blu) of MSNs of dyskinetic Ras-GRF1 mutants and control animals. b,d) The graphs provide quantitative data of the percentage of phospho-S6 and phospho-H3 positive cells over the total NeuN-positive neurons. Two-way ANOVA revealed a significant reduction in the phosphorylation level of H3 in dyskinetic Ras-GRF1 mutants (Tukey's HSD test , *p<.001 genotype effect) whereas S6 activation is not affected by Ras-GRF1 ablation.

# Conclusions and future perspectives

The striatum, the input nucleus of the basal ganglia circuit, integrates excitatory glutamatergic signals from the cortex, thalamus and limbic areas with modulatory dopaminergic signals from midbrain neurons located in the SNc and in the ventral tegmental area.

Thus, signal integration is necessary for normal striatal functions and for the development of various forms of behavioural plasticity, including learning of procedural actions and motor skills, habit formation and reward mechanisms. In addition, the abnormal potentiation of dopamine- and glutamate-dependent signalling, including ERK activation, is implicated in neurological diseases such as L-DOPA induced dyskinesia and drug addiction (Fasano and Brambilla, 2011, Hervé et al., 2001; Cenci et al., 2007; Santini et al., 2007). In particular, psychostimulants and L-DOPA are able to promote cAMP-dependent signalling in the striatum trigger ERK1/2 and MSK-1 signalling specifically in the striatonigral pathway, through phosphorylation of DARPP-32 at Thr34 (Santini et al., 2007; Valjent et al., 2000); this activation of ERK1/2 and MSK1, which depends on the concerted activation of D1Rs and glutamate receptors, mediates also the concomitant increase in the state of phosphorylation of histone H3 and S6 ribosomal protein (Brami-Cherrier et al, 2005; Santini et al, 2007). Conversely, in the striatopallidal pathway, cAMP signalling is controlled by the opposite actions of A2ARs, which increase cAMP production through Gαolf, and D2Rs, which reduce cAMP production through Gαi/o. Therefore, haloperidol and other D2R antagonists promote cAMP/PKA/DARPP-32 signalling, thus increasing the state of phosphorylation of ERK, S6 and histone H3 (Bertran-Gonzalez et al., 2008, 2009; Valjent et al., 2011). This effect has been attributed to the removal of the inhibitory tone exerted by D2Rs on adenylyl cyclase, which leads to the accumulation of cAMP and activation of PKA. The ability of D2R antagonists to promote cAMP/PKA signaling depends on A2ARs which maintain basal adenylyl cyclase activity via activation of Gαolf (Bertran-Gonzalez et al., 2009).

In this work, I showed the development of a new experimental approach in acute striatal slices obtained from the mature brain that has allowed me to characterize the regulation of the Ras-ERK pathway in the striatum with a single-cell definition.

The first aspect to be highlighted is that this ex-vivo system provides some advantages with respect to the other traditional techniques that have been used so far to study signal transduction. For instance, my approach represents a more physiological setting in comparison to the dissociated neuronal cultures (either embryonic or early postnatal ones), in which the cytoarchitecture of the brain structures is completely lost and the cell composition is likely to be altered. In addition, differently from the common use of organotypic cultures obtained from post-natal rodents, this

system uses adult slices that, following the incubation in a perfusion chamber, can be challenged with specific agonists and antagonists and the induction of signaling events, including the ERK cascade, can be monitored using specific antibodies against phosphorylated or unphosphorylated proteins.

In the initial phase of the project, I tested the ability of glutamate to elicit ERK activation using Western blot analysis and I confirmed the induction of ERK following 10 min stimulation with glutamate 100 μM. However, since Western blot analysis examines an average of signaling events in a mixed neuronal population without discriminating between different cell types I decided to develop a system to target specific cell populations in the striatum, also by using transgenic mouse lines expressing EGFP in restricted cell types, including MSNs from the direct and in the indirect pathways.

In particular, I monitored the phosphorylation of two proteins downstream ERK, S6 ribosomal protein and histone H3, respectively a cytoplasmic and a nuclear marker, by immunofluorescence analysis, demonstrating that glutamate, the D1 agonist SKF-38393 or BDNF are able to induce a robust S6 phosphorylation, assessed at Ser235/236 sites. Similarly, I found that the Lys14-acetylated form of histone H3, an important target of MSK1 in striatal neurons (Brami-Cherrier et al., 2005, Santini et al., 2007), is strongly phosphorylated following the application of glutamate, SKF38393 or BDNF.

These observations, together with the demonstration that upon MEK blockade the glutamate-dependent activation of either S6 and H3 is completely abolished, indicate that it is possible to study at a single-cell level both cytoplasmic and nuclear events induced by ERK activation and that these phosphorylation sites on S6 ribosomal protein and histone H3 are reliable indicators of the Ras-ERK pathway. Regarding S6 phosphorylation, my findings are partially in agreement with a previous study conducted on mammalian cells challenged with several stimuli, including serum and growth factors; in fact, these experiments have shown that S6 phosphorylation at the dual site Ser235/236 occurs either via p70 S6 kinase 1 (S6K1) and via the p90 ribosomal S6 kinases (RSKs), which are activated by ERK independently from mTORC1 (Roux et al., 2007). Consistently, I found that S6 phosphorylation at Ser235/236 is totally dependent on ERK activation, strongly suggesting that both S6K1 and RSKs require to be fully activated by ERK1/2 in order to phosphorylate these two sites.

Having validated this experimental setting, we next investigated the integration between dopaminergic and glutamatergic signaling underlying striatal plasticity. Recently, the interactions between NMDARs and dopamine receptors has been extensively studied, given their essential physiological role but also their involvement in pathological conditions; for instance, it has been

documented that the integration of these two signalling pathways, finely balanced in the intact brain, controls a variety of functions according to the area in which they occur, including motor control in the dorsal striatum (Cepeda and Levine, 1998) and working memory and cognition in the frontal cortex (Castner et al., 2007); however, the disruption of this homeostasis may contribute to pathological states, including addiction. The classical paradigm of NMDARs interactions with dopamine receptors is that these take place through the crosstalk between their signalling transduction cascades; for instance, in the striatum, upon stimulation D1Rs are able to enhance NMDARs responses by cAMP-PKA-DARPP-32 pathway that leads to the phosphorylation of the NR1 subunit of NMDARs (Snyder et al., 1998) and activation of voltage-gated channels (Cepeda et al., 1998), but also exerts an inhibitory action on striatal-enriched tyrosine phosphatase (STEP) and protein phosphatase-1 (PP-1) (Valjent et al., 2005). In contrast, when the D1 receptor is blocked, activation of D2 receptors reduces the PKA-mediated phosphorylation of both DARPP-32 and NR1 subunits (Edwards et al., 2002) and inhibits NMDAR-mediated calcium influx (Higley and Sabatini, 2010).

Besides the indirect crosstalk between NMDARs and dopamine receptors, other studies have found physical interactions between these receptors; for instance, the interaction of the C-terminal tails of D1Rs with NR1 NMDAR subunit enables an increased membrane insertion of D1Rs and it is also implicated in the attenuation of NMDAR-dependent excitotoxicity through a PI-3 kinase-dependent pathway (Pei et al., 2004). In addition, the C-terminal tails of D1Rs have also been found to interact with NR2A NMDAR subunit in hippocampus, and this event results in the inhibition of NMDARs-gated currents, via a decrease in the number of cell surface receptors (Lee et al., 2002).

It is now known that ERK cascade is a common downstream target of glutamate and dopamine pathways in different brain regions, since its triggering requires both calcium influx from AMPARs/NMDARs and D1Rs activation (Bertran-Gonzales et al., 2008; Kaphzan et al., 2006; Valjent et al., 2005). In addition, both NMDARs/AMPARs and D1Rs are potently activated during rewarding experiences and exposure to addictive drugs, and the integration between the signalling pathways harboring from the two classes of receptors modulates the enduring changes in synaptic plasticity underlying addictive behaviour. For instance, in vivo studies have demonstrated that mice treated with cocaine show a robust activation of ERK1/2, dependent on the concomitant stimulation of NMDARs/AMPARs and D1Rs; in addition, ERK activation is involved in the long lasting behavioural changes induced by cocaine, including psychomotor sensitization and conditioned place preference (Valjent et al., 2006; Fasano et al., 2009). More recently, it has been shown that D1R-mediated tyrosine phosphorylation of NR2 subunit of NMDARs is necessary to trigger cocaine-induced ERK activation (Pascoli et al., 2010). Furthermore, previous experiments

conducted in our laboratory have clearly demonstrated an additive effect of SKF38393- and glutamate-dependent signalling on ERK1/2 activation in organotypic slices, an effect completely lost in Ras-GRF1 knock out mice, suggesting that Ras-GRF1 acts as integrator of dopaminergic and glutamatergic signalling in striatum (Fasano et al., 2009).

These observations, together with the availability of M4-EGFP mice expressing EGFP in the striatonigral pathway, have prompted us to investigate the integration of dopaminergic and glutamatergic signalling specifically in the direct and in the indirect pathway in adult striatal slices.

However, before using M4-EGFP mice, we first characterized these animals calculating the proportions of EGFP-expressing MSNs with respect to MSNs that do not express EGFP, considering that it is highly believed that the cellular composition belonging to the direct and the indirect pathway is quite similar. The result demonstrated that the percentage of EGFP-positive cells is similar to the percentage of EGFP-negative cells (48% of striatonigral MSNs and 52% of striatopallidal MSNs), suggesting that M4-EGFP mice may represent a good model to study and compare the signaling pathways in the two populations of MSNs.

Having validated M4-EGFP mice, we next determined the lowest concentration of both glutamate and SKF38393 able to efficiently activate S6 and histone H3 after a stimulation of 10 min. The treatment with different doses of glutamate and SKF38393 has demonstrated that both agonists affect in a dose-dependent manner the level of S6 and histone H3 phosphorylation and 20 μM of either glutamate and SFK38393 is able to induce the maximal activation of S6 and histone H3 after 10 min stimulation.

On the basis of these preliminary observations, we wanted to further explore the interplay between the glutamatergic and the dopaminergic signaling in the two striatal pathways, using M4-EGFP mice. In particular, our results confirm that an additive integration between glutamate and SKF38393 converges on S6 phosphorylation. Interestingly, this effect seems to be restricted to the striatonigral pathway. In addition, we found that the basal level of S6 activation, that is MEK-dependent, is two fold higher in the indirect pathway in comparison to the direct pathway. This last observation seems to be in accordance with previous electrophysiological observations suggesting a generally higher excitability of the striatopallidal MSNs (Cepeda et al., 2008; Day et al., 2008).

Furthermore, we also found that the application of SKF38393 activates S6 ribosomal protein also in the indirect pathway, even though at a lower level in comparison to what observed in the striatonigral MSNs. This finding, quite unexpected since SKF38393 is supposed to be a D1R-like specific agonist, has prompted us to further investigate the effect of D1Rs blockade on SKF38393-induced S6 activation; our data clearly demonstrate that S6 phosphorylation observed in the indirect pathway depends directly on D1Rs stimulation since the D1Rs antagonist SCH233390 completely

abolishes SKF38393-induced S6 activation in both pathways. Thus, the exact mechanism, either direct or indirect, by which SKF38393 is able to induce S6 activation in the striatopallidal neurons still remains to be elucidated. However, in this regard, it has to be noted that, although several neuroanatomical and functional studies support the selective distribution of D1/5Rs and D2/3/4Rs respectively in the striatonigral and in the striatopallidal pathway, other studies have disclosed a partial overlap between the expression of the two receptor classes (Aizman et al., 2000, Bertran-Gonzales et al., 2008). The fact that the degree of overlap has been continuously questioned is a clear indication of this controversy but a recent study estimated that only 5% of MSNs co-expresses the D1s and D2Rs in the dorsal striatum and in the NAc core, whereas co-expressing neurons are more abundant in the NAc shell (about 17%) (Bertran-Gonzales et al., 2008). These findings, although still under debate, might partially explain our observations since SKF38393-induced S6 phosphorylation in the indirect pathway might be mediated by D1Rs localized in the subset of striatopallidal MSNs expressing both types of dopamine receptors. Another possibility to be considered is that SKF38393-induced S6 activation in the indirect pathway might be mediated indirectly by D1Rs that, for instance, might trigger signaling pathways that finally modulate other receptors, including A2ARs, thereby leading to S6 phosphorylation in the indirect pathway. The final possibility is that some EGFP negative cells in the M4-EGFP model are indeed part of the indirect pathway despite they do not express the fluorescence marker (see comment further below). This possibility will be explored in the near future by using a BAC transgenic mouse specifically expressing EGFP in the indirect pathway, i.e. the A2A-EGFP line (Fasano et al., 2010).

We next wanted to investigate the effect of the co-stimulation of glutamate receptors and D1Rs on histone H3 phosphorylation but, in contrast to what observed for S6, we have not found an additive integration between glutamate and SKF38393. A possible explanation of this result is that histone H3 is already maximally phosphorylated at the doses used of glutamate and SKF38393, as we also observed in the dose-response curves.

Our results also confirm and extend previous evidence from our laboratory that suggested, by Western blot analysis, a reciprocal dependence of both glutamate and SKF38393 on NMDARs and D1Rs activation in organotypic slices extracts (Fasano et al., 2009). This finding was unique to the striatum since in hippocampus only dopaminergic activity requires NMDAR activation to trigger ERK cascade (Kaphzan et al., 2007). Accordingly to what published by Fasano et al. in 2009, we found that D1Rs-mediated signalling depends on glutamatergic activity since SKF38393-dependent S6 activation is totally abolished either in the direct and indirect pathway not only by the treatment with the D1Rs antagonist SCH23390 but also when SKF38393 is applied in combination with the NMDAR antagonist AP5. Conversely, glutamatergic activity does not completely depend on

dopaminergic signalling since glutamate-mediated S6 phosphorylation is only partially inhibited (48% of inhibition) when glutamate is applied in combination with SCH23390. In addition, when I compared the direct and the indirect pathways, my results highlighted a difference in the level of glutamate-induced S6 activation in the slices pre-treated with SCH23390. In particular, in the direct pathway, S6 activation seems to be more inhibited (55 % of inhibition) by SCH23390 with respect to the indirect pathway (41% of inhibition). Regarding all these findings, it should be noted once again that, whereas the data referred to the direct pathway are certainly reliable, we are planning to perform further experiments in A2A-EGFP mice, expressing EGFP in the indirect pathway, to confirm the results concerning the indirect pathway.

In fact, although we estimated that the number of the EGFP-expressing cells is quite similar to the number of EGFP-negative cells in the whole striatum, we also observed that the fluorescence is not always distributed homogeneously within the different striatal slices, possibly resulting in an underestimation of the EGFP positive cells. Therefore, the data relative to the striatopallidal pathway may appear overestimated by counting the EGFP-negative cells in the specific fields that we considered.

As future perspective, another step forward may be represented by the genetic manipulation of Ras-ERK components in EGFP mice, for instance by injecting viral vectors with cell-specific promoters in the direct or in the indirect pathways.

In the last part of the project, we also investigated the role of Ras-ERK signalling in L-DOPA induced dyskinesia (LID), a severe and disabling pathology characterized by involuntary choredystonic movements that develop as consequence of chronic L-DOPA treatment in parkinsonian patients. Several lines of evidence have suggested that LID largely results from the pulsatile stimulation of dopamine receptors, triggering a complex cascade of molecular changes including ERK activation that concur to modify neuronal firing patterns in the basal ganglia-thalamocortical networks. Unfortunately, at present only two therapeutic options are used for the treatment of severe LID. The first strategy is the neurosurgical intervention targeting the deep basal nuclei (deep brain stimulation, DBS) but, in addition to being expensive and invasive, can only be offered to selected parkinsonian patients responding to specific criteria (Lang et al., 2006); the second strategy is a pharmacological therapy using NMDA receptor antagonist amantadine; however, the main disadvantage of this type of treatment is given by its modest antidyskinetic efficacy since amantadine is able to reduce dyskinesia in the range of 40-60% in the best responding patients.

However, in recent years the study of the molecular changes occurring in the striatum during the development of LID and the role of the specific components of the signalling machinery has

revealed potential new therapeutic targets. For instance, the recent discovered NOP receptor has been suggested as a possible target for treating PD and motor disorders. In particular, NOP receptor antagonists have been found to reverse experimental parkinsonism thereby suggesting a possible application in PD treatment (Marti et al., 2005; Marti et al., 2008; Volta et al., 2010). In addition, NOP receptor antagonists might affect the dyskinesiogenic activity of L-DOPA since they elevate striatal DA (Marti et al., 2004) and raphe serotonin (Tao et al., 2007; Nazzaro et al., 2009) levels. On the other hand, NOP receptor agonists (N/OFQ) impair the firing activity of ascending DA and serotonin neurons, and inhibit DA (Flau et al., 2002; Olianas et al., 2008) and serotonin (Sbrenna et al., 2002) released presynaptically. Therefore, these observations, together with the recent finding that N/OFQ counteracts striatal D1 signalling postsynaptically , have suggested a possible anti-dyskinetic effect of N/OFQ.

In this direction, Morari and collaborators have recently performed experiments either in 6-OHDA lesioned rats and in MPTP-treated macaques to evaluate whether NOP receptors agonists and antagonists affected the expression of dyskinetic movements. They demonstrated that N/OFQ is able to reduce dyskinesia in both these animal models without impairing the antiparkinsonian effect of L-DOPA. Therefore, on the basis of these observations, we wondered whether the antidyskinetic property of N/OFQ might correlate with a negative modulation of D1Rs-mediated signalling. To support this idea I decided to use the ex-vivo system I developed on striatal slices obtained from naive mice; my results clearly indicate that the application of N/OFQ completely prevents S6 activation induced by D1Rs stimulation, thereby suggesting that N/OFQ is able to block D1Rs-mediated ERK signalling pathway.

Another perspective for pharmacological treatments of LID is given by the demonstration that LID is causally linked to ERK hyperactivation and thus it can be prevented in 6-OHDA mice by the treatment with SL237, a MEK inhibitor (Santini et al., 2007). From this point of view, the striatal signalling machinery controlled by ERK may represent an appealing drug target but, since ERK cascade is involved in a number of important biological processes including cell proliferation, differentiation and neuronal plasticity, a complete blockade of this pathway may produce negative side effects, including neuronal cell loss. To overcome this problem, Fasano et al. (2010, 2011) have suggested that Ras-GRF1, a brain-specific Ras exchange factor, may represent an alternative target for pharmacological treatment of LID. In fact, they demonstrated that LID is significantly reduced both in Ras-GRF1 KO mice and in mice injected in the dorsal striatum with lentiviral vectors causing Ras-GRF1 knockdown (Fasano et al., 2010).

In this work, I wanted to investigate the effect of Ras-GRF1 ablation in LID by monitoring the changes in ERK1/2, S6 and histone H3 phosphorylation in dyskinetic Ras-GRF1 KO mice. Our

data confirmed previous evidence (Fasano et al., 2010; Santini et al., 2009), demonstrating that ERK, S6 and histone H3 are hyperactivated in the dorsolateral striatum of dyskinetic mice.

In addition, I showed that the lack of Ras-GRF1 prevents histone H3, but not S6 hyperactivation following chronic L-DOPA treatment. Altogether these findings suggest that the chronic treatment with L-DOPA produces some adaptive processes that may bypass Ras-GRF1 and possibly ERK requirement; for instance, in neuronal cells, ERK signalling is promoted not only via calcium-dependent activation of Ras-GRF1 but also by other calcium-sensitive Ras-GEFs, including the striatal-enriched members of Ras-GRP/CalDAG GEFs family (Ebinu et al., 1998). In addition, other lines of evidence have demonstrated that LID is also associated with a persistent enhancement of mTORC1 signalling, leading to an increased S6 phosphorylation, assessed both at Ser 235/236 sites and Ser 240/244 sites (Santini et al., 2009) and this event may be related to an enhanced local protein synthesis underlying LID. Thus, it is possible that mTOR pathway may converge to activate S6 in dyskinetic Ras-GRF1 KO mice bypassing ERK. In order to test our hypothesis, further experiments will need to be performed, for instance by treating dyskinetic wild type and Ras-GRF1 KO mice or striatal slices obtained from these animals with MEK inhibitor, to investigate the effect of ERK blockade on L-DOPA induced S6 hyperactivation in this pathological condition.

# References

Aizman, O., H. Brismar, P. Uhlen, E. Zettergren, A. I. Levey, H. Forssberg, P. Greengard, and A. Aperia. "Anatomical and Physiological Evidence for D1 and D2 Dopamine Receptor Colocalization in Neostriatal Neurons." *Nat Neurosci* 3, no. 3 (2000): 226-30.

Andersson, M., A. Hilbertson, and M. A. Cenci. "Striatal Fosb Expression Is Causally Linked with L-Dopa-Induced Abnormal Involuntary Movements and the Associated Upregulation of Striatal Prodynorphin Mrna in a Rat Model of Parkinson's Disease." *Neurobiol Dis* 6, no. 6 (1999): 461-74.

Aoki, Y., T. Niihori, Y. Narumi, S. Kure, and Y. Matsubara. "The Ras/Mapk Syndromes: Novel Roles of the Ras Pathway in Human Genetic Disorders." *Hum Mutat* 29, no. 8 (2008): 992-1006.

Atkins, C. M., J. C. Selcher, J. J. Petraitis, J. M. Trzaskos, and J. D. Sweatt. "The Mapk Cascade Is Required for Mammalian Associative Learning." *Nat Neurosci* 1, no. 7 (1998): 602-9.

Aubert, I., C. Guigoni, K. Hakansson, Q. Li, S. Dovero, N. Barthe, B. H. Bioulac, C. E. Gross, G. Fisone, B. Bloch, and E. Bezard. "Increased D1 Dopamine Receptor Signaling in Levodopa-Induced Dyskinesia." *Ann Neurol* 57, no. 1 (2005): 17-26.

Baldassa, S., R. Zippel, and E. Sturani. "Depolarization-Induced Signaling to Ras, Rap1 and Mapks in Cortical Neurons." *Brain Res Mol Brain Res* 119, no. 1 (2003): 111-22.

Barbacid, M. "Ras Genes." *Ann. Rev. Biochem.* 56, (1987): 779-827.

Benabid, A. L., A. Benazzouz, P. Limousin, A. Koudsie, P. Krack, B. Piallat, and P. Pollak. "Dyskinesias and the Subthalamic Nucleus." *Ann Neurol* 47, no. 4 Suppl 1 (2000): S189-92.

Benabid, A. L., S. Chabardes, E. Seigneuret, V. Fraix, P. Krack, P. Pollak, R. Xia, B. Wallace, and F. Sauter. "Surgical Therapy for Parkinson's Disease." *J Neural Transm Suppl*, no. 70 (2006): 383-92.

Benabid, A. L., S. Chabardes, N. Torres, B. Piallat, P. Krack, V. Fraix, and P. Pollak. "Functional Neurosurgery for Movement Disorders: A Historical Perspective." *Prog Brain Res* 175, (2009): 379-91.

Bentires-Alj, M., M. I. Kontaridis, and B. G. Neel. "Stops Along the Ras Pathway in Human Genetic Disease." *Nat Med* 12, no. 3 (2006): 283-5.

Berman, D. E., S. Hazvi, V. Neduva, and Y. Dudai. "The Role of Identified Neurotransmitter Systems in the Response of Insular Cortex to Unfamiliar Taste: Activation of Erk1-2 and Formation of a Memory Trace." *J Neurosci* 20, no. 18 (2000): 7017-23.

Berthet, A., and E. Bezard. "Dopamine Receptors and L-Dopa-Induced Dyskinesia." *Parkinsonism Relat Disord* 15 Suppl 4, (2009): S8-12.

Berthet, A., G. Porras, E. Doudnikoff, H. Stark, M. Cador, E. Bezard, and B. Bloch. "Pharmacological Analysis Demonstrates Dramatic Alteration of D1 Dopamine Receptor Neuronal Distribution in the Rat Analog of L-Dopa-Induced Dyskinesia." *J Neurosci* 29, no. 15 (2009): 4829-35.

Bertran-Gonzalez, J., C. Bosch, M. Maroteaux, M. Matamales, D. Herve, E. Valjent, and J. A. Girault. "Opposing Patterns of Signaling Activation in Dopamine D1 and D2 Receptor-Expressing Striatal Neurons in Response to Cocaine and Haloperidol." *J Neurosci* 28, no. 22 (2008): 5671-85.

Bertran-Gonzalez, J., K. Hakansson, A. Borgkvist, T. Irinopoulou, K. Brami-Cherrier, A. Usiello, P. Greengard, D. Herve, J. A. Girault, E. Valjent, and G. Fisone. "Histone H3 Phosphorylation Is under the Opposite Tonic Control of Dopamine D2 and Adenosine A2a Receptors in Striatopallidal Neurons." *Neuropsychopharmacology*, (2009).

Besnard, A., N. Bouveyron, V. Kappes, V. Pascoli, C. Pages, N. Heck, P. Vanhoutte, and J. Caboche. "Alterations of Molecular and Behavioral Responses to Cocaine by Selective Inhibition of Elk-1 Phosphorylation." *J Neurosci* 31, no. 40 (2011): 14296-307.

Blum, S., A. N. Moore, F. Adams, and P. K. Dash. "A Mitogen-Activated Protein Kinase Cascade in the Ca1/Ca2 Subfield of the Dorsal Hippocampus Is Essential for Long-Term Spatial Memory." *J Neurosci* 19, no. 9 (1999): 3535-44.

Bos, J. L. "All in the Family? New Insights and Questions Regarding Interconnectivity of Ras, Rap1 and Ral." *Embo J* 17, no. 23 (1998): 6776-82.

Bourne, H. R., D. A. Sanders, and F. McCormick. "The Gtpase Superfamily: A Conserved Switch for Diverse Cell Functions." *Nature* 348, (1990): 125-132.

Braithwaite, S. P., M. Adkisson, J. Leung, A. Nava, B. Masterson, R. Urfer, D. Oksenberg, and K. Nikolich. "Regulation of Nmda Receptor Trafficking and Function by Striatal-Enriched Tyrosine Phosphatase (Step)." *Eur J Neurosci* 23, no. 11 (2006): 2847-56.

Brambilla, R., N. Gnesutta, L. Minichiello, G. White, A. J. Roylance, C. E. Herron, M. Ramsey, D. P. Wolfer, V. Cestari, C. Rossi-Arnaud, S. G. N. Grant, P. F. Chapman, H.-P. Lipp, E. Sturani, and R. Klein. "A Role for the Ras Signalling Pathway in Synaptic Transmission and Long-Term Memory." *Nature* 390, (1997): 281-286.

Brami-Cherrier, K., E. Valjent, D. Herve, J. Darragh, J. C. Corvol, C. Pages, S. J. Arthur, J. A. Girault, and J. Caboche. "Parsing Molecular and Behavioral Effects of Cocaine in Mitogen- and Stress-Activated Protein Kinase-1-Deficient Mice." *J Neurosci* 25, no. 49 (2005): 11444-54.

Brems, H., M. Chmara, M. Sahbatou, E. Denayer, K. Taniguchi, R. Kato, R. Somers, L. Messiaen, S. De Schepper, J. P. Fryns, J. Cools, P. Marynen, G. Thomas, A. Yoshimura, and E. Legius. "Germline Loss-of-Function Mutations in Spred1 Cause a Neurofibromatosis 1-Like Phenotype." *Nat Genet* 39, no. 9 (2007): 1120-6.

Brems, H., E. Pasmant, R. Van Minkelen, K. Wimmer, M. Upadhyaya, E. Legius, and L. Messiaen. "Review and Update of Spred1 Mutations Causing Legius Syndrome." *Hum Mutat* 33, no. 11 (2012): 1538-46.

Campbell, S. L., R. Khosravi-Far, K. L. Rossman, G. J. Clark, and C. J. Der. "Increasing Complexity of Ras Signaling." *Oncogene* 17, no. 11 Reviews (1998): 1395-413.

Castner, S. A., and G. V. Williams. "Tuning the Engine of Cognition: A Focus on Nmda/D1 Receptor Interactions in Prefrontal Cortex." *Brain Cogn* 63, no. 2 (2007): 94-122.

Cenci, M. A. "Dopamine Dysregulation of Movement Control in L-Dopa-Induced Dyskinesia." *Trends Neurosci* 30, no. 5 (2007): 236-43.

Cepeda, C., V. M. Andre, I. Yamazaki, N. Wu, M. Kleiman-Weiner, and M. S. Levine. "Differential Electrophysiological Properties of Dopamine D1 and D2 Receptor-Containing Striatal Medium-Sized Spiny Neurons." *Eur J Neurosci* 27, no. 3 (2008): 671-82.

Cepeda, C., N. A. Buchwald, and M. S. Levine. "Neuromodulatory Actions of Dopamine in the Neostriatum Are Dependent Upon the Excitatory Amino Acid Receptor Subtypes Activated." *Proc Natl Acad Sci U S A* 90, no. 20 (1993): 9576-80.

Cepeda, C., and M. S. Levine. "Dopamine and N-Methyl-D-Aspartate Receptor Interactions in the Neostriatum." *Dev Neurosci* 20, no. 1 (1998): 1-18.

Chadee, D. N., M. J. Hendzel, C. P. Tylipski, C. D. Allis, D. P. Bazett-Jones, J. A. Wright, and J. R. Davie. "Increased Ser-10 Phosphorylation of Histone H3 in Mitogen-Stimulated and Oncogene-Transformed Mouse Fibroblasts." *J Biol Chem* 274, no. 35 (1999): 24914-20.

Citro, S., S. Malik, E. A. Oestreich, J. Radeff-Huang, G. G. Kelley, A. V. Smrcka, and J. H. Brown. "Phospholipase Cepsilon Is a Nexus for Rho and Rap-Mediated G Protein-Coupled Receptor-Induced Astrocyte Proliferation." *Proc Natl Acad Sci U S A* 104, no. 39 (2007): 15543-8.

Coleman, M. L., C. J. Marshall, and M. F. Olson. "Ras and Rho Gtpases in G1-Phase Cell-Cycle Regulation." *Nat Rev Mol Cell Biol* 5, no. 5 (2004): 355-66.

Costa-Mattioli, M., W. S. Sossin, E. Klann, and N. Sonenberg. "Translational Control of Long-Lasting Synaptic Plasticity and Memory." *Neuron* 61, no. 1 (2009): 10-26.

Crosio, C., E. Heitz, C. D. Allis, E. Borrelli, and P. Sassone-Corsi. "Chromatin Remodeling and Neuronal Response: Multiple Signaling Pathways Induce Specific Histone H3 Modifications and Early Gene Expression in Hippocampal Neurons." *J Cell Sci* 116, no. Pt 24 (2003): 4905-14.

D'isa, R., S.L. Clapcote, V. Voikar, D. P. Wolfer, K.-P. Giese, R. Brambilla, and S. Fasano. "Mice Lacking Ras-Grf1 Have Fear Conditioning but Not Spatial Memory Impairments: Convergent Evidence from the Two Independent Murine Mutant Lines Ras-Grf1 Ko and Gena 53." *Front Behav Neurosci* in press, (2011).

Davis, S., and S. Laroche. "Mitogen-Activated Protein Kinase/Extracellular Regulated Kinase Signalling and Memory Stabilization: A Review." *Genes Brain Behav* 5 Suppl 2, (2006): 61-72.

Day, M., D. Wokosin, J. L. Plotkin, X. Tian, and D. J. Surmeier. "Differential Excitability and Modulation of Striatal Medium Spiny Neuron Dendrites." *J Neurosci* 28, no. 45 (2008): 11603-14.

Dobrossy, M., A. Klein, N. Janghra, G. Nikkhah, and S. B. Dunnett. "Validating the Use of M4-Bac-Gfp Mice as Tissue Donors in Cell Replacement Therapies in a Rodent Model of Huntington's Disease." *J Neurosci Methods* 197, no. 1 (2011): 6-13.

Ebinu, J. O., D. A. Bottorff, E. Y. Chan, S. L. Stang, R. J. Dunn, and J. C. Stone. "Rasgrp, a Ras Guanyl Nucleotide- Releasing Protein with Calcium- and Diacylglycerol-Binding Motifs." *Science* 280, no. 5366 (1998): 1082-6.

Edwards, S., D. L. Simmons, D. G. Galindo, J. M. Doherty, A. M. Scott, P. D. Hughes, and R. E. Wilcox. "Antagonistic Effects of Dopaminergic Signaling and Ethanol on Protein Kinase a-Mediated Phosphorylation of Darpp-32 and the Nr1 Subunit of the Nmda Receptor." *Alcohol Clin Exp Res* 26, no. 2 (2002): 173-80.

English, J. D., and J. D. Sweatt. "Activation of P42 Mitogen-Activated Protein Kinase in Hippocampal Long Term Potentiation." *J Biol Chem* 271, no. 40 (1996): 24329-32.

Fahn, S. "The Spectrum of Levodopa-Induced Dyskinesias." *Ann Neurol* 47, no. 4 Suppl 1 (2000): S2-9; discussion S9-11.

_____. "Description of Parkinson's Disease as a Clinical Syndrome." *Ann N Y Acad Sci* 991, (2003): 1-14.

Farnsworth, C. L., N. W. Freshney, Rosen L. B., A. Ghosh, M. E. Greenberg, and L. A. Feig. "Calcium Activation of Ras Mediated by Neuronal Exchange Factor Ras-Grf." *Nature* 376, (1995): 524-526.

Fasano, S., E. Bezard, A. D'Antoni, M. Indrigo, V. Francardo, L. Qin, S. Dovero, M. Cerovic, M. A. Cenci, and R. Brambilla. "Inhibition of Ras-Grf1 in the Striatum Reverts Motor Symptoms Associated to L-Dopa Induced Dyskinesia." *Proc Natl Acad Sci U S A* Epub, 29 Nov, (2010).

Fasano, S., and R. Brambilla. "Ras-Erk Signaling in Behavior: Old Questions and New Perspectives." *Front. Behav. Neurosci* in press, (2011).

Fasano, S., A. D'Antoni, P. C. Orban, E. Valjent, E. Putignano, H. Vara, T. Pizzorusso, M. Giustetto, B. Yoon, P. Soloway, R. Maldonado, J. Caboche, and R. Brambilla. "Ras-Guanine Nucleotide-Releasing Factor 1 (Ras-Grf1) Controls Activation of Extracellular Signal-Regulated Kinase (Erk) Signaling in the Striatum and Long-Term Behavioral Responses to Cocaine." *Biol Psychiatry*, (2009).

Ferguson, S. M., S. Fasano, P. Yang, R. Brambilla, and T. E. Robinson. "Knockout of Erk1 Enhances Cocaine-Evoked Immediate Early Gene Expression and Behavioral Plasticity." *Neuropsychopharmacology* 31, no. 12 (2006): 2660-8.

Feyder, M., A. Bonito-Oliva, and G. Fisone. "L-Dopa-Induced Dyskinesia and Abnormal Signaling in Striatal Medium Spiny Neurons: Focus on Dopamine D1 Receptor-Mediated Transmission." *Front Behav Neurosci* 5, (2011): 71.

Flau, K., A. Redmer, S. Liedtke, M. Kathmann, and E. Schlicker. "Inhibition of Striatal and Retinal Dopamine Release Via Nociceptin/Orphanin Fq Receptors." *Br J Pharmacol* 137, no. 8 (2002): 1355-61.

Follett, K. A. "Comparison of Pallidal and Subthalamic Deep Brain Stimulation for the Treatment of Levodopa-Induced Dyskinesias." *Neurosurg Focus* 17, no. 1 (2004): E3.

Gerfen, C. R. "D1 Dopamine Receptor Supersensitivity in the Dopamine-Depleted Striatum Animal Model of Parkinson's Disease." *Neuroscientist* 9, no. 6 (2003): 455-62.

Guridi, J., M. C. Rodriguez-Oroz, J. Arbizu, M. Alegre, E. Prieto, I. Landecho, M. Manrique, J. Artieda, and J. A. Obeso. "Successful Thalamic Deep Brain Stimulation for Orthostatic Tremor." *Mov Disord* 23, no. 13 (2008): 1808-11.

Hakansson, K., S. Galdi, J. Hendrick, G. Snyder, P. Greengard, and G. Fisone. "Regulation of Phosphorylation of the Glur1 Ampa Receptor by Dopamine D2 Receptors." *J Neurochem* 96, no. 2 (2006): 482-8.

Hebert, A. E., and P. K. Dash. "Extracellular Signal-Regulated Kinase Activity in the Entorhinal Cortex Is Necessary for Long-Term Spatial Memory." *Learning & memory* 9, no. 4 (2002): 156-66.

Hernandez-Lopez, S., T. Tkatch, E. Perez-Garci, E. Galarraga, J. Bargas, H. Hamm, and D. J. Surmeier. "D2 Dopamine Receptors in Striatal Medium Spiny Neurons Reduce L-Type Ca2+ Currents and Excitability Via a Novel Plc[Beta]1-Ip3-Calcineurin-Signaling Cascade." *J Neurosci* 20, no. 24 (2000): 8987-95.

Herve, D., C. Le Moine, J. C. Corvol, L. Belluscio, C. Ledent, A. A. Fienberg, M. Jaber, J. M. Studler, and J. A. Girault. "Galpha(Olf) Levels Are Regulated by Receptor Usage and Control Dopamine and Adenosine Action in the Striatum." *J Neurosci* 21, no. 12 (2001): 4390-9.

Higley, M. J., and B. L. Sabatini. "Competitive Regulation of Synaptic Ca2+ Influx by D2 Dopamine and A2a Adenosine Receptors." *Nat Neurosci* 13, no. 8 (2010): 958-66.

Hurley, M. J., D. C. Mash, and P. Jenner. "Dopamine D(1) Receptor Expression in Human Basal Ganglia and Changes in Parkinson's Disease." *Brain Res Mol Brain Res* 87, no. 2 (2001): 271-9.

Indrigo, M., A. Papale, D. Orellana, and R. Brambilla. "Lentiviral Vectors to Study the Differential Function of Erk1 and Erk2 Map Kinases." *Methods Mol Biol* 661, (2010): 205-20.

Jenner, P. "Molecular Mechanisms of L-Dopa-Induced Dyskinesia." *Nat Rev Neurosci* 9, no. 9 (2008): 665-77.

Johannessen, M., and U. Moens. "Multisite Phosphorylation of the Camp Response Element-Binding Protein (Creb) by a Diversity of Protein Kinases." *Front Biosci* 12, (2007): 1814-32.

Kaphzan, H., K. J. O'Riordan, K. P. Mangan, J. M. Levenson, and K. Rosenblum. "Nmda and Dopamine Converge on the Nmda-Receptor to Induce Erk Activation and Synaptic Depression in Mature Hippocampus." *PLoS ONE* 1, (2006): e138.

Kaplan, D. R., and F. D. Miller. "Neurotrophin Signal Transduction in the Nervous System." *Curr Opin Neurobiol* 10, no. 3 (2000): 381-91.

Kelleher, R. J., 3rd, A. Govindarajan, and S. Tonegawa. "Translational Regulatory Mechanisms in Persistent Forms of Synaptic Plasticity." *Neuron* 44, no. 1 (2004): 59-73.

Kelly, A., S. Laroche, and S. Davis. "Activation of Mitogen-Activated Protein Kinase/Extracellular Signal-Regulated Kinase in Hippocampal Circuitry Is Required for Consolidation and Reconsolidation of Recognition Memory." *The Journal of neuroscience : the official journal of the Society for Neuroscience* 23, no. 12 (2003): 5354-60.

Kennedy, M. B., H. C. Beale, H. J. Carlisle, and L. R. Washburn. "Integration of Biochemical Signalling in Spines." *Nat Rev Neurosci* 6, no. 6 (2005): 423-34.

Kim, J. H., H. K. Lee, K. Takamiya, and R. L. Huganir. "The Role of Synaptic Gtpase-Activating Protein in Neuronal Development and Synaptic Plasticity." *J Neurosci* 23, no. 4 (2003): 1119-24.

Klann, E., and T. E. Dever. "Biochemical Mechanisms for Translational Regulation in Synaptic Plasticity." *Nat Rev Neurosci* 5, no. 12 (2004): 931-42.

Konitsiotis, S., P. J. Blanchet, L. Verhagen, E. Lamers, and T. N. Chase. "Ampa Receptor Blockade Improves Levodopa-Induced Dyskinesia in Mptp Monkeys." *Neurology* 54, no. 8 (2000): 1589-95.

Krack, P., P. Pollak, P. Limousin, A. Benazzouz, and A. L. Benabid. "Stimulation of Subthalamic Nucleus Alleviates Tremor in Parkinson's Disease." *Lancet* 350, no. 9092 (1997): 1675.

Krapivinsky, G., L. Krapivinsky, Y. Manasian, A. Ivanov, R. Tyzio, C. Pellegrino, Y. Ben-Ari, D. E. Clapham, and I. Medina. "The Nmda Receptor Is Coupled to the Erk Pathway by a Direct Interaction between Nr2b and Rasgrf1." *Neuron* 40, no. 4 (2003): 775-84.

Lang, A. E., J. L. Houeto, P. Krack, C. Kubu, K. E. Lyons, E. Moro, W. Ondo, R. Pahwa, W. Poewe, A. I. Troster, R. Uitti, and V. Voon. "Deep Brain Stimulation: Preoperative Issues." *Mov Disord* 21 Suppl 14, (2006): S171-96.

Langston, J. W., and P. A. Ballard, Jr. "Parkinson's Disease in a Chemist Working with 1-Methyl-4-Phenyl-1,2,5,6-Tetrahydropyridine." *N Engl J Med* 309, no. 5 (1983): 310.

Lee, F. J., S. Xue, L. Pei, B. Vukusic, N. Chery, Y. Wang, Y. T. Wang, H. B. Niznik, X. M. Yu, and F. Liu. "Dual Regulation of Nmda Receptor Functions by Direct Protein-Protein Interactions with the Dopamine D1 Receptor." *Cell* 111, no. 2 (2002): 219-30.

Lefloch, R., J. Pouyssegur, and P. Lenormand. "Single and Combined Silencing of Erk1 and Erk2 Reveals Their Positive Contribution to Growth Signaling Depending on Their Expression Levels." *Mol Cell Biol* 28, no. 1 (2008): 511-27.

Limousin, P., P. Krack, P. Pollak, A. Benazzouz, C. Ardouin, D. Hoffmann, and A. L. Benabid. "Electrical Stimulation of the Subthalamic Nucleus in Advanced Parkinson's Disease." *N Engl J Med* 339, no. 16 (1998): 1105-11.

Mahadevan, L. C., A. C. Willis, and M. J. Barratt. "Rapid Histone H3 Phosphorylation in Response to Growth Factors, Phorbol Esters, Okadaic Acid, and Protein Synthesis Inhibitors." *Cell* 65, no. 5 (1991): 775-83.

Marshall, C. J. "Ras Effectors." *Curr Opin Cell Biol* 8, no. 2 (1996): 197-204.

Marti, M., F. Mela, M. Fantin, S. Zucchini, J. M. Brown, J. Witta, M. Di Benedetto, B. Buzas, R. K. Reinscheid, S. Salvadori, R. Guerrini, P. Romualdi, S. Candeletti, M. Simonato, B. M. Cox, and M. Morari. "Blockade of Nociceptin/Orphanin Fq Transmission Attenuates Symptoms and Neurodegeneration Associated with Parkinson's Disease." *J Neurosci* 25, no. 42 (2005): 9591-601.

Marti, M., F. Mela, C. Veronesi, R. Guerrini, S. Salvadori, M. Federici, N. B. Mercuri, A. Rizzi, G. Franchi, L. Beani, C. Bianchi, and M. Morari. "Blockade of Nociceptin/Orphanin Fq Receptor Signaling in Rat Substantia Nigra Pars Reticulata Stimulates Nigrostriatal Dopaminergic Transmission and Motor Behavior." *J Neurosci* 24, no. 30 (2004): 6659-66.

Marti, M., D. Rodi, Q. Li, R. Guerrini, S. Fasano, I. Morella, A. Tozzi, R. Brambilla, P. Calabresi, M. Simonato, E. Bezard, and M. Morari. "Nociceptin/Orphanin Fq Receptor Agonists Attenuate L-Dopa-Induced Dyskinesias." *J Neurosci* 32, no. 46 (2012): 16106-16119.

Marti, M., C. Trapella, and M. Morari. "The Novel Nociceptin/Orphanin Fq Receptor Antagonist Trap-101 Alleviates Experimental Parkinsonism through Inhibition of the Nigro-Thalamic Pathway: Positive Interaction with L-Dopa." *J Neurochem* 107, no. 6 (2008): 1683-96.

Martin, K. C., M. Barad, and E. R. Kandel. "Local Protein Synthesis and Its Role in Synapse-Specific Plasticity." *Curr Opin Neurobiol* 10, no. 5 (2000): 587-92.

Matamales, M., and J. A. Girault. "Signaling from the Cytoplasm to the Nucleus in Striatal Medium-Sized Spiny Neurons." *Front Neuroanat* 5, (2011): 37.

Mattingly, R. R. "Phosphorylation of Serine 916 of Ras-Grf1 Contributes to the Activation of Exchange Factor Activity by Muscarinic Receptors." *J Biol Chem* 274, no. 52 (1999): 37379-84.

Mayergoyz, I. D., Z. Zhang, and G. Miano. "Analysis of Dynamics of Excitation and Dephasing of Plasmon Resonance Modes in Nanoparticles." *Phys Rev Lett* 98, no. 14 (2007): 147401.

Mazzucchelli, C., C. Vantaggiato, A. Ciamei, S. Fasano, A. Porrazzo, P. C. Orban, P. Pakhotin, W. Krezel, H. Wezl, D. P. Wolfer, G. Pages, O. Valverde, A. Marowsky, R. Maldonado, M. U. Ehrengruber, V. Cestari, H.-P. Lipp, P. F. Chapman, J. Pouyssegur, and R. Brambilla. "Knockout of Erk1 Map Kinase Enhances Synaptic Plasticity in the Striatum and Facilitates Striatal-Mediated Learning and Memory." *Neuron* 34, (2002): 807-820.

Miyamoto, E. "Molecular Mechanism of Neuronal Plasticity: Induction and Maintenance of Long-Term Potentiation in the Hippocampus." *J Pharmacol Sci* 100, no. 5 (2006): 433-42.

Nazzaro, C., S. Marino, M. Barbieri, and A. Siniscalchi. "Inhibition of Serotonin Outflow by Nociceptin/Orphaninfq in Dorsal Raphe Nucleus Slices from Normal and Stressed Rats: Role of Corticotropin Releasing Factor." *Neurochem Int* 54, no. 5-6 (2009): 378-84.

Nicklas, W. J., I. Vyas, and R. E. Heikkila. "Inhibition of Nadh-Linked Oxidation in Brain Mitochondria by 1-Methyl-4-Phenyl-Pyridine, a Metabolite of the Neurotoxin, 1-Methyl-4-Phenyl-1,2,5,6-Tetrahydropyridine." *Life Sci* 36, no. 26 (1985): 2503-8.

Nutt, J. G. "Levodopa-Induced Dyskinesia: Review, Observations, and Speculations." *Neurology* 40, no. 2 (1990): 340-5.

Nutt, J. G., W. R. Woodward, J. H. Carter, and S. T. Gancher. "Effect of Long-Term Therapy on the Pharmacodynamics of Levodopa. Relation to on-Off Phenomenon." *Arch Neurol* 49, no. 11 (1992): 1123-30.

Olianas, M. C., S. Dedoni, M. Boi, and P. Onali. "Activation of Nociceptin/Orphanin Fq-Nop Receptor System Inhibits Tyrosine Hydroxylase Phosphorylation, Dopamine Synthesis, and

Dopamine D(1) Receptor Signaling in Rat Nucleus Accumbens and Dorsal Striatum." *J Neurochem* 107, no. 2 (2008): 544-56.

Pagès, G., S. Guerin, D. Grall, F. Bonino, A. Smith, F. Anjuere, P. Auberger, and J. Pouysségur. "Defective Thymocyte Maturation in P44 Map Kinase (Erk 1) Knockout Mice." *Science* 286, no. 5443 (1999): 1374-7.

Pandit, B., A. Sarkozy, L. A. Pennacchio, C. Carta, K. Oishi, S. Martinelli, E. A. Pogna, W. Schackwitz, A. Ustaszewska, A. Landstrom, J. M. Bos, S. R. Ommen, G. Esposito, F. Lepri, C. Faul, P. Mundel, J. P. Lopez Siguero, R. Tenconi, A. Selicorni, C. Rossi, L. Mazzanti, I. Torrente, B. Marino, M. C. Digilio, G. Zampino, M. J. Ackerman, B. Dallapiccola, M. Tartaglia, and B. D. Gelb. "Gain-of-Function Raf1 Mutations Cause Noonan and Leopard Syndromes with Hypertrophic Cardiomyopathy." *Nat Genet* 39, no. 8 (2007): 1007-12.

Pascoli, V., A. Besnard, D. Herve, C. Pages, N. Heck, J. A. Girault, J. Caboche, and P. Vanhoutte. "Cyclic Adenosine Monophosphate-Independent Tyrosine Phosphorylation of Nr2b Mediates Cocaine-Induced Extracellular Signal-Regulated Kinase Activation." *Biol Psychiatry* 69, no. 3 (2010): 218-27.

Pavon, N., A. B. Martin, A. Mendialdua, and R. Moratalla. "Erk Phosphorylation and Fosb Expression Are Associated with L-Dopa-Induced Dyskinesia in Hemiparkinsonian Mice." *Biol Psychiatry* 59, no. 1 (2006): 64-74.

Pearson, G., F. Robinson, T. Beers Gibson, B. E. Xu, M. Karandikar, K. Berman, and M. H. Cobb. "Mitogen-Activated Protein (Map) Kinase Pathways: Regulation and Physiological Functions." *Endocr Rev* 22, no. 2 (2001): 153-83.

Pei, L., F. J. Lee, A. Moszczynska, B. Vukusic, and F. Liu. "Regulation of Dopamine D1 Receptor Function by Physical Interaction with the Nmda Receptors." *J Neurosci* 24, no. 5 (2004): 1149-58.

Przedborski, S., and V. Jackson-Lewis. "Mechanisms of Mptp Toxicity." *Mov Disord* 13 Suppl 1, (1998): 35-8.

Razzaque, M. A., T. Nishizawa, Y. Komoike, H. Yagi, M. Furutani, R. Amo, M. Kamisago, K. Momma, H. Katayama, M. Nakagawa, Y. Fujiwara, M. Matsushima, K. Mizuno, M. Tokuyama, H. Hirota, J. Muneuchi, T. Higashinakagawa, and R. Matsuoka. "Germline Gain-of-Function Mutations in Raf1 Cause Noonan Syndrome." *Nat Genet* 39, no. 8 (2007): 1013-7.

Richter, J. D., and N. Sonenberg. "Regulation of Cap-Dependent Translation by Eif4e Inhibitory Proteins." *Nature* 433, no. 7025 (2005): 477-80.

Robinson, K. N., K. Manto, R. J. Buchsbaum, J. I. MacDonald, and S. O. Meakin. "Neurotrophin-Dependent Tyrosine Phosphorylation of Ras Guanine-Releasing Factor 1 and Associated Neurite Outgrowth Is Dependent on the Hike Domain of Trka." *J Biol Chem* 280, no. 1 (2005): 225-35.

Rodriguez-Viciana, P., P. H. Warne, B. Vanhaesebroeck, M. D. Waterfield, and J. Downward. "Activation of Phosphoinositide 3-Kinase by Interaction with Ras and by Point Mutation." *EMBO J.* 15, no. 10 (1996): 2442-2451.

Roux, P. P., D. Shahbazian, H. Vu, M. K. Holz, M. S. Cohen, J. Taunton, N. Sonenberg, and J. Blenis. "Ras/Erk Signaling Promotes Site-Specific Ribosomal Protein S6 Phosphorylation Via Rsk and Stimulates Cap-Dependent Translation." *J Biol Chem* 282, no. 19 (2007): 14056-64.

Rubino, T., G. Forlani, D. Vigano, R. Zippel, and D. Parolaro. "Modulation of Extracellular Signal-Regulated Kinases Cascade by Chronic Delta 9-Tetrahydrocannabinol Treatment." *Mol Cell Neurosci* 25, no. 3 (2004): 355-62.

Ruvinsky, I., and O. Meyuhas. "Ribosomal Protein S6 Phosphorylation: From Protein Synthesis to Cell Size." *Trends Biochem Sci* 31, no. 6 (2006): 342-8.

Saba-El-Leil, M. K., F. D. Vella, B. Vernay, L. Voisin, L. Chen, N. Labrecque, S. L. Ang, and S. Meloche. "An Essential Function of the Mitogen-Activated Protein Kinase Erk2 in Mouse Trophoblast Development." *EMBO Rep* 4, no. 10 (2003): 964-8.

Samuels, I. S., S. C. Saitta, and G. E. Landreth. "Map'ing Cns Development and Cognition: An Erksome Process." *Neuron* 61, no. 2 (2009): 160-7.

Santini, E., C. Alcacer, S. Cacciatore, M. Heiman, D. Herve, P. Greengard, J. A. Girault, E. Valjent, and G. Fisone. "L-Dopa Activates Erk Signaling and Phosphorylates Histone H3 in the Striatonigral Medium Spiny Neurons of Hemiparkinsonian Mice." *J Neurochem* 108, no. 3 (2009): 621-33.

Santini, E., M. Heiman, P. Greengard, E. Valjent, and G. Fisone. "Inhibition of Mtor Signaling in Parkinson's Disease Prevents L-Dopa-Induced Dyskinesia." *Sci Signal* 2, no. 80 (2009): ra36.

Santini, E., E. Valjent, and G. Fisone. "Mtorc1 Signaling in Parkinson's Disease and L-Dopa-Induced Dyskinesia: A Sensitized Matter." *Cell Cycle* 9, no. 14: 2713-8.

Santini, E., E. Valjent, A. Usiello, M. Carta, A. Borgkvist, J. A. Girault, D. Herve, P. Greengard, and G. Fisone. "Critical Involvement of Camp/Darpp-32 and Extracellular Signal-Regulated Protein Kinase Signaling in L-Dopa-Induced Dyskinesia." *J Neurosci* 27, no. 26 (2007): 6995-7005.

Satoh, Y., S. Endo, T. Ikeda, K. Yamada, M. Ito, M. Kuroki, T. Hiramoto, O. Imamura, Y. Kobayashi, Y. Watanabe, S. Itohara, and K. Takishima. "Extracellular Signal-Regulated Kinase 2 (Erk2) Knockdown Mice Show Deficits in Long-Term Memory; Erk2 Has a Specific Function in Learning and Memory." *J Neurosci* 27, no. 40 (2007): 10765-76.

Sbrenna, S., M. Marti, M. Morari, G. Calo, R. Guerrini, L. Beani, and C. Bianchi. "Modulation of 5-Hydroxytryptamine Efflux from Rat Cortical Synaptosomes by Opioids and Nociceptin." *Br J Pharmacol* 130, no. 2 (2000): 425-33.

Schafe, G. E., C. M. Atkins, M. W. Swank, E. P. Bauer, J. D. Sweatt, and J. E. LeDoux. "Activation of Erk/Map Kinase in the Amygdala Is Required for Memory Consolidation of Pavlovian Fear Conditioning." *J Neurosci* 20, no. 21 (2000): 8177-87.

Schubbert, S., K. Shannon, and G. Bollag. "Hyperactive Ras in Developmental Disorders and Cancer." *Nat Rev Cancer* 7, no. 4 (2007): 295-308.

Selcher, J. C., C. M. Atkins, J. M. Trzaskos, R. Paylor, and J. D. Sweatt. "A Necessity for Map Kinase Activation in Mammalian Spatial Learning." *Learn Mem* 6, no. 5 (1999): 478-90.

Sgambato, V., C. Pages, M. Rogard, M. J. Besson, and J. Caboche. "Extracellular Signal-Regulated Kinase (Erk) Controls Immediate Early Gene Induction on Corticostriatal Stimulation." *J Neurosci* 18, no. 21 (1998): 8814-25.

Sheng, M., and M. J. Kim. "Postsynaptic Signaling and Plasticity Mechanisms." *Science* 298, no. 5594 (2002): 776-80.

Shou, C., A. Wurmser, K. Ling, M. Barbacid, and L. A. Feig. "Differential Response of the Ras Exchange Factor, Ras-Grf to Tyrosine Kinase and G Protein Mediated Signal." *Oncogene* 10, (1995): 1887-1893.

Snyder, G. L., A. A. Fienberg, R. L. Huganir, and P. Greengard. "A Dopamine/D1 Receptor/Protein Kinase a/Dopamine- and Camp-Regulated Phosphoprotein (Mr 32 Kda)/Protein Phosphatase-1 Pathway Regulates Dephosphorylation of the Nmda Receptor." *J Neurosci* 18, no. 24 (1998): 10297-303.

Stornetta, R. L., and J. J. Zhu. "Ras and Rap Signaling in Synaptic Plasticity and Mental Disorders." *Neuroscientist* 17, no. 1 (2011): 54-78.

Svenningsson, P., A. Nishi, G. Fisone, J. A. Girault, A. C. Nairn, and P. Greengard. "Darpp-32: An Integrator of Neurotransmission." *Annu Rev Pharmacol Toxicol* 44, (2004): 269-96.

Swank, M. W. "Conditioned C-Fos in Mouse Nts During Expression of a Learned Taste Aversion Depends on Contextual Cues." *Brain research* 862, no. 1-2 (2000): 138-44.

Sweatt, J. D. "The Neuronal Map Kinase Cascade: A Biochemical Signal Integration System Subserving Synaptic Plasticity and Memory." *J Neurochem* 76, no. 1 (2001): 1-10.

Tao, R., Z. Ma, M. M. Thakkar, R. W. McCarley, and S. B. Auerbach. "Nociceptin/Orphanin Fq Decreases Serotonin Efflux in the Rat Brain but in Contrast to a Kappa-Opioid Has No Antagonistic Effect on Mu-Opioid-Induced Increases in Serotonin Efflux." *Neuroscience* 147, no. 1 (2007): 106-16.

Thomas, G. M., and R. L. Huganir. "Mapk Cascade Signalling and Synaptic Plasticity." *Nat Rev Neurosci* 5, no. 3 (2004): 173-83.

Toda, H., C. Hamani, and A. Lozano. "Deep Brain Stimulation in the Treatment of Dyskinesia and Dystonia." *Neurosurg Focus* 17, no. 1 (2004): E2.

Toki, S., H. Kawasaki, N. Tashiro, D. E. Housman, and A. M. Graybiel. "Guanine Nucleotide Exchange Factors Caldag-Gefi and Caldag-Gefii Are Colocalized in Striatal Projection Neurons." *J Comp Neurol* 437, no. 4 (2001): 398-407.

Trifilieff, P., J. Lavaur, V. Pascoli, V. Kappes, K. Brami-Cherrier, C. Pages, J. Micheau, J. Caboche, and P. Vanhoutte. "Endocytosis Controls Glutamate-Induced Nuclear Accumulation of Erk." *Mol Cell Neurosci* 41, no. 3 (2009): 325-36.

Turjanski, N., A. J. Lees, and D. J. Brooks. "In Vivo Studies on Striatal Dopamine D1 and D2 Site Binding in L-Dopa-Treated Parkinson's Disease Patients with and without Dyskinesias." *Neurology* 49, no. 3 (1997): 717-23.

Vaillant, A. R., P. Zanassi, G. S. Walsh, A. Aumont, A. Alonso, and F. D. Miller. "Signaling Mechanisms Underlying Reversible, Activity-Dependent Dendrite Formation." *Neuron* 34, no. 6 (2002): 985-98.

Valjent, E., J. Bertran-Gonzalez, H. Bowling, S. Lopez, E. Santini, M. Matamales, A. Bonito-Oliva, D. Herve, C. Hoeffer, E. Klann, J. A. Girault, and G. Fisone. "Haloperidol Regulates the State of Phosphorylation of Ribosomal Protein S6 Via Activation of Pka and Phosphorylation of Darpp-32." *Neuropsychopharmacology* 36, no. 12 (2011): 2561-70.

Valjent, E., J. C. Corvol, J. M. Trzaskos, J. A. Girault, and D. Herve. "Role of the Erk Pathway in Psychostimulant-Induced Locomotor Sensitization." *BMC Neurosci* 7, (2006): 20.

Valjent, E., V. Pascoli, P. Svenningsson, S. Paul, H. Enslen, J. C. Corvol, A. Stipanovich, J. Caboche, P. J. Lombroso, A. C. Nairn, P. Greengard, D. Herve, and J. A. Girault. "Regulation of a Protein Phosphatase Cascade Allows Convergent Dopamine and Glutamate Signals to Activate Erk in the Striatum." *Proc Natl Acad Sci U S A* 102, no. 2 (2005): 491-6.

Vanhoutte, P., J. V. Barnier, B. Guibert, C. Pages, M. J. Besson, R. A. Hipskind, and J. Caboche. "Glutamate Induces Phosphorylation of Elk-1 and Creb, Along with C-Fos Activation, Via an Extracellular Signal-Regulated Kinase-Dependent Pathway in Brain Slices." *Mol Cell Biol* 19, no. 1 (1999): 136-46.

Vantaggiato, C., I. Formentini, A. Bondanza, C. Bonini, L. Naldini, and R. Brambilla. "Erk1 and Erk2 Mitogen-Activated Protein Kinases Affect Ras-Dependent Cell Signaling Differentially." *J Biol* 5, no. 5 (2006): 14.

Voisin, L., M. K. Saba-El-Leil, C. Julien, C. Fremin, and S. Meloche. "Genetic Demonstration of a Redundant Role of Extracellular Signal-Regulated Kinase 1 (Erk1) and Erk2 Mitogen-Activated Protein Kinases in Promoting Fibroblast Proliferation." *Mol Cell Biol* 30, no. 12 (2010): 2918-32.

Volta, M., M. Marti, J. McDonald, S. Molinari, V. Camarda, M. Pela, C. Trapella, and M. Morari. "Pharmacological Profile and Antiparkinsonian Properties of the Novel Nociceptin/Orphanin Fq Receptor Antagonist 1-[1-Cyclooctylmethyl-5-(1-Hydroxy-1-Methyl-Ethyl)-1,2,3,6-Tetrahydro-Pyridin-4-Y L]-3-Ethyl-1,3-Dihydro-Benzoimidazol-2-One (Gf-4)." *Peptides* 31, no. 6 (2010): 1194-204.

Walz, R., I. C. Rockenbach, O. B. Amaral, J. Quevedo, and R. Roesler. "Mapk and Memory." *Trends Neurosci* 22, no. 11 (1999): 495.

Wennerberg, K., K. L. Rossman, and C. J. Der. "The Ras Superfamily at a Glance." *J Cell Sci* 118, no. Pt 5 (2005): 843-6.

Westin, J. E., L. Vercammen, E. M. Strome, C. Konradi, and M. A. Cenci. "Spatiotemporal Pattern of Striatal Erk1/2 Phosphorylation in a Rat Model of L-Dopa-Induced Dyskinesia and the Role of Dopamine D1 Receptors." *Biol Psychiatry* 62, no. 7 (2007): 800-10.

York, R. D., H. Yao, T. Dillon, C. L. Ellig, S. P. Eckert, E. W. McCleskey, and P. J. Stork. "Rap1 Mediates Sustained Map Kinase Activation Induced by Nerve Growth Factor [See Comments]." *Nature* 392, no. 6676 (1998): 622-6.

Zhu, J. J., Y. Qin, M. Zhao, L. Van Aelst, and R. Malinow. "Ras and Rap Control Ampa Receptor Trafficking During Synaptic Plasticity." *Cell* 110, no. 4 (2002): 443-55.

Zippel, R., N. Gnesutta, N. Matus-Leibovitch, E. Mancinelli, D. Saya, Z. Vogel, and E. Sturani. "Ras-Grf, the Activator of Ras, Is Expressed Preferentially in Mature Neurons of the Central Nervous System." *Mol. Brain Res.* 48, (1997): 140-144.

# Acknowledgements

Giunta alla fine di questo percorso, vorrei ringraziare tutti coloro che mi sono stati di supporto in questi ultimi anni.

Innanzitutto, un enorme grazie va a mamma e papà per il sostegno, l'incoraggiamento e per i sacrifici fatti per farmi felice.

Vorrei inoltre esprimere la mia gratitudine alla Prof. Renata Zippel, per avermi fatto appassionare a questo lavoro, incoraggiandomi a intraprendere il dottorato e soprattutto perchè la sua porta è stata sempre aperta per me. E' stato sicuramente un onore e un privilegio essere un suo studente.

Vorrei anche ringraziare Riccardo che mi ha accolto nel suo laboratorio, seguendomi con disponibilità e attenzione nonostante i numerosi impegni, e mi ha insegnato a lavorare con serietà e rigore.

Inoltre, vorrei ringraziare Stefania, Marzia, Milica, Alessandro, Nicola, Raffaele, per la collaborazione e l'aiuto che mi hanno dato tutte le volte in cui ne ho avuto bisogno, ma anche per avermi fatto sorridere, rendendo piu' leggeri questi ultimi mesi. Grazie anche ai nuovi arrivi Livia, Francesca ed Elena e agli ex Daniel, Martina e Aura, per il supporto morale.

Grazie Loris e Francesco per avermi fatto divertire molto, ma soprattutto per essere stati dei buoni amici su cui ho potuto contare.

Infine, ringrazio gli ex colleghi del 5B degli Edifici Biologici: Graziano, per la risaputa pazienza e saggezza, nonchè Enrico, Silvia, Alessandra, Francesca e Renato.

# PART II

## List of papers included:

Marti M., Rodi D., Li Q., Guerrini R., Fasano S., **Morella I.**, Tozzi A., Brambilla R., Calabresi P., Simonato M., Bezard E., and Morari M. "Nociceptin/Orphanin FQ Receptor Agonists Attenuate L-DOPA-Induced Dyskinesias" published in The Journal of Neuroscience, November 14, 2012; 32(46):16106 –16119

Orellana D., **Morella I.**, Indrigo M., Papale A., and Brambilla R. "The Extracellular Signal-Regulated Kinase (ERK) Cascade in Neuronal Cell Signaling" published in Protein Kinase Technologies, Neuromethods, vol. 68, Hideyuki Mukai (ed.), DOI 10.1007/978-1-61779-824-5_8

Longoni M., Moncini S., Cisternino M., **Morella I.**, Ferraiuolo S., Russo S., Mannarino S., Brazzelli V., Coi P., Zippel R., Venturin M., and Riva P. "Noonan Syndrome Associated With Both a New Jnk-Activating Familial SOS1 and a De Novo RAF1 Mutations" published in American Journal of Medical Genetics, September 2010; 152A(9):2176-84

Cerovic M., Picconi B., Ghiglieri V., Fasano S., **Morella I.**, Heuer A., Marchisella F., Camaleonti L., Hardingham N., Calabresi P., and Brambilla R. "Ras-GRF1 controls ERK-mediated long-term potentiation at the cortico-striatal synapse: implications for L-DOPA induced Dyskinesia" submitted to PNAS, under review

Neurobiology of Disease

# Nociceptin/Orphanin FQ Receptor Agonists Attenuate L-DOPA-Induced Dyskinesias

**Matteo Marti,[1] Donata Rodi,[1] Qin Li,[2] Remo Guerrini,[3] Stefania Fasano,[4] Ilaria Morella,[4] Alessandro Tozzi,[5,6] Riccardo Brambilla,[4] Paolo Calabresi,[5,6] Michele Simonato,[1] Erwan Bezard,[2,7,8] and Michele Morari[1]**

[1]Department of Experimental and Clinical Medicine, Section of Pharmacology, University of Ferrara and National Institute of Neuroscience, 44100 Ferrara Italy; [2]Institute of Laboratory Animal Sciences, China Academy of Medical Sciences, 100864 Beijing, China; [3]Department of Pharmaceutical Sciences, University of Ferrara, Ferrara, 44100 Italy; [4]Institute of Experimental Neurology, Division of Neuroscience, San Raffaele Scientific Institute and University, 20123 Milano, Italy; [5]Clinica Neurologica, Dip. Specialità Medico-Chirurgiche e Sanità Pubblica, Università di Perugia, Ospedale Santa Maria della Misericordia, 06123 Perugia, Italy; [6]Fondazione Santa Lucia, Istituto di Ricovero e Cura a Carattere Scientifico, 00179 Rome, Italy; [7]Université de Bordeaux, Institut des Maladies Neurodégénératives, UMR 5293, Bordeaux, F-33000 France; and [8]Centre National de la Recherche Scientifique, Institut des Maladies Neurodégénératives, UMR 5293, Bordeaux, F-33000 France

**In the present study we investigated whether the neuropeptide nociceptin/orphanin FQ (N/OFQ), previously implicated in the pathogenesis of Parkinson's disease, also affects L-DOPA-induced dyskinesia. In striatal slices of naive rodents, N/OFQ (0.1–1 $\mu$M) prevented the increase of ERK phosphorylation and the loss of depotentiation of synaptic plasticity induced by the D1 receptor agonist SKF38393 in spiny neurons. *In vivo*, exogenous N/OFQ (0.03–1 nmol, i.c.v.) or a synthetic N/OFQ receptor agonist given systemically (0.01–1 mg/Kg) attenuated dyskinesias expression in 6-hydroxydopamine hemilesioned rats primed with L-DOPA, without causing primary hypolocomotive effects. Conversely, N/OFQ receptor antagonists worsened dyskinesia expression. *In vivo* microdialysis revealed that N/OFQ prevented dyskinesias simultaneously with its neurochemical correlates such as the surge of nigral GABA and glutamate, and the reduction of thalamic GABA. Regional microinjections revealed that N/OFQ attenuated dyskinesias more potently and effectively when microinjected in striatum than substantia nigra (SN) reticulata, whereas N/OFQ receptor antagonists were ineffective in striatum but worsened dyskinesias when given in SN. Quantitative autoradiography showed an increase in N/OFQ receptor binding in striatum and a reduction in SN of both unprimed and dyskinetic 6-hydroxydopamine rats, consistent with opposite adaptive changes of N/OFQ transmission. Finally, the N/OFQ receptor synthetic agonist also reduced dyskinesia expression in 1-methyl-4-phenyl-1,2,3,6-tetrahydropyridine-treated dyskinetic macaques without affecting the global parkinsonian score. We conclude that N/OFQ receptor agonists may represent a novel strategy to counteract L-DOPA-induced dyskinesias. Their action is possibly mediated by upregulated striatal N/OFQ receptors opposing the D1 receptor-mediated overactivation of the striatonigral direct pathway.**

## Introduction

Nociceptin/orphanin FQ (N/OFQ) (Meunier et al., 1995; Reinscheid et al., 1995) and its receptor (NOP) represent a neuropeptide system bearing structural and functional analogies with classical opioid systems but unique pharmacological profile (Calò et al., 2000). NOP receptor expression and binding are widespread throughout the rodent and primate brain, supporting the role of the N/OFQ-NOP receptor system in the modulation of central functions such as sensory nociceptive processing, learning and memory, reward, mood, feeding, stress, and movement (Mogil and Pasternak, 2001; Lambert, 2008).

Preclinical and clinical studies revealed a link between N/OFQ and Parkinson's disease (PD) (Marti et al., 2005, 2010). Indeed, an increase of N/OFQ expression (Marti et al., 2005, 2010; Gouty et al., 2010) and release (Marti et al., 2005) in the substantia nigra (SN) of parkinsonian animals was found, together with an elevation of N/OFQ levels in the CSF of parkinsonian patients (Marti et al., 2010). Consistent with a pathogenic role of endogenous N/OFQ, NOP receptor antagonists reversed parkinsonian-like motor deficits (Marti et al., 2005, 2008; Viaro et al., 2008; Volta et al., 2010), also synergizing with L-3,4-dihydroxyphenylalanine (L-DOPA) (Marti et al., 2007; Visanji et al., 2008; Viaro et al., 2010). Contrary to substantia nigra reticulata (SNr), a reduction in N/OFQ expression was found in the dopamine (DA)-depleted striatum (Marti et al., 2010), suggesting a different adaptive response of striatal N/OFQ transmission in PD. The striatal N/OFQ-NOP receptor system has so far received little attention, possibly due to the low expression of N/OFQ and NOP receptor in the rodent striatum (Neal et al., 1999a,b). Nonetheless, N/OFQ

Received Dec. 22, 2011; revised Sept. 11, 2012; accepted Sept. 14, 2012.

Author contributions: M.M., R.B., P.C., M.S., E.B., and M.M. designed research; M.M., D.R., Q.L., S.F., I.M., and A.T. performed research; R.G. contributed unpublished reagents/analytic tools; M.M., M.S., E.B., and M.M. analyzed data; M.M. wrote the paper.

This work was supported by the Italian Ministry of the University (FIRB n. RBIN047W33, PRIN 2008 n. 2008EJ85RS to M.M.) and the Italian Ministry of Health (Progetto Giovani Ricercatori 2008).

The authors declare no competing financial interests.

Correspondence should be addressed to Michele Morari, Department of Experimental and Clinical Medicine, Section of Pharmacology, University of Ferrara, via Fossato di Mortara 17–19, 44100 Ferrara, Italy. E-mail: m.morari@unife.it.

DOI:10.1523/JNEUROSCI.6408-11.2012

 0270-6474/12/3216106-14$15.00/0

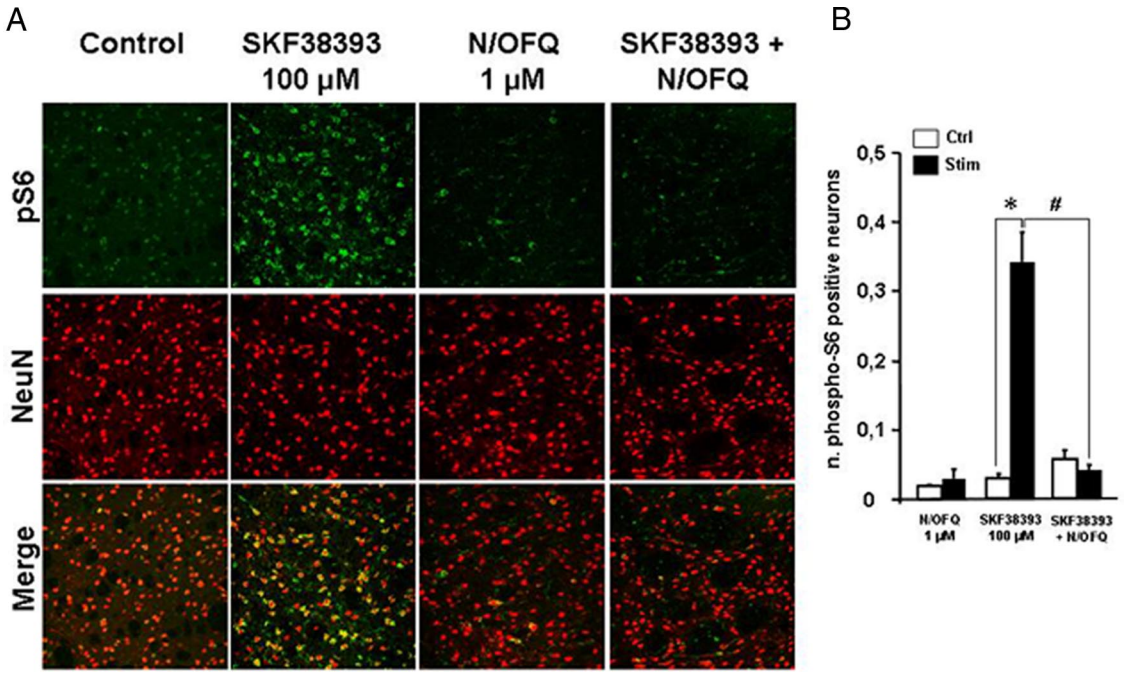


**Figure 1.** N/OFQ inhibited D1 receptor-mediated activation of ERK signaling in mouse striatal slices. ***A***, Representative photomicrographs showing ERK-dependent ribosomal protein S6 phosphorylation (pS6 Thr235/236) (green) and NeuN (red) immunofluorescence in mouse striatal slices in response to SKF38393 (100 $\mu$M), N/OFQ (1 $\mu$M), or their combination. ***B***, Phospho-S6 levels were significantly increased in striatal neurons stimulated with SKF38393 (Student's *t* test, Control vs SKF38393, $t_{(10)} = -6.452$, $^*p = 0.0006$). N/OFQ, ineffective by itself, prevented the effect of SKF38393 (Student's *t* test, Control vs SKF38393 + N/OFQ, $t_{(12)} = 0.947$, $p = 0.363$). One-way ANOVA revealed a significant effect of treatment $F_{(5,31)} = 27.235$, $p > 0.0001$. Bonferroni's *post hoc*, SKF38393 vs SKF38393 + N/OFQ, $\#p < 0.0001$. Data are expressed as number ± SEM of pS6 positive cells with respect to NeuN positive cells. $^*p < 0.05$ different from control. $\#p < 0.05$ different from SKF38393 alone.

impairs the firing activity of ascending DA (Marti et al., 2004) and serotonin (Tao et al., 2007; Nazzaro et al., 2009) neurons, and inhibits DA (Flau et al., 2002; Olianas et al., 2008) and serotonin (Sbrenna et al., 2000) release presynaptically. N/OFQ also postsynaptically counteracts the D1 receptor-stimulated cAMP accumulation in striatal neurons (Olianas et al., 2008), overall suggesting that endogenous N/OFQ might control striatal function. This control might be more relevant in the primate caudate/putamen due to the much greater expression of NOP receptors (Berthele et al., 2003; Bridge et al., 2003). We therefore investigated whether NOP receptor agonists and antagonists affect the expression of L-DOPA-induced dyskinesias (LID) in rats (Cenci et al., 1998) and nonhuman primates (Bézard et al., 2003). Indeed, LID are a major motor complication of L-DOPA pharmacotherapy thought to originate from aberrant striatal plasticity (Calabresi et al., 2010). LID are involuntary choreodystonic movements (Nutt and Gancher, 1994) that develop as a consequence of DA denervation and nonphysiological DA release from both residual DA and serotonin striatal terminals (Carta et al., 2007; Navailles et al., 2010). This leads to "pulsatile" DA receptor stimulation and upregulation of D1 signaling (Andersson et al., 1999; Aubert et al., 2005), increased activity along the Ras/MEK/ERK kinase pathway (Valjent et al., 2005; Feyder et al., 2011) and loss of neuronal depotentiation after long-term potentiation (LTP) induction in striatonigral spiny neurons (Picconi et al., 2003).

## Materials and Methods

### *In vitro* experiments

#### *Immunohistochemistry*

Anesthetized 2-month-old C57BL/6 mice were decapitated and the brains rapidly removed. Slices (200 $\mu$m thick) were cut using a vibratome keeping the brain submerged in ice-cold carboxygenated sucrose-based dissecting solution containing the following (in mM): 87 NaCl, 2.5 KCl, 7 $MgCl_2$, 1 $NaH_2PO_4$, 75 sucrose, 25 $NaHCO_3$, 10 D-glucose, 0.5 $CaCl_2$, and 2 kynurenic acid. The slices were transferred into BSC1 chambers (Scientific System Design) and constantly perfused with carboxygenated artificial CSF solution containing the following (in mM): 124 NaCl, 5 KCl, 1.3 $MgSO_4$, 1.2 $NaH_2PO_4$, 25 $NaHCO_3$, 10 D-glucose, and 2.4 $CaCl_2$ at a constant rate of 2 ml/min at 32°C for 1 h. Slices were then stimulated for 10 min with 100 $\mu$M SKF38393, 1 $\mu$M N/OFQ, or their combination, and fixed in 4% paraformaldehyde in 0.1 M sodium phosphate buffer, pH 7.4, at room temperature for 15 min. Slices were then rinsed three times for 20 min in 0.1 M sodium phosphate buffer, pH 7.4, at room temperature and cryoprotected in 30% sucrose overnight at 4°C.

Eighteen micrometer cryosections were cut and washed three times for 10 min with Dulbecco's PBS (D-PBS). After blocking in D-PBS containing 5% normal goat serum and 0.1% Triton X-100 for 1 h at room temperature, sections were incubated overnight at 4°C with the primary antibodies: anti-phospho-S6 ribosomal protein (Thr235/236) (1:200; Cell signaling Technology) and anti-NeuN (1:1000; Chemicon). Sections were then washed three times for 10 min with D-PBS and incubated for 1 h at room temperature with the secondary antibodies: Alexa Fluor 546 goat anti-mouse (1:200) and Alexa Fluor 488 goat anti-rabbit (1:500) (Invitrogen).

Following the incubation with the secondary antibodies, the sections were washed three times for 10 min with D-PBS and the coverslips were mounted using the fluorescent mounting medium (Dako).

Single- and double-labeled images were obtained using a laser scanning confocal microscopy (Leica SP2), equipped with the corresponding lasers and the appropriate filter sets to avoid cross talk between the fluorophores. Neuronal quantification was performed with ImageJ software on images taken at 40× magnification by counting phospho-S6-immunoreactive neurons among NeuN positive neurons in each slice.

#### *Electrophysiology*

Corticostriatal coronal slices (270 $\mu$m thick) were cut from 1- to 2-month-old male Wistar rats ($n = 12$; Harlan) using a vibratome, as previously described (Calabresi et al., 1998; Picconi et al., 2003). A single

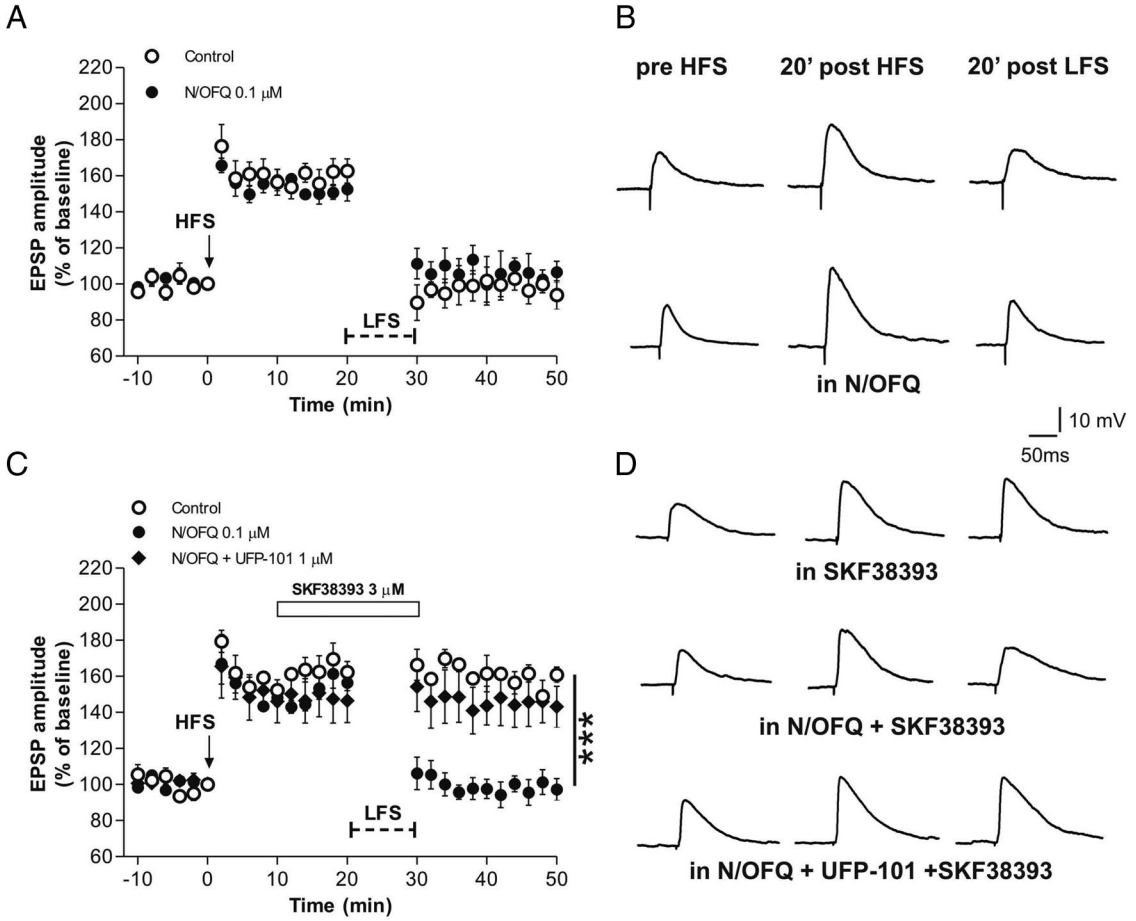


**Figure 2.** N/OFQ restored synaptic depotentiation of MSNs in the presence of a D1 receptor agonist. ***A***, Time course of the HFS-induced LTP followed by the LFS-induced depotentiation of MSN EPSPs in control conditions ($n = 3$, open circles) and in the presence of 0.1 $\mu$M N/OFQ ($n = 3$, filled circles). ***B***, EPSP traces recorded in representative MSNs before HFS (left), and 20 min post-HFS (middle) or LFS (right) in control conditions and in the presence of 0.1 $\mu$M N/OFQ. ***C***, Time course of HFS followed by LFS in the presence of 3 $\mu$M D1 receptor agonist SKF38393 applied for 20 min (white bar). SKF38393 alone prevented depotentiation in MSNs (control, $n = 3$, open circles) whereas N/OFQ reversed this effect ($n = 5$, filled circles). The NOP receptor antagonist UFP-101 (0.1 $\mu$M) counteracted the effect of N/OFQ ($n = 4$, diamonds). ***D***, EPSP traces acquired before HFS and after HFS or LFS in the presence of SKF38393 applied 10 min after HFS (top), N/OFQ + SKF38393 (middle), and N/OFQ + SKF38393 in the presence of UFP-101 (bottom). ***$p < 0.001$ different from control.

slice was then transferred to a recording chamber and submerged in a continuously flowing (2.5–3 ml/min) carboxygenated (95% $O_2$-5% $CO_2$) Krebs solution (in mM): 126 NaCl, 2.5 KCl, 1.2 $MgCl_2$, 1.2 $NaH_2PO_4$, 2.4 $CaCl_2$, 10 glucose, and 25 $NaHCO_3$ kept at 34°C. Drugs were bath applied by switching the solution to one containing known concentrations of drugs. Total replacement of the medium in the chamber occurred within 1 min. Intracellular recordings of striatal medium spiny neurons (MSNs) were obtained with sharp microelectrodes pulled from borosilicate glass pipettes backfilled with 2 M KCl (30–60 M$\Omega$). An Axoclamp 2B amplifier (Molecular Devices) was connected in parallel to an oscilloscope to monitor the signal in "bridge" mode and to a PC for acquisition of the traces using a pClamp9 software (Molecular Devices). Only neurons electrophysiologically identified as MSNs were considered for experiment (Calabresi et al., 1992).

A glutamatergic EPSP was evoked every 10 s by means of a bipolar electrode connected to a stimulator unit (Grass Telefactor). The stimulating electrode was located in the cortical areas close to the recording electrode or in the white matter between the cortex and the striatum to activate corticostriatal fibers. The recording electrodes were invariably placed within the striatum. The experiments were conducted in a $Mg^{2+}$-free Krebs' solution to unmask the NMDA glutamate (Glu) receptor component of the EPSP. After 10–15 min the acquisition of EPSPs of stable amplitude, a high-frequency stimulation protocol (HFS), consisting of three trains of stimuli at 100 Hz (20 s intertrain interval), was delivered to the slice to induce LTP of the EPSP (Calabresi et al., 1992). Twenty minutes after the HFS protocol a low-frequency stimulation protocol (LFS), consisting of repeated stimuli applied at 2 Hz for 10 min, was applied to induce depotentiation of the EPSP amplitude to pre-HFS conditions (Picconi et al., 2003). Quantitative data are expressed as a percentage of the EPSP amplitudes in respect to the relative control amplitude values, the latter representing the mean of responses recorded during a stable period. EPSP amplitudes were measured 20 min after HFS or LFS and compared with pre-HFS baseline. Off-line analysis was performed using Clampfit (Molecular Devices) and GraphPad Prism 5 software.

### *Autoradiography*

Twenty micrometer coronal sections were obtained from the frozen brains of sham-operated, untreated 6-hydroxydopamine (OHDA) lesioned and dyskinetic 6-OHDA lesioned (killed 48 h after last L-DOPA injection) male Sprague Dawley rats (see below). Sections were cut at two different brain levels from bregma: anteroposterior (AP) −0.30 to −0.92 and −3.60 to −5.80 (Paxinos and Watson, 1986) using a cryostat (13−15°C). Sets of five slides (three slides for total binding and two slides for nonspecific binding) were used for each group. Iodination of [Arg$^{14}$Lys$^{15}$Tyr$^{18}$(di)iodo]N/OFQ-$NH_2$ was performed according to the Chloramine T method (Hunter and Greenwood, 1962). Briefly, 5 $\mu$g of peptide was incubated in 0.05 M phosphate buffer, pH 7.4, for 30 s in the presence of 0.5 mCi (18.5 MBq) of Na$^{125}$I and 220 nmol of Chloramine T in a total volume of 85 $\mu$l. The mono-iodinated peptide was then immediately purified by HPLC on a C18 Jupiter 300 column (250 × 4,6 mm; Phenomenex) with 0.1% trifluoroacetic acid and acetonitrile as

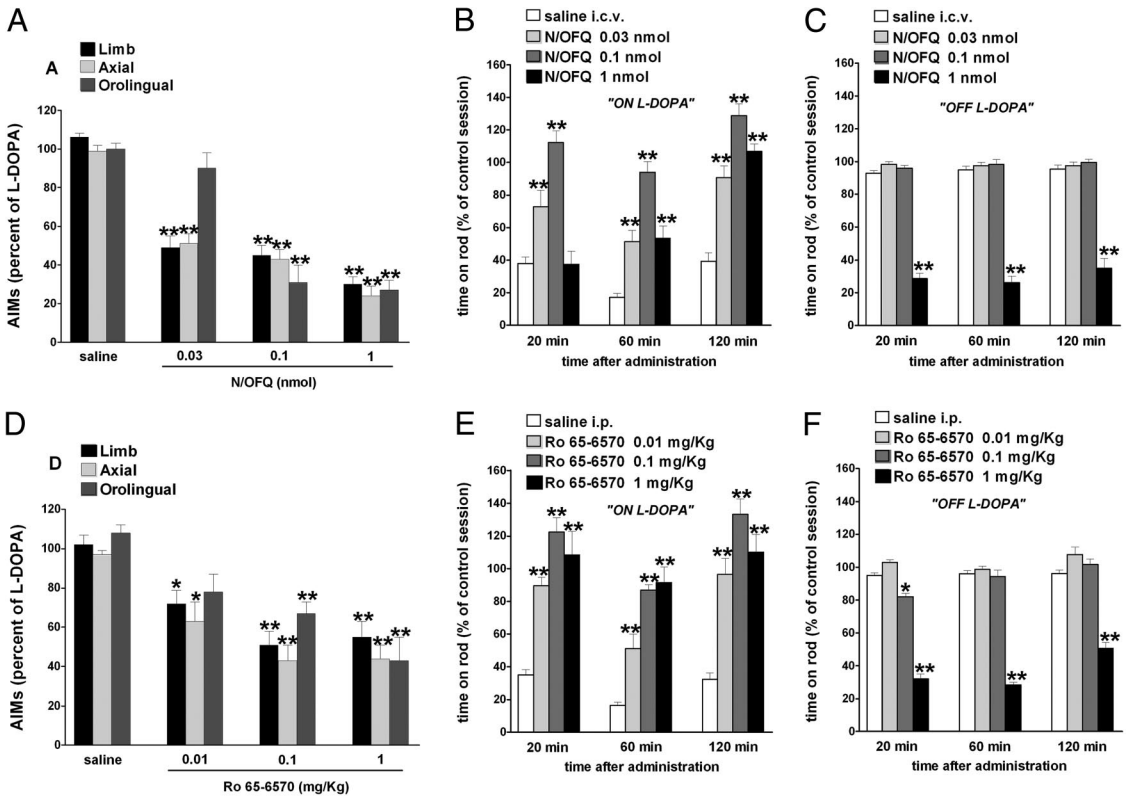


**Figure 3.** NOP receptor agonists attenuated LID. Effect of N/OFQ (0.03–1 nmol, i.c.v.) and Ro 65–6570 (0.01–1 mg/kg, i.p.) on ALO AIMs induced by L-DOPA (6 mg/kg plus benserazide 15 mg/kg, i.p.). N/OFQ (***A***) or Ro 65–6570 (***D***), given 5 and 30 min before L-DOPA, respectively, attenuated the severity of dyskinesias in a dose-related fashion. N/OFQ and Ro 65–6570 improved rotarod performance ON L-DOPA (***B***, ***E***) but worsened it OFF L-DOPA (***C***, ***F***). Data are expressed as percentage of the L-DOPA effect measured in the same animal in the last training session, and represent the mean ± SEM of 10 determinations. Statistical analysis was performed by conventional (***A***, ***D***) or RM (***B***, ***C***, ***E***, ***F***) one-way ANOVA followed by the Newman–Keuls test for multiple comparisons. ***A***, Significant effect of treatment ($F_{(11,153)} = 24.78$, $p < 0.0001$). ***B***, Significant effect of treatment ($F_{(3,114)} = 77.29$, $p < 0.0001$), time ($F_{(2,114)} = 35.08$, $p < 0.0001$), and time × treatment interaction ($F_{(6,114)} = 5.42$, $p < 0.0001$). ***C***, Significant effect of treatment ($F_{(3,114)} = 400.64$, $p < 0.0001$), but not time ($F_{(2,114)} = 1.21$, $p = 0.30$) or time × treatment interaction ($F_{(6,114)} = 0.64$, $p = 0.70$). ***D***, Significant effect of treatment ($F_{(11,147)} = 11.27$, $p < 0.0001$). ***E***, Significant effect of treatment ($F_{(3,114)} = 68.86$, $p < 0.0001$) and time ($F_{(2,114)} = 18.24$, $p < 0.0001$) but not time × treatment interaction ($F_{(6,114)} = 1.10$, $p = 0.36$). ***F***, Significant effect of treatment ($F_{(3,114)} = 387.52$, $p < 0.0001$), time ($F_{(2,114)} = 20.66$, $p < 0.0001$), and time × treatment interaction ($F_{(6,114)} = 5.39$, $p < 0.0001$). *$p < 0.05$, **$p < 0.01$, significantly different from saline.

mobile phases. The specific activity of the iodinated peptides corresponds to 2000 cpm/fmol or 1212 Ci/mmol.

The binding method used in this study was adapted from (Bridge et al., 2003). Tissue sections were thawed at room temperature and preincubated for 30 min in a solution containing: 50 mM Tris-HCl, pH 7.4; 5 mM $MgCl_2$; and 0.2% bovine serum albumin (BSA). They were then incubated at room temperature for 90 min in the same buffer solution, to which 5 mg/ml Bacitracin and 150 pM $^{125}$I[Tyr$^{14}$]N/OFQ were added. Nonspecific binding was determined by adding 1 $\mu$M cold ligand to the mixture. Slides were then rinsed in the preincubation solution without BSA (four rinses, 1 min each), then in distilled water at 4°C (15 s, to remove the excess of salts) and air dried. Kodak Scientific Biomax MS films were juxtaposed onto the slides for 3 d at room temperature. Films were developed in D-19 (Kodak developer) and fixed in Kodak fixer. Image analysis was performed using a computerized image analysis system (MCID; InterFocus GmbH). Specific binding was determined by subtracting nonspecific binding from total binding taken from adjacent sections. Calibration was performed on a standard curve generated using polymer [C$^{14}$]-microscale standards (GE Healthcare), thereby enabling conversion of relative optical intensity units, directly measured from autoradiograms, to binding site density expressed in fmol/mg.

### *In vivo* experiments in rats

Male Sprague Dawley rats (150 g; Harlan) were kept under regular lighting conditions (12 h light/dark cycle) and given food and water *ad libitum*. The experimental protocols performed in rodents were in accordance with the European Communities Council Directive of November 24, 1986 (86/609/EEC), and were approved by the Italian Ministry of Health (license #194/2008-B) and the Ethical Committee of the University of Ferrara. Adequate measures were taken to minimize the number of animals used and animal pain and discomfort.

#### *Experimental design*

*Experiments in rats.* A total of 126 6-OHDA hemilesioned dyskinetic, 10 6-OHDA hemilesioned naive and 14 sham-operated rats were used. Pharmacological treatments were randomized and usually administered every 3 d. A maintenance dose of L-DOPA was administered the day before treatment, and animals were scored. In experiment using NOP agonists (see Fig. 3), 20 dyskinetic animals implanted with an intracerebroventricular cannula received either saline or three doses of N/OFQ, ON and OFF L-DOPA ($n = 10$ each condition). Another group of 20 animals was treated with saline or three different doses of Ro 65–6570 (i.p.), ON and OFF L-DOPA ($n = 10$ each condition). In microdialysis experiments (see Fig. 5), six dyskinetic animals were implanted with a cannula (i.c.v.) and two microdialysis probes in SNr and the ventromedial thalamus (VMTh). Microdialysis was performed for 4 d and treatments (saline, L-DOPA, N/OFQ, and L-DOPA + N/OFQ) were given in a randomized fashion. In experiments using NOP antagonists (see Fig. 6), 10 dyskinetic animals implanted with an intracerebroventricular cannula received L-DOPA in combination with saline or UFP-101 (i.c.v.), whereas another group of 10 animals received L-DOPA in combination with saline or J-113397 (i.p.). In separate experiments, saline, UFP-101 and J-113397 were also given OFF L-DOPA to measure the impact of NOP receptor antagonists alone on rotarod performance. Control group

was injected with saline in both areas. In experiments using regional microinjections (see Fig. 7) 20 dyskinetic rats had a cannula implanted either in the SNr or dorsolateral striatum (DLS) ($n = 10$ each group) and received saline or three doses of N/OFQ in combination with L-DOPA. Another group of 10 animals was implanted both in the SNr and DLS, and received a single dose of N/OFQ in DLS, SNr, or both. In combination experiments (see Fig. 8), 20 dyskinetic animals implanted with a cannula in DLS or SNr ($n = 10$ each) received saline, N/OFQ (0.1 nmol), UFP-101 (10 nmol), or N/OFQ + UFP-101, in combination with L-DOPA. In autoradiography experiment (see Fig. 9) brain slices were obtained from 8 sham-operated, 10 6-OHDA hemilesioned, and 10 dyskinetic rats.

*Experiments in nonhuman primates.* Five macaques rendered stably parkinsonian with 1-methyl-4-phenyl-1,2,3,6-tetrahydropyridine (MPTP) and dyskinetic with L-DOPA (see below)(see Fig. 10).

### *Unilateral lesion with 6-OHDA*

Unilateral lesion of DA neurons was induced in isoflurane-anesthetized Sprague Dawley male rats by stereotaxically injecting 8 $\mu$g of 6-OHDA (dissolved in 4 $\mu$l of saline containing 0.02% ascorbic acid) into the medial forebrain bundle (Marti et al., 2005), according to the following coordinates from bregma: AP −4.4 mm, mediolateral (ML) −1.2 mm, and dorsoventral (DV) −7.8 mm below dura (Paxinos and Watson, 1986). Sham-operated animals were injected with 4 $\mu$l of saline (containing 0.02% ascorbic acid). Two weeks after 6-OHDA injection, denervation was evaluated with a test dose of amphetamine (5 mg/kg, i.p.). Rats showing ipsilateral turning >7 turns/min were enrolled in the study (Marti et al., 2002a, 2007).

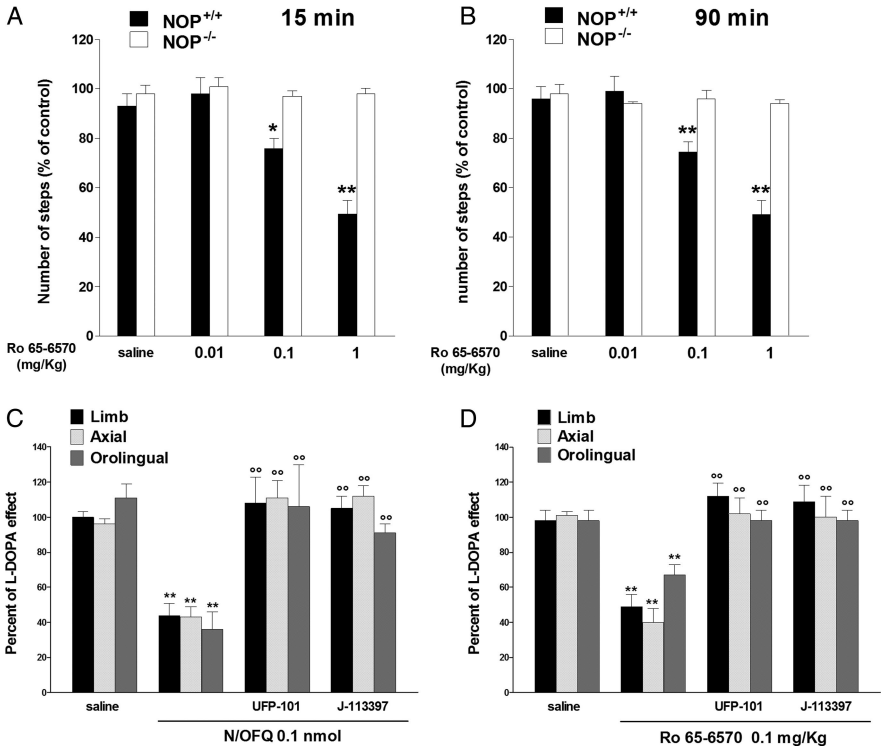


**Figure 4.** *In vivo* specificity of NOP receptor agonists. ***A***, ***B***, Ro 65–6570 (0.01–1 mg/kg, i.p.) inhibited stepping activity in the drag test in NOP $^{+/+}$ mice, being ineffective in NOP $^{-/-}$ mice. Each experiment consisted of three different sessions: a control session followed by two other sessions performed 15 min (***A***) and 90 min (***B***) after saline or drug administration. Data are expressed as percentages of motor performance in the control session and are means ± SEM 6–7 determinations per group. ***C***, ***D***, NOP receptor antagonists prevent the antidyskinetic effect of NOP receptor agonists. UFP-101 (10 nmol, i.c.v.) was administered simultaneously with N/OFQ (0.1 nmol, i.c.v.; ***C***) or 5 min before Ro 65–6570 (0.1 mg/kg, i.p.; ***D***). J-113397 (3 mg/kg, i.p.) was administered 15 min before NOP agonists. Data are expressed as percentages of L-DOPA effect, and are means ± SEM of 10–12 determinations per group. Statistical analysis was performed by one-way ANOVA followed by the Newman–Keuls test for multiple comparisons. ***A***, Significant effect of treatment in NOP $^{+/+}$ mice ($F_{(3,23)} = 17.61$, $p < 0.0001$). ***B***, Significant effect of treatment in NOP $^{+/+}$ mice ($F_{(3,23)} = 19.89$, $p < 0.0001$). *$p < 0.05$, **$p < 0.01$, different from saline. °°$p < 0.01$, different from N/OFQ or Ro 65–6570 alone.

### *L-DOPA treatment and Abnormal Involuntary Movement Scale rating*

Two weeks after amphetamine testing, DA-depleted rats were made dyskinetic by a 21 d course of L-DOPA treatment (6 mg/kg + benserazide 15 mg/kg, i.p., once daily). Quantification of abnormal involuntary movements (Abnormal Involuntary Movement Scale; AIMs), a correlate of dyskinesia (Cenci et al., 1998), was performed as extensively described in previous papers (Lundblad et al., 2002; Muñoz et al., 2008; Berthet et al., 2009; Mela et al., 2010). Briefly, rats were observed individually for 1 min every 20 min during the 3 h that followed L-DOPA injection. Dyskinetic movements were classified based on their topographic distribution into three subtypes: (1) axial AIMs, i.e., twisted posture or choreiform twisting of the neck and upper body toward the side contralateral to the lesion; (2) forelimb AIMs, i.e., jerky or dystonic movements of the contralateral forelimb and/or purposeless grabbing movement of the contralateral paw; and (3) orolingual AIMs, i.e., orofacial muscle twitching, empty masticatory movements and contralateral tongue protrusion. Each AIM subtype was rated on a frequency scale from 0 to 4 (1, occasional; 2, frequent; 3, continuous but interrupted by sensory distraction; and 4, continuous, severe, and not interrupted by sensory distraction) on each monitoring period (Cenci et al., 1998). In addition, the amplitude of these AIMs was scored based on a scale from 0 to 4 as described by (Cenci and Lundblad, 2007). Axial, forelimb, and orolingual (ALO) AIMs were calculated as the sum of the product of amplitude and frequency scores from all monitoring periods (Cenci and Lundblad, 2007), and presented either separately or together (global score). AIMs scoring was performed five times during L-DOPA treatment; dyskinetic rats showing total AIMs score > 100 in the last session were enrolled in the study. The theoretical maximal total AIMs score for each animal is 432 (48 each of the nine 20 minute sessions).

Tyrosine immunohistochemistry analysis revealed that dyskinetic rats were fully DA denervated since the ratio of optical density in the ipsilateral versus contralateral side was 99.1 ± 0.2% in sham-operated and 0.1 ± 0.01% in dyskinetic rats ($n = 6$ both).

### *Rotarod experiments*

The rotarod test was used to quantify the degree of motor impairment both ON and OFF L-DOPA. Dyskinetic rats were tested before (control session) and 20, 60, and 120 min after acute drug treatment (L-DOPA, NOP ligands or their combination). These windows were selected based on the AIMs time course (data not shown), showing a peak after 60–80 min and extinction after 180 min from L-DOPA administration. The speed of rotating cylinder was stepwise increased (180 s each step) from 5 rpm until animals fell off the rod (Marti et al., 2004). Dyskinesias negatively correlated with rotarod performance ($r = -0.75$, Spearman's nonparametric correlation test, $p < 0.001$), with a maximal reduction of ~85% at peak (data not shown).

### *Drug microinjections in dyskinetic rats*

Under isoflurane anesthesia, a stainless steel infusion cannula (15 mm long, 24 gauge) was stereotaxically lowered over the lateral ventricle [intracerebroventricular: AP = −0.9 mm; ML = −1.4 mm; ventrodorsal (VD) = −2.0 mm; DLS: AP = +0.7 mm; ML = +3.5 mm; VD = −3.2 mm; and/or SNr: AP = −5.5 mm; ML = −2.2 mm; VD = −7.3 mm] ipsilateral to the lesioned side. A stainless steel stylet was inserted into the

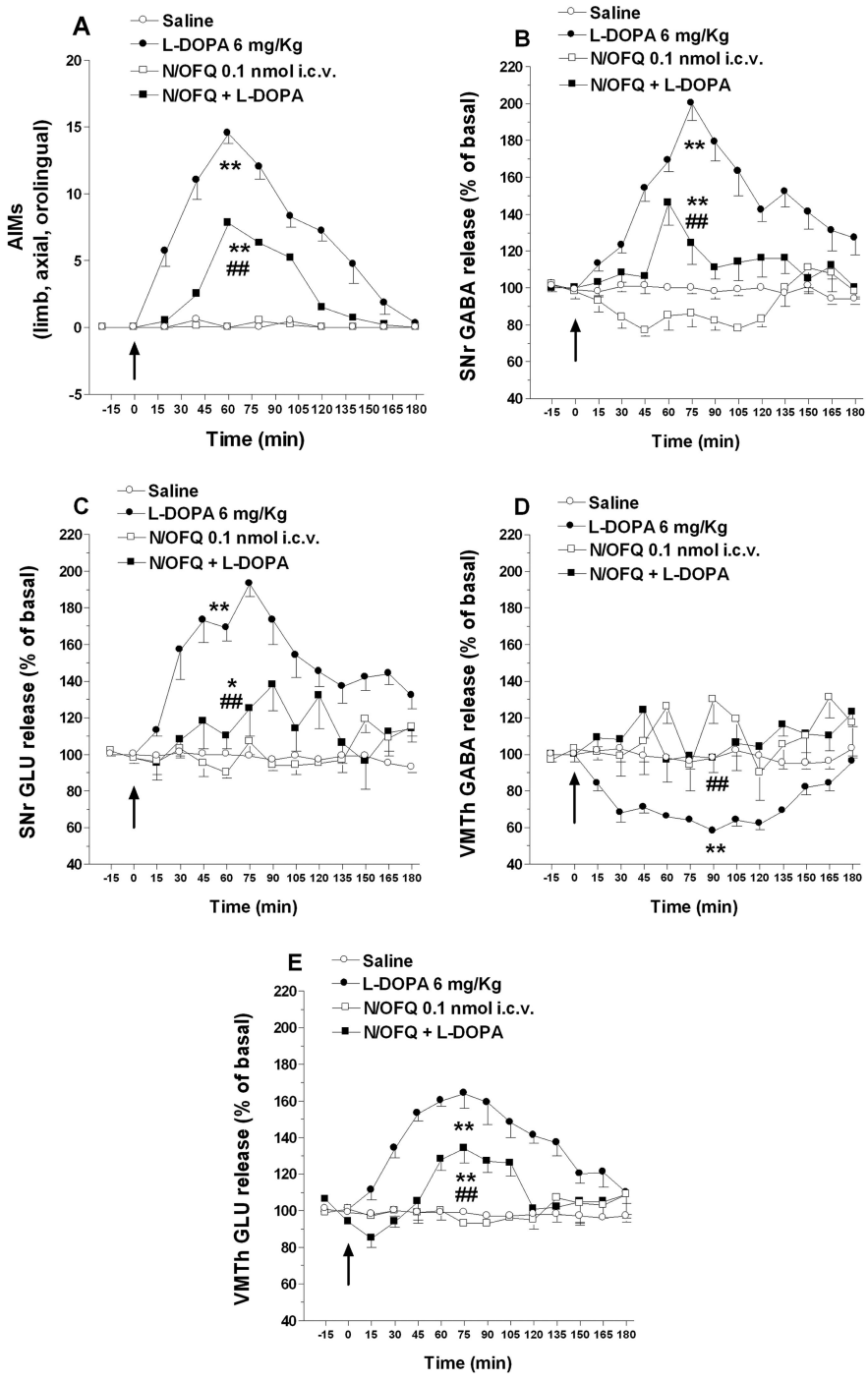


**Figure 5.** N/OFQ attenuated the elevation of nigral amino acids and the reduction of thalamic GABA associated with LID. Dyskinetic rats were implanted with one microdialysis probe in the lesioned SNr and another in ipsilateral VMTh. Twenty-four hours later, rats were acutely challenged with saline, L-DOPA (6 mg/kg plus 15 mg/kg benserazide, i.p.), N/OFQ (0.1 nmol, i.c.v.), or their combination (N/OFQ given 5 min before). In control rats, saline was injected (i.c.v.) and, 5 min later, administered (i.p.). ALO AIMs in arbitrary units (***A***) were monitored (for 1 min every 15 min) simultaneously with GABA and Glu levels in SNr (***B***, ***C***) and VMTh (***D***, ***E***) up to 180 min from L-DOPA administration. Microdialysis data were expressed as percentage of basal pretreatment levels (calculated as the mean of the two samples preceding the treatment). Data are means ± SEM of six animals. Basal dialysate GABA and Glu levels were 13.4 ± 1.0 and 190.6 ± 9.7 nM, respectively, in SNr, and 16.7 ± 0.9 and 204.8 ± 8.7 nM, respectively, in VMTh. Statistical analysis was performed on area-under-the-curve values by two-way ANOVA followed by Newman–Keuls test for multiple comparisons. ***A***, Main effect of N/OFQ ($F_{(1,1)} = 80.75, p < 0.0001$), L-DOPA ($F_{(1,1)} = 472.44, p < 0.0001$), and their interaction ($F_{(1,20)} = 78.63, p < 0.0001$). ***B***, Main effect of N/OFQ ($F_{(1,1)} = 56.64, p < 0.0001$), L-DOPA ($F_{(1,1)} = 158.69, p < 0.0001$), and their interaction ($F_{(1,20)} = 21.64, p < 0.0001$). ***C***, Main effect of N/OFQ ($F_{(1,1)} = 24.30, p < 0.0001$), L-DOPA ($F_{(1,1)} = 88.86, p < 0.0001$), and their interaction ($F_{(1,20)} = 32.30, p < 0.0001$). ***D***, Main effect of N/OFQ ($F_{(1,1)} = 40.09, p < 0.0001$), L-DOPA ($F_{(1,1)} = 17.42, p < 0.0001$), and their interaction ($F_{(1,20)} = 12.01, p < 0.0001$). ***E***, Main effect of N/OFQ ($F_{(1,1)} = 33.25, p < 0.0001$), L-DOPA ($F_{(1,1)} = 169.20, p < 0.0001$), and their interaction ($F_{(1,20)} = 46.30, p < 0.0001$). *$p < 0.05$, **$p < 0.01$ significantly different from saline. ##$p < 0.01$, significantly different from L-DOPA.

cannula to avoid its occlusion. Animals were allowed 6 d to recover, during which they were handled to familiarize with the operator and injection procedures. On the day of experiment, the rat was gently restrained by the operator, the stylet was removed and 0.5 μl of saline (control rats) or saline containing NOP receptor peptide ligands (N/OFQ and UFP-101) was injected without the use of anesthesia. Alternatively, systemic (i.p.) administration of saline, Ro 65–6570 or J-113397, was performed. In combination studies, NOP ligands were given 5 min (N/OFQ and UFP-101), 15 min (J-113397), or 30 min (Ro 65–6570) before L-DOPA.

### *Microdialysis*

Two microdialysis probes (1 mm dialyzing membrane, AN69; Hospal) were implanted in the DA-lesioned SNr (AP −5.5, ML −2.2, VD −8.3) and ipsilateral VMTh (AP −2.3, ML −1.4, VD −7.4) of isoflurane-anesthetized dyskinetic rats, as previously described (Marti et al., 2007, 2008). In the same surgery session, animals were also implanted with an intracerebroventricular cannula (coordinated as above). Twenty-four hours after surgery, probes were perfused with a modified Ringer's solution (1.2 mM $CaCl_2$, 2.7 mM $MgCl_2$, 148 mM NaCl, and 0.85 mM $MgCl_2$) at a 3 μl/min flow rate and, after 6 h rinsing, samples were collected every 15 min. L-DOPA (6 mg/kg plus benserazide 15 mg/kg) was administered systemically (i.p.), whereas N/OFQ 0.1 nmol was injected (i.c.v., 5 min before L-DOPA). In control rats, saline was injected (i.c.v.) and, 5 min later, administered intraperitoneally. AIMs monitoring was performed every 15 (for 1 min). At the end of the experiments, animals were killed and the correct placement of the probes was verified histologically.

### *Endogenous Glu and GABA analysis*

Glu and GABA were measured by HPLC coupled with fluorometric detection following *o*-phthaldialdehyde/mercaptoethanol derivatization (Marti et al., 2007). Glu and GABA were separated in a 5-C18 Chromsep analytical column (Chrompack) perfused at 0.48 ml/min with a mobile phase containing 0.1 M sodium acetate, 10% methanol and 2.2% tetrahydrofuran, pH 6.5). Glu and GABA were detected by a FP-2020 Plus spectrophotometer (Jasco) with the excitation and the emission wavelengths set at 370 and 450 nm, respectively. The limits of detection for Glu and GABA were ~1 and ~0.5 nM, and their retention times were ~3.5 and ~ 18.0 min, respectively.

## *In vivo* experiments in mice

To investigate the *in vivo* selectivity of Ro 65–6570, motor activity was evaluated in NOP $^{+/+}$ and NOP $^{-/-}$ naive mice (25–30 g; 12–15 weeks old) (Nishi et al., 1997) by means of the drag test. This test measures the ability of the animal to balance its body posture with forelimbs in response to an externally imposed dynamic stimulus (backward dragging) (Marti et al., 2005). The animal was gently lifted from the tail allowing the forepaws to rest on the table,

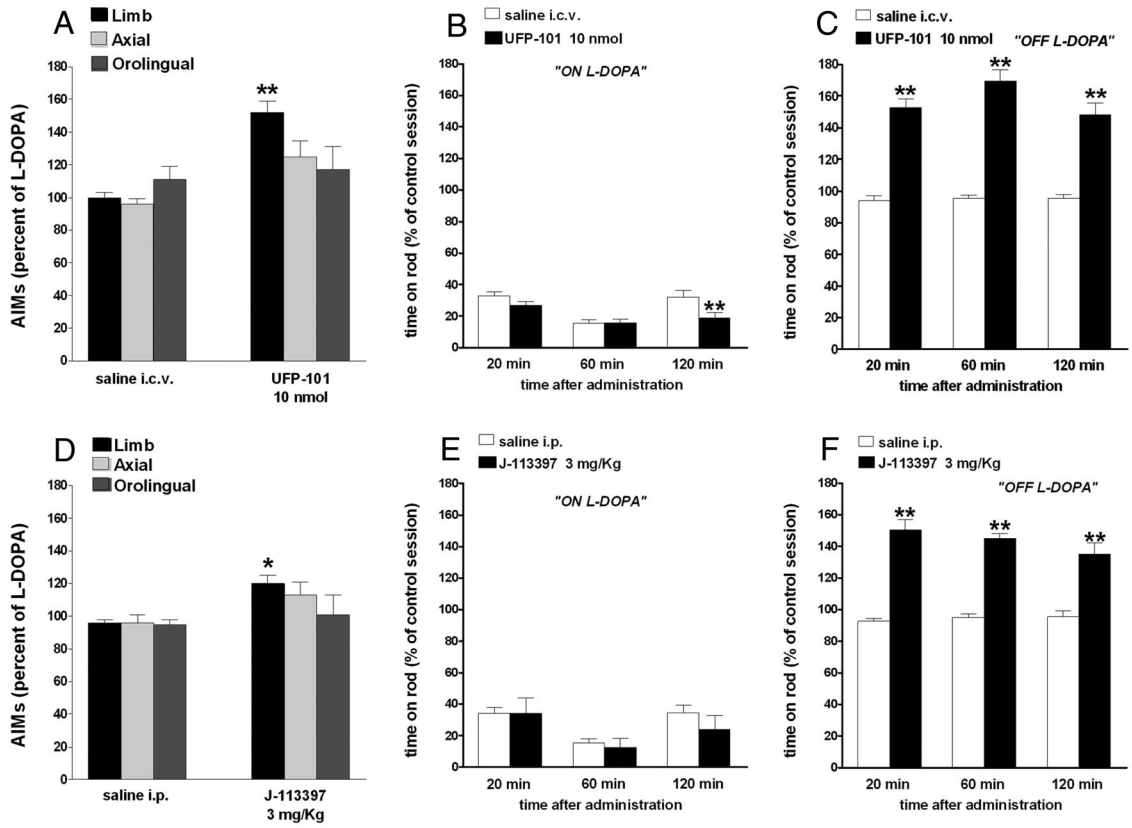


**Figure 6.** NOP receptor antagonists worsened LID. Effect of UFP-101 (10 nmol, i.c.v.) and J-113397 (3 mg/kg, i.p.) on ALO AIMs induced by L-DOPA (6 mg/kg plus benserazide 15 mg/kg, i.p.). UFP-101 (***A***) and J-113397 (***D***), given 5 and 15 min before L-DOPA, respectively, worsened limb AIMs without affecting axial and orolingual AIMs. UFP-101 also slightly worsened rotarod performance ON L-DOPA (***B***) while J-113397 left it unaffected (***E***). Both compounds improved rotarod performance OFF L-DOPA (***C***, ***F***). Data are expressed as percentage of the L-DOPA effect measured in the same animal in the last training session, and represent the mean ± SEM 10 determinations. Statistical analysis was performed by conventional (***A***, ***D***) or RM (***B***, ***C***, ***E***, ***F***) one-way ANOVA followed by the Newman–Keuls test for multiple comparisons. ***A***, Significant effect of treatment ($F_{(5,60)} = 5.99, p < 0.0001$). ***B***, Significant effect of treatment ($F_{(1,54)} = 7.02, p = 0.0106$) and time ($F_{(2,54)} = 12.95, p < 0.0001$) but not time × treatment interaction ($F_{(2,54)} = 2.83, p = 0.0678$). ***C***, Significant effect of treatment ($F_{(1,60)} = 115.65, p < 0.0001$), time ($F_{(2,60)} = 17.11, p < 0.0001$), and time × treatment interaction ($F_{(2,60)} = 3.29, p = 0.0441$). ***D***, Significant effect of treatment ($F_{(5,84)} = 3.056, p < 0.0001$). ***E***. Significant effect of time ($F_{(2,54)} = 5.41, p = 0.0072$) but not treatment ($F_{(1,54)} = 0.79, p = 0.37$) or time × treatment interaction ($F_{(2,54)} = 0.37, p = 0.69$). ***F***, Significant effect of treatment ($F_{(1,54)} = 175.12, p < 0.0001$) but not time ($F_{(2,54)} = 1.09, p = 0.3448$) or time × treatment interaction ($F_{(2,54)} = 1.95, p = 0.15$). *$p < 0.05$, **$p < 0.01$, significantly different from saline.

and dragged backwards at a constant speed (~20 cm/s) for a fixed distance (100 cm). The number of steps made with each paw was recorded by two distinct observers.

### *In vivo* experiments in nonhuman primates

Experiments were conducted according to previously published procedures and methods (Bézard et al., 2003; Aubert et al., 2005; Fasano et al., 2010). Five cynomolgus monkeys (*Macaca fascicularis*; SAH/Xierxin) were housed in individual primate cages under controlled conditions of humidity (50 ± 5%), temperature (24 ± 1°C), and light (12 h light/dark cycles, time lights on 8:00 A.M.) with food and water *ad libitum*. Experiments were performed in accordance with European Communities Council Directive of November 24, 1986 (86/609/EEC) for care of laboratory animals in an Association for Assessment and Accreditation of Laboratory Animal Care -accredited facility following acceptance of study design by the Institute of Lab Animal Science (Chinese Academy of Science, Beijing, China) Institutional Animal Care and Use Committee. Veterinarians skilled in the healthcare and maintenance of nonhuman primates supervised animal care.

Animals were treated daily (9:00 A.M.) with MPTP hydrochloride (0.2 mg/kg, i.v.) dissolved in saline (Bezard et al., 2001a). Following stabilization of the MPTP-induced syndrome (2 months), animals received a tailored dose (16–19 mg/kg) of an L-DOPA/carbidopa combination (100/25 mg) designed to optimally reverse the parkinsonian features of each animal, twice daily for 3 months. Animals developed severe and reproducible dyskinesias, presenting choreic-athetoid (characterized by constant writhing and jerking motions), dystonic, and sometimes ballistic movements (large-amplitude flinging and flailing movements). These animals were not terminated after completion of experiments, but we demonstrated in several occasions that animals intoxicated with this regimen display a dramatic reduction of DAergic nigrostriatal markers (>95%) compared with control animals (Bezard et al., 2001b; Guigoni et al., 2005; Fernagut et al., 2010).

#### *Behavioral experiments*

Macaque's behavior was first recorded in the OFF state for 0.5 h in an observation cage (dimensions: 1.1 × 1.5 × 1.1 m). Drugs were then administered, and behavior was recorded for at least a further 4 h in the observation cage. The parkinsonian condition (and its reversal) was assessed on a validated parkinsonian monkey rating scale by *post hoc* analysis of video recordings by observers blinded to treatment. The parkinsonian disability score is a combination of the range of movement, bradykinesia, posture, and tremor scores according to the following formula: range of movement + bradykinesia + postural abnormality + tremor (Bézard et al., 2003; Aubert et al., 2005; Fasano et al., 2010). The severity of dyskinesia is rated using the Dyskinesia Disability Scale: 0, dyskinesia absent; 1, mild, fleeting, and rare dyskinetic postures and movements; 2, moderate, more prominent abnormal movements, but not interfering significantly with normal behavior; 3, marked, frequent and, at times, continuous dyskinesia intruding on the normal repertoire of activity; or, 4, severe, virtually continuous dyskinetic activity replacing normal behavior and disabling to the animal. Locomotor activity is con-

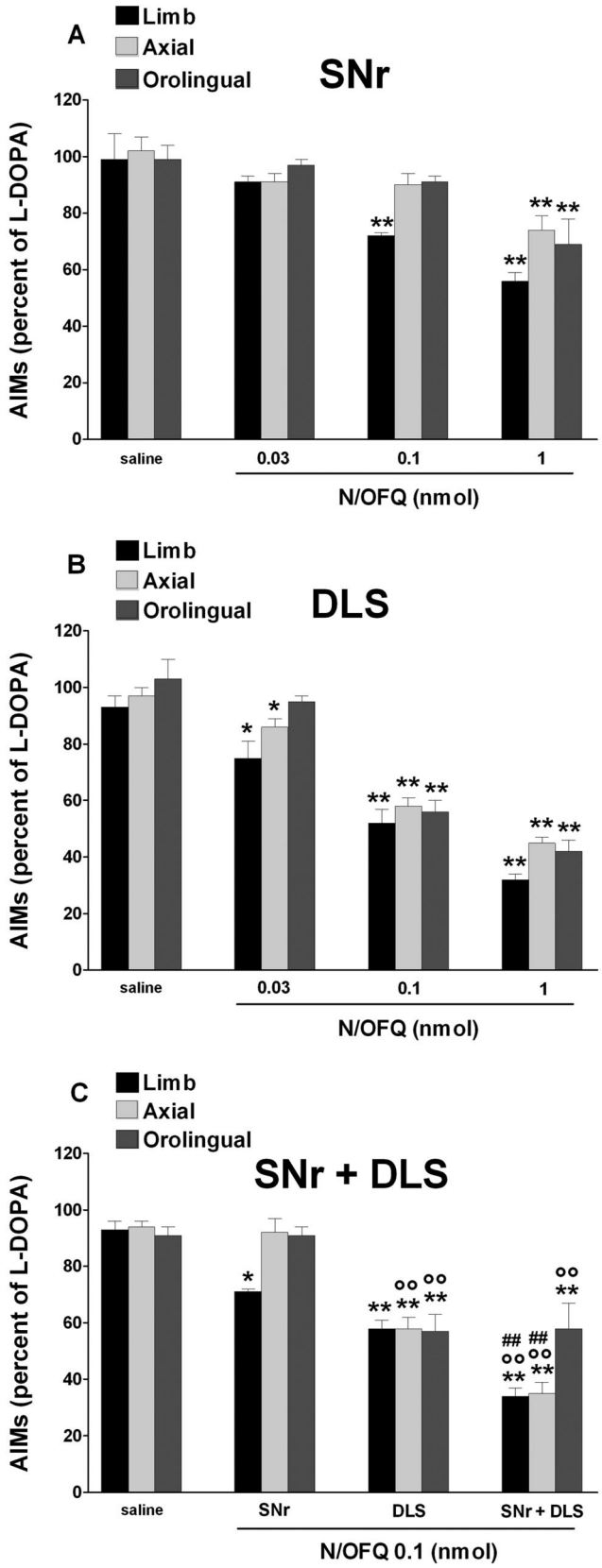


**Figure 7.** N/OFQ attenuated LID when injected in SNr and DLS. Effect of N/OFQ (0.03–1 nmol, i.c.v.) injected in SNr (***A***), DLS (***B***), or both (at 0.1 nmol; ***C***) on ALO AIMs induced by L-DOPA (6 mg/kg plus benserazide 15 mg/kg, i.p.). N/OFQ given 5 min before L-DOPA attenuated the severity of dyskinesias in a dose-related fashion, being more potent when injected in DLS than SNr. Coinjection of N/OFQ in SNr and DLS produced an additive antidyskinetic effect (***C***). Saline was simultaneously injected in SNr and DLS. Data are expressed as percentage of the L-DOPA effect measured in the same animal in the last training session, and represent the mean ± SEM of 10 determinations. Statistical analysis was performed by one-way (***A***, ***B***) or two-way (***C***) ANOVA followed by the Newman–Keuls test for multiple comparisons. ***A***, Significant effect of treatment ($F_{(11,71)} = 9.58, p < 0.0001$). ***B***, Significant effect of treatment ($F_{(11,71)} = 38.8, p < 0.0001$). ***C***, Main effect of N/OFQ ($F_{(3,60)} = 528.64, p < 0.0001$), brain area ($F_{(2,60)} = 33.94, p < 0.0001$), and their interaction ($F_{(6,60)} = 23.76, p < 0.0001$). $^{**}p < 0.01$, $^{*}p < 0.05$, significantly different from saline. $^{\circ\circ}p < 0.01$, significantly different from SNr injection. $\#\#p < 0.01$, significantly different from DLS injection.

comitantly monitored with infrared activity monitors, providing a mobility count every 5 min (Bézard et al., 2003; Aubert et al., 2005; Fasano et al., 2010).

### Data presentation and statistical analysis

Behavior (Figs. 3, 4, 6) and autoradiography (Fig. 9) data were analyzed using conventional or repeated measure (RM) one-way ANOVA as appropriate, followed by the Newman–Keuls test for multiple comparisons. Conventional two-way ANOVA with a 2 × 2 factorial design was used to analyze drug interactions (Figs. 5, 7, 8). Nonparametric one-way RM ANOVA followed by the Dunn's test for multiple comparisons was used to treat behavioral scores in nonhuman primates (Fig. 10). $p$ values $<0.05$ were considered to be statistically significant.

### Materials

D-Amphetamine sulfate, benserazide hydrochloride, L-DOPA methylester hydrochloride, MPTP hydrochloride, 6-OHDA hydrobromide, and SKF38393 were purchased from Sigma. N/OFQ, UFP-101, J-113397, and Ro 65–6570 were synthesized in our laboratory. All drugs were readily dissolved in saline.

## Results

### Effects of N/OFQ on D1 receptor-induced ERK phosphorylation and loss of synaptic depotentiation

Upregulation of striatal D1 signaling in LID is associated with an increased activity along the Ras/MEK/ERK kinase pathway (Valjent et al., 2005; Feyder et al., 2011) and a loss of neuron capability to depotentiate striatal synaptic response after LTP induction (Picconi et al., 2003). To investigate the effect of NOP receptor activation on these D1 receptor-dependent biochemical correlates of LID, we explored whether N/OFQ could prevent ERK phosphorylation and restore a physiological depotentiation of synaptic plasticity in striatal slices of naive animals stimulated with the D1 receptor agonist SKF38393.

To quantify ERK phosphorylation, we used a recently established *ex vivo* system, in which brain slices prepared from adult mice can be stimulated with appropriate agonists and antagonists. For ERK signaling activation we monitored the ribosomal protein S6 phosphorylation at the Thr235/236 site (Orellana et al., 2012). D1 receptor activation by 100 $\mu$M SKF38393 application dramatically elevated ERK signaling by ~10-fold (Fig. 1*A*,*B*). N/OFQ 1 $\mu$M was ineffective alone but prevented the D1 agonist effect (Fig. 1*A*,*B*).

Cortically evoked EPSPs were measured in electrophysiologically identified striatal MSNs (Fig. 2). In a first group of control slices, after acquiring EPSPs of stable amplitudes for 10 min, LTP of synaptic transmission was induced by HFS protocol (EPSP amplitude post-HFS, 162.7 ± 6.7%). A subsequent application of LFS protocol in these recorded MSNs produced a depotentiation of the synaptic response to pre-HFS conditions (EPSP amplitude post-LFS, 93.9 ± 7.9%; Fig. 2*A*,*B*). Bath application of 3 $\mu$M D1 receptor agonist SKF38393 prevented depotentiation of MSN synaptic plasticity (EPSP amplitude post-LFS, 160.8 ± 4.3%; Fig. 2*C*,*D*). Bath application of 0.1 $\mu$M N/OFQ did not affect LTP or

depotentiation in MSNs (EPSP amplitude post-HFS, 152.6 ± 6.5%; EPSP amplitude post-LFS 106.7 ± 6.0%; Fig. 2*A*,*B*). However, when 3 μM SKF38393 was bath applied for 20 min in the presence of 0.1 μM N/OFQ, depotentiation of MSN synaptic transmission was fully restored (EPSP amplitude, post-LFS 97.3 ± 5.9%, SKF38393 vs SKF38393 + N/OFQ, $p < 0.001$; Fig. 2*C*,*D*). To verify the selectivity of N/OFQ action, we bath applied 3 μM SKF38393 and 0.1 μM N/OFQ with 1 μM NOP receptor antagonist UFP-101. In these conditions, LFS protocol did not produce depotentiation, confirming that N/OFQ action was accomplished through the NOP receptor.

### Effect of NOP receptor agonists on dyskinesias and rotarod performance in rats

Data obtained *in vitro* predict that NOP receptor agonists might selectively target LID pathways and attenuate LID. We therefore administered exogenous N/OFQ and the NOP receptor synthetic agonist Ro 65–6570 (Röver et al., 2000) to dyskinetic rats challenged with L-DOPA. N/OFQ (i.c.v.) dose-dependently attenuated LID appearance (Fig. 3*A*) and rescued rotarod performance (Fig. 3*B*) in the 0.03–1 nmol range. The rescue effect at 1 nmol was, however, less pronounced than at lower doses, consistent with the finding that N/OFQ caused primary hypolocomotive effect OFF L-DOPA at this dose (Fig. 3*C*). To prove the antidyskinetic potential of NOP receptor agonists, the small molecule Ro 65–6570 was used at doses selective for NOP receptor stimulation (0.01–1 mg/kg, i.p.). Indeed, in this dose range Ro 65–6570 reduced stepping activity in NOP $^{+/+}$ mice but was ineffective in NOP $^{-/-}$ mice (Fig. 4*A*,*B*). Ro 65–6570, given 30 min before L-DOPA, attenuated AIMs appearance at 0.01 mg/kg (Fig. 3*D*), and maximally at 1 mg/kg. This antidyskinetic effect was accompanied by restoration of rotarod performance (Fig. 3*E*). Conversely, Ro 65–6570 markedly impaired rotarod performance OFF L-DOPA at 1 mg/kg (Fig. 3*F*). To confirm the pharmacological specificity of the antidyskinetic action of NOP agonists, UFP-101 and J-113397 prevented the antidyskinetic effect of N/OFQ and Ro 65–6570 (Fig. 4*C*,*D*).

### Effects of intracerebroventricular injections of N/OFQ on LID and neurochemical correlates in SNr and VMTh

Microdialysis was used to investigate whether the antidyskinetic action of N/OFQ was accompanied by changes of the nigral output. AIMs expression (Fig. 5*A*) was associated with a ~2-fold elevation of GABA and Glu in SNr (Fig. 5*B*,*C*) as well as a ~40% reduction of GABA and a ~60% elevation of Glu in VMTh (Fig. 5*D*,*E*). Injection of 0.1 nmol N/OFQ (i.c.v.) attenuated (~60%) LID severity (Fig. 5*A*) and simultaneously blunted the surge in nigral amino acids (Fig. 5*B*,*C*). In addition, N/OFQ prevented the GABA inhibition and attenuated the Glu surge in VMTh (Fig. 5*D*,*E*).

### Effect of NOP receptor antagonists on dyskinesias and rotarod performance in rats

To investigate whether not only exogenous but also endogenous N/OFQ affected LID, peptidic (UFP-101) (Calo et al., 2002) and nonpeptidic (J-113397) (Kawamoto et al., 1999) NOP receptor antagonists were used at maximal antiparkinsonian doses (Marti et al., 2005) against a prodyskinetic dose of L-DOPA. UFP-101 (10 nmol, i.c.v.; Fig. 6*A*) or J-113397 (3 mg/kg, i.p.; Fig. 6*D*) worsened limb without affecting axial and orolingual AIMs. Consistently, neither antagonist attenuated the impairment of rotarod performance associated with LID (ON L-DOPA; Fig. 6*B*,*E*). Conversely, UFP-101 (Fig. 6*C*) and J-113397 (Fig. 6*F*) facilitated rotarod performance OFF L-DOPA.

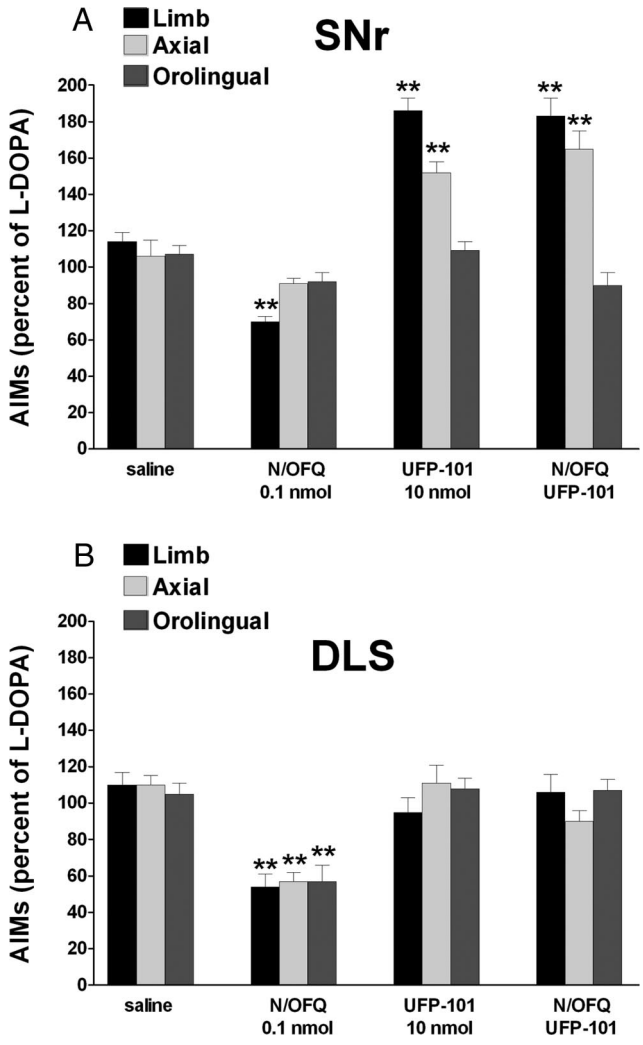


**Figure 8.** UFP-101 worsened LID when given in SNr but not DLS, preventing N/OFQ action in both regions. Effect of injections of N/OFQ (0.1 nmol, i.c.v.), UFP-101 (10 nmol, i.c.v.), or their combinations in SNr (***A***) or DLS (***B***) on ALO AIMs induced by L-DOPA (6 mg/kg plus benserazide 15 mg/kg, i.p.). UFP-101 was administered 5 min before L-DOPA, simultaneously with N/OFQ. Data are expressed as percentage of the L-DOPA effect measured in the same animal in the last training session, and represent the mean ± SEM of 10 determinations. Statistical analysis was performed by two-way ANOVA followed by the Newman–Keuls test for multiple comparisons. ***A***, Limb AIMs, main effect of N/OFQ ($F_{(1,1)} = 12.95$, $p = 0.0012$), UFP-101 ($F_{(1,1)} = 16.00$, $p = 0.0004$), and their interaction ($F_{(1,28)} = 29.18$, $p < 0.0001$); axial AIMs, main effect of N/OFQ ($F_{(1,1)} = 13.63$, $p = 0.0012$), UFP-101 ($F_{(1,1)} = 45.11$, $p < 0.0001$), and their interaction ($F_{(1,28)} = 12.38$, $p = 0.0015$); orolingual AIMs, main effect of N/OFQ ($F_{(1,1)} = 26.90$, $p < 0.0001$), UFP-101 ($F_{(1,1)} = 24.54$, $p < 0.0001$), and their interaction ($F_{(1,28)} = 22.93$, $p < 0.0001$). ***B***, Limb AIMs, main effect of N/OFQ ($F_{(1,1)} = 192.51$, $p < 0.0001$), UFP-101 ($F_{(1,1)} = 12.64$, $p = 0.0014$), and their interaction ($F_{(1,28)} = 9.42$, $p = 0.0047$); axial AIMs, main effect of N/OFQ ($F_{(1,1)} = 64.43$, $p < 0.0001$) but not UFP-101 ($F_{(1,1)} = 0.01$, $p = 0.89$) or their interaction ($F_{(1,28)} = 3.65$, $p = 0.07$); orolingual AIMs, main effect of UFP-101 ($F_{(1,1)} = 8.99$, $p = 0.0056$) but not N/OFQ ($F_{(1,1)} = 0.02$, $p = 0.98$) or their interaction ($F_{(1,28)} = 0.10$, $p = 0.74$). **$p < 0.01$, significantly different from saline.

### Effect of regional injections of N/OFQ in the SNr and DLS of dyskinetic rats

To investigate the brain areas involved in the antidyskinetic and prodyskinetic effects of NOP receptor ligands, N/OFQ and UFP-101 were microinjected in SNr and/or DLS. Intranigral N/OFQ slightly reduced limb AIMs at 0.1 nmol providing a greater and

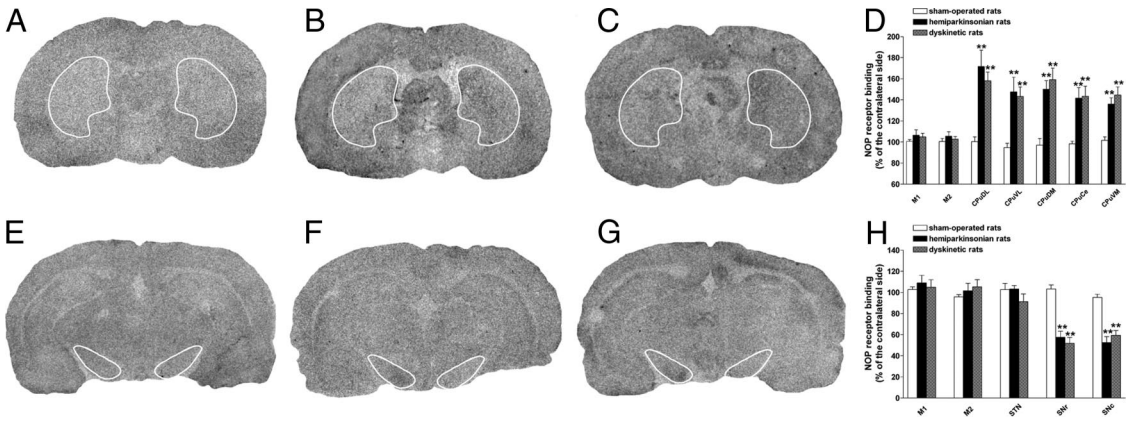


**Figure 9.** LID was associated with an elevation of NOP receptor binding in the striatum and a reduction in the SN. Representative total binding of $^{125}$I[Tyr $^{14}$]N/OFQ to NOP receptors in cortical and subcortical areas of sham-operated (***A***, ***E***), hemiparkinsonian (***B***, ***F***), and dyskinetic (***C***, ***G***) rats. Twenty micrometer coronal sections were cut at two different brain levels from bregma: AP −0.30 to −0.92 and −3.60 to −5.80. Specific binding values, given in Table 1, were obtained by subtraction of nonspecific from total binding. Binding changes are expressed as percentage of the contralateral hemisphere (***D***, ***H***) and are means ± SEM of 6–10 animals. Statistical analysis was performed by one-way ANOVA followed by Newman–Keuls test for multiple comparisons. $^{**}p < 0.01$, significantly different from sham-operated rats.

**Table 1. Autoradiographical binding of $^{125}$I[Tyr $^{14}$]N/OFQ to the NOP receptor in cortical and subcortical areas of sham-operated, untreated 6-OHDA lesioned (hemiparkinsonian), and dyskinetic rats**

| | Sham operated | Hemiparkinsonian | Dyskinetic |
|---|---|---|---|
| Level AP −0.30 to −0.92 mm | | | |
| M1 | | | |
| Ipsi | 71.6 ± 6.7 | 89.8 ± 14.9 | 94.6 ± 6.1 |
| C/L | 77.2 ± 7.6 | 83.8 ± 14.1 | 90.6 ± 6.2 |
| M2 | | | |
| Ipsi | 80.8 ± 8.6 | 90.9 ± 14.9 | 100.3 ± 6.8 |
| C/L | 81.1 ± 6.1 | 90.0 ± 13.7 | 97.5 ± 6.9 |
| CPuDL | | | |
| Ipsi | 22.7 ± 4.8 | 30.6 ± 6.2 | 31.5 ± 3.5 |
| C/L | 23.0 ± 4.9 | 20.9 ± 4.5 | 21.5 ± 3.0 |
| CPuVL | | | |
| Ipsi | 24.8 ± 4.7 | 30.1 ± 3.9 | 34.3 ± 3.1 |
| C/L | 25.9 ± 4.7 | 22.5 ± 3.8 | 25.9 ± 2.8 |
| CPuDM | | | |
| Ipsi | 24.8 ± 4.9 | 28.6 ± 3.0 | 30.4 ± 3.4 |
| C/L | 26.1 ± 4.7 | 19.2 ± 1.5 | 21.6 ± 3.1 |
| CPuCe | | | |
| Ipsi | 27.0 ± 6.4 | 27.7 ± 4.2 | 30.6 ± 3.7 |
| C/L | 27.7 ± 6.5 | 20.7 ± 3.4 | 23.1 ± 3.6 |
| CPuVM | | | |
| Ipsi | 29.7 ± 3.0 | 39.5 ± 6.3 | 36.9 ± 3.1 |
| C/L | 29.5 ± 3.1 | 30.0 ± 5.3 | 27.1 ± 3.0 |
| Level AP −3.60 to −5.80 mm | | | |
| M1 | | | |
| Ipsi | 72.4 ± 6.8 | 89.7 ± 13.9 | 96.6 ± 7.2 |
| C/L | 75.4 ± 8.6 | 84.8 ± 12.1 | 94.6 ± 7.3 |
| M2 | | | |
| Ipsi | 78.4 ± 5.0 | 85.7 ± 14.0 | 90.1 ± 7.5 |
| C/L | 76.4 ± 8.6 | 84.8 ± 13.0 | 91.0 ± 7.8 |
| STN | | | |
| Ipsi | 17.4 ± 1.7 | 32.3 ± 6.1 | 35.4 ± 7.0 |
| C/L | 18.5 ± 4.1 | 30.9 ± 6.0 | 38.5 ± 7.4 |
| SNr | | | |
| Ipsi | 25.5 ± 1.3 | 16.0 ± 4.6 | 16.6 ± 4.4 |
| C/L | 25.1 ± 2.7 | 28.1 ± 4.9 | 26.8 ± 4.7 |
| SNc | | | |
| Ipsi | 22.9 ± 0.6 | 17.7 ± 3.9 | 19.9 ± 3.4 |
| C/L | 24.6 ± 1.8 | 34.7 ± 3.2 | 32.1 ± 4.8 |

Twenty micrometer coronal sections were cut at two different brain levels from bregma: AP −0.30 to −0.92 and −3.60 to −5.80. Absolute binding values are given as fmol/mg tissue. Ce, Cerebellar; CPu, caudate-putamen; DL, dorsolateral; DM, dorsomedial; VL, ventrolateral; VM, ventromedial.

more generalized effect at 1 nmol (Fig. 7*A*). Conversely, intrastriatal N/OFQ caused a marked reduction of limb and axial AIMs yet at 0.03 nmol (Fig. 7*B*). Combined intranigral and intrastriatal injections of 0.1 nmol N/OFQ (Fig. 7*C*) caused greater AIMs attenuation than each injection alone. Contrary to N/OFQ, UFP-101 (10 nmol) worsened limb and axial AIMs when injected in SNr (Fig. 8*A*) but not striatum (Fig. 8*B*). In both cases, however, UFP-101 prevented the antidyskinetic effect of locally injected N/OFQ.

### NOP receptor binding associated with parkinsonism and dyskinesias

To investigate whether LID is associated with changes of NOP receptor binding, quantitative autoradiography was used (Fig. 9). In sham-operated rats, binding appeared highest in motor cortex (M1 and M2), intermediate in striatum and SN, and lowest in the subthalamic nucleus of (Fig. 9*A*,*E*) (Table 1). 6-OHDA lesioning (Fig. 9*B*,*F*) caused an increase of ipsilateral binding throughout the striatum and a reduction in both SN subdivisions (Fig. 9*D*,*H*). Similar patterns were observed in the brain of dyskinetic rats (Fig. 9*C*,*D*,*G*–*H*).

### NOP receptor agonists in dyskinetic nonhuman primates

To confirm the antidyskinetic potential of NOP receptor agonists, Ro 65–6570 was systemically injected in MPTP-lesioned dyskinetic macaques (Fig. 10*A*). Ro 65–6570 significantly reduced dyskinetic movements at 0.01 mg/kg (i.m.) but not lower dose (Fig. 9*B*). Ro 65–6570 was effective against dystonia, although a trend for inhibition of chorea was clearly observed (Fig. 10*B*). Time-course analysis (Fig. 10*C*,*D*) revealed that Ro 65–6570 attenuated the peak and shortened the duration of dyskinetic movements. Ro 65–6570 did not affect the therapeutic effects of L-DOPA on movement range, bradykinesia, and tremor, and even improved posture at the higher dose (Table 2).

## Discussion

Opposite adaptive changes of N/OFQ transmission have been observed in the basal ganglia of the parkinsonian rodent brain: elevation of N/OFQ expression (and release) accompanied by reduction of NOP receptor binding in SNr, and reduction of N/OFQ expression accompanied by elevation of NOP receptor binding in striatum. These changes underlie the different behav-

ioral responses to NOP receptor ligands in PD models. Indeed, we have previously reported that NOP receptor antagonists exert a symptomatic antiparkinsonian effect (Marti et al., 2005, 2008; Viaro et al., 2008, 2010; Visanji et al., 2008; Volta et al., 2010), and that such effect is mediated by blockade of SNr NOP receptors (Marti et al., 2005, 2010). We now report that NOP receptor agonists provide an antidyskinetic effect, which is faithfully replicated by intrastriatal N/OFQ injections, suggesting the involvement of striatal NOP receptors. LIDs are associated with hyperesponsiveness of upregulated D1 receptors on striatonigral MSNs (Aubert et al., 2005; Berthet et al., 2009) leading to an increased activity along the Ras/MEK/ERK kinase pathway (Valjent et al., 2005; Feyder et al., 2011) and a loss of neuron capability to depotentiate striatal synaptic response after LTP induction (Picconi et al., 2003). *In vitro* and *in vivo* data revealed that NOP receptor activation opposes D1 signaling in striatum. Indeed, N/OFQ prevented the D1 receptor-mediated increase in ERK phosphorylation and loss of striatal depotentiation of striatal plasticity in striatal MSNs, without being per se effective. These data add to the previous finding that N/OFQ inhibited the D1 receptor stimulated cAMP accumulation in striatal slices (Olianas et al., 2008) and suggest the existence of a negative interaction between the NOP and D1 receptor on the membranes of striatal MSNs. The NOP receptor is expressed not only presynaptically on nigrostriatal DA terminals (Norton et al., 2002) but also postsynaptically on striatal GABAergic MSNs neurons (Olianas et al., 2008). The postsynaptic action of N/OFQ might be favored under dyskinetic conditions, since in the striatum of L-DOPA primed and unprimed 6-OHDA hemilesioned rats, NOP receptor binding is upregulated, probably to compensate for the reduction of N/OFQ expression following DA denervation (Marti et al., 2010). Thus, NOP receptor agonists would reinstate an inhibitory control mediated by endogenous N/OFQ over striatal D1 signaling, which has been lost following DA denervation.

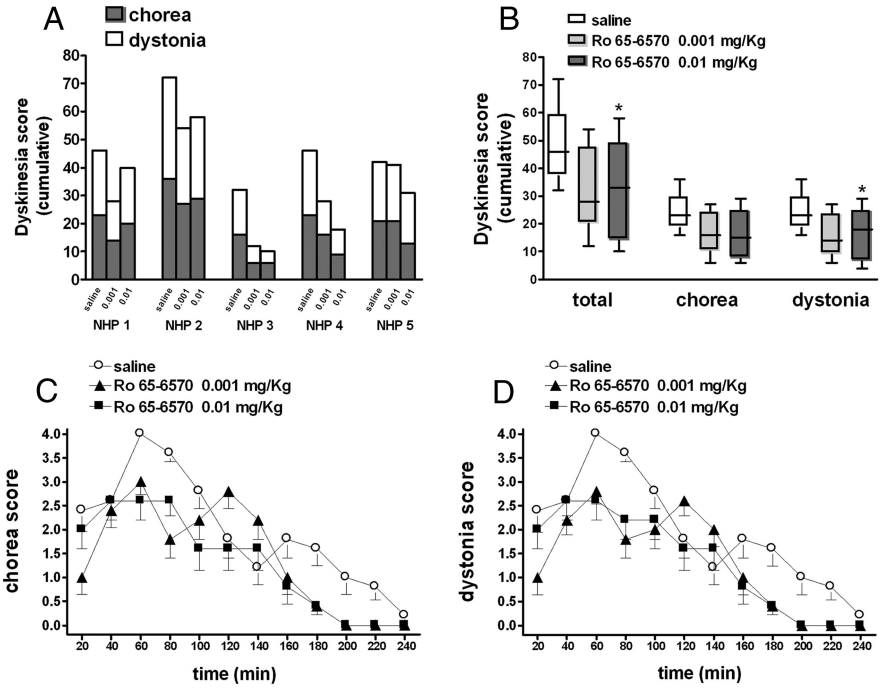


**Figure 10.** Ro 65–6570 attenuated LID in MPTP-treated macaques. Five stably parkinsonian macaques were made dyskinetic by chronic L-DOPA treatment, and then challenged with L-DOPA combined with Ro 65–6570 (0.001 and 0.01 mg/kg, i.m.) or saline (***A***). Dyskinetic conditions were assessed on a Dyskinesia Disability Scale (see Materials and Methods) evaluating choreiform and dystonic components (***A***, ***B***). The time courses of these motor responses are shown in ***C*** and ***D***. Data are expressed as absolute dyskinesia scores in each animal (***A***), medians with lower and upper quartiles (***B***), or means ± SEM (***C***, ***D***). Statistical analysis was performed by one-way nonparametric RM ANOVA (Friedman test) followed by the Dunn's test for multiple comparisons. $*p < 0.05$, significantly different from saline.

**Table 2. Motor behavior of MPTP-treated macaques before (OFF score) and after (ON score) L-DOPA and Ro 65–6570 administration**

| | | ON score | | |
|---|---|---|---|---|
| | OFF score | Saline | Ro 65–6570 0.001 mg/kg | Ro 65–6570 0.01 mg/kg |
| Chorea | 0.0 ± 0.0 | 23.8 ± 3.3 | 16.8 ± 3.5 | 15.4 ± 4.1 |
| Dystonia | 0.0 ± 0.0 | 23.8 ± 3.3 | 15.8 ± 3.6 | 16.0 ± 4.4* |
| Total dyskinesia | 0.0 ± 0.0 | 47.6 ± 6.6 | 32.8 ± 7.1 | 31.4 ± 8.4* |
| Movement | 2.4 ± 2.4 | 39.4 ± 1.9 | 39.4 ± 1.5 | 40.0 ± 1.7 |
| Bradykinesia | 36.0 ± 0.0 | 9.4 ± 1.7 | 8.6 ± 2.2 | 8.6 ± 3.0 |
| Posture | 19.2 ± 2.9 | 7.2 ± 1.5 | 3.6 ± 1.6 | 1.8 ± 1.1* |
| Tremor | 2.4 ± 2.4 | 0.6 ± 0.6 | 1.0 ± 0.5 | 3.2 ± 1.4 |
| Total parkinsonian disability | 103.2 ± 6.1 | 25.8 ± 4.7 | 21.8 ± 4.9 | 21.4 ± 6.2 |

Five stably parkinsonian macaques were made dyskinetic by chronic L-DOPA treatment. Macaques were then challenged with L-DOPA combined with Ro 65–6570 (0.001 and 0.01 mg/kg, i.m.) or saline. Parkinsonian condition was assessed on a parkinsonian nonhuman primate rating scale scoring movement range, bradykinesia, posture, tremor, and total parkinsonian disability (see Materials and Methods). Dyskinetic condition was assessed on a Dyskinesia Disability Scale evaluating choreiform, dystonic, and total dyskinesia movements (see Materials and Methods). Data are means ± means from five animals. Statistical analysis was performed by nonparametric one-way RM ANOVA followed by Dunn's test for multiple comparisons. $*p < 0.05$, versus saline.

Indirect evidence that the negative NOP receptor modulation of D1 signaling is relevant for *in vivo* conditions was provided by microdialysis experiments showing that centrally administered N/OFQ attenuated LID simultaneously with the surge of GABA levels in SNr. In fact, the same responses were observed in dyskinetic rats by pairing systemic L-DOPA with intrastriatal perfusion of a D1 receptor antagonist (Mela et al., 2012). This endorses the view that the antidyskinetic effect of N/OFQ is possibly mediated by upregulated postsynaptic NOP receptors opposing the overactivation of the direct striatonigral pathway induced by L-DOPA via D1 receptors. Consistently, microdialysis also revealed that LID was associated with inhibition of thalamic GABA release, and that the antidyskinetic action of N/OFQ was accompanied by blockade of this response. Indeed, inhibition of thalamic GABA might reflect overinhibition of nigrothalamic neurons by direct striatonigral pathway activation, as previously demonstrated for the anti-akinetic effect of L-DOPA in hemiparkinsonian rats (Marti et al., 2007). This lends neurochemical support to the notion that overinhibition of nigrothalamic GABA neurons by striatonigral direct pathway activation underlies both the motor promoting and prodyskinetic actions of L-DOPA.

Remarkably, the antidyskinetic action of N/OFQ was not accompanied by motor inhibition. Indeed, it is well known that one of the main consequences of central NOP receptor stimulation is motor impairment (Reinscheid et al., 1995; Devine et al., 1996; Jenck et al., 1997; Marti et al., 2004, 2009). However, the antidyskinetic effect of N/OFQ and Ro 65–6570 was observed at doses approximately 30- to 100-fold lower than those causing hypolocomotion, suggesting it was not related to motor impair-

ment. Thus, NOP receptor agonists might behave as functional DA antagonists that can be dosed in a way to improve LID without affecting movement in the OFF state.

N/OFQ also attenuated dyskinesia when injected into SNr. Indeed, SNr is involved in LID (Meissner et al., 2006; Westin et al., 2006; Lindgren et al., 2010). In particular, conversion of L-DOPA to DA in SNr (Sarre et al., 1998) generates abnormal nigral DA levels (Lindgren et al., 2010) thereby triggering dyskinetic movements through activation of both D1 and D2 nigral receptors (Mela et al., 2012). However, different from striatum, the hypolocomotive and antidyskinetic doses of N/OFQ given intranigrally largely overlapped, suggesting that attenuation of LID is due to unspecific motor inhibition. Indeed, exogenous N/OFQ microinjected in the SNr of naive rats inhibits movement (Marti et al., 2004, 2009), possibly through elevation of the excitatory Glu (Marti et al., 2002b) and attenuation of the inhibitory GABA inputs (Marti et al., 2007; Mabrouk et al., 2010) impinging over nigrothalamic neurons. Alternatively, we could speculate that dyskinesia pathways in SNr are less sensitive to N/OFQ, or even that N/OFQ itself is less active in the DA-depleted SNr. Indeed, the enhancement of the N/OFQ tone in SNr along with the reduction of the NOP receptor binding (present study) and expression following DA depletion (Marti et al., 2005, 2010) predict a higher NOP receptor saturation by endogenous N/OFQ, which favors the motor promoting and antiparkinsonian action of NOP receptor antagonists (Marti et al., 2007, 2008; Volta et al., 2011).

Previous studies have demonstrated the potential therapeutic benefit of a combination of subthreshold doses of an NOP receptor antagonist with L-DOPA in parkinsonian rodents (Marti et al., 2007; Viaro et al., 2010). We now report that an NOP receptor antagonist given in SNr worsens dyskinesia severity when combined with dyskinesiogenic doses of L-DOPA. This corroborates the view that NOP receptor blockade in SNr potentiates the antiparkinsonian action of L-DOPA at the cost of inducing dyskinesia, as also observed in marmosets (Visanji et al., 2008). Although the prodyskinetic effect induced by intracerebroventricular UFP-101 and systemic J-113397 was mild, limited to limb dyskinesia and observed at maximal antagonist doses, this finding warns of the potential motor side effects of overdosing NOP antagonists as an adjunct to L-DOPA therapy.

The antidyskinetic effect of Ro 65–6570 was also replicated in the gold-standard model of LID, the dyskinetic macaque. The effect of Ro 65–6570 was milder than in rats, but occurred in the same dose range. Axial symptoms such as gait and balance disturbances are very common and disabling in PD patients (Jankovic, 2008). The finding that an NOP agonist improved posture in L-DOPA-treated dyskinetic macaques might contrast with previous findings that an NOP antagonist improved balance in MPTP-treated L-DOPA-unprimed macaques (Viaro et al., 2008). The apparent contradiction that an NOP agonist and an antagonist have the same impact on axial symptoms might be explained on the basis of an action at NOP receptors (possibly located in different brain areas/circuits) that are differently saturated by endogenous N/OFQ. Moreover, we should recall that the models and timing of administration were different in the two studies. Indeed, the overall behavioral patterns were different since the NOP antagonist also improved bradykinesia, tremor, hypokinesia, and rigidity, whereas the NOP agonist did not.

### Concluding remarks

A major side effect of long-term therapy with L-DOPA is the development of dyskinesias (Nutt and Gancher, 1994; Bezard et al., 2001a; Obeso et al., 2004; Calabresi et al., 2010), which represent a clinical challenge due to the poor therapeutic armamentarium available to neurologists, essentially limited to amantadine (Verhagen Metman et al., 1998). Here we report that exogenous N/OFQ and the small molecule NOP receptor agonist Ro 65–6570 inhibited LID expression in dyskinetic rats and macaques without attenuating the antiparkinsonian effect of L-DOPA. We also provide evidence that N/OFQ inhibited biochemical, electrophysiological, and neurochemical correlates of striatal D1 receptor activation in the naive or dyskinetic striatum, which suggests that NOP receptor agonists exert a selective antidyskinetic effect by activating striatal NOP receptors that oppose D1 signaling. However, further mechanistic studies in 6-OHDA lesioned dyskinetic and nondyskinetic rats need to be performed to confirm this hypothesis. The possibility that NOP receptor agonists exert an antidyskinetic effect through striatal NOP receptor does not contradict our previous finding that NOP receptor antagonists exert antiparkinsonian effects through blockade of NOP receptors in SNr. Indeed, an NOP receptor antagonist is expected to act primarily where the N/OFQ tone is elevated (i.e., in SNr), whereas an NOP receptor agonist where N/OFQ is low or absent (i.e., in striatum).

In conclusion, NOP receptor agonists have been proven effective for treating pain (Ko et al., 2009), anxiety (Jenck et al., 1997), and drug dependence (Zaveri, 2011). The concordance of the antidyskinetic effects in rats and nonhuman primates suggests that NOP receptor agonists may also prove effective in attenuating LID and rescuing motor activity in dyskinetic PD patients.

## References


Andersson M, Hilbertson A, Cenci MA (1999) Striatal fosB expression is causally linked with l-DOPA-induced abnormal involuntary movements and the associated upregulation of striatal prodynorphin mRNA in a rat model of Parkinson's disease. Neurobiol Dis 6:461–474. CrossRef Medline

Aubert I, Guigoni C, Håkansson K, Li Q, Dovero S, Barthe N, Bioulac BH, Gross CE, Fisone G, Bloch B, Bezard E (2005) Increased D1 dopamine receptor signaling in levodopa-induced dyskinesia. Ann Neurol 57:17–26. CrossRef Medline

Berthele A, Platzer S, Dworzak D, Schadrack J, Mahal B, Büttner A, Assmus HP, Wurster K, Zieglgänsberger W, Conrad B, Tölle TR (2003) [3H]-nociceptin ligand-binding and nociceptin opioid receptor mrna expression in the human brain. Neuroscience 121:629–640. CrossRef Medline

Berthet A, Porras G, Doudnikoff E, Stark H, Cador M, Bezard E, Bloch B (2009) Pharmacological analysis demonstrates dramatic alteration of D1 dopamine receptor neuronal distribution in the rat analog of L-DOPA-induced dyskinesia. J Neurosci 29:4829–4835. CrossRef Medline

Bezard E, Brotchie JM, Gross CE (2001a) Pathophysiology of levodopa-induced dyskinesia: potential for new therapies. Nat Rev Neurosci 2:577–588. CrossRef Medline

Bezard E, Boraud T, Chalon S, Brotchie JM, Guilloteau D, Gross CE (2001b) Pallidal border cells: an anatomical and electrophysiological study in the 1-methyl-4-phenyl-1,2,3,6-tetrahydropyridine-treated monkey. Neuroscience 103:117–123. CrossRef Medline

Bézard E, Ferry S, Mach U, Stark H, Leriche L, Boraud T, Gross C, Sokoloff P (2003) Attenuation of levodopa-induced dyskinesia by normalizing dopamine D3 receptor function. Nat Med 9:762–767. CrossRef Medline

Bridge KE, Wainwright A, Reilly K, Oliver KR (2003) Autoradiographic localization of (125)i[Tyr(14)] nociceptin/orphanin FQ binding sites in macaque primate CNS. Neuroscience 118:513–523. CrossRef Medline

Calabresi P, Pisani A, Mercuri NB, Bernardi G (1992) Long-term potentiation in the striatum is unmasked by removing the voltage-dependent magnesium block of NMDA receptor channels. Eur J Neurosci 4:929–935. CrossRef Medline

Calabresi P, Centonze D, Pisani A, Sancesario G, Gubellini P, Marfia GA, Bernardi G (1998) Striatal spiny neurons and cholinergic interneurons express differential ionotropic glutamatergic responses and vulnerability:

implications for ischemia and Huntington's disease. Ann Neurol 43:586–597. CrossRef Medline

Calabresi P, Di Filippo M, Ghiglieri V, Tambasco N, Picconi B (2010) Levodopa-induced dyskinesias in patients with Parkinson's disease: filling the bench-to-bedside gap. Lancet Neurol 9:1106–1117. CrossRef Medline

Calò G, Guerrini R, Rizzi A, Salvadori S, Regoli D (2000) Pharmacology of nociceptin and its receptor: a novel therapeutic target. Br J Pharmacol 129:1261–1283. CrossRef Medline

Calo G, Rizzi A, Rizzi D, Bigoni R, Guerrini R, Marzola G, Marti M, McDonald J, Morari M, Lambert DG, Salvadori S, Regoli D (2002) [Nphe1,Arg14,Lys15]nociceptin-NH2, a novel potent and selective antagonist of the nociceptin/orphanin FQ receptor. Br J Pharmacol 136:303–311. CrossRef Medline

Carta M, Carlsson T, Kirik D, Björklund A (2007) Dopamine released from 5-HT terminals is the cause of L-DOPA-induced dyskinesia in parkinsonian rats. Brain 130:1819–1833. CrossRef Medline

Cenci MA, Lundblad M (2007) Ratings of L-DOPA-induced dyskinesia in the unilateral 6-OHDA lesion model of Parkinson's disease in rats and mice. Curr Protoc Neurosci Chapter 9:Unit 9.25.

Cenci MA, Lee CS, Björklund A (1998) L-DOPA-induced dyskinesia in the rat is associated with striatal overexpression of prodynorphin- and glutamic acid decarboxylase mRNA. Eur J Neurosci 10:2694–2706. CrossRef Medline

Devine DP, Reinscheid RK, Monsma FJ Jr, Civelli O, Akil H (1996) The novel neuropeptide orphanin FQ fails to produce conditioned place preference or aversion. Brain Res 727:225–229. CrossRef Medline

Fasano S, Bezard E, D'Antoni A, Francardo V, Indrigo M, Qin L, Doveró S, Cerovic M, Cenci MA, Brambilla R (2010) Inhibition of Ras-guanine nucleotide-releasing factor 1 (Ras-GRF1) signaling in the striatum reverts motor symptoms associated with L-dopa-induced dyskinesia. Proc Natl Acad Sci U S A 107:21824–21829. CrossRef Medline

Fernagut PO, Li Q, Dovero S, Chan P, Wu T, Ravenscroft P, Hill M, Chen Z, Bezard E (2010) Dopamine transporter binding is unaffected by L-DOPA administration in normal and MPTP-treated monkeys. PLoS One 5:e14053. CrossRef Medline

Feyder M, Bonito-Oliva A, Fisone G (2011) L-DOPA-induced dyskinesia and abnormal signaling in striatal medium spiny neurons: focus on dopamine D1 receptor-mediated transmission. Front Behav Neurosci 5:71. Medline

Flau K, Redmer A, Liedtke S, Kathmann M, Schlicker E (2002) Inhibition of striatal and retinal dopamine release via nociceptin/orphanin FQ receptors. Br J Pharmacol 137:1355–1361. CrossRef Medline

Gouty S, Brown JM, Rosenberger J, Cox BM (2010) MPTP treatment increases expression of pre-pro-nociceptin/orphanin FQ mRNA in a subset of substantia nigra reticulata neurons. Neuroscience 169:269–278. CrossRef Medline

Guigoni C, Dovero S, Aubert I, Li Q, Bioulac BH, Bloch B, Gurevich EV, Gross CE, Bezard E (2005) Levodopa-induced dyskinesia in MPTP-treated macaques is not dependent on the extent and pattern of nigrostrial lesioning. Eur J Neurosci 22:283–287. CrossRef Medline

Hunter WM, Greenwood FC (1962) Preparation of iodine-131 labelled human growth hormone of high specific activity. Nature 194:495–496. CrossRef Medline

Jankovic J (2008) Parkinson's disease: clinical features and diagnosis. J Neurol Neurosurg Psychiatry 79:368–376. CrossRef Medline

Jenck F, Moreau JL, Martin JR, Kilpatrick GJ, Reinscheid RK, Monsma FJ Jr, Nothacker HP, Civelli O (1997) Orphanin FQ acts as an anxiolytic to attenuate behavioral responses to stress. Proc Natl Acad Sci U S A 94:14854–14858. CrossRef Medline

Kawamoto H, Ozaki S, Itoh Y, Miyaji M, Arai S, Nakashima H, Kato T, Ohta H, Iwasawa Y (1999) Discovery of the first potent and selective small molecule opioid receptor-like (ORL1) antagonist: 1-[(3R,4R)-1-cyclooctylmethyl-3-hydroxymethyl-4-piperidyl]-3-ethyl-1, 3-dihydro-2H-benzimidazol-2-one (J-113397). J Med Chem 42:5061–5063. CrossRef Medline

Ko MC, Woods JH, Fantegrossi WE, Galuska CM, Wichmann J, Prinssen EP (2009) Behavioral effects of a synthetic agonist selective for nociceptin/orphanin FQ peptide receptors in monkeys. Neuropsychopharmacology 34:2088–2096. CrossRef Medline

Lambert DG (2008) The nociceptin/orphanin FQ receptor: a target with broad therapeutic potential. Nat Rev Drug Discov 7:694–710. CrossRef Medline

Lindgren HS, Andersson DR, Lagerkvist S, Nissbrandt H, Cenci MA (2010) L-DOPA-induced dopamine efflux in the striatum and the substantia nigra in a rat model of Parkinson's disease: temporal and quantitative relationship to the expression of dyskinesia. J Neurochem 112:1465–1476. CrossRef Medline

Lundblad M, Andersson M, Winkler C, Kirik D, Wierup N, Cenci MA (2002) Pharmacological validation of behavioural measures of akinesia and dyskinesia in a rat model of Parkinson's disease. Eur J Neurosci 15:120–132. CrossRef Medline

Mabrouk OS, Marti M, Morari M (2010) Endogenous nociceptin/orphanin FQ (N/OFQ) contributes to haloperidol-induced changes of nigral amino acid transmission and parkinsonism: a combined microdialysis and behavioral study in naive and nociceptin/orphanin FQ receptor knockout mice. Neuroscience 166:40–48. CrossRef Medline

Marti M, Mela F, Bianchi C, Beani L, Morari M (2002a) Striatal dopamine-NMDA receptor interactions in the modulation of glutamate release in the substantia nigra pars reticulata in vivo: opposite role for D1 and D2 receptors. J Neurochem 83:635–644. CrossRef Medline

Marti M, Guerrini R, Beani L, Bianchi C, Morari M (2002b) Nociceptin/orphanin FQ receptors modulate glutamate extracellular levels in the substantia nigra pars reticulata. A microdialysis study in the awake freely moving rat. Neuroscience 112:153–160. CrossRef Medline

Marti M, Mela F, Veronesi C, Guerrini R, Salvadori S, Federici M, Mercuri NB, Rizzi A, Franchi G, Beani L, Bianchi C, Morari M (2004) Blockade of nociceptin/orphanin FQ receptor signaling in rat substantia nigra pars reticulata stimulates nigrostriatal dopaminergic transmission and motor behavior. J Neurosci 24:6659–6666. CrossRef Medline

Marti M, Mela F, Fantin M, Zucchini S, Brown JM, Witta J, Di Benedetto M, Buzas B, Reinscheid RK, Salvadori S, Guerrini R, Romualdi P, Candeletti S, Simonato M, Cox BM, Morari M (2005) Blockade of nociceptin/orphanin FQ transmission attenuates symptoms and neurodegeneration associated with Parkinson's disease. J Neurosci 25:9591–9601. CrossRef Medline

Marti M, Trapella C, Viaro R, Morari M (2007) The nociceptin/orphanin FQ receptor antagonist J-113397 and L-DOPA additively attenuate experimental parkinsonism through overinhibition of the nigrothalamic pathway. J Neurosci 27:1297–1307. CrossRef Medline

Marti M, Trapella C, Morari M (2008) The novel nociceptin/orphanin FQ receptor antagonist Trap-101 alleviates experimental parkinsonism through inhibition of the nigro-thalamic pathway: positive interaction with L-DOPA. J Neurochem 107:1683–1696. CrossRef Medline

Marti M, Viaro R, Guerrini R, Franchi G, Morari M (2009) Nociceptin/orphanin FQ modulates motor behavior and primary motor cortex output through receptors located in substantia nigra reticulata. Neuropsychopharmacology 34:341–355. CrossRef Medline

Marti M, Sarubbo S, Latini F, Cavallo M, Eleopra R, Biguzzi S, Lettieri C, Conti C, Simonato M, Zucchini S, Quatrale R, Sensi M, Candeletti S, Romualdi P, Morari M (2010) Brain interstitial nociceptin/orphanin FQ levels are elevated in Parkinson's disease. Mov Disord 25:1723–1732. CrossRef Medline

Meissner W, Ravenscroft P, Reese R, Harnack D, Morgenstern R, Kupsch A, Klitgaard H, Bioulac B, Gross CE, Bezard E, Boraud T (2006) Increased slow oscillatory activity in substantia nigra pars reticulata triggers abnormal involuntary movements in the 6-OHDA-lesioned rat in the presence of excessive extracellular striatal dopamine. Neurobiol Dis 22:586–598. CrossRef Medline

Mela F, Millan MJ, Brocco M, Morari M (2010) The selective D(3) receptor antagonist, S33084, improves parkinsonian-like motor dysfunction but does not affect L-DOPA-induced dyskinesia in 6-hydroxydopamine hemi-lesioned rats. Neuropharmacology 58:528–536. CrossRef Medline

Mela F, Marti M, Bido S, Cenci MA, Morari M (2012) In vivo evidence for a differential contribution of striatal and nigral D1 and D2 receptors to l-DOPA induced dyskinesia and the accompanying surge of nigral amino acid levels. Neurobiol Dis 45:573–582. CrossRef Medline

Meunier JC, Mollereau C, Toll L, Suaudeau C, Moisand C, Alvinerie P, Butour JL, Guillemot JC, Ferrara P, Monsarrat B (1995) Isolation and structure of the endogenous agonist of opioid receptor-like ORL1 receptor. Nature 377:532–535. CrossRef Medline

Mogil JS, Pasternak GW (2001) The molecular and behavioral pharmacology of the orphanin FQ/nociceptin peptide and receptor family. Pharmacol Rev 53:381–415. Medline

Muñoz A, Li Q, Gardoni F, Marcello E, Qin C, Carlsson T, Kirik D, Di Luca M, Björklund A, Bezard E, Carta M (2008) Combined 5-HT1A and

5-HT1B receptor agonists for the treatment of L-DOPA-induced dyskinesia. Brain 131:3380–3394. CrossRef Medline

Navailles S, Bioulac B, Gross C, De Deurwaerdère P (2010) Serotonergic neurons mediate ectopic release of dopamine induced by L-DOPA in a rat model of Parkinson's disease. Neurobiol Dis 38:136–143. CrossRef Medline

Nazzaro C, Marino S, Barbieri M, Siniscalchi A (2009) Inhibition of serotonin outflow by nociceptin/orphaninFQ in dorsal raphe nucleus slices from normal and stressed rats: role of corticotropin releasing factor. Neurochem Int 54:378–384. CrossRef Medline

Neal CR Jr, Mansour A, Reinscheid R, Nothacker HP, Civelli O, Watson SJ Jr (1999a) Localization of orphanin FQ (nociceptin) peptide and messenger RNA in the central nervous system of the rat. J Comp Neurol 406:503–547. CrossRef Medline

Neal CR Jr, Mansour A, Reinscheid R, Nothacker HP, Civelli O, Akil H, Watson SJ Jr (1999b) Opioid receptor-like (ORL1) receptor distribution in the rat central nervous system: comparison of ORL1 receptor mRNA expression with (125)I-[(14)Tyr]-orphanin FQ binding. J Comp Neurol 412:563–605. CrossRef Medline

Nishi M, Houtani T, Noda Y, Mamiya T, Sato K, Doi T, Kuno J, Takeshima H, Nukada T, Nabeshima T, Yamashita T, Noda T, Sugimoto T (1997) Unrestrained nociceptive response and dysregulation of hearing ability in mice lacking the nociceptin/orphaninFQ receptor. EMBO J 16: 1858–1864. CrossRef Medline

Norton CS, Neal CR, Kumar S, Akil H, Watson SJ (2002) Nociceptin/orphanin FQ and opioid receptor-like receptor mRNA expression in dopamine systems. J Comp Neurol 444:358–368. CrossRef Medline

Nutt JG, Gancher ST (1994) Parkinson's disease dyskinesias. Neurology 44: 1187; author reply 1187–1188. CrossRef Medline

Obeso JA, Rodriguez-Oroz M, Marin C, Alonso F, Zamarbide I, Lanciego JL, Rodriguez-Diaz M (2004) The origin of motor fluctuations in Parkinson's disease: importance of dopaminergic innervation and basal ganglia circuits. Neurology 62 [Suppl 1]:S17–S30. CrossRef Medline

Olianas MC, Dedoni S, Boi M, Onali P (2008) Activation of nociceptin/orphanin FQ-NOP receptor system inhibits tyrosine hydroxylase phosphorylation, dopamine synthesis, and dopamine D(1) receptor signaling in rat nucleus accumbens and dorsal striatum. J Neurochem 107:544–556. CrossRef Medline

Orellana D, Morella I, Indrigo M, Papale A, Brambilla R (2012) The Ras-ERK pathway in neuronal cell signalling. In: Protein kinase technologies (Mukai H, ed.). New York: Springer.

Paxinos G, Watson C (1986) The rat brain in stereotaxic coordinates, Ed 2. Orlando, FL: Academic.

Picconi B, Centonze D, Håkansson K, Bernardi G, Greengard P, Fisone G, Cenci MA, Calabresi P (2003) Loss of bidirectional striatal synaptic plasticity in L-DOPA-induced dyskinesia. Nat Neurosci 6:501–506. Medline

Reinscheid RK, Nothacker HP, Bourson A, Ardati A, Henningsen RA, Bunzow JR, Grandy DK, Langen H, Monsma FJ Jr, Civelli O (1995) Orphanin-Fq— a neuropeptide that activates an opioid-like g-protein-coupled receptor. Science 270:792–794. CrossRef Medline

Röver S, Adam G, Cesura AM, Galley G, Jenck F, Monsma FJ Jr, Wichmann J, Dautzenberg FM (2000) High-affinity, non-peptide agonists for the ORL1 (orphanin FQ/nociceptin) receptor. J Med Chem 43:1329–1338. CrossRef Medline

Sarre S, Vandeneede D, Ebinger G, Michotte Y (1998) Biotransformation of L-DOPA to dopamine in the substantia nigra of freely moving rats: effect of dopamine receptor agonists and antagonists. J Neurochem 70: 1730–1739. Medline

Sbrenna S, Marti M, Morari M, Calò G, Guerrini R, Beani L, Bianchi C (2000) Modulation of 5-hydroxytryptamine efflux from rat cortical synaptosomes by opioids and nociceptin. Br J Pharmacol 130:425–433. CrossRef Medline

Tao R, Ma Z, Thakkar MM, McCarley RW, Auerbach SB (2007) Nociceptin/orphanin FQ decreases serotonin efflux in the rat brain but in contrast to a kappa-opioid has no antagonistic effect on mu-opioid-induced increases in serotonin efflux. Neuroscience 147:106–116. CrossRef Medline

Valjent E, Pascoli V, Svenningsson P, Paul S, Enslen H, Corvol JC, Stipanovich A, Caboche J, Lombroso PJ, Nairn AC, Greengard P, Hervé D, Girault JA (2005) Regulation of a protein phosphatase cascade allows convergent dopamine and glutamate signals to activate ERK in the striatum. Proc Natl Acad Sci U S A 102:491–496. CrossRef Medline

Verhagen Metman L, Del Dotto P, van den Munckhof P, Fang J, Mouradian MM, Chase TN (1998) Amantadine as treatment for dyskinesias and motor fluctuations in Parkinson's disease. Neurology 50:1323–1326. CrossRef Medline

Viaro R, Sanchez-Pernaute R, Marti M, Trapella C, Isacson O, Morari M (2008) Nociceptin/orphanin FQ receptor blockade attenuates MPTP-induced parkinsonism. Neurobiol Dis 30:430–438. CrossRef Medline

Viaro R, Marti M, Morari M (2010) Dual motor response to l-dopa and nociceptin/orphanin FQ receptor antagonists in 1-methyl-4-phenyl-1,2,5,6-tetrahydropyridine (MPTP) treated mice: paradoxical inhibition is relieved by D(2)/D(3) receptor blockade. Exp Neurol 223:473–484. CrossRef Medline

Visanji NP, de Bie RM, Johnston TH, McCreary AC, Brotchie JM, Fox SH (2008) The nociceptin/orphanin FQ (NOP) receptor antagonist J-113397 enhances the effects of levodopa in the MPTP-lesioned nonhuman primate model of Parkinson's disease. Mov Disord 23:1922–1925. CrossRef Medline

Volta M, Mabrouk OS, Bido S, Marti M, Morari M (2010) Further evidence for an involvement of nociceptin/orphanin FQ in the pathophysiology of Parkinson's disease: a behavioral and neurochemical study in reserpinized mice. J Neurochem 115:1543–1555. CrossRef Medline

Volta M, Viaro R, Trapella C, Marti M, Morari M (2011) Dopamine-nociceptin/orphanin FQ interactions in the substantia nigra reticulata of hemiparkinsonian rats: involvement of D2/D3 receptors and impact on nigro-thalamic neurons and motor activity. Exp Neurol 228:126–137. CrossRef Medline

Westin JE, Lindgren HS, Gardi J, Nyengaard JR, Brundin P, Mohapel P, Cenci MA (2006) Endothelial proliferation and increased blood-brain barrier permeability in the basal ganglia in a rat model of 3,4-dihydroxyphenyl-L-alanine-induced dyskinesia. J Neurosci 26:9448–9461. CrossRef Medline

Zaveri NT (2011) The nociceptin/orphanin FQ receptor (NOP) as a target for drug abuse medications. Curr Top Med Chem 11:1151–1156. CrossRef Medline

# Chapter 8

# The Extracellular Signal-Regulated Kinase (ERK) Cascade in Neuronal Cell Signaling

**Daniel Orellana, Ilaria Morella, Marzia Indrigo, Alessandro Papale, and Riccardo Brambilla**

## Abstract

The Ras-controlled extracellular signal-regulated kinase (ERK) pathway mediates a large number of cellular events, from proliferation to survival, from synaptic plasticity to memory formation. In order to study the role of the two major ERK isoforms in the brain, ERK1 and ERK2, we have generated GFP fusion proteins of both protein kinases. In addition, we have produced two swapped constructs in which the N-term tail of ERK1, the domain responsible for its unique properties, has either been removed from ERK1 or attached to ERK2. We demonstrated that all four GFP proteins are properly expressed in vitro in mouse embryo fibroblasts. However, only ERK1 and ERK2 > 1 overexpression resulted in a significant growth retardation. In addition, we have expressed all four GFP fusion constructs in vivo, in the adult brain, using lentiviral vector-assisted transgenesis and found that they are predominantly neuronal. Finally, we have devised an ex-vivo system, in which brain slices prepared from adult mice can be stimulated with glutamate and the activation of both cytoplasmic and nuclear substrates of ERK can be detected. Since phosphorylation of both the ribosomal protein S6 and of the histone H3 is completely prevented by a chemical inhibition of the ERK pathway, this ex-vivo system can be exploited in the future to investigate the regulation of the ERK cascade using slices from LV-injected or conventional transgenic animals.

**Key words:** Ras-ERK signaling, Cell proliferation, Lentiviral vectors, Glutamate, MEK inhibitors, Brain slices, Immunofluorescence

## 1. Introduction

Cell communication is a major process controlling life of both unicellular and multicellular organisms. Within cells, a broad range of different signaling pathways is involved in these communications. Among them, special attention has been pointed to the mitogen-activated protein (MAP) kinase system, a major signal transduction pathway mediating the transfer of extracellular stimuli to the

Hideyuki Mukai (ed.), *Protein Kinase Technologies*, Neuromethods, vol. 68,
DOI 10.1007/978-1-61779-824-5_8, © Springer Science+Business Media, LLC 2012

nucleus. The MAPK system is highly conserved throughout eukaryotic evolution, from yeast to humans. The core component of this pathway is made up of a three-tier protein kinase system which is upstream regulated, at the cell membrane, by members of the Ras superfamily of small GTPases. The MAPK family of cellular pathways in mammalian cells is divided into four distinct subfamilies named following the last protein kinase of the signal transduction cascade: ERK (extracellular signal-regulated kinase), JNK (c-Jun *N-terminal* kinase), p38 SAPK (stress-activated protein kinase), and ERK5/BMK1 (big MAP kinase1) subfamily (1–4).

Once activated, ERK signaling may be involved, depending on the cell type and on the physiological context, in a wide range of processes, ranging from embryogenesis, cell differentiation, cell survival, cell proliferation, and cancer. In the brain, this cascade provides a link between ionotropic, metabotropic, and neurotrophin receptors to cytosolic (regulation of ion channels and of protein translation) and nuclear events, leading to gene transcription, de novo protein synthesis and changes either in synaptic remodeling and plasticity, memory formation, or neuronal survival, depending on the context. Once activated by neurotransmitter receptors through GTP/GDP exchange factors, the small GTPases belonging to the Ras class (p21 H-, K- and N-Ras gene products) stimulate sequentially the cascade of protein kinases consisting of serine/threonine kinases of the Raf subfamily (mainly c-Raf and B-Raf, the MAPK Kinase Kinase tier), the threonine/tyrosine dual-specificity kinases MEK1/2 (MAPK Kinase), and finally ERK1/2 proteins (the MAPK component) (5). More specifically, activation of MEK1/2 leads to a selective interaction with ERK proteins through specific docking domains which result in phosphorylation of the conserved recognition motif of threonine and tyrosine (TEY domain), within the activation loop of ERK1/2 (6). ERK1 and ERK2, also known as p44/p42MAPK, respectively, are homologous isoforms produced by two genes, erk1 (MAPK3) and erk2 (MAPK1). Both of them have nearly 85% amino acid identity with much greater identity in the core regions and are expressed in essentially all cells, even if ERK2 is the predominant isoform in brain and hematopoietic cells (7). Once activated, ERK1 and ERK2, the two major MAPK in the brain, are able to translocate into the nucleus. There, they can activate, either directly or indirectly (via the kinases of the RSK families), transcription factors, including the CREB-like class of transcriptional regulators, or to regulate chromatin remodeling (via the kinases of the MSK family) by for instance phosphorylating histone H3 (8–10). The ability of ERK in regulating gene expression and chromatin organization is believed to be a crucial step not only in the processes of neural adaptations underlying normal cognitive processes but also in the onset of several neuropsychiatric disorders (11–15). In addition, this signaling pathway also controls protein translation in the

cytosol and in the dendrites by activating the mTor pathway that regulates a number of factors including the S6 kinase which directly phosphorylate the S6 ribosomal protein (16).

ERK1 and ERK2 are activated by the same stimuli and are believed to bear similar substrate recognition properties and subcellular localization (17). Because of their great similarity, the two isoforms have been considered for a long time as largely interchangeable, with mostly overlapping functions, and are traditionally designated as a single ERK1/2 entity; this concept is also derived from the use, in several studies of the ERK pathway, of MEK inhibitors (such as U0126 or SL327) that do not discriminate between MEK1 and MEK2 (18–20). Although some studies still claim that ERK isoforms contribute to ERK signaling according to the ratio of their expression levels and not to their specific properties, recent evidence has highlighted critical functional differences between these two isoforms. A strong support in this direction derives from the results obtained using ERK1 or ERK2 knockout (KO) mice. ERK2 KO mice die early in development, showing that ERK1 cannot compensate for ERK2 in the embryo (21–26). On the contrary, *erk1* gene ablation is fully compatible with the adult life (27–29). Experiments at the molecular level in a variety of cell types showed that in ERK1-deficient cells (taken from ERK1 KO mice) the stimulus-dependent activation of ERK2 was enhanced, without any compensatory increase in ERK2 protein levels (27, 29). Other studies have used RNA interference techniques to silence the activity of ERK1, obtaining its knockdown in cells: as a result, cell growth was facilitated (7, 30). Interestingly, the phenotype caused by ERK1 knockdown, i.e., an enhancement of ERK2 activity, strongly parallel that observed when a constitutive active form of MEK1 is overexpressed via lentiviral vectors into mouse embryo fibroblasts (MEF) cells. On the contrary, the ERK2 knockdown phenotype is similar to what observed with a dominant negative form of MEK1 (30). Importantly, ERK2 activity enhancement in the nervous system of ERK1 mutant mice has been linked to improvement of certain forms of learning and memory (29, 31). The model put forward to explain these functional differences between ERK1 and ERK2 is that while ERK2 appears to be the main MAPK isoform transducing the signal to the nucleus, ERK1 seems to act like a partial agonist, antagonizing the binding of ERK2 with interacting partners. Importantly, the structural basis of these differences has recently been located to the unique N-terminal moiety of ERK1, which causes a significant delay in the nuclear/cystoplamic shuttling. Indeed, a final confirmation that the N-terminal portion of ERK1 is responsible for the observed phenotype comes from the swap of this domain between the two ERK isoforms: ERK1 without its N-term behaves in proliferating cells like ERK2 while ERK2 fused to the ERK1 N-term causes a ERK1-like phenotype (17).

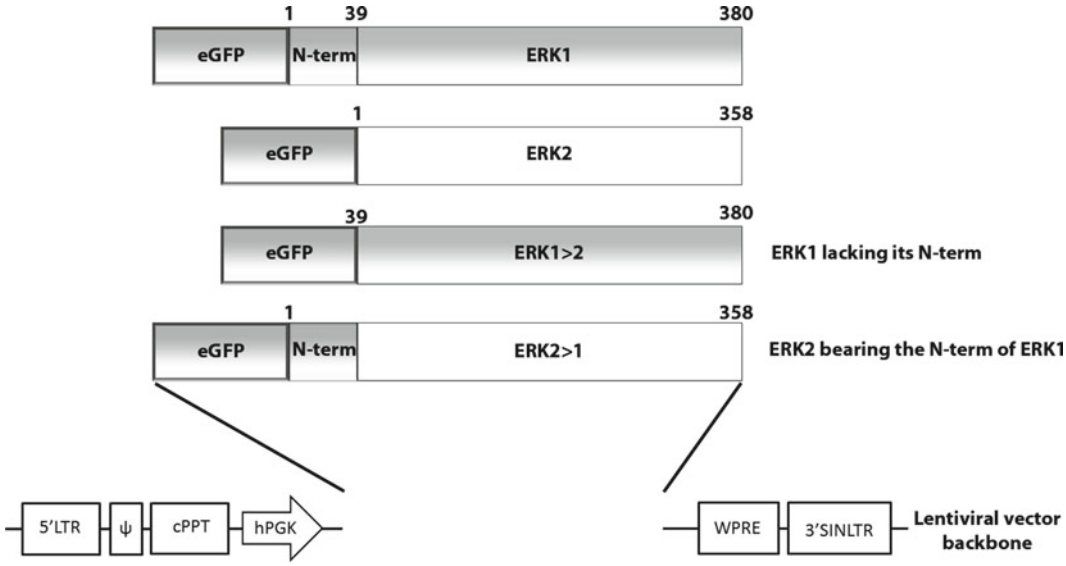


Fig. 1. Lentiviral vectors for ERK1, ERK2, and their swapped GFP fusion proteins. Schematic representation of the different ERK constructs in which the N-term moiety (1-39aa) of ERK1, conferring unique properties, is either present or absent. The ERK constructs were subcloned in a LV vector (pCCLsin.PPT.hPGK.eGFP.PRE) for in vivo expression studies.

In order to study in vivo in the brain the functional differences between ERK1 and ERK2, we generated GFP fusion proteins not only of ERK1 and ERK2 but also of their swapped counterparts: ERK1>2 (ERK1 deprived of its N-term) and ERK2>1 (ERK2 with the ERK1 N-term attached) (Fig. 1). These constructs have been introduced in a lentiviral vector (LV) and high-titer viral preparations have been obtained. LV is a powerful and efficient tool to modify gene expression in primary cells without the need to use a selection marker, which is a major complication for in vitro study of cell proliferation. Supporting the competition model described above, here we show that the overexpression of ERK1 and of ERK2>1 fusion proteins into MEF causes a reduction in the cell growth (Fig. 2). On the contrary, overexpression of ERK2 and of ERK1>2 fusion proteins results in a growth advantage. Importantly, once validated their activity in vitro, these LV constructs can now be used to study the function of ERK1 and ERK2 kinases in the brain. Stereotactic injections at the dorsal striatum of the mouse brain of such LV lead to a strong visualization of all four GFP fusion proteins. These proteins can be observed within 4 weeks from the surgical procedure. Superimposition of the fluorescence signals of GFP expressing cells (in green) with either a neuron-specific marker (NeuN, in red, Fig. 3a) or with a glial-specific staining (GFAP, in red, Fig. 3b) demonstrates a preferential neuronal localization of all four LV-expressed ERK–GFP fusion constructs. In order to study biochemically the function of these

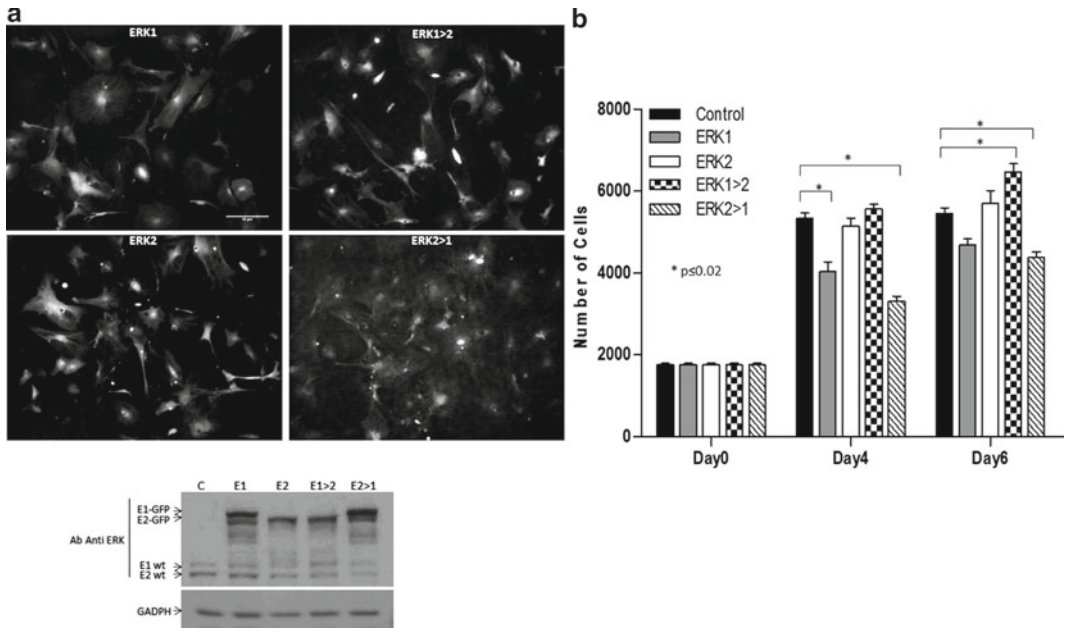


Fig. 2. Effects of ERK constructs in MEF proliferation. (**a**) Images of MEF cells infected with the LV expressing different GFP fusion proteins (MOI = 5). MEF cells were infected with LV vectors expressing ERK1, ERK2, and their swapped counterparts ERK1 > 2 and ERK2 > 1. Four days after infection, the GFP protein was found expressed ubiquitously in the cell. Bar = 50 μm. In the low left insert a representative Western blot is shown. A whole-cell extract was immunoblotted for ERK and GADPH (loading control). The GFP fusion proteins of ERK1, ERK2, and their swapped counterparts were easily detected by immunoblotting. (**b**) Proliferation assay on MEF transduced with LV for ERK1, ERK2, and their swapped versions. Proliferation was assessed by counting every day the cells using a Coulter Counter. $1.25 \times 10^5$ cells/well were seeded in six-well plate and maintained in culture medium. The following day (day 0), cells were transduced at MOI = 5 with lentiviral vectors expressing ERK1, ERK2, and their swapped counterparts or GFP as a control. At the end of the experiment (day 6), a significant growth retardation was observed in cells infected with LV for ERK1 and ERK2 > 1. Results are the mean of $n = 6$.

GFP fusion proteins, we have also set up an ex-vivo system in which brain slices can be freshly prepared from adult mice, incubated in a perfusing chamber and stimulated with appropriate agonist and antagonists. As shown in Figs. 4 and 5, striatal slices can be challenged with glutamate and induction of ERK signaling can be monitored at the single cell level using phospho-specific antibodies either against ribosomal protein S6 (pS6) or histone H3 (pH3). Quantification of double pS6 or pH3 (in red) and anti-NeuN staining (in green) allow us to monitor changes in ERK activity. Importantly, pretreating the slices with U0126, a specific MEK1/2 inhibitor, completely blocks S6 and H3 phosphorylation. Having validated this ex-vivo system, brain slices can in the future be prepared from LV-injected mice and/or from other transgenic animals and the activity of the ERK pathway can be easily assessed with a tight spatio-temporal resolution.

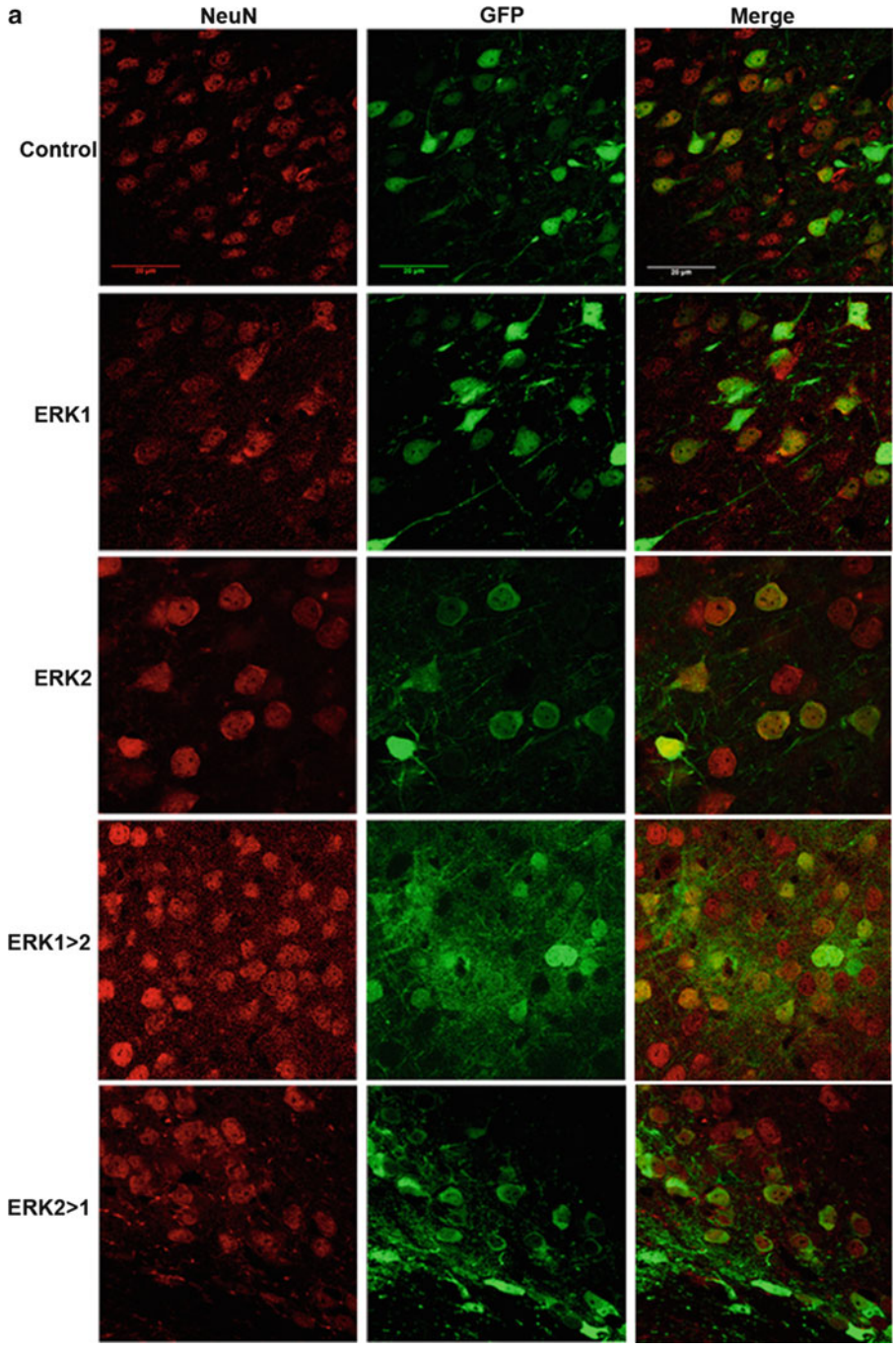


Fig. 3. In vivo expression of the LV constructs in the mouse brain. Images from the mouse striatum infected with LV for the different ERK constructs. Sections of the mouse brain were studied by immunofluorescence at 4 weeks following dorsal striatum injections. Immunofluorescence for either (**a**) NeuN (a neuron-specific marker, in *red*) or, (**b**) GFAP (a glial-specific marker, in *red*) demonstrated a preferential neuronal expression mediated by the lentiviral vectors. Smaller neurons show obvious colocalization of GFP and the primarily nuclear NeuN expression. Some neurons do not include the nucleus in the confocal optical plane of section and thus do not appear NeuN-positive in these images, although they would show co-localization in subsequent focal planes. Bar = 20 μm.

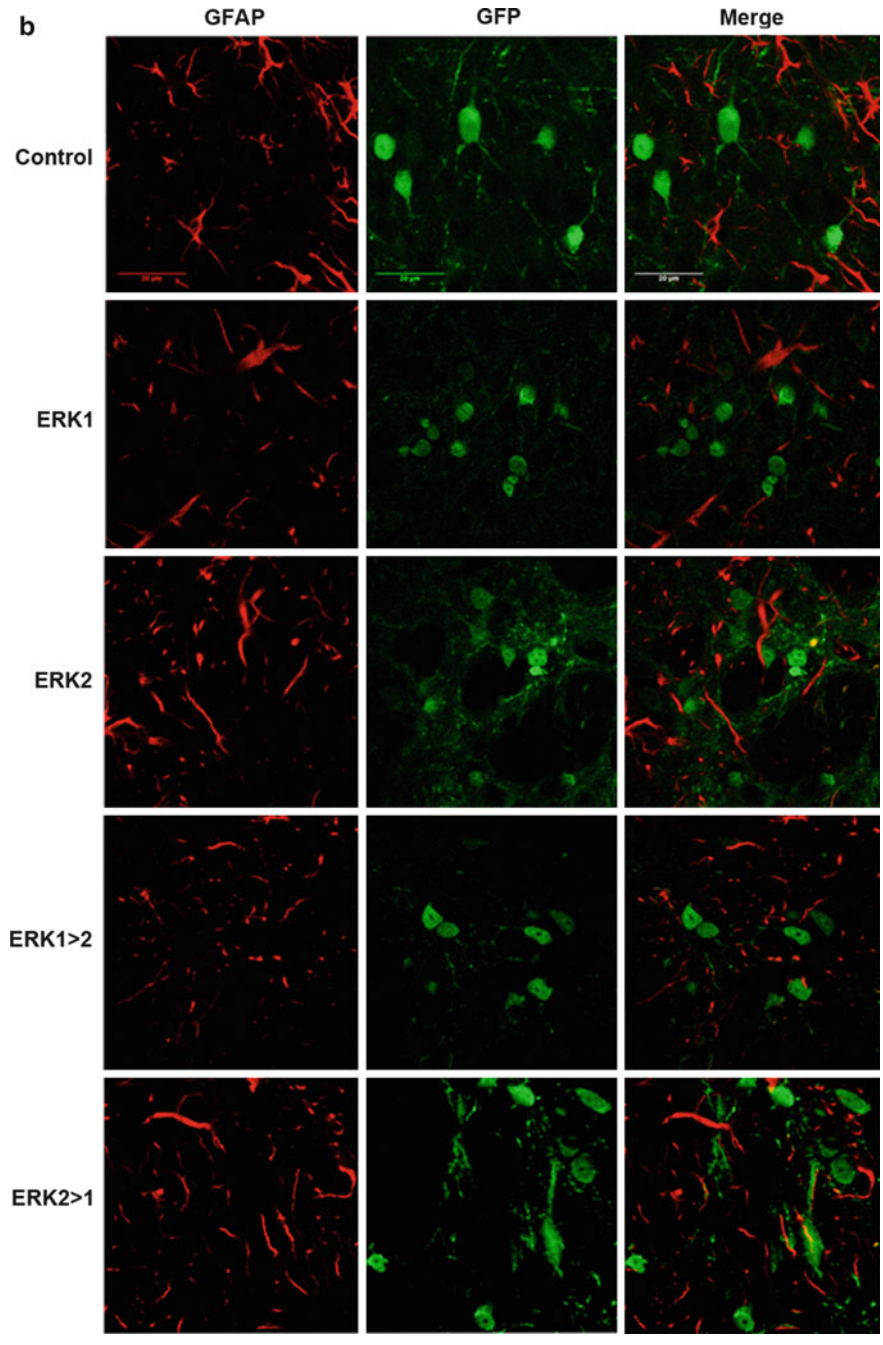


Fig. 3. (continued)

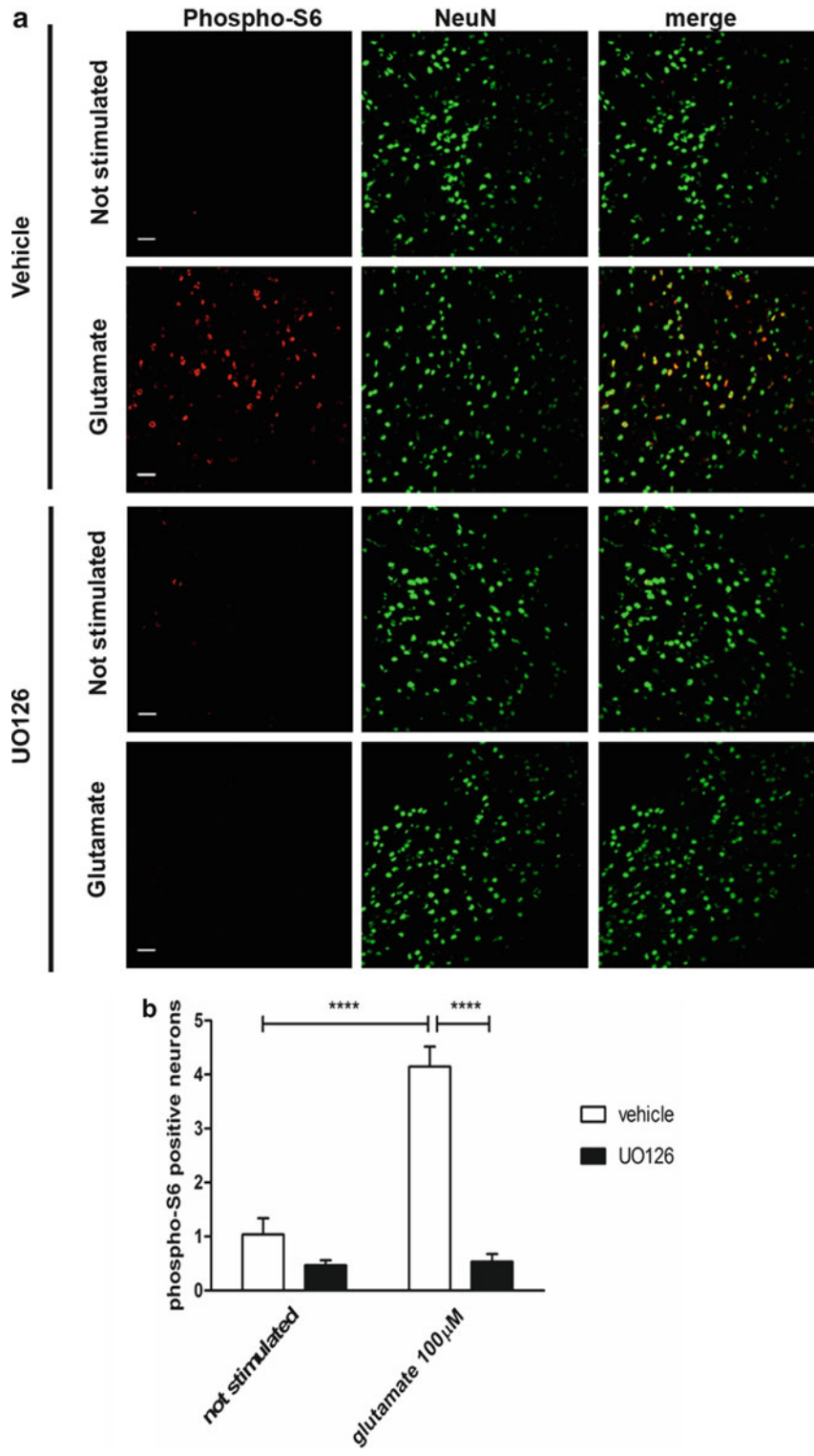


Fig. 4. S6 ribosomal protein phosphorylation is prevented by MEK inhibitor UO126 in a model of mature striatal slices. (**a**) Double immunolabeling of phospho S6 ribosomal protein (Ser235/236) (*red*) and NeuN (*green*) in adult striatal slices stimulated or not with glutamate 100 μM for 10 min in the presence of the vehicle or 20 μM UO126. (**b**) The data from the quantification are represented in the graph as mean ± SEM ($n = 7$ and $n = 8$ for the groups treated with vehicle and respectively stimulated or not with glutamate, $n = 9$ for the groups treated with UO126). Statistical analysis was performed using two-way ANOVA and post-hoc comparisons between groups using Bonferroni test (****$p < 0.0001$). Scale bars: 30 μm.

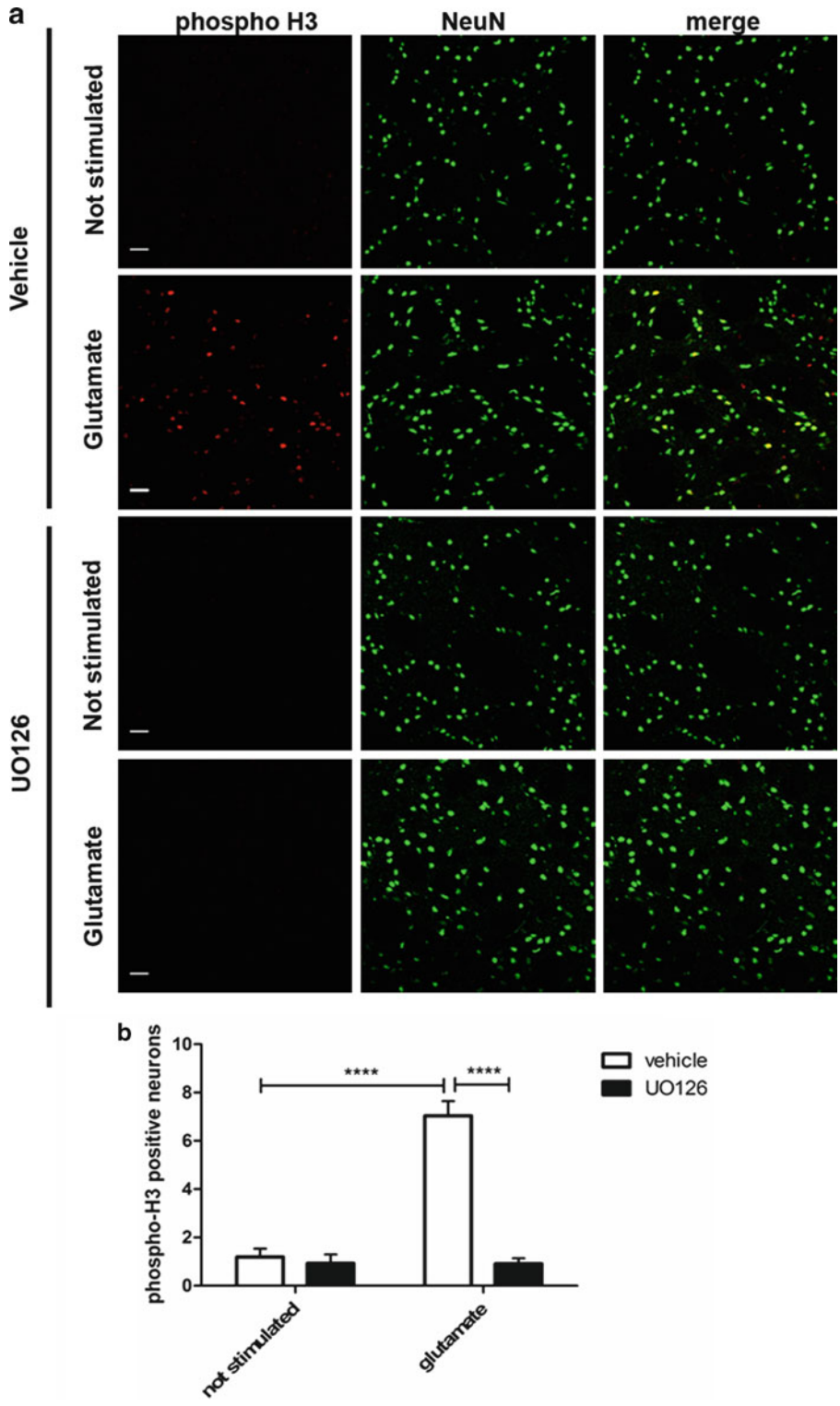


Fig. 5. Histone H3 phosphorylation is prevented by MEK inhibitor UO126 in a model of mature striatal slices. (**a**) Double immunolabeling of phospho-histone H3 (*red*) and NeuN (*green*) in adult striatal slices stimulated or not with glutamate 100 μM for 10 min in the presence of the vehicle or 20 μM UO126. (**b**) The data from the quantification are represented in the graph as mean ± SEM ($n = 4$ and $n = 3$ for the groups treated with vehicle and respectively stimulated or not with glutamate, $n = 6$ and $n = 5$ for the groups treated with UO126 vehicle and respectively stimulated or not with glutamate). Statistical analysis was performed using two-way ANOVA and post-hoc comparisons between groups using Bonferroni test (****$p < 0.0001$). Scale bars: 30 μm.

## 2. Materials

### 2.1. Cell Culture, Transfection, and Viral Vector Production

1. Dulbecco's Modified Eagle Medium with GlutaMax (DMEM GlutaMax, GIBCO).
2. Iscove's Modified Dulbecco Medium (IMDM, SIGMA).
3. Fetal Bovine Serum (FBS, EUROCLONE).
4. 100× Glutamine (200 mM Glutamine) (GIBCO).
5. 100× Pen/Strept (10,000 U/ml Penicillin, 10,000 μg/ml Streptomycin, GIBCO).
6. Sodium butyrate (SIGMA).
7. Dulbecco's Phosphate Saline Buffer (PBS, EUROCLONE).
8. Trypsin solution (0.05% Trypsin/ethylenediaminetetraacetic acid) (GIBCO).
9. Tris–EDTA (TE) buffer 1× [10 mM Tris (SIGMA) pH 8.0; 1 mM EDTA, SIGMA].
10. Collagenase (SIGMA).
11. 100 mm, 150 mm and six-well plates (CORNING).
12. 2× HBS pH 7.09: 281 mM NaCl, 100 mM HEPES (SIGMA), 1.5 mM $Na_2HPO_4$ (SIGMA), filter sterilized and stored at –20°C.
13. 2.5 M $CaCl_2$ solution (SIGMA) filtered (0.22 μm) and stored at –20°C.
14. Sterile water (DIACO).
15. Syringe-driven filter units (0.22 μm) MILLEX GP (MILLIPORE).
16. Dimethylsulfoxide (DMSO, SIGMA).

### 2.2. Proliferation Curve

1. Fixing solution: 2% Paraformaldehyde (SIGMA) in PBS.
2. Cell Coulter Z1 (BECKMAN).
3. Saline solution (0.9% NaCl solution in sterile water, DIACO).

### 2.3. Sodium Dodecyl Sulfate–PolyAcrylamide Gel Electrophoresis (SDS–PAGE)

1. Stacking Gel: 125 mM Tris/HCl pH 6.8; 4.5% Acrylamide-bis (37.5:1) (MERCK); 0.1% SDS (SIGMA); 0.2% Ammonium persulphate (SIGMA); 0.2% *N*,*N*,*N*′,*N*′-Tetramethylethylenediamine (TEMED, BIORAD).
2. Running Gel: 375 mM Tris/HCl pH 8.8; 12% Acrylamide-bis (37.5:1); 0.1% SDS; 0.1% Ammonium persulphate; 0.1% TEMED.
3. Running Buffer pH 8.8: 25 mM Tris; 190 mM Glycine (SIGMA); 0.1% SDS.

4. Sample Buffer 5×: 250 mM Tris/HCl pH 6.8; 10% SDS; 50% Glycerol; 0.02% Bromophenol Blue (SIGMA); 110 mM Dithiothreitol (DTT, SIGMA).
5. Lysis Buffer: 125 mM Tris/HCl pH 6.8, 2.5% SDS.

### 2.4. Western Blot

1. Transfer Buffer: 25 mM Tris; 190 mM Glycine, 20% Methanol (MERCK).
2. Protran Nitrocellulose membrane (WHATMAN).
3. Tris Buffered Saline buffer (TBS): 20 mM Tris/HCl pH 7.4; 150 mM NaCl, (SIGMA)) with 0.1% Tween (SIGMA) (TBS-TW).
4. Blocking buffer: 5% Bovine Serum Albumin, (SIGMA) in TBS-TW.
5. Antibody buffer: 3% BSA in TBS-TW.
6. Antibodies: p44-42 MAPK #SC-153 (SANTA CRUZ BIOTECHNOLOGY), GAPDH #SC-25778 (SANTA CRUZ BIOTECHNOLOGY).

### 2.5. In Vivo Injection

1. C57/BL6 male mice 26g (Charles River). All experimental procedures must be performed in accordance with National and Institutional Guidelines for the use of laboratory animals.
2. Anesthetic solution: 100 mg/kg Ketamine (KETAVET, INTERVET), 10 mg/kg Xilazina (Rompun, BAYER) in physiologic solution.
3. Microscope (L-0940SD, INAMI).
4. Stereotaxic Frame (Kopf Instruments).

### 2.6. Perfusion and Preparation of Free-Floating Slices

1. Phosphate Buffer (PB): pH 7.4 ($Na_2HPO_4$ 81 mM, $NaH_2PO_4$ 18.84 mM).
2. Perfusion solution: Paraformaldehyde (PFA) 4% in PB.
3. Sucrose 30% in PB.
4. Anti-Freeze: $Na_2HPO_4 \cdot 2H_2O$ 30.62 mM, $NaH_2PO_4 \cdot H_2O$ 11.38 mM, 33.33% ethylene glycol, 33.33% glycerol.
5. Microtome (MICROM HM 430).

### 2.7. Preparation of Acute Striatal Slices

1. C57/BL6 mice 2–3 months old (Charles River) (see Note 1). All experimental procedures must be performed in accordance with National and Institutional Guidelines for the use of laboratory animals.
2. Artificial cerebrospinal fluid (ACSF): 124 mM NaCl, 5 mM KCl, 1.3 mM $MgSO_4 \cdot 7H_2O$, 1.2 mM $NaH_2PO_4 \cdot H_2O$, 25 mM $NaHCO_3$, 10 mM D-glucose 2.4 mM $CaCl_2$ (1 M stock) in $dH_2O$. This solution should be prepared fresh on the day of the experiment and saturated with carbogen (95% $O_2$, 5% $CO_2$) for 10 min before use.

3. Sucrose-based dissecting solution: 87 mM NaCl, 2.5 mM KCl, 7 mM $MgCl_2$ 1 mM $NaH_2PO_4$, 75 mM sucrose, 25 mM $NaHCO_3$, 10 mM D-glucose, 0.5 mM $CaCl_2$ (1 M stock), and 2 mM kynurenic acid in $dH_2O$. This solution should be prepared fresh on the day of the experiment and saturated with carbogen for 10 min before use.
4. L-glutamic acid 100 μM (>99%, Sigma-Aldrich).
5. UO126 20 μM (Tocris Bioscience) diluted in DMSO.
6. Fixative solution: 4% paraformaldehyde in 0.1 M sodium phosphate buffer pH 7.4. This solution should be prepared fresh on the day of the experiment. This solution is harmful, and it must be used in ventilated hood wearing gloves.
7. Cryoprotectant solution: 30% sucrose in 0.1 M sodium phosphate buffer pH 7.4. This solution should be prepared fresh on the day of the experiment.
8. Dissection tools for removing the brains (scissors, forceps, and spatula).
9. Cyanoacrylate glue.
10. Vibratome (VT1000S, Leica Microsystems).
11. Brain slice chamber-BSC1 (Scientific System design Inc., Mississauga, ON, Canada).
12. Proportional temperature controller (Scientific System design Inc., Mississauga, ON, Canada).
13. Two peristaltic pumps (Minipuls 3, Gilson) with R8 medium flow pump heads (see Note 2).
14. Silicone peristaltic tubing and connectors (Gilson).

### 2.8. Slices Sectioning

1. Cryostat.
2. Embedding medium for frozen sectioning.
3. Superfrost slides.

### 2.9. Immunofluorescence

1. Dulbecco's Phosphate Saline Buffer (PBS, EUROCLONE).
2. Blocking solution:
   (a) NeuN antibody: 5% NGS (normal goat serum), 0.1% Triton100 in PBS.
   (b) GFAP antibody: 10% NGS, 0.1% Triton100, BSA 1 mg/ml in PBS.
3. Primary Antibodies: anti-phospho-S6 ribosomal protein (Thr235/236) (Cell signaling Technology) 1:100, anti-phospho (Ser10)-acetyl (Lys14)-histone H3 (1:1000) (Upstate), Alexa Fluor 488 conjugate antiGFP (1:500) (A21311, Invitrogen), NeuN (1:500) (MAB-377, CHEMICON), rabbit anti-GFAP (1:500) (DAKO).

4. Secondary Antibodies: Alexa Fluor 546 goat anti-mouse (1:200) (A11003, Invitrogen), Alexa Fluor 555 goat anti-mouse (1:1000) (A21422, Molecular Probes), Alexa Fluor 546 goat anti-rabbit (1:200) (A-11035, Molecular Probes), Alexa Fluor 488 goat anti-mouse (1:200) (A11001, Invitrogen).
5. PapPen (Sigma).
6. Fluorescence Mounting Medium (S3023, Dako).
7. Microscope Slide Superfrost Plus (Thermo Scientific) and coverslips.
8. Leica confocal microscope.

## 3. Methods

### *3.1. Mouse Embryonic Fibroblasts Preparation*

MEF cultures are prepared from wild-type E13.5 embryos obtained from commercially available C57 B/6 mice (Charles River) (see Note 3).

1. Dissection is carried out in PBS.
2. Remove the internal organs and the head, reduce the remaining tissues in small pieces and transfer in a 50 ml tube.
3. Centrifuge at 3,000 rcf for 5 min.
4. Wash in PBS and incubate for 1 h at 37°C in a solution of 0.25% collagenase and 20% FBS in PBS.
5. Dissociate tissues using a syringe.
6. Centrifuge at 3,000 rcf for 5 min at room temperature.
7. Resuspend the cells in DMEM GlutaMax containing 10% FBS, 1× Pen/Strept.
8. Count the cells and seed $5 \times 10^6$ cells on 15 mm plates.
9. Freeze the cells at confluence in 95% serum and 5% DMSO.

### *3.2. Lentiviral Vectors Production*

We use all third-generation LV, modifications of the originally described backbone (see Note 4).

1. Seed and incubate $9 \times 10^6$ HEK 293T cells [ATCC, CRL-11268] in 150 mm dishes, approximately 24 h before transfection. The medium used is DMEM GlutaMax containing 10% FBS, 1× Pen/Strept. Use low passage cells (not more than P12–15) and do not ever let cells grow to confluence.
2. Change medium 2 h before transfection: IMDM supplemented with 10% FBS, 1× Pen/Strept, 1× glutamine (22 ml final volume).
3. Prepare the plasmid DNA mix by adding together: 9 µg ENV plasmid (VSV-G), 12.5 µg packaging plasmid (pMDLg/pRRE

or CMV R8.74), 6.25 μg of pRSV-REV, and 32 μg of gene transfer plasmid. The plasmid mix solution is made up to a final volume of 1,125 μl with 0.1× TE Buffer (1: 10 mM Tris pH 8.0; 1 mM EDTA pH 8.0 in water). Finally, 125 μl of 2.5 M $CaCl_2$ is added.

4. Leave the mix 15 min at room temperature.
5. The precipitate is formed by dropwise addition of 1,250 μl of 2× HBS (281 mM NaCl, 100 mM HEPES, 1.5 mM $Na_2PO_4$, pH 7.06–7.12) solution to the 1,250 μl DNA–TE–$CaCl_2$ mixture from step 3 while vortexing at full speed. The precipitate should be added to HEK 293T-cell immediately following the addition of the 2 HBS. High magnification microscopy of the cells should reveal a very small granular precipitate of $CaPO_4$-precipitate plasmid DNA, initially above the cell monolayer and after incubation in 37°C incubator overnight, on the bottom of the plate in the large spaces between the cells.
6. The $CaPO_4$-precipitate plasmid DNA should be allowed to stay on the cells for 14–16 h, after which the media should be replaced with fresh medium (IMDM with 10% FBS, 1× Pen/Strept, 1× glutamine and 1 M sodium butyrate).
7. Collect the cell supernatants at 36 h after changing the medium, filter (0.22 μm) and centrifuge at 20,000 rpm, at 20°C for 2 h (Beckman Ultracentrifuge, SW32Ti rotor).
8. Discard the supernatant and resuspend the pellet in sterile PBS 1×.
9. Aliquot and store at −80°C.

### 3.3. Titration of the Lentiviral Vectors

1. Seed and incubate $5 \times 10^4$ HEK 293T cells in 35 mm dishes, 12–14 h before the infection.
2. Make serial dilution of the LV in the growing medium (DMEM GlutaMAX, 10% FBS, 1× Pen/Strept) and transduce the cells with the desired dilutions in a final volume of 1 ml.
3. After 5 days, collect the cells, wash in PBS with 1% FBS, and resuspend in 2% paraformaldehyde in PBS 1×.
4. The titer (transforming units, TU) is determined by using FACS calibur (BD BIOSCIENCE) and counting the percentage of GFP-positive cells in each dilution. When the percentage is between 2.5 and 25%, the titer can be determined using the following formula:

$$\text{Titer}(\text{T.U.}/\text{ml}) = \frac{\text{Percentage of GFP positive cells} \times \text{Cells plated the first day}(5 \times 10^4)}{\text{Dilution}}.$$

### 3.4. Proliferation Assays

Cells are initially plated in the exponential phase and followed for 5 days, till they reached a subconfluent stage (see Note 5).

1. The day before the infection seed $1.25 \times 10^5$ MEF cells/well in six-well plates. It is better to use low passage cells, in this case P4–5 cells were used. Prepare one plate for each day of counting for each condition.
2. The day after (day 0) count one plate for each condition. The count is performed following the next protocol:
   (a) Detach the cells with the trypsin solution for 5 min at 37°C.
   (b) Collect the cells and wash carefully the wells with PBS 1× with 1% serum to be sure to take all the cells.
   (c) Centrifuge at 1,500 rcf for 5 min at RT.
   (d) Resuspend the cells in 1 ml of fixing solution.
   (e) Dilute 200 µl of cell suspension in 10 ml of saline and determine the cell number with the coulter counter.
3. Tranduce (MOI=5 in 1 ml of fresh medium) cells in the remaining plates.
4. Every day count one plate for each condition and change medium in the others.
5. At day 2 after infection, cells are controlled for GFP expression in order to check the efficiency of the process.

### 3.5. In Vivo Lentiviral Injection

1. Anesthetize the mouse.
2. Secured the animal in a steroetaxic frame equipped with a mouse adaptor.
3. Unilateral LV injection is performed into two different sites of the motor dorsal striatum:
   (a) 1° SITE: AP +1; L –2.1; DV –2.6.
   (b) 2° SITE: AP +0.3; L –2.3; DV –2.4.

### 3.6. Brain Perfusion and Preparation of Free-Floating Slices

1. Anesthetize the mouse.
2. Perfuse the mice with cold physiologic solution at 35 rpm for 2 min.
3. Perfuse the mice with cold perfusion solution at 35 rpm for 5 min.
4. Carefully, extract the brain and post-fix it in cold perfusion solution, overnight at 4°C.
5. Discard the perfusion solution, wash the brain with PB and incubate with sucrose 30% for 24 h at 4°C.
6. Cut the brain at 35 µm with a microtome and stock the slices in antifreeze at –20°C.

### 3.7. Free Floating Immunofluorescence

1. Rinse the slices three times for 10 min in PBS.
2. Preincubate the slices for 1 h at room temperature with blocking solution.
3. Incubated overnight at 4°C with primary antibodies.
4. Rinse the slices three times for 10 min in PBS.
5. Incubated 1 h at room temperature with secondary antibodies.
6. Rinse the slices three times for 10 min in PBS.
7. Mount the slices on microscope slides, leave them dry and cover with a cover slip. Close it with the mounting medium.

### 3.8. Preparation of Acute Striatal Slices

1. Prepare the ACSF solutions containing 20 μM UO126 or the vehicle. Carboxygenate these solutions for at least 10 min and let them flow into the brain slice chamber at a constant rate of 2 ml/min at 32°C. The height of the perfusion fluid should be adjusted so that it forms a thin film over the slices.
2. Anesthetize a mouse and decapitate it with scissors, rapidly remove the brain in ice-cold sucrose-based dissecting solution oxygenated with 95% $O_2$ and 5% $CO_2$ (see Note 6).
3. Mount the brain on the vibratome stage on a drop of cyanoacrylate glue.
4. Cut 200 μm-thick slices keeping the brain submerged in ice-cold carboxygenated sucrose-based dissecting solution. The vibration rate of the blade should be fast and the speed nearly minimal.
5. Transfer the slices into the brain slice chamber placing them upon a lens paper (up to four slices in every chamber) and let them recover for 1 h at 32°C, constantly perfusing carboxygenated ACSF in the presence of the inhibitor or the vehicle.
6. After the recovery period, infuse 100 μM glutamate in the chamber for 10 min.
7. Remove the slices from the chamber and rapidly fix them in 4% PFA for 15 min at room temperature (see Note 7).
8. Rinse extensively (three times for 20 min with gentle agitation) in 0.1 M sodium phosphate buffer pH 7.4 at room temperature.
9. Incubate the slices in the cryoprotectant overnight at 4°C. Slices should not be incubated longer than overnight.

### 3.9. Slices Sectioning

1. Set the temperature of the cryostat chamber to −22°C.
2. Mount a piece of embedding medium on a metal specimen holder and cut the surface to make it flat.
3. Wrap a glass slide with parafilm and place the slice on this surface on a drop of embedding medium.

4. Transfer the slice onto the embedding medium flat surface and let it freeze.
5. Cut 18 μm cryosections and collect them onto Superfrost slides. Store in the cryostat until the cutting is completed (see Note 8).

### 3.10. Acute Striatal Slices Immunofluorescence

1. Draw a hydrophobic ring around the slices using a PapPen.
2. Rinse the slides with PBS three times for 10 min.
3. Pipette 100–200 μl blocking solution on each slide and incubate for 1 h at room temperature in a humid chamber (see Note 9).
4. Discard the blocking solution and pipette 100–200 μl primary antibodies solution on each slide. Incubate in a humid chamber overnight at 4°C.
5. Rinse the slides with PBS three times for 10 min.
6. Pipette 100–200 μl secondary antibodies on each slide and incubate in a humid chamber for 1 h at room temperature.
7. Rinse the slides with PBS three times for 10 min.
8. Discard PBS without drying the sections and mount the coverslips using the fluorescent mounting medium.
9. Store the slides at 4°C overnight in the dark before the examination at the microscope.

### 3.11. Microscopy and Image Analysis

Single and double-labeled images were obtained using a laser scanning confocal microscopy (Leica SP2), equipped with the corresponding lasers and the appropriate filters sets to avoid the cross-talk between the fluorochromes. Images were obtained with a 40× and 63× objectives. Neuronal quantification was performed with ImageJ software by counting phospho-S6/phospho-H3 immunoreactive neurons among NeuN-positive neurons in each slice. Statistical analysis was performed using two-way ANOVA and post-hoc comparisons between groups were made using Bonferroni test (****$p < 0.0001$).

## 4. Notes

1. Brain slices obtained from young animals are more viable.
2. The height of the perfusion fluid in the brain slice chamber can be better regulated when the inflow and the outflow in the chamber are controlled by two independent pumps.
3. Mouse embryonic fibroblasts, prepared following this protocol, are cells with a relatively low proliferative potential and they should exclusively be used at low passages (maximum two

times after thawing) since they rapidly undergo senescence. We never refreeze MEF after the initial freezing. Although MEF normally grow at 10% FBS and can be starved at 0.5–1% FBS for inducing entering into the $G_0$ phase of the cell cycle, they can also be grown at 5% FBS, as done in our proliferation assays. Since MEF are resistant to plasmid transfection, we use for the experiments in Figs. 2 and 3 LV-assisted infection with the constructs described in Note 4. Using our infection conditions (multiplicity of infection, MOI = 5), transduction efficiency of MEF is very high (<90% of GFP-positive cells).

4. All lentiviral vectors used for the MEF proliferation assays and in-vivo injections (Figs. 2 and 3) are self-inactivating, third-generation vectors (32). The plasmids used for packaging, kindly provided by Luigi Naldini, were pREV (expressing REV protein), pVSVG (expressing the envelope: G glycoprotein of Vesicular Stomatitis Virus), and pRRE (expressing capsid, polymerase, protease, and integrase proteins). The lentiviral vector used as control in the MEF proliferation and in-vivo injection assay is pCCLsin.PPT.hPGK.eGFP.PRE (33). This vector allows the expression of eGFP under the human phosphoglycerate kinase (hPGK) promoter. The four LV used for overexpressing ERK1, ERK2, ERK1>2, and ERK2>1 were derived from the previously described constructs (7). The expression of the ERK constructs in the LV is under the hPGK promoter.
5. At the proliferation assays, the following cell densities (mean ± SEM) were reached. For Day 4: control vector, 5,338.06 ± 65.95 cells/mm$^2$; ERK1, 4,035.72 ± 116.09 cells/mm$^2$; ERK2, 5,142.39 ± 99.53 cells/mm$^2$; ERK1>2, 5,570.61 ± 56.04 cells/mm$^2$; ERK2>1, 3,310.61 ± 58.43 cells/mm$^2$. For Day 6: control vector, 5,453.83 ± 71.30 cells/mm$^2$; ERK1, 4,681.61 ± 74.49 cells/mm$^2$; ERK2, 5,700.06 ± 156.69 cells/mm$^2$; ERK1>2, 6,475.61 ± 94.57 cells/mm$^2$; ERK2>1, 4,376.17 ± 68.44 cells/mm$^2$. Statistical analysis was performed using two-way ANOVA and post-hoc comparisons between groups was made using Bonferroni test (*$p \leq 0.02$).
6. Speed is essential for good results: the brain should be removed within 1–2 min after the decapitation.
7. The duration of fixation can be changed depending on the primary antibody and the brain region.
8. The cryosections should not be stored too long in the freezer. Best results are achieved processing the sections for immunofluorescence immediately after cutting.
9. The sections must never dry during the entire staining procedure in order to avoid high levels of background fluorescence.

## Acknowledgments

This work was supported by the Michael J Fox Foundation for Parkinson's Research and the Parkinson's UK as well as by the Italian Ministry of Health, the Fondazione CARIPLO and the Compagnia di San Paolo (to RB). Daniel Orellana conducted this study as partial fulfillment of his PhD in Molecular Medicine, Program in Neuroscience, Vita-Salute San Raffaele University, Milan, Italy. Part of this work was carried out in ALEMBIC, an advanced microscopy laboratory established by the San Raffaele Scientific Institute and the Vita-Salute San Raffele University.

### References

1. Pearson G et al (2001) Mitogen-activated protein (MAP) kinase pathways: regulation and physiological functions. Endocr Rev 22(2):153–183
2. Rubinfeld H, Seger R (2005) The ERK cascade: a prototype of MAPK signaling. Mol Biotechnol 31(2):151–174
3. Shaul YD, Seger R (2006) The MEK/ERK cascade: from signaling specificity to diverse functions. Biochim Biophys Acta 1773(8):1213–1226
4. Ramos JW (2008) The regulation of extracellular signal-regulated kinase (ERK) in mammalian cells. Int J Biochem Cell Biol 40(12):2707–2719
5. Orban PC, Chapman PF, Brambilla R (1999) Is the Ras-MAPK signalling pathway necessary for long-term memory formation? Trends Neurosci 22(1):38–44
6. Chuderland D, Seger R (2005) Protein-protein interactions in the regulation of the extracellular signal-regulated kinase. Mol Biotechnol 29(1):57–74
7. Vantaggiato C et al (2006) ERK1 and ERK2 mitogen-activated protein kinases affect Ras-dependent cell signaling differentially. J Biol 5(5):14
8. Thomas GM, Huganir RL (2004) MAPK cascade signalling and synaptic plasticity. Nat Rev 5(3):173–183
9. Sweatt JD (2004) Mitogen-activated protein kinases in synaptic plasticity and memory. Curr Opin Neurobiol 14(3):311–317
10. Davis S, Laroche S (2006) Mitogen-activated protein kinase/extracellular regulated kinase signalling and memory stabilization: a review. Genes Brain Behav 5(Suppl 2):61–72
11. Samuels IS, Saitta SC, Landreth GE (2009) MAP'ing CNS development and cognition: an ERKsome process. Neuron 61(2):160–167
12. Santini E, Valjent E, Fisone G (2008) Parkinson's disease: levodopa-induced dyskinesia and signal transduction. FEBS J 275(7): 1392–1399
13. Girault JA, Valjent E, Caboche J, Herve D (2007) ERK2: a logical AND gate critical for drug-induced plasticity? Curr Opin Pharmacol 7(1):77–85
14. Kim EK, Choi EJ (2010) Pathological roles of MAPK signaling pathways in human diseases. Biochim Biophys Acta 1802(4):396–405
15. Tidyman WE, Rauen KA (2009) The RASopathies: developmental syndromes of Ras/MAPK pathway dysregulation. Curr Opin Genet Dev 19(3):230–236
16. Klann E, Dever TE (2004) Biochemical mechanisms for translational regulation in synaptic plasticity. Nat Rev 5(12):931–942
17. Marchi M et al (2008) The N-terminal domain of ERK1 accounts for the functional differences with ERK2. PLoS One 3(12):e3873
18. Dudley DT, Pang L, Decker SJ, Bridges AJ, Saltiel AR (1995) A synthetic inhibitor of the mitogen-activated protein kinase cascade. Proc Natl Acad Sci U S A 92(17):7686–7689
19. Favata MF et al (1998) Identification of a novel inhibitor of mitogen-activated protein kinase kinase. J Biol Chem 273(29):18623–18632
20. Sebolt-Leopold JS, Herrera R (2004) Targeting the mitogen-activated protein kinase cascade to treat cancer. Nat Rev Cancer 4(12):937–947
21. Saba-El-Leil MK et al (2003) An essential function of the mitogen-activated protein kinase

Erk2 in mouse trophoblast development. EMBO Rep 4(10):964–968

22. Yao Y et al (2003) Extracellular signal-regulated kinase 2 is necessary for mesoderm differentiation. Proc Natl Acad Sci U S A 100(22):12759–12764
23. Hatano N et al (2003) Essential role for ERK2 mitogen-activated protein kinase in placental development. Genes Cells 8(11): 847–856
24. Meloche S, Vella FD, Voisin L, Ang SL, Saba-El-Leil M (2004) Erk2 signaling and early embryo stem cell self-renewal. Cell Cycle 3(3):241–243
25. Fischer AM, Katayama CD, Pages G, Pouyssegur J, Hedrick SM (2005) The role of erk1 and erk2 in multiple stages of T cell development. Immunity 23(4):431–443
26. Satoh Y et al (2007) Extracellular signal-regulated kinase 2 (ERK2) knockdown mice show deficits in long-term memory; ERK2 has a specific function in learning and memory. J Neurosci 27(40):10765–10776
27. Pagès G et al (1999) Defective thymocyte maturation in p44 MAP kinase (Erk 1) knockout mice. Science 286(5443):1374–1377
28. Selcher JC, Nekrasova T, Paylor R, Landreth GE, Sweatt JD (2001) Mice lacking the ERK1 isoform of MAP kinase are unimpaired in emotional learning. Learn Mem 8(1):11–19
29. Mazzucchelli C et al (2002) Knockout of ERK1 MAP kinase enhances synaptic plasticity in the striatum and facilitates striatal-mediated learning and memory. Neuron 34:807–820
30. Indrigo M, Papale A, Orellana D, Brambilla R (2010) Lentiviral vectors to study the differential function of ERK1 and ERK2 MAP kinases. Methods Mol Biol 661:205–220
31. Tronson NC et al (2008) Regulatory mechanisms of fear extinction and depression-like behavior. Neuropsychopharmacology 33(7):1570–1583
32. Naldini L, Blomer U, Gage FH, Trono D, Verma IM (1996) Efficient transfer, integration, and sustained long-term expression of the transgene in adult rat brains injected with a lentiviral vector. Proc Natl Acad Sci U S A 93(21):11382–11388
33. Follenzi A, Ailles LE, Bakovic S, Geuna M, Naldini L (2000) Gene transfer by lentiviral vectors is limited by nuclear translocation and rescued by HIV-1 pol sequences. Nat Genet 25(2):217–222

RESEARCH ARTICLE

AMERICAN JOURNAL OF medical genetics PART A

# Noonan Syndrome Associated With Both a New Jnk-Activating Familial *SOS1* and a De Novo *RAF1* Mutations

**Mauro Longoni,[1] Silvia Moncini,[1] Mariangela Cisternino,[2] Ilaria M. Morella,[3] Serena Ferraiuolo,[4] Silvia Russo,[4] Savina Mannarino,[2] Valeria Brazzelli,[5] Paola Coi,[2] Renata Zippel,[3] Marco Venturin,[1] and Paola Riva[1]***

[1]Dipartimento di Biologia e Genetica per le Scienze Mediche, Università degli Studi di Milano, Milano, Italy

[2]Dipartimento di Pediatria, Fondazione IRCCS Policlinico S. Matteo, Università di Pavia, Pavia, Italy

[3]Dipartimento di Scienze Biomolecolari e Biotecnologie, Università degli Studi di Milano, Milano, Italy

[4]IRCCS Istituto Auxologico Italiano, Cusano, Milano, Italy

[5]Dipartimento di Patologia Umana Ereditaria, Istitute di Dermatologia, Fondazione IRCCS Policlinico S. Matteo, Università di Pavia, Pavia, Italy

Received 8 July 2009; Accepted 23 May 2010

Noonan syndrome is a genetic condition characterized by congenital heart defects, short stature, and characteristic facial features. Familial or de novo mutations in *PTPN11*, *RAF1*, *SOS1*, *KRAS*, and *NRAS* are responsible for 60–75% of the cases, thus, additional genes are expected to be involved in the pathogenesis. In addition, the genotype–phenotype correlation has been hindered by the highly variable expressivity of the disease. For all these reasons, expanding the genotyped and clinically evaluated case numbers will benefit the clinical community. A mutation analysis has been performed on *RAF1*, *SOS1*, and *GRB2*, in 24 patients previously found to be negative for *PTPN11* and *KRAS* mutations. We identified four mutations in *SOS1* and one in *RAF1*, while no *GRB2* variants have been found. Interestingly, the *RAF1* mutation was present in a patient also carrying a newly identified p.R497Q familial *SOS1* mutation, segregating with a typical Noonan Syndrome *SOS1* cutaneous phenotype. Functional analysis demonstrated that the R497Q *SOS1* mutation leads to Jnk activation, but has no effect on the Ras effector Erk1. We propose that this variant might contribute to the onset of the peculiar ectodermal traits displayed by the propositus amidst the more classical Noonan syndrome presentation. To our knowledge, this is the first reported case of a patient harboring mutations in two genes, with an involvement of both Ras and Rac1 pathways, indicating that *SOS1* may have a role of modifier gene that might contribute the variable expressivity of the disease, evidencing a genotype–phenotype correlation in the family. 

**Key words:** Noonan syndrome; Jnk activation; genotype–phenotype correlation; *SOS1*; *RAF1*; *GRB2*; mutational analysis

**How to Cite this Article:**
Longoni M, Moncini S, Cisternino M, Morella IM, Ferraiuolo S, Russo S, Mannarino S, Brazzelli V, Coi P, Zippel R, Venturin M, Riva P. 2010. Noonan syndrome associated with both a new Jnk-activating familial *SOS1* and a de novo *RAF1* mutations. Am J Med Genet Part A 152A:2176–2184.

## INTRODUCTION

Noonan syndrome (NS [OMIM63950]) is an autosomal dominant genetic condition, characterized by short stature, dysmorphic facial features, skeletal abnormalities, and congenital heart defects. Its estimated incidence ranges from 1/1,000 to 1/2,500 live births [Allanson, 1987; Sharland et al., 1992]. Noonan syndrome is diagnosed by a clinical-based scoring system, comprising major and minor criteria [van der Burgt et al., 1994].

Noonan syndrome is genetically heterogeneous with four causal genes identified to date. *PTPN11* encodes a protein phosphatase and it harbors gain-of-function mutations in approximately 50% of patients [Tartaglia and Gelb, 2005]. *KRAS*, *SOS1*, and *RAF1* have been recently implicated in a minority of patients [Carta et al., 2006; Schubbert et al., 2006; Pandit et al., 2007; Razzaque et al., 2007; Roberts et al., 2007; Tartaglia et al., 2007]. All genes so far identified belong to the conserved Ras-MAPK signaling pathway. *SOS1* is

Additional supporting information may be found in the online version of this article.

Grant sponsor: 2007 Academic Grant (FIRST).

Mauro Longoni and Silvia Moncini contributed equally to this work.

*Correspondence to:
Paola Riva, Ph.D., Department of Biology and Genetics for Medical Science, University of Milan, Via Viotti, 3/5 20133 Milano (MI), Italy.
E-mail: paola.riva@unimi.it

Published online 3 August 2010 in Wiley Online Library (wileyonlinelibrary.com).
DOI 10.1002/ajmg.a.33564

mapped to chromosome 2p22.1 and encodes for a 150 kDa Ras-GEF (guanine exchange factor) protein. When a growth factor binds to its tyrosine kinase receptor, SOS1, associated with the adaptor GRB2, is recruited to the plasma membrane where it participates in the activation of Ras by catalyzing the exchange of GDP with GTP [Quilliam et al., 2002]. SOS1 is also known to activate a distinct pathway mediated by Rac1, a GTPase belonging to the Rho-family [Sini et al., 2004].

*SOS1* mutations account for 10–13% of Noonan syndrome patients [Roberts et al., 2007]. Those patients have been reported to show phenotypic elements reminiscent of cardiofaciocutaneous syndrome [MIM115150], particularly concerning the dysmorphic features, macrocephaly and peculiar ectodermal traits, although this observation lacks statistical significance [Tartaglia et al., 2007]. *RAF1* was identified as a causative gene for hypertrophic cardiomyopathy (HCM) in Noonan syndrome and LEOPARD syndrome-2 [MIM611554], and accounts for about a third of *PTPN11* mutation negative patients [Pandit et al., 2007; Razzaque et al., 2007]. *RAF1* is a known oncogene mapped to 3p25, and encodes for a serine–threonine kinase downstream of Ras signaling pathway [Li et al., 1991].

Although different genes have been implicated in the pathogenesis of Noonan syndrome, about 30% of patients remain genetically uncharacterized, thus additional genes are expected to be involved and should be searched for. In addition, the correlation between the phenotypic traits and the specific genetic defect has been limited by the highly variable expressivity of the disease and by the relatively small number of published genotyped cases, thus further patients should be genotyped.

We here report on the mutational study on *SOS1*, *RAF1*, in a cohort of 24 patients affected with Noonan syndrome, who previously tested negative for *PTPN11* and *KRAS*. Additionally, we report the mutational screening of the candidate gene *GRB2*. We found four *SOS1* mutations and one *RAF1* mutation, interestingly shown by a patient also carrying a familial *SOS1* mutation.

## MATERIALS AND METHODS

### Patients and Samples

Twenty-four patients affected by Noonan syndrome and negative for *PTPN11* and *KRAS* mutations were included in the study. All matched the diagnostic criteria for Noonan syndrome, as defined by van der Burgt et al. [1994] and were referred as sporadic instances of the disease at the time of referral. Genetic exams were performed by experienced physicians (M.C., S.M., P.C.).

Peripheral lymphocyte DNA was obtained from patients, parents, and controls using the QIAamp DNA Blood Mini Kit (Qiagen, Valencia, CA), according to the manufacturer's instructions.

### Mutation Screening

PCR products were bi-directionally sequenced using the Terminator v3.1 Cycle Sequencing Kit (Applied Biosystems, Foster City, CA), and run on an automated ABI-3130xl DNA genetic analyzer (Applied Biosystems). Output data were analyzed by SeqScape® software v2.6 (Applied Biosystems). Sequencing was performed on the nine exons of *SOS1*, and two exons of *RAF1*, where mutations had been previously identified [Pandit et al., 2007; Roberts et al., 2007; Tartaglia et al., 2007]. *GRB2* mutation screening has been carried out on the whole coding region by using the conditions indicated in Table I.

Alternatively, PCR products were run on WAVE® Nucleic Acid Fragment Analysis System 3500HT (Transgenomic, Glasgow, UK), and data analyzed by Navigator™ Software (Transgenomic). Primer sequences are published elsewhere [Pandit et al., 2007; Tartaglia et al., 2007].

### Plasmids and Mutagenesis

hSOS1 was a kind gift of G. Scita (IFOM Milano); HA-JNK and HA-ERK1 have been previously described [Innocenti et al., 1999]. The hSOS1 plasmid was used as template for site-directed mutagenesis, performed using the QuikChange Site-Directed Mutagenesis Kit (Agilent Technologies, Santa Clara, CA) according to the manufacturer's instructions. Pairs of complementary mutagenic primers (R497Q-Fw: AAAAGTTTTTATGCAAAAGGTACAAATTA and R497Q-Rev: TTAATTTGTACCTTTGCATAAAAAACTTTT; M269R-Fw: AAGATACAGTAGAAAGGACAGATGAAGGCAG and M269R-Rev: CTGCCTTCATCTGTCCTTTCTACTGTATCTT) were designed.

### Biochemical Analysis

HEK293 cells were grown in DMEM plus 10% FBS and antibiotics. Cells were transiently transfected with equal amount of the full-

TABLE I. *GRB2* Primers

| EXON | Primer | Sequence | Annealing temperature (°C) | Fragment size (bp) |
|---|---|---|---|---|
| 2 | *EX2A* | 5′-CGAGGCTGAAAAGAGG AAGA-3′ | 58 | 467 |
| | *EX2B* | 5′-TGTGTGTAATCAGGGCGAAA-3′ | | |
| 3 | EX3A | 5′-CGAGTGAAACCGTTCACAGA-3′ | 58 | 298 |
| | EX3B | 5′-TGACATCCATCCCAGTGATCT-3′ | | |
| 4 | *EX4A* | 5′-GGCTGGAT ATCCCGTTTCTT-3′ | 56 | 250 |
| | *EX4B* | 5′-AACGGCTTCACAATTTGGAT-3′ | | |
| 5 | *EX5A* | 5′-ACCCTCGATTTGCCAAGTTA-3′ | 58 | [1,0]295 |
| | *EX5B* | 5′-CAGGAATGCACACTGAGGAG-3′ | | |
| 6 | *EX6A* | 5′-GGGAGATGGGAGGTGAGTTT-3′ | 58 | 399 |
| | *EX6B* | 5′-AGAGGCAGCTTGTGGGTTTA-3′ | | |

length hSOS1 or of the mutated isoforms of hSOS1 and either hemagglutinin (HA)-tagged c-Jun NH2-terminal kinase (JNK) or HA-tagged extracellular regulated kinase1 (ERK1) using the JetPEI (Polyplus, New York, NY) method according to manufacturer's instructions. Twenty-four hours after transfection the medium was replaced with serum deprived medium and left for 18 hr. Cells were then stimulated with EGF (20 ng/ml) for the indicated intervals. Cells were then collected in lysis buffer (Tris–HCl 50 mM, pH 7.5, NaCl 150 mM, Triton X-100 1%, glycerol 10%, NaF 50 mM, $NaVO_3$ 1 mM, and cocktail of proteases inhibitors) and equal amount of proteins were immunoprecipitated using anti-HA antibodies (BABCO, Richmond, CA) and subsequently incubated with protein G slurry. Beads were washed and resuspended in SDS sample buffer. Samples were run on SDS–PAGE and then transferred to nitrocellulose membranes. The membranes were then immunodecorated with anti-HA, anti-pERK2 (Cell signalling, Danvers, MA), pJNK (Cell signalling), or anti-SOS1 (Santa Cruz Biotechnology, Santa Cruz, CA). Antibodies were visualized by enhanced chemioluminescence detection (ECL; Amersham Pharmacia Biotech, Milan, Italy) using horseradish peroxidase-conjugated secondary antibodies (Jackson Immunoresearch Laboratories, West Grove, PA). Band intensities were quantified by densitometry with Scion Image Program (Scion Corporation, Frederick, MD).

## Bioinformatic Analysis

The potential effects of the novel *SOS1* sequence variant were analyzed using the following programs: ClustalX 2.0 (ftp://ftp.ebi.ac.uk/pub/software/clustalw2) for multiple sequence alignment, NACCESS (http://www.bioinf.manchester.ac.uk/naccess/), HBPLUS 3.0 (http://www.biochem.ucl.ac.uk/bsm/hbplus/home.html), LIGPLOT 4.4.2 (http://www.biochem.ucl.ac.uk/bsm/ligplot/ligplot.html), and PyMOL v1.1 (http://pymol.sourceforge.net/) for the analysis and the visualization of amino acids interactions. Three-dimensional structures of SOS1 domains were retrieved from RCSB Protein Data Bank (http://www.rcsb.org/pdb/home/home.do).

# RESULTS

## Mutation Analysis

We ascertained 24 carefully phenotyped patients with Noonan syndrome, who were determined to be negative for *PTPN11* and *KRAS* mutations. The clinical features of the propositi are detailed in Table II. Following sequencing of *SOS1* and *RAF1* exons implicated in Noonan syndrome pathogenesis, we identified two novel heterozygous mutations, c.1430A > G (p.Q477R) and c.1490G > A (p.R497Q), and two previously described mutations, c.806T > C (p.M269T) and c.2104T > C (p.Y702H) [Tartaglia et al., 2007; Zenker et al., 2007] in *SOS1*, and one known mutation, c.781C > T (p.P261S), in *RAF1* [Pandit et al., 2007; Razzaque et al., 2007] (Table III). It is noteworthy that both *SOS1* p.R497Q and *RAF1* p.P261S mutations were present in the same patient. Mutations p.M269T and p.Q477R were de novo, while p.R497Q and p.Y702H were inherited. Segregation tests were run on every propositus-parent group with a set of highly polymorphic micro-

**TABLE II. Comparative Clinical Features in 24 Individuals With Noonan Syndrome**

| | Patient ID | | | | | | | | | | | | | | | | | | | | | | | | |
|---|---|---|---|---|---|---|---|---|---|---|---|---|---|---|---|---|---|---|---|---|---|---|---|---|---|
| | 1 | 2 | 3 | 4 | 5 | 6 | 7 | 8 | 9 | 10 | 11 | 12 | 13 | 14 | 15 | 16 | 17 | 18 | 19 | 20 | 21 | 22 | 23 | 24 |
| Sex | M | M | M | F | F | F | M | F | F | M | F | F | F | M | F | F | M | M | M | M | F | F | M | M |
| Congenital hearth defect | PS, HCM | PS | SD | — | AC | — | PS | PS | PS, SD | PS | PS | PS | PS, SD | SD | AC | PS SD | AS SD | SD | na | — | SD | — | — | — |
| Short stature | — | — | + | + | + | — | ± | — | + | + | + | + | + | + | + | + | + | — | + | + | + | + | — | + |
| Learning impairment | — | — | — | — | + | — | + | — | + | — | — | — | — | + | — | — | + | — | — | + | + | + | + | + |
| Facial features | + | + | + | — | + | + | + | + | + | + | + | + | + | + | + | + | + | + | + | + | + | + | + | + |
| Thorax deformity | + | + | — | — | + | + | + | + | + | + | — | — | + | + | — | + | — | + | + | + | — | + | — | + |
| Cryprorchidism | — | — | + | na | na | na | + | na | na | — | na | na | na | — | na | na | — | — | + | + | na | na | — | — |
| Ectodermal anomalies | CAL, KP | CAL, KP, CH | — | Naevi | Naevi | — | KP | Naevi | — | CAL | — | — | — | — | — | — | — | — | CAL Naevi | — | — | — | — | — |

M, male; F, female; AC, aortic coarctation; SD, septal defect; HCM, hypertrophic cardiomyopathy; PS, pulmonary stenosis; AS, aortic stenosis; +, below 5th centile; ±, 5th–10th centile; –, above 10th centile; na, not applicable; CAL, Caféaaunalait spots; KP, keratosis pilaris; CH, curly hair.

TABLE III. SOS1 and *RAF1* Mutations

| Patient | Gene | Mutation | | Inheritance |
|---|---|---|---|---|
| 1 | *SOS1* | c.1490G > A | R497Q | Familial |
| 1 | *RAF1* | c.781C > T | P261S | De novo |
| 2 | *SOS1* | c.806T > C | M269T | De novo |
| 7 | *SOS1* | c.1430A > G | Q477R | De novo |
| 8 | *SOS1* | c.2104T > C | Y702H | Familial |

satellites, confirming paternity in every instance (data not shown). The patients also underwent a mutational analysis of *GRB2*, a gene encoding an adaptor protein with the function of recruiting and activating SOS1 [Benfield et al., 2007], which has never been shown to be implicated in Noonan syndrome so far. *GRB2* was not found to be mutated in the analyzed patients.

The *SOS1* p.M269T mutation was identified in Patient 2. This is an already described pathogenetic variant [Zenker et al., 2007] affecting a residue, which, if mutated, leads to increased levels of RAS-ERK activation [Roberts et al., 2007]. The *SOS1* p.Y702H mutation, carried by Patient 8 and her mother, is also a known change deemed as pathogenetic [Tartaglia et al., 2007; Zenker et al., 2007].

Of the two novel mutations, the *SOS1* p.Q477R change, identified in Patient 7, is a non-conservative substitution and affects a conserved amino acid. The same residue was found to be mutated in a patient carrying the p.Q477H/P478L variants [Zenker et al., 2007].

The second novel mutation, *SOS1* p.R497Q, was found in Patient 1, who turned out to bear also the known pathogenetic *RAF1* p.P261S variant. This is the first instance of a Noonan syndrome patient harboring mutations in two genes of the Ras-MAPK pathway. In addition, Patient 1's father and paternal grandfather were found to share with the propositus the same *SOS1* mutation and to carry some cutaneous anomalies, typically observed in *SOS1* mutated patients. DHPLC analysis on 300 control chromosomes of unaffected individuals with matched geographic origin revealed that the p.R497Q sequence variant is a private mutation in this family. These findings prompted us to carry out functional studies to characterize the p.R497Q mutation and to assess whether this variant could contribute to Patient 1's phenotype.

## Functional Studies of SOS1 p.R497Q

To investigate whether the SOS1 p.R497Q variant can activate the Ras pathway, we transfected HEK293 cells with the wild type human

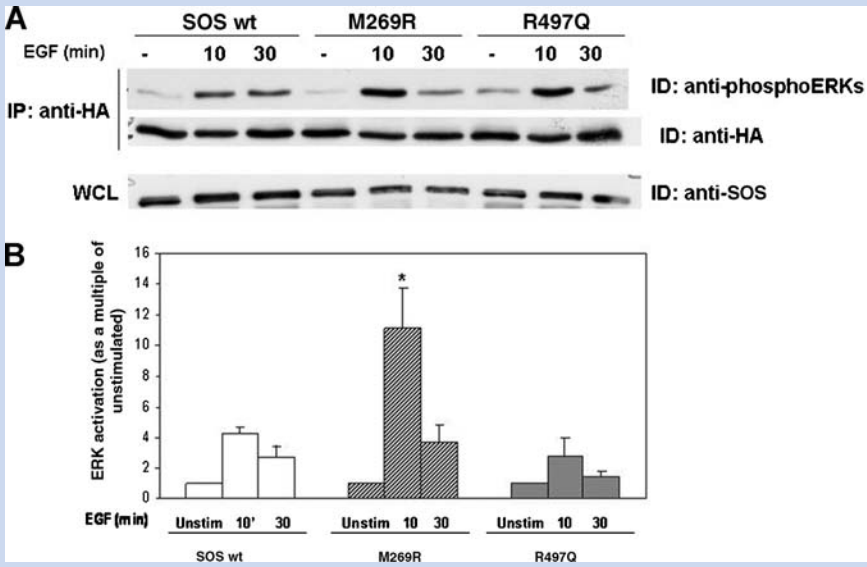


**FIG. 1. Erk activation assay. A: hSOS1 (SOS WT) or M269R or R497Q together with HA-ERK1 were expressed in HEK293 cells. Cells were serum starved and then stimulated with EGF (20 ng/ml) for the time indicated. HA-ERK1 was immunoprecipitated with anti-HA antibodies and the level of phosphorylated ERK1 (A, upper row) and HA-ERK1 (A, middle row) in the immunoprecipitates was detected with pERKs and HA antibodies, respectively. The level of the different SOS1 constructs was detected in total cell extracts with antibodies against SOS1 (A, bottom row). A representative time course experiment is shown. B: Quantification of relative pERK1 level after normalization with HA-ERK1 intensity in the immunoprecipitates. The quantification was done on three independent experiments and the data are expressed as fold increase over the basal (unstimulated) condition for each SOS1 construct. Error bars represent SD, *$P < 0.05$ compared to the SOS1 wild type condition at 10 min of stimulation.**

SOS1, the mutant isoform p.M269R, previously reported to activate the Ras-Erk pathway [Roberts et al., 2007], or the new p.R497Q mutant. In Figure 1, we show that, after epidermal growth factor (EGF) stimulation, the p.M269R mutant significantly activates Erk signaling, as expected, while the p.R497Q substitution does not induce Erk1 phosphorylation above the level of the wild type (Fig. 1). As SOS1 is also involved in Rac1 pathway signal transduction, we sought to determine whether this pathway might be affected. HEK293 cells transfected with the p.R497Q plasmid showed activated Jnk, after stimulation with EGF. On the contrary, Jnk is not significantly activated under EGF stimulation in cells transfected either with the wild type SOS1 or the p.M269R mutant (Fig. 2).

## Structural Analysis of the SOS1 p.R497Q Variant

In order to characterize the SOS1 p.R497Q mutant from a structural point of view, we performed a bioinformatic study. Conservation analysis revealed that SOS1 p.R497 is highly conserved in evolution, from insects to *Homo sapiens*. The only exception is in worms, where there is a conservative substitution from arginine to hystidine (Fig. 3A).

p.R497 lies within the PH domain of SOS1; based upon the crystal structure of SOS1 PH-DH-cat domain (Protein Data Bank entry 1XD4), it is oriented towards the outside of the protein and face in the same direction as p.R552. Sondermann et al. [2005] provided evidence, by means of a combined approach exploiting computational docking, X-ray scattering and binding assays, that p.R552 interacts with two aspartic residues (p.D140 and p.D169) of SOS1 histone fold (HF) domain, whose crystal structure was independently determined (Protein Data Bank entry 1Q9C). The p.R552G mutation resulted in increased and prolonged Ras activation and also in augmented pErk levels, and this effect is likely to be caused by the disruption of p.R522 interaction with p.D140 and p.D169 [Tartaglia et al., 2007].

We therefore wondered if p.R497 could also interact with a negatively charged residue of SOS1 HF domain. According to the validated docking model of HF domain onto DH-PH-cat domain, p.R497 is located opposite to p.D174 in HF domain (Fig. 3B) [Sondermann et al., 2005]. p.D174 is also a very conserved residue, except in *Caenorhabditis elegans*, where, based on multiple alignments, there is glutamate [Innocenti et al., 2002]. The presence of the two conservative substitutions p.Q174D and p.H497R in *C. elegans* is suggestive of a functional interaction between the two residues. The analysis of amino acids interactions, carried out by means of HBPLUS 3.0 and LIGPLOT 4.4.2 programs, predicts that p.R497 and p.D174 interact via hydrophobic bonds (see supporting information which may be found in the online version of this article). The analysis of the mutated residue shows that p.Q497 may still hydrophobically interact with p.D174 but, unlike p.R497, it also forms a hydrogen bond with p.M496 (Fig. 3C, and see supporting information which may be found in the online version of this article). This might lead to a conformational change of the sur-

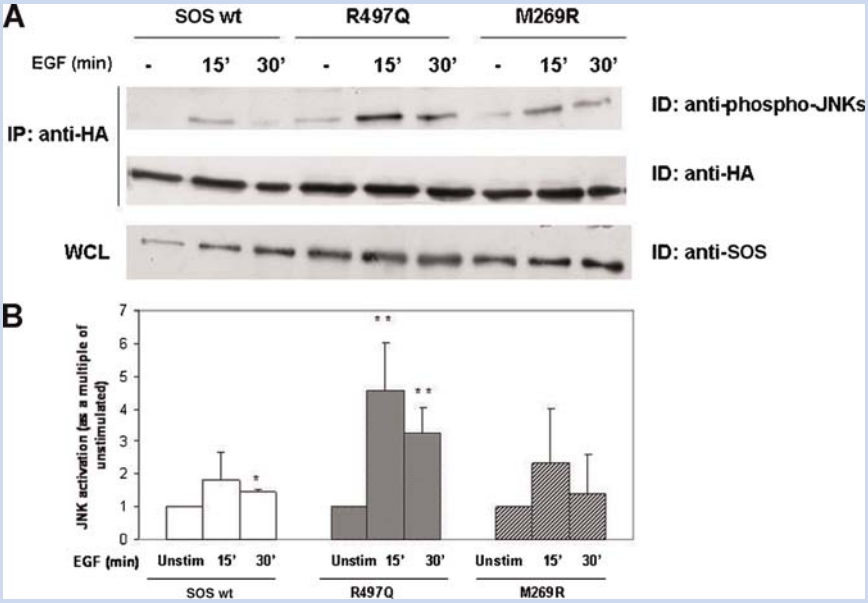


**FIG. 2. Jnk-activation assay. A: hSOS1 (SOS WT) or M269R or R497Q together with HA-JNK were expressed in HEK293 cells. Cells were serum starved and then stimulated with EGF (20 ng/ml) for the time indicated. Ha-JNK was immunoprecipitated with anti-Ha antibodies and the level of phosphorylated JNK (A, upper row) and HA-JNK (A, middle row) in the immunoprecipitates was detected with pJNK and HA antibodies, respectively. The level of the different SOS1 constructs was detected in total cell extracts with antibodies against SOS1 (A, bottom row). A representative time course experiment is shown (B) quantification of relative pJNK level after normalization with HA-JNK intensity in the immunoprecipitates. The quantification was assayed on three independent experiments and the data is expressed as fold increase over the basal (unstimulated) condition for each SOS1 construct. Error bars represent SD, $^{**}P < 0.001$ compared to the unstimulated condition for the same SOS1 construct.**

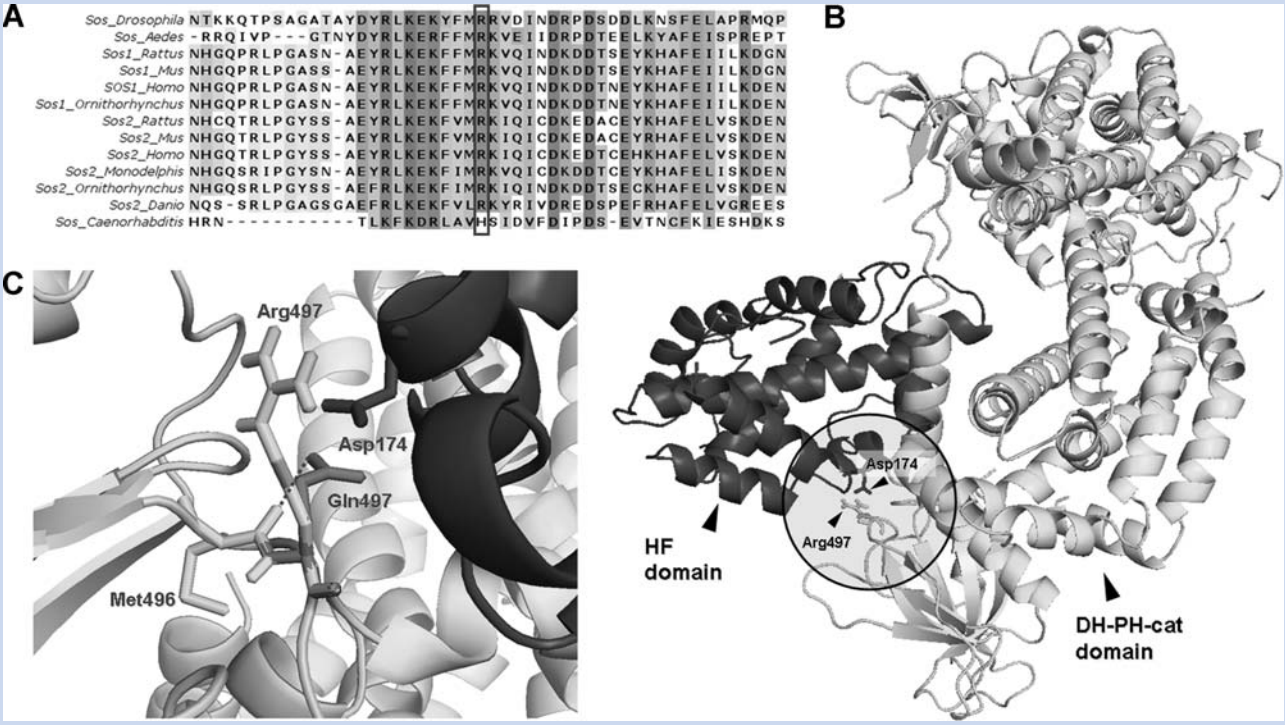


**FIG. 3. Bioinformatic analysis of p.R497Q. A: Multiple sequence alignment of *Sos1* orthologs, in the region surrounding p.R497 (black rectangle), as computed by ClustalX 2.0.6. B: Three-dimensional docking model of SOS1 HF domain (PDB 1Q9C, black) onto SOS1 PH-DH-cat domain (PDB 1XD4, light gray), showing the interaction between p.R497 and p.D174. C: Prediction of p.R497Q consequences. The PH domain p.R497 residue (light gray) is predicted to contact the HF domain p.D174 (black) via hydrophobic interactions. The mutated p.Q497 (dark gray) forms an additional hydrogen bond with the flanking p.M496 (dashed line), which should cause a local conformational change affecting the interaction between PH-DH-cat and HF domains. [Color figure can be viewed in the online issue, which is available at wileyonlinelibrary.com.]**

rounding region, altering the interaction between the HF and the DH-PH domains, with a deleterious effect on the correct functioning of the protein.

## DISCUSSION

We carried out the sequence analysis of *SOS1*, *RAF1*, and *GRB2* genes in a cohort of 24 patients affected with Noonan syndrome, previously found to be negative for *PTPN11* and *KRAS* mutations. We found one patient with mutated *RAF1* and four patients with mutated *SOS1*, two of whom showing a new mutation (p.Q477R and p.R497Q, respectively). Interestingly, this latter was inherited and was present in the propositus, who also carries the identified *RAF1* mutation, and in two unaffected relatives showing a peculiar abnormal cutaneous phenotype. No *GRB2* variants have been identified.

The *SOS1* p.Q477R change, identified in Patient 7, is a non conservative substitution and affects a conserved amino acid. The same residue was found to be mutated in a patient carrying the p.Q477H/P478L variants [Zenker et al., 2007]. Together, these findings might indicate that p.Q477 is important for SOS1 function, even if the amino acid is located in a PH domain loop, whose function is unknown [Zenker et al., 2007].

The known p.Y702H *SOS1* mutation [Tartaglia et al., 2007] was identified in Patient 8 and her mother, who had a medical history of transitory GH deficiency treated with hormone replacement and delayed puberty and was treated with replacement therapy. After genetic counseling, it was agreed to extend the analysis to the maternal uncle, born with cryptorchidism, and to both maternal grandparents. The uncle and the maternal grandfather both harbored the p.Y702H mutation. The propositus' family members carrying the *SOS1* mutation showed a subclinical Noonan syndrome phenotype, including facial features and medical history of delayed puberty in all members, cryptorchidism in the uncle and short stature as well as GH deficiency in the mother. This observation underlines the occurrence of milder phenotypes related to *SOS1* mutations. Subclinical phenotypes have previously been reported in *PTPN11* and *SOS1* mutation carriers [Tartaglia et al., 2007] that are usually parents diagnosed after their progeny expressing the full phenotype.

Patient 1 was unusual in that he showed both a *SOS1* and a *RAF1* variant. This is the first instance of a Noonan syndrome patient harboring mutations in two genes of the Ras-MAPK pathway.

The p.P261S *RAF1* mutation has been previously demonstrated to increase RAF1 kinase activity downstream of EGFR in an experimental cell model and is likely to be responsible for the

Noonan syndrome phenotype observed in the patient [Pandit et al., 2007].

Patient 1, his father and the paternal grandfather were also found to carry the novel *SOS1* sequence variant p.R497Q. The lack of this variant in a matched control population suggests that it is likely a private mutation segregating within the family. The presence in the propositus and in the two relatives of cutaneous anomalies peculiar to *SOS1* mutated patients [Tartaglia et al., 2007] raised the hypothesis that this substitution might have contributed to these ectodermal features.

SOS1 functions as a GEF for both Ras and Rac1. SOS1 may be Ras -specific, leading to Erk and Jnk activation, when alone or in association with GRB2, or be Rac1 specific, causing Jnk activation alone, when in complex with Eps8 and E3b1. SOS1 is therefore involved in two separate and differentially regulated RTK initiated signaling cascades [Innocenti et al., 2002; Khandhay et al., 2006]. The p.R497Q construct showed an increased activation of Jnk in EFG-stimulated HEK293 cells, while wild type SOS1 and the Noonan syndrome associated p.M269R mutant did not. As p.R497Q substitution induces Erk1 phosphorylation to levels comparable with those induced by the wild type (Fig. 1), we propose that the *SOS1* p.R497Q mutation particularly affects the Rac1-Jnk pathway, differently from the Ras-activating p.M269R mutation.

The in silico structural analysis suggests that the SOS1 p.R497 residue is important for the interaction between the HF and the DH -PH domains. The p.R497Q mutant is likely to alter this function and, unlike what has been seen for other *SOS1* mutations, it might be that this variant affects only the regulation of the DH-PH domain, which is known to be responsible for Jnk activation through Rac1 stimulation [Nimnual et al., 1998], but not the activity of the Rem-Cdc25 catalytic domain, which serves as guanine nucleotide exchange factor for Ras, possibly explaining why this mutation leads to Jnk but not Ras activation.

Within family 1 (Fig. 4), only the propositus, carrier of both *SOS1* p.R497Q and *RAF1* p.P261S mutations, is consistent with the diagnosis of Noonan syndrome. He displays a classic phenotype, including the characteristic facial features (Fig. 4). Additionally, he showed cutaneous xerosis and keratosis pilaris, a café-au-lait spot on the abdomen, hypertrichosis, left foot fifth finger overlapping the fourth finger and a mild thorax deformity. His cardiac phenotype was also consistent, and included pulmonary valve stenosis, HCM, and mitral valve prolapse. *RAF1* mutations affecting the CR2 domain, like p.P261S, are thought to be frequently associated with HCM [Pandit et al., 2007]. The finding of hyperpigmented cutaneous lesions in *RAF1* mutated Noonan syndrome patients includes multiple nevi, lentigines and café-au-lait spots. On the other hand, Patient 1 also displays uncommon features in *RAF1* mutated patients, such as keratosis, hypertrichosis and left foot fifth finger overlapping the fourth one (Fig. 4).

*SOS1* mutated patients typically have ectodermal abnormalities, normal stature, and normal mental development [Tartaglia et al., 2007]. In the relatives of Patient 1 who carry the private *SOS1* p.R497Q mutation, we identified some ectodermal abnormalities. A recently published mutational study on a different cohort de-

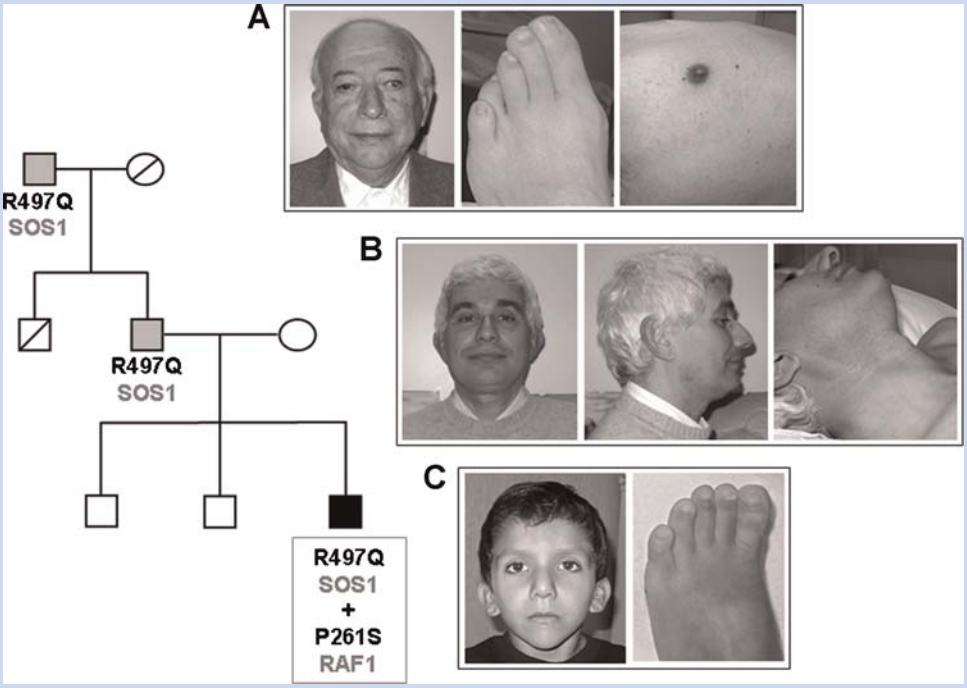


**FIG. 4. Pedigree and clinical features of family 1: the black box indicates the fully penetrant Noonan syndrome phenotype in the propositus; gray boxes indicate mild phenotype in his father and in his grandfather. A: Grandfather: keratosis pilaris on the trunk, left foot fifth finger overlapping the fourth finger. B: Father: mildly low set and posteriorly rotated ears, high arched and thick eyebrows, thick and prematurely white hair, keratosis pilaris of the neck. C: Propositus: characteristic Noonan syndrome facial features, left foot fifth finger overlapping the fourth finger, as observed in his grandfather, keratosis pilaris.**

scribed a similarly looking keratosis pilaris rubra and additional ectodermal features in a Noonan patient with a de novo *SOS1* p.K170R mutation [Denayer et al., 2010].

The propositus' father has no clinical signs of Noonan syndrome, as determined by careful physical and dysmorphologic exam, with the exception of mild lowset and posteriorly angulated ears, and high arched and thick eyebrows (Fig. 4). Echocardiography showed a borderline enlargement of the ventricular septum, which was determined to be within range of normal upon further evaluation by chest magnetic resonance. The father, however, displayed a cutaneous phenotype characterized by thick and precociously white hair, since 20 years of age, and by keratosis pilaris of the neck skin (Fig. 4). The grandfather of Patient 1, who also carries the *SOS1* variant, has no clinical signs of Noonan syndrome. His heart is normal examination by echocardiogram and electrocardiogram. Like Patient 1, he has a left foot fifth finger overlapping the fourth (Fig. 4). Multiple keratosis is also present on the chest. Both the propositus and the family members carrying the *SOS1* mutation showed normal stature and normal mental development.

Although the full Noonan syndrome phenotype is clearly determined by the *RAF1* p.P261S mutation in Patient 1, it seems reasonable to hypothesize that the *SOS1* p.R497Q mutation, which we showed to activate the Rac1-Jnk pathway, have concurred in determining the cutaneous anomalies also shared by his father and grandfather, acting as a modifier gene for the propositus phenotype.

It is worth noting that the activation of Jnk, through Rac1 pathway, might be related to the peculiar ectodermal phenotype exhibited by some patients carrying a *SOS1* mutation, raising the possibility that some phenotypic characteristics of *SOS1* mutation carriers may also be determined by alternative pathways and not only by the canonical Ras pathway. Interestingly, Rac1 has been reported to regulate the epidermal stem cell compartment, and conditional epidermal deletion of Rac1 in mice generates an early phenotype characterized by thickening of the interfollicular epidermis with increased numbers of living and cornified cell layers and expansion of the infundibulum [Benitah et al., 2005]. On the basis of these findings we speculate that the abnormal cutaneous traits, often expressed in *SOS1* mutated Noonan syndrome patients, may be exacerbated by the concurrent activation of the Rac1-Jnk pathway besides the Ras-Erk1 pathway. As a cautionary note, the apparent incomplete penetrance reported for some *SOS1* alleles present in the undiagnosed parents of some patients [Tartaglia et al., 2007; Zenker et al., 2007], might represent another known or unknown mutated gene that is the real cause of Noonan syndrome.

In addition, the expression of atypical traits in the contest of a classical Noonan phenotype might be explained by the co-occurrence of different mutations in genes belonging to the Ras-Erk1 and related signaling pathways, one major pathogenetic variant, causing per se the onset of the Noonan phenotype, and one minor variant, that in such cases should act as modifier to the overall phenotype, constituting a possible mechanism which contributes to the highly variable expressivity of the syndrome. Although our hypothesis needs to be substantiated by other similar cases, this may illustrate the importance of a re-evaluation of the functional significance of *SOS1* variants that do not cause an overt Noonan syndrome phenotype, extending the mutation screening to the other pathogenetic genes, addressing genotype–phenotype correlation studies that will ultimately improve genetic counseling and molecular diagnosis of Noonan syndrome.

## ACKNOWLEDGMENTS

This work was supported by a 2007 Academic grant (FIRST) to P.R.

## REFERENCES

Allanson JE. 1987. Noonan syndrome. J Med Genet 24:9–13.

Benfield AP, Whiddon BB, Clements JH, Martin SF. 2007. Structural and energetic aspects of Grb2-SH2 domain-swapping. Arch Biochem Biophys 462:47–53.

Benitah SA, Frye M, Glogauer M, Watt FM. 2005. Stem cell depletion through epidermal deletion of Rac1. Science 309:933–935.

Carta C, Pantaleoni F, Bocchinfuso G, Stella L, Vasta I, Sarkozy A, Digilio C, Palleschi A, Pizzuti A, Grammatico P, Zampino G, Dallapiccola B, Gelb BD, Tartaglia M. 2006. Germline missense mutations affecting KRAS isoform B are associated with a severe Noonan syndrome phenotype. Am J Hum Genet 79:129–135.

Denayer E, Devriendt K, de Ravel T, Van Buggenhout G, Smeets E, Francois I, Sznajer Y, Craen M, Leventopoulos G, Mutesa L, Vandecasseye W, Massa G, Kayserili H, Sciot R, Fryns JP, Legius E. 2010. Tumor spectrum in children with Noonan syndrome and SOS1 or RAF1 mutations. Genes Chromosomes Cancer. 49:242–252.

Innocenti M, Zippel R, Brambilla R, Sturani E. 1999. CDC25(Mm)/Ras-GRF1 regulates both Ras and Rac signaling pathways. FEBS Lett 460:357–362.

Innocenti M, Tenca P, Frittoli E, Faretta M, Tocchetti A, Di Fiore PP, Scita G. 2002. Mechanisms through which Sos-1 coordinates the activation of Ras and Rac. J Cell Biol 156:125–136.

Khandhay FA, Santhanam L, Kasuno K, Yamamori T, Naqvi A, DeRicco J, Bugayenko A, Mattagajasingh I, Distanza A, Scita G, Kaikobad Irani K. 2006. Sos-mediated activation of rac1 by p66shc. J Cell Biol 172:817–822.

Li P, Wood K, Mamon H, Haser W, Roberts T. 1991. Raf-1: A kinase currently without a cause but not lacking in effects. Cell 64:479–482.

Nimnual AS, Yatsula BA, Bar-Sagi D. 1998. Coupling of Ras and Rac guanosine triphosphatases through the Ras exchanger Sos. Science 279:560–563.

Pandit B, Sarkozy A, Pennacchio LA, Carta C, Oishi K, Martinelli S, Pogna EA, Schackwitz W, Ustaszewska A, Landstrom A, Bos JM, Ommen SR, Esposito G, Lepri F, Faul C, Mundel P, López Siguero JP, Tenconi R, Selicorni A, Rossi C, Mazzanti L, Torrente I, Marino B, Digilio MC, Zampino G, Ackerman MJ, Dallapiccola B, Tartaglia M, Gelb BD. 2007. Gain-of-function RAF1 mutations cause Noonan and LEOPARD syndromes with hypertrophic cardiomyopathy. Nat Genet 39:1007–1012.

Quilliam LA, Rebhun JF, Castro AF. 2002. A growing family of guanine nucleotide exchange factors is responsible for activation of Ras-family GTPases. Prog Nucleic Acid Res Mol Biol 71:391–444.

Razzaque MA, Nishizawa T, Komoike Y, Yagi H, Furutani M, Amo R, Kamisago M, Momma K, Katayama H, Nakagawa M, Fujiwara Y, Matsushima M, Mizuno K, Tokuyama M, Hirota H, Muneuchi J, Higashinakagawa T, Matsuoka R. 2007. Germline gain-of-function mutations in RAF1 cause Noonan syndrome. Nat Genet 39:1013–1017.

Roberts AE, Araki T, Swanson KD, Montgomery KT, Schiripo TA, Joshi VA, Li L, Yassin Y, Tamburino AM, Neel BG, Kucherlapati RS. 2007. Germline gain-of-function mutations in SOS1 cause Noonan syndrome. Nat Genet 39:70–74.

Schubbert S, Zenker M, Rowe SL, Böll S, Klein C, Bollag G, van der Burgt I, Musante L, Kalscheuer V, Wehner LE, Nguyen H, West B, Zhang KY, Sistermans E, Rauch A, Niemeyer CM, Shannon K, Kratz CP. 2006. Germline KRAS mutations cause Noonan syndrome. Nat Genet 38: 331–336.

Sharland M, Burch M, McKenna WM, Paton MA. 1992. A clinical study of Noonan syndrome. Arch Dis Child 67:178–183.

Sini P, Cannas A, Koleske AJ, Di Fiore PP, Scita G. 2004. Abl-dependent tyrosine phosphorylation of Sos-1 mediates growth-factor-induced Rac activation. Nat Cell Biol 6:268–274.

Sondermann H, Nagar B, Bar-Sagi D, Kuriyan J. 2005. Computational docking and solution x-ray scattering predict a membrane-interacting role for the histone domain of the Ras activator son of sevenless. Proc Natl Acad Sci USA 102:16632–16637.

Tartaglia M, Gelb BD. 2005. Noonan syndrome and related disorders: Genetics and pathogenesis. Annu Rev Genomics Hum Genet 6:45–68.

Tartaglia M, Pennacchio LA, Zhao C, Yadav KK, Fodale V, Sarkozy A, Pandit B, Oishi K, Martinelli S, Schackwitz W, Ustaszewska A, Martin J, Bristow J, Carta C, Neri C, Vasta I, Curry CJ, Siguero JP, Digilio MC, Zampino G, Dallapiccola B, Bar-Sagi D, Gelb BD. 2007. Gain-of-function SOS1 mutations cause a distinctive form of Noonan syndrome. Nat Genet 39:75–79.

van der Burgt I, Berends E, Lommen E, van Beersum S, Hamel B, Mariman E. 1994. Clinical and molecular studies in a large Dutch family with Noonan syndrome. Am J Med Genet 53:187–191.

Zenker M, Horn D, Wieczorek D, Allanson J, Pauli S, van der Burgt I, Doerr HG, Gaspar H, Hofbeck M, Gillessen-Kaesbach G, Koch A, Meinecke P, Mundlos S, Nowka A, Rauch A, Reif S, von Schnakenburg C, Seidel H, Wehner LE, Zweier C, Bauhuber S, Matejas V, Kratz CP, Thomas C, Kutsche K. 2007. SOS1 is the second most common Noonan gene but plays no major role in cardio-facio-cutaneous syndrome. J Med Genet 44:651–656.

# Ras-GRF1 controls ERK-mediated long-term potentiation at the cortico-striatal synapse: implications for L-DOPA induced Dyskinesia

**Milica Cerovic[a], Barbara Picconi[b], Veronica Ghiglieri[b], Stefania Fasano[c], Ilaria Morella[c], Andreas Heuer[a], Francesca Marchisella[c], Loris Camaleonti[c], Neil Hardingham[a], Paolo Calabresi[b,d], and Riccardo Brambilla[c,a, §]**

[a] School of Biosciences, Cardiff University, Cardiff, UK

[b] Lab. Neurophysiology, Fondazione Santa Lucia, IRCCS, 00143, Rome, Italy

[c] Institute of Experimental Neurology, Division of Neuroscience, San Raffaele Scientific Institute and University, Via Olgettina 58, 20132 Milano, Italy

[d] Clinica Neurologica, University of Perugia, Ospedale S. Maria della Misericordia, 06156, Perugia, Italy

[§] Correspondence should be addressed to:
Riccardo Brambilla, e-mail:brambilla.riccardo@hsr.it

This paper is dedicated to the memory of Prof. Renata Zippel (1948-2011)

**Abstract**

Bidirectional long-term plasticity at the cortico-striatal synapse has been proposed as a central cellular mechanism governing dopamine (DA)-mediated behavioral adaptations in the basal ganglia system. A fine balance between the activity of medium spiny neurons (MSNs) of the direct and of the indirect striatal pathway is essential for normal striatal function. This balance is disrupted in Parkinson's disease (PD) and in L-DOPA induced dyskinesia (LID), a common motor complication of current pharmacotherapy. Here we show that the Ras-ERK pathway, a signal transduction cascade previously implicated in behavioral plasticity, is essential for the induction of high frequency stimulation long-term potentiation (HFS-LTP) in the dorsal striatum but it is not needed for establishing long-term depression (HFS-LTD). In addition, in a mouse model, ablation of Ras-GRF1 a neuronal specific activator of Ras proteins, causes a specific loss of HFS-LTP in the direct pathway MSNs, without affecting LTP in the indirect pathway. Furthermore, synapses of 6-OHDA unilaterally lesioned animals rendered dyskinetic with a repeated L-DOPA treatment cannot be depotentiated from a potentiated state to baseline levels, but in the Ras–GRF1 KO animals this form of synaptic plasticity is partially restored. These data demonstrate a central role for Ras-ERK signaling in striatal LTP and support at the cellular level, previous observations indicating that targeting of Ras-GRF1 and ERK may result in a significant attenuation of LID.

## Introduction

Changes in the synaptic efficacy at the cortico-striatal synapse are believed to be central not only in the regulation of normal cellular functions of the basal ganglia system but also in pathological conditions such as Parkinson's Disease (PD) and motor complications associated to prolonged dopamine (DA) replacement pharmacotherapy using L-DOPA or dopaminergic agonists (L-DOPA induced Dyskinesia, LID) (1-5). The synaptic correlates of these behavioral alterations most frequently studied in recent years are long-term potentiation (LTP) and long-term depression (LTD) in the dorsal striatum. Bidirectional synaptic plasticity can be induced in most medium spiny neurons (MSNs), the largest neuronal population of the striatum. MSNs are believed to consist of two distinct populations, the striatonigral (direct) pathway and the striatopallidal (indirect) pathway, which predominantly express dopamine (DA) D1-like and D2-like receptors, respectively. LTP and LTD can both be induced using repeated high frequency stimulation (HFS) protocol at 100 Hz. In order to induce LTP rather than LTD either magnesium ($Mg^{2+}$) is removed from the extracellular medium or the neuron is depolarized to more positive potentials to allow stronger activation of glutamate NMDA receptors (1, 6-8). Importantly, while HFS-LTD seems to be dependent on both D1 and D2 receptors, HFS-LTP induction requires D1 receptors but it is blocked, most likely through an indirect mechanism, by D2 receptors antagonists. Both forms of long-term plasticity are lost in DA depleted experimental models, such as the unilateral 6-hydroxydopamine (6-OHDA)-lesion system, and they can be promptly restored in chronically L-DOPA administered animals. Two recently identified synaptic alterations have been specifically linked to abnormal involuntary movements (AIMs), the rodent correlate of LID. Firstly, striatal slices from highly dyskinetic animals fail to depotentiate, a condition normally obtained when a low frequency stimulation (LFS) protocol is applied after the induction of HFS-LTP (9, 10). Secondly, HFS-LTD cannot be restored in highly dyskinetic animals, unless phosphodiesterase (PDE) inhibitors are administered. PDE treatment also reduces LID formation (11).

In recent years, the availability of transgenic mice expressing green fluorescent protein (GFP) under the control of BAC transgenes, has allowed several groups to specifically record, from individual MSNs belonging to either the striatonigral pathway or the striatopallidal pathway (12). Using this technology Surmeier's group performed a number of studies using whole cell voltage-clamp recordings inducing different forms of synaptic plasticity, including a HFS-LTD protocol coupled to depolarization as well as spike-timing-dependent plasticity (STDP)(13, 14). In marked contrast with previous findings a study using HFS-LTD showed that this form of plasticity could only be induced in indirect-pathway MSNs (identified using BAC transgenic mice expressing EGFP under the D2R promoter) but not in direct pathway MSN (shown by means of

M4-EGFP transgenic mice), (15). However, a more recent study suggests that the apparent lack of LTD in direct pathway detected in could be due to the electrophysiological abnormalities intrinsic to the D1-EGFP transgenic mice (16), shown by recordings in both EGFP-positive and EGFP-negative MSNs of these BAC transgenic mice .

At present, although intracellular mechanisms underlying synaptic plasticity in the dorsal striatum have been extensively investigated in physiological and pathological condition (5), little is known about the specific role of Ras-ERK signaling. This evolutionarily conserved signaling cassette has been implicated in a number of important cellular responses, including memory formation, synaptic plasticity and behavioral adaptations in the central nervous system, as well as in cell proliferation and survival in most cell types (17-24). In the striatum, the Ras-ERK pathway has been shown to control instrumental learning and memory, responses to drugs of abuse and to chronic L-DOPA in experimental models of LID (25-36) (37). Surprisingly, to date the role of Ras-ERK in cortico-striatal plasticity has not been assessed; neither in normal conditions or in DA depleted animals subjected to chronic L-DOPA administration. Moreover, little attempt has been made to correlate changes in cellular plasticity in the dorsal striatum with behavioral alterations in experimental animal models of PD and LID. Here we show that ERK signaling is crucial in the induction of HFS-LTP at the cortico-striatal synapse but it is not required for HSF-LTD. In addition, we identified a crucial brain specific component of this pathway, Ras-GRF1, which specifically modulates LTP in the direct striatal pathway and controls both LID onset and expression in both murine and non human primate (NHP) models of PD.

## Results

**ERK signaling is necessary for HFS-LTP at the cortico-striatal synapse.** Recent evidence indicates that the Ras-ERK signaling pathway in the dorsal portion of the striatum is abnormally activated in responses to both drugs of abuse and L-DOPA (23, 38). Thus, hyperactivation of this signaling cascade may represent a key pathological factor for both drug addiction and LID, two conditions both relying on abnormal DA adaptations in the basal ganglia system. In particular, we recently showed that Ras-GRF1, a neuronal specific GDP/GTP Ras-exchange factor, plays a crucial role in the regulation of ERK mediated cellular and behavioral responses to psychostimulants, by sensing and integrating DA and glutamate (GLU) signaling in the striatum. In addition, Ras-GRF1 inhibition, both in murine and NHP models of LID, significantly improves the behavioral symptoms linked to repeated L-DOPA administration (30, 36). Thus, in order to

identify the synaptic correlates of the observed behavioral responses in MSNs we investigated the role of Ras-GRF1 and ERK signaling in long-term plasticity at the cortico-striatal synapse.

We first used extracellular field recordings on wild-type (WT) slices exposed to the MEK inhibitor U0126 (which blocks ERK signaling). This treatment did not affect basal synaptic responses which were consistent within a whole range of stimulus intensities (Fig. 1A: treatment effect, two way ANOVA, $p>0.05$). When HFS was delivered in the presence of physiological $Mg^{2+}$ concentration, robust LTD was induced in both controls and U0126 treated slices (Fig. 1B: time effect, two way ANOVA, $p<0.0001$). Lack of U0126 effect was further confirmed by analyzing the mean amplitudes of 60 min post tetanic LTD (Fig1C: DMSO=69.58±2.5, U0126=74.03±3.5, Student's t test, $p>0.05$). Interestingly, in the absence of magnesium, while HFS-LTP was efficiently induced in the control slices, this form of long-term plasticity was completely abolished by the pre-treatment with U0126 (Fig.1D: treatment effect, two way ANOVA, $p<0.0001$). Analysis of the post tetanic mean amplitudes (60min) further confirm the effect of U0126 treatment (Fig. 1E: DMSO=102.6±3.5, U0126=166±10.2, Student's t test, $p<0.0001$). We obtained the same result using intracellular recordings where LTP induction in all recorded cells was abolished by 5μM U0126 treatment (Supplementary Fig 1A: time effect two way ANOVA, $P>0.05$, supplementary Fig 1B). Finally, when U0126 was applied 20 minutes after tetanus, it did not affect LTP expression (Fig. 1F: LTP pre= 178.4±16.1 vs. post=180.47±16.3 U0126 application, Student's t test, $p>0.05$). Altogether, these data indicate that ERK signaling is necessary for the induction of HFS-LTP in the dorsal striatum but it is not required either for LTP expression, for HFS-LTD and for basal synaptic transmission.

**Ras-GRF1 controls HFS-LTP in the striatonigral pathway.** The data above suggest a specific role for ERK signaling in the induction of HFS-LTP but does not necessarily implicate Ras-GRF1 in the striatal synaptic plasticity. In order to address this point, we performed electrophysiological recordings using intracellular sharp electrodes in slices from WT and Ras-GRF1 KO mice (6, 7, 39). With physiological $Mg^{2+}$ concentrations in the medium, HFS of cortical afferents induced a normal LTD in both WT and mutant mice (Fig. 2A: LTD time effect, two way ANOVA, $p<0.001$). Analysis of the 40 min post tetanic mean amplitudes confirm the lack of genotype effect (Fig. 2B: WT=60.3±4.3, Ras-GRF1 KO=58.3±6.1, Student's t test, $p>0.05$). However, when $Mg^{2+}$ was removed to unblock NMDA receptors, the same HFS protocol reliably induced LTP of cortico-striatal synaptic transmission in WT mice, whereas approximately 50% of the striatal MSNs recorded from Ras-GRF1 KO mice did not potentiate (Fig. 2C: group effect, two way ANOVA, $p<0.001$). Comparison of the 40 min post tetanic mean amplitudes indicate that only one subpopulation of Ras-GRF1 KO MSNs significantly lack LTP (Fig. 2D: WT=143.0±4.52, Ras-

GRF1 first population=160.5±4.52, Ras-GRF1 second population=95.2±4.57)(WT vs. Ras-GRF1 second population, Student's t test, $p<0.01$; Ras-GRF1 KO first population vs. Ras-GRF1 KO-second population, $p<0.001$). These data confirm that ERK signaling in the dorsal striatum is necessary for HFS-LTP but not for HFS-LTD and also indicate that Ras-GRF1 is likely to play a role in a specific subset of MSNs.

Since we have previously established that the Ras-GRF1 is equally expressed in both striatonigral and striatopallidal MSNs, the pathway-specific involvement of Ras-GRF1 in LTP is likely due to its specific engagement by a subclass of these striatal cells (36). In order to clarify which subpopulation of MSNs is affected by the loss of Ras-GRF1, we took advantage of two types of bacterial artificial chromosome (BAC) transgenic mice expressing enhanced green fluorescent protein (EGFP) specifically in striatonigral or striatopallidal MSNs; M4-EGFP mice (striatonigral neurons, direct pathway) and adenosine receptor A2A-EGFP mice (striatopallidal neurons, indirect pathway) (12). In order to study the role of Ras-GRF1 in the two different subpopulations of MSNs we combined these BAC transgenic mutants with Ras-GRF1 KO mice, to obtain double mutants (M4-EGFP/Ras-GRF1-KO and A2A- EGFP/Ras-GRF1-KO).We first performed whole cell patch clamp recordings from M4-EGFP and A2A-EGFP single transgenics, to ensure that LTP could be reliably induced in EGFP positive and EGFP negative cells in both transgenic lines. For this purpose, cells were visualized with a microscope with fluorescent and infrared imaging systems. Only cells with electrophysiological and morphological features typical for MSN were recorded. Fluorescent dye Alexa 594 was icluded in the patch pipette to allow the visualization of cell morphology during and after recordings (Fig. 3A and 3B).

We were able to induce a robust LTP, with the similar amplitude and time course, in the both fluorescent and non fluorescent MSNs from M4-EGFP mice (Fig. 3C: time effect, two way ANOVA, $p<0.0001$) (Fig. 3D: direct pathway MSNs=181.1± 4.1% vs. indirect pathway MSNs=187.4±14.5%, Student's t test, $p>0.05$). Similarly, A2A-EGFP mice also showed robust LTP in both cell populations (Fig. 3E: time effect, two way ANOVA, $p<0.0001$) (Fig.3F: Direct pathway MSNs=172.3±14.7% vs. indirect pathway MSN=177.3±15.4%, Student's t test, $p>0.05$). On the other hand, when we subsequently recorded in slices obtained from M4-EGFP/Ras-GRF1 KO double mutants, LTP could only be induced in striatopallidal /indirect pathway MSNs (Fig. 3G: group effect, two way ANOVA, $p<0.001$) (Fig.3H: direct pathway MSNs=93.1±3.9% vs. indirect pathway MSNs=178.4±15.2%, Student's t test $p<0.001$). As a further confirmation that Ras-GRF1 is essential for LTP in the striatonigral MSNs, we also recorded from A2A-EGFP/Ras-GRF1 KO double mutants (Fig. 3I: group effect, two way ANOVA, $p<0.0001$) (Fig. 3J: direct pathway, MSNs=93.11±3.9% vs. indirect pathway MSNs=178.4±15.2%, Student's t test, $p<0.0001$). This

finding provides evidence of the selective involvement of Ras-GRF1 in the control of HFS-LTP in the direct striatal pathway.

To further clarify the role of ERK and Ras-GRF1 in HFS-LTP induction we used immunofluorescence on acute cortico-straital slices to measure directly the phosphorilation levels of ribosomal protein 6S (p-6S), which is phosphorylated downstream of ERK, in response to HFS protocol. Phosphorilation levels were significantly higher in stimulated slices compared to controls (Supp. Fig 2. E: HFS stimulated= 29.54±3.34% vs. non stimulated slice= 11.05±3.15% of p-S6 positive neurons over total number of neurons; Student's t test, $P<0.001$). In the other hand in Ras-GRF1 KO, the increase in S6 phosporilation was attenuated but still significant(HFS stimulated=19.10±6.05% vs. control=8.78±4.2% Student's t test $P<0.05$). Furthermore we showed that the pre-treatment with 5μM U0126 prevents the increase in phosphorilation of S6 in response to HFS protocol, as expected ( Suplementary fig 2E: 6.7±3.2% of p-S6 positive cells over total number of NeuN pos cells ).

We used the same EGFP expressing mice, as in previous experiment, to distinguish between two different pathways. Even though the increase in p-S6 was significant in both pathways, the levels of p-S6 in the indirect pathway were substantially higher, either in basal conditions or after HFS stimulation (Supplementary fig 2 F,G: direct pathway, control 4.34±1.01% vs. HFS 8.71±1.49% stimulated $P<0.01$: indirect pathway control, control 18±5.09% vs. HFS 41±7.05% $P<0.01$; percentages are expressed as number of p-S6 positive cells over number of cells in direct or indirect pathway). Interestingly in M4-EGFP/Ras GRF1 KO mice only indirect pathway neurons showed significantly increased levels of p-S6 after HFS (Suppelementary fig 2 F,G: control 3.02±1.10% vs. HFS 3.5±1.02 $P>0.05$; 18±5.09)

**Ras-GRF1 controls DA-mediated adaptations in the murine model of LID.** Parkinson's disease (PD) is a neurodegenerative disorder characterized by a slow and inexorable loss of substantia nigra pars compacta dopaminergic neurons and by an ensuing depletion of dopamine (DA) input to the striatum. DA replacement therapy, using the DA precursor L-DOPA, has been and remains the most effective treatment for PD, but its prolonged use is associated with a series of complications including motor fluctuations and abnormal involuntary movements (AIMs), also termed L-DOPA induced dyskinesia (LID), which can become treatment-limiting over time (40-43). Considering the central role played by Ras-GRF1 and ERK signaling in HFS-LTP, we then assessed the possibility that this intracellular pathway may be implicated in LID formation and in synaptic alterations in response to both DA depletion and replacement with L-DOPA. We first generated a unilateral 6-hydroxydopamine (6-OHDA) lesioned model of PD and LID by injecting the neurotoxin into the

right medial forebrain bundle of both Ras-GRF1 KO mice and littermate controls. Two weeks after surgery, we measured spontaneous ipsilateral rotations as an efficacy index of the lesion. The rotational behavior was similar in the two genotypes (Supplementary Fig 3A: 6-OHDA WT=24.7±1.4 vs. 6-OHDA Ras- GRF1 KO=28.1±2.5 turns/10 min, Student's t test, $p>0.05$), suggesting an equivalent sensitivity to the neurotoxic damage .

To elicit axial, limb, and orolingual AIMs, a validated model of LID in mice, we administered an ascending dose regimen of L-DOPA (1.5, 3, 6 mg/kg, twice daily) to both 6-OHDA-lesioned WT and Ras-GRF1 mutant animals for 9 consecutive days (36). Daily scoring of AIMs revealed a gradual development of dyskinetic symptoms in both genotypes, which affected the trunk, limb and orolingual regions on the side of the body contralateral to the lesion. However, for all doses of L-DOPA, the AIMs scores were significantly reduced in Ras-GRF1 KO mice in comparison to their littermate controls (Supplementary Fig 3B: genotype effect, two way ANOVA, $p<0.001$). Analysis of the cumulative AIMS over the 8 days time period confirm a significant reduction of LID in the Ras-GRF1 KO animals (Supplementary Fig 3C: WT + L-DOPA=42.6±3 vs. Ras-GRF1 KO + L-DOPA=25.6±6.7, Student's t test, $p<0.05$). These results are consistent with our previous data showing that the absence of Ras-GRF1 strongly attenuates LID induction in mice (36).

At the electrophysiological level, following 6-OHDA lesion, all MSNs recorded either from WT or from Ras-GRF1 KO mice lost the ability to show LTP, an expected consequence of DA denervation (Fig. 4D) (Fig. 4E: mean 40 min after tetanus EPSP as % of control, WT=89.3±5.0 vs. Ras-GRF1 KO=86±8.1, Student's t test, $p>0.05$) (6, 8). Chronic L-DOPA treatment has been shown to rescue LTP in DA-denervated animals but, concomitantly with the development of AIMs, depotentiation is occluded (9). We next examined the induction of LTP and its reversal by LFS in slices from Ras-GRF1 KO mice and WT littermates with 6-OHDA lesions and given chronic L-DOPA treatment. As indicated in Figure 4B, Ras-GRF1 KO mice showed significantly lower AIM scores than the control WT group. Accordingly, all MSNs recorded from the mildly dyskinetic Ras-GRF1 KO mice displayed normal LTP after HFS, and a significant but not complete depotentiation of the synaptic activity upon LFS (Fig. 4F), suggesting that cortico-striatal plasticity parallels the low dyskinetic profile of these mutants. Conversely, while LTP was normal in the highly dyskinetic WT controls, depotentiation was absent (Fig 4F; Dys Ras-GRF1 KO: pre vs. post LFS, Student's t test, $p<0.05$; Dys WT vs. Dys Ras-GRF1 KO post LFS, post hoc Bonferroni, $p<0.05$).

Thus, Ras-GRF1 KO mice, which showed less dyskinetic symptoms than the control WT animals, not only displayed normal LTP after HFS but also showed significant depotentiation upon low frequency stimulation (LFS), substantially different from the dyskinetic wild type animals which did not depotentiate.

## Discussion

The striatum, as a part of basal ganglia circuit, receives a complex set of inputs comprising excitatory afferents from the cortex and the thalamus as well as midbrain dopaminergic innervation (3, 44, 45). For normal striatal function different neurotransmitter inputs, receptor activations and intracellular signaling cascades involved in the regulation of striatal plasticity need to be correctly balanced. Changes at the striatal synapses controlled by ERK signaling are believed to be crucial for learning of procedural actions as well as for habit formation and reward mechanisms (21, 24). In addition, alterations of striatal synaptic plasticity are linked to pathological states such as L-DOPA induced dyskinesia (9), drug addiction (46) and obsessive-compulsive disorder (OCD) (47).

The Ras-ERK signaling pathway is activated in MSNs by a combined engagement of DA and glutamate receptors, making it a suitable candidate for having a regulatory role in striatal synaptic plasticity (21, 23, 43). Importantly, it is now well established that distinct chemical stimuli are able to activate ERK signaling in specific MSN subpopulations. For example, psychostimulants in intact animals and L-DOPA in denervated animals selectively activate the ERK cascade in MSNs of the direct pathway. This activation involves DA D1-like receptors which also activate DARPP-32, a known indirect activator of ERK signaling. Conversely, ERK activation in the indirect pathway MSNs can be achieved by a specific blockade of D2-like receptors through the administration of receptor antagonists and this effect also implicate the activation of adenosine A2A receptors, PKA and DARPP-32 (48-50). Our own data from the current study provides an initial evidence of a complex role of Ras-ERK signaling in cortico-striatal plasticity which highlights interesting differences from the defined role in drug-dependent plasticity. Firstly, ERK is vital for LTP in both cellular pathways, indicating that HFS at the cortico-striatal synapse is able to overcome the negative effect exerted by D2 receptors on ERK activation. Secondly, the mechanism of ERK activation in response to HFS is distinctly different in the two cell types. In fact, in striatonigral MSN, LTP is Ras-GRF1 dependent while in striatopallidal MSN LTP is Ras-GRF1 independent. This evidence is rather unexpected since we previously demonstrated that Ras-GRF1 is expressed in both MSN subpopulations (36). One possibility is that Ras-GRF1 loss in the indirect pathway is either compensated by other Ras specific exchange factors or that DARPP-32 activation is sufficient to increase ERK activity by acting downstream in the pathway, effectively bypassing Ras requirements. The third aspect to be highlighted is our observation that HSF-LTD does not require ERK signaling. In order to support this evidence we have provided data both using a chemical inhibition of ERK, U0126 and using Ras-GRF1 mutant mice. In both cases, HFS-LTD is spared. Interestingly, this form of plasticity is instead disrupted by blocking CREB function in the

dorsal striatum (51). Considering that ERK signaling is a major determinant of CREB phosphorylation and is activated in many physiological conditions, our evidence suggests a differential regulation of the activity of this transcription factor in HFS-LTP and HFS-LTD, the latter being ERK independent. In addition, since both CREB inhibition and Ras-GRF1 loss in the striatum result in procedural memory impairment in operant conditioning tasks, but only LTP is impaired in both animal models, it is possible to hypothesize that this form of long-term plasticity is more relevant for striatum-dependent memory formation than LTD (30, 51).

Finally, we believe that the role of Ras-GRF1 in controlling HFS-LTP in the dorsal striatum has profound consequences for our understanding of the cellular mechanisms underlying L-DOPA induced dyskinesia. We recently published that the loss of Ras-GRF1 functions in the striatum significantly attenuates LID both in a murine and in a non human primate (NHP) model of this disease. Although our recent report suggests that the inability of cortico-striatal synapses to rescue LTD correlates well with a highly dyskinetic status (11), it is also conceivable, based on our observation that Ras-GRF1 does not play a role in HFS-LTD. Moreover, we tend to confirm that occlusion of the scaling down of synaptic activity (loss of depotentiation and LTD) at the cortico-striatal synapse plays an important role in LID, since in the Ras-GRF1 mutants an almost normal depotentiation is accompanied by a significant attenuation of abnormal involuntary movements, the rodent correlate of LID. Interestingly, while L-DOPA does not cause LID in the Ras-GRF1 mutants, it does fully restore HFS-LTP in both direct and indirect MSNs pathways. Since LTP in the direct pathway is absent in naïve Ras-GRF1 mutants, we suggest that some L-DOPA dependent mechanism may occur in this subset of MSN upon DA denervation that may bypass the Ras-GRF1 requirement. Once again, a likely possibility is that D1 receptor sensitization in the direct pathway of denervated animals may be responsible for that. Altogether, our findings strongly support the idea that the Ras-GRF1 plays an important role in LID by regulating both LTP and depotentiation at the cortico-striatal synapse.

## Materials and Methods

**Animals.** Generation of Ras-GRF1 KO mice has been prevously described (30, 39). BAC-EGFP mice (M4-EGFP and A2A EGFP) were originally generated by the GENSAT (Gene Expression Nervous System Atlas) program at the Rockefeller University (www.gensat.org).Transgenic mice and littermate controls were kept in C57BL/6 background and housed under a 12 hour-light-dark cycle with *ad libitum* access to the food.

**Lesion Surgery.** Ras-GRF1 WT (n=20) and KO (n=20) mice were anesthetized with Isofluorane

(Baxter Medical AB, Sweden) and secured in a stereotaxic frame equipped with a mouse adaptor. 1µl of 6-OHDA-HCL (3µg/µl) was injected into the right ascending medium forebrain bundle (MFB) at the following coordinates according to the mouse brain atlas: AP -0.7; L -1.2; DV -4.7 from dural surface using a glass capillary attached to a 10µl Hamilton syringe. Severity of DA denervation was assessed at the end of the experiments analyzing striatal levels of tyrosine hydroxylase (TH) and nigral cell loss using immunohistochemical labelling.

**Motor impairment and AIM induction.** Two weeks after lesion, mice were evaluated in the open field in order to estimate the success rate of lesion. Starting from day 18, they were treated twice a day, for 9 consecutive days with an escalating L-DOPA dosing regimen (1.5, 3, 6 mg/kg) plus benserazide (12 mg/kg) (Ras-GRF1 wt, n=9 and Ras-GRF1 KO, n=9) or with saline (Ras-GRF1 wt, n=6 and Ras-GRF1 KO, n=6). Abnormal involuntary movements were scored using a 0-4 rating scale according to validated mouse model of LID (36). At the end of treatment respectively (n=7) WT mice and (n=7) KO develops dyskinetic movements. Every morning, mice were individually placed in large transparent boxes and observed for 1 min

**Electrophysiology**

***Extracellular recordings*.** Coronal brain slices (350µm) from 35-50d old male C57BL/6 mice were cut in ice-cold modified artificial cerebrospinal fluid (aCSF) containing the following (in mM): 87 NaCl, 2.5 KCl, 1 $NaH_2PO_4$, 75 Sucrose, 7 $MgCl_26H_2O$, 24 $NaHCO_3$, 11 D-glucose, and 0.5 $CaCl_2$. Slices where then transferred into incubating chamber, submerged in a normal aCSF containing in mM 130 NaCl, 3.5 KCl, 1.2 $NaH_2PO_4$, 1.3 $MgCl_26H_2O$, 25 $NaHCO_3$, 11 D-glucose, 2mM CaCl and constantly provided with 95%$O_2$ and 5%$CO_2$ at room temperature. Slices were stored in this condition for at least 1h before registration**.** During registrations, slices were transferred in a submerged recording chamber, perfused at a constant rate of 2ml/min with aCSF, maintained at constant temperature of 28-30 ºC and constantly bubbled with 95%$O_2$ and 5%$CO_2$. Extracellular field recordings of glutamate driven population spikes (PS) were obtained in the dorsolateral striatum using glass micropipettes filled with 3M NaCl. Stimuli were delivered via a Constant Voltage Isolated Stimulator (Digitimer Ltd., Welwyn Garden City, UK) through bipolar twisted Ni/Cr stimulating electrodes placed in the proximity of the white matter overlaying the dorsal striatum. Data were amplified and filtered (low filter 10Hz, high filter 3kHz) by a DAM 80 AC Differential Amplifier (World Precision Instruments, Sarasota, FL), and digitized at 10 KHz by a Digidata 1322 (Axon Instruments, Sunnyvale, CA) (Molecular Devices, Foster City, CA). LTP and LTD were induced by the following high-frequency (HFS) stimulation protocol: 4 trains, 1s

duration, 100 Hz frequency, 10s inter-train interval. During LTP experiments $Mg^{2+}$ ions were omitted from the medium and the concentration of $Ca^{2+}$ ions was 2.4 mM .

***Intracellular recordings.*** Corticostriatal coronal slices (270-300μm thickness) were prepared from tissue blocks of brain from WT and Ras-GRF1 KO mice with the use of a vibratome (Leica VT1200S, Heidelberger, Germany). A single slice was transferred to a recording chamber and submerged in a continuously flowing artificial CSF (ACSF) solution (32°C, 2±3ml/min) gassed with 95% O2/5% CO2. The composition of the ACSF solution was (in mM): 126 NaCl, 2.5 KCl, 1.2 MgCl2, 1.2 NaH2PO4, 2.4 CaCl2, 11 glucose and 25 NaHCO3. Intracellular current clamp recordings were performed to study the synaptic plasticity of striatal spiny neurons (46, 52, 53). The sharp electrodes were filled with 2 M KCl (30–60MΩ). An AxoClamp 2B amplifier (Axon Instruments, USA) was used for recordings in current clamp mode. The headstage signal was continuously monitored on a separate oscilloscope. Traces were displayed on an oscilloscope and stored on a digital system (pClamp 9, Axon Instruments, USA). For synaptic stimulation, bipolar electrodes were used and were located in the white matter between the cortex and the striatum. $Mg^{2+}$ ions were omitted from the medium to better disclose the NMDA-mediated component of the evoked excitatory post synaptic potential (EPSP). Under this experimental condition, high frequency stimulation (HFS; 3 trains, 3 s duration, 100 Hz frequency, 20 s inter-train interval) of corticostriatal fibres was used as a long term potentiation (LTP)-inducing protocol. The same HFS protocol in the presence of 1.2mM $Mg^{2+}$ was used to induce the long term depression (LTD) in striatal spiny neurons. Quantitative data on EPSP modifications induced by tetanic stimulation are expressed as a percentage of the controls, the latter representing the mean of responses recorded during a stable period (15–20 min) before the tetanus.

***Whole cell recordings.*** Coronal corticostriatal brain slices (300 μm thick) were transferred to a submerged recording chamber and constantly perfused with the ACSF at a rate of 2 ml/min. ACSF was constantly bubbled with the 95% O2 and 5% CO2. Cells were visualized with the 40X water immersion objectives using Olympus BX51WI upright microscope equipped with the reflected fluorescence as well as IR/DIC (infrared/ differential interference contrast) observation systems. Whole cell recordings were performed using borosilicate patch pipettes (6-8 MΩ) filled with a solution containing (in mM): 115 K-gluconate, 20 KCl, 10 HEPES, 2 MgCl2, 2 Mg-ATP, 2 Na2-ATP, 0.3 GTP (pH 7.3). A bipolar twisted Ni/Cr stimulating electrode was used to evoke the responses. All patch clamp experiments were peformed in current clamp mode. For LTP experiments $Mg^{2+}$ was removed from the bath solution and the $Ca^{2+}$ was increased to 2.5 mM. After a stable evoked EPSP has been recorded for at least 10 min, high frequency induction protocol consisting of 3 trains of 1s at 100 Hz with 20 s intervals between trains was used to induce LTP.

The stimulation intensity during HFS was transiently increased to the superthreshold levels if necessary. Data were acquired using a Multiclamp 700B amplifier and pClamp 10 software (Molecular Device), and sampled at 10 kHz with a Digidata 1322 (Molecular Device)

**Fluorescence imaging.** During electrophysiological recordings neurons were filled, through patch pipette, with the fluorescent dye Alexa fluor 594 hydrazide sodium (invitrogen). Brain slices were post-fixed with 4% paraformaldehyde at 4ºC in phosphate buffer solution (PBS) for 20 min, and washed in PBS. Slices were then left overnight at 4ºC in PBS and mounted on slides using ProLong Gold antifade reagent (Invitrogen). Images were acquired with Leica TCS-SP2 laser-scanning confocal microscope.

**Statistical analyses.**

Electrophysiological data given in the text and in the figures are mean ± SEM of changes in the respective cell populations. Statistical analysis of the time courses was done using two way ANOVA for repeated measures, followed by Bonferroni's test for post-hoc comparison, in the case interactions were significant. Paired Student's t test was used to compare mean amplitudes of post HFS responses. These analyses were done using Prism 4.0 software.

Global AIMs scores were analyzed by two way ANOVA for repeated measures and relevant differences within or between groups were analyzed pairwise by Tukey's HSD test. These analyses were done using Statistics.

**ACKOWLEDGEMENTS**

This work was supported by the Michael J. Fox Foundation for Parkinson's Research (to RB), by Parkinson's UK (to RB), the Italian Ministry of Health (to RB and PC), the Compagnia di San Paolo (to RB and PC) and the European Community (EC) contract number 222918 (REPLACES) FP7 - Thematic priority HEALTH (to PC).

We would also like to thank Prof. Paul Kemp for granting us the laboratory space as well as Dr. Marianne Benoit-Marand for her precious help with technical issues.

**References**

1. Calabresi P, Picconi B, Tozzi A, & Di Filippo M (2007) Dopamine-mediated regulation of corticostriatal synaptic plasticity. *Trends Neurosci* 30(5):211-219.
2. Surmeier DJ, Ding J, Day M, Wang Z, & Shen W (2007) D1 and D2 dopamine-receptor

modulation of striatal glutamatergic signaling in striatal medium spiny neurons. *Trends Neurosci* 30(5):228-235.

3. Kreitzer AC & Malenka RC (2008) Striatal plasticity and basal ganglia circuit function. *Neuron* 60(4):543-554.
4. Surmeier DJ, Plotkin J, & Shen W (2009) Dopamine and synaptic plasticity in dorsal striatal circuits controlling action selection. *Curr Opin Neurobiol* 19(6):621-628.
5. Calabresi P, Di Filippo M, Ghiglieri V, Tambasco N, & Picconi B (2010) Levodopa-induced dyskinesias in patients with Parkinson's disease: filling the bench-to-bedside gap. *Lancet neurology* 9(11):1106-1117.
6. Calabresi P, Maj R, Pisani A, Mercuri NB, & Bernardi G (1992) Long-term synaptic depression in the striatum: physiological and pharmacological characterization. *J Neurosci* 12(11):4224-4233.
7. Calabresi P, Pisani A, Mercuri NB, & Bernardi G (1992) Long term potentiation in the striatum is unmasked by removing the voltage-dependent blockade of NMDA receptor channel. *Eur J Neurosci* 4:929-935.
8. Centonze D*, et al.* (1999) Unilateral dopamine denervation blocks corticostriatal LTP. *Journal of neurophysiology* 82(6):3575-3579.
9. Picconi B*, et al.* (2003) Loss of bidirectional striatal synaptic plasticity in L-DOPA-induced dyskinesia. *Nature neuroscience* 6(5):501-506.
10. Picconi B*, et al.* (2005) Pathological Synaptic Plasticity in the Striatum: Implications for Parkinson's Disease. *Neurotoxicology*.
11. Picconi B*, et al.* (2010) Inhibition of phosphodiesterases rescues striatal long-term depression and reduces levodopa-induced dyskinesia. *Brain* 134(Pt 2):375-387.
12. Gong S*, et al.* (2003) A gene expression atlas of the central nervous system based on bacterial artificial chromosomes. *Nature* 425(6961):917-925.
13. Wang Z*, et al.* (2006) Dopaminergic control of corticostriatal long-term synaptic depression in medium spiny neurons is mediated by cholinergic interneurons. *Neuron* 50(3):443-452.
14. Shen W, Flajolet M, Greengard P, & Surmeier DJ (2008) Dichotomous dopaminergic control of striatal synaptic plasticity. *Science (New York, N.Y* 321(5890):848-851.
15. Kreitzer AC & Malenka RC (2007) Endocannabinoid-mediated rescue of striatal LTD and motor deficits in Parkinson's disease models. *Nature* 445(7128):643-647.
16. Bagetta V*, et al.* (2011) Dopamine-dependent long-term depression is expressed in striatal spiny neurons of both direct and indirect pathways: implications for Parkinson's disease. *J Neurosci* 31(35):12513-12522.

17. Orban PC, Chapman PF, & Brambilla R (1999) Is the Ras-MAPK signalling pathway necessary for long-term memory formation? *Trends Neurosci* 22(1):38-44.
18. Sweatt JD (2001) The neuronal MAP kinase cascade: a biochemical signal integration system subserving synaptic plasticity and memory. *Journal of neurochemistry* 76(1):1-10.
19. Fasano S & Brambilla R (2002) Cellular mechanisms of striatum-dependent behavioral plasticity and drug addiction. *Curr Mol Med* 2(7):649-665.
20. Davis S & Laroche S (2006) Mitogen-activated protein kinase/extracellular regulated kinase signalling and memory stabilization: a review. *Genes, brain, and behavior* 5 Suppl 2:61-72.
21. Girault JA, Valjent E, Caboche J, & Herve D (2007) ERK2: a logical AND gate critical for drug-induced plasticity? *Curr Opin Pharmacol* 7(1):77-85.
22. Santini E, Valjent E, & Fisone G (2008) Parkinson's disease: levodopa-induced dyskinesia and signal transduction. *The FEBS journal* 275(7):1392-1399.
23. Fasano S & Brambilla R (2011) Ras-ERK Signaling in Behavior: Old Questions and New Perspectives. *Front Behav Neurosci* 5:79.
24. Shiflett MW & Balleine BW (2010) Contributions of ERK signaling in the striatum to instrumental learning and performance. *Behavioural brain research* 218(1):240-247.
25. Valjent E*, et al.* (2000) Involvement of the extracellular signal-regulated kinase cascade for cocaine-rewarding properties. *J Neurosci* 20(23):8701-8709.
26. Mazzucchelli C*, et al.* (2002) Knockout of ERK1 MAP kinase enhances synaptic plasticity in the striatum and facilitates striatal-mediated learning and memory. *Neuron* 34:807-820.
27. Valjent E, Pages C, Herve D, Girault JA, & Caboche J (2004) Addictive and non-addictive drugs induce distinct and specific patterns of ERK activation in mouse brain. *Eur J Neurosci* 19(7):1826-1836.
28. Ferguson SM, Fasano S, Yang P, Brambilla R, & Robinson TE (2006) Knockout of ERK1 enhances cocaine-evoked immediate early gene expression and behavioral plasticity. *Neuropsychopharmacology* 31(12):2660-2668.
29. Santini E*, et al.* (2007) Critical involvement of cAMP/DARPP-32 and extracellular signal-regulated protein kinase signaling in L-DOPA-induced dyskinesia. *J Neurosci* 27(26):6995-7005.
30. Fasano S*, et al.* (2009) Ras-Guanine Nucleotide-Releasing Factor 1 (Ras-GRF1) Controls Activation of Extracellular Signal-Regulated Kinase (ERK) Signaling in the Striatum and Long-Term Behavioral Responses to Cocaine. *Biol Psychiatry*.
31. Gerfen CR, Miyachi S, Paletzki R, & Brown P (2002) D1 dopamine receptor supersensitivity in the dopamine-depleted striatum Results from a switch in the regulation of

ERK1/2/MAP kinase. *J Neurosci* 22(12):5042-5054.

32. Pavon N, Martin AB, Mendialdua A, & Moratalla R (2006) ERK phosphorylation and FosB expression are associated with L-DOPA-induced dyskinesia in hemiparkinsonian mice. *Biol Psychiatry* 59(1):64-74.
33. Westin JE, Vercammen L, Strome EM, Konradi C, & Cenci MA (2007) Spatiotemporal pattern of striatal ERK1/2 phosphorylation in a rat model of L-DOPA-induced dyskinesia and the role of dopamine D1 receptors. *Biol Psychiatry* 62(7):800-810.
34. Bezard E*, et al.* (2005) L-DOPA reverses the MPTP-induced elevation of the arrestin2 and GRK6 expression and enhanced ERK activation in monkey brain. *Neurobiology of disease* 18(2):323-335.
35. Schuster S*, et al.* (2008) The 3-hydroxy-3-methylglutaryl-CoA reductase inhibitor lovastatin reduces severity of L-DOPA-induced abnormal involuntary movements in experimental Parkinson's disease. *J Neurosci* 28(17):4311-4316.
36. Fasano S*, et al.* (2010) Inhibition of Ras-guanine nucleotide-releasing factor 1 (Ras-GRF1) signaling in the striatum reverts motor symptoms associated with L-dopa-induced dyskinesia. *Proc Natl Acad Sci U S A* 107(50):21824-21829.
37. Shiflett MW, Brown RA, & Balleine BW (2010) Acquisition and performance of goal-directed instrumental actions depends on ERK signaling in distinct regions of dorsal striatum in rats. *J Neurosci* 30(8):2951-2959.
38. Murer MG & Moratalla R (2011) Striatal Signaling in L-DOPA-Induced Dyskinesia: Common Mechanisms with Drug Abuse and Long Term Memory Involving D1 Dopamine Receptor Stimulation. *Front Neuroanat* 5:51.
39. Brambilla R*, et al.* (1997) A role for the Ras signalling pathway in synaptic transmission and long-term memory. *Nature* 390:281-286.
40. Calabresi P, Di Filippo M, Ghiglieri V, & Picconi B (2008) Molecular mechanisms underlying levodopa-induced dyskinesia. *Mov Disord* 23 Suppl 3:S570-579.
41. Cenci MA (2007) Dopamine dysregulation of movement control in L-DOPA-induced dyskinesia. *Trends Neurosci* 30(5):236-243.
42. Jenner P (2008) Molecular mechanisms of L-DOPA-induced dyskinesia. *Nature reviews* 9(9):665-677.
43. Feyder M, Bonito-Oliva A, & Fisone G (2011) L-DOPA-Induced Dyskinesia and Abnormal Signaling in Striatal Medium Spiny Neurons: Focus on Dopamine D1 Receptor-Mediated Transmission. *Front Behav Neurosci* 5:71.
44. Bolam JP, Hanley JJ, Booth PA, & Bevan MD (2000) Synaptic organisation of the basal

ganglia. *J Anat* 196 ( Pt 4):527-542.

45. Gerfen CR (2000) Molecular effects of dopamine on striatal-projection pathways. *Trends Neurosci. (Suppl. Basal Ganglia, Parkinson's Disease and Levodopa Therapy)* 23:S64-S70.
46. Centonze D*, et al.* (2006) Chronic cocaine prevents depotentiation at corticostriatal synapses. *Biol Psychiatry* 60(5):436-443.
47. Allendes FE, Lozano AM, & Hutchison WD (2008) Attenuation of long-term depression in human striatum after anterior capsulotomy. *Stereotact Funct Neurosurg* 86(4):224-230.
48. Bertran-Gonzalez J*, et al.* (2008) Opposing patterns of signaling activation in dopamine D1 and D2 receptor-expressing striatal neurons in response to cocaine and haloperidol. *J Neurosci* 28(22):5671-5685.
49. Bertran-Gonzalez J*, et al.* (2009) Histone H3 Phosphorylation is Under the Opposite Tonic Control of Dopamine D2 and Adenosine A2A Receptors in Striatopallidal Neurons. *Neuropsychopharmacology*.
50. Santini E*, et al.* (2009) L-DOPA activates ERK signaling and phosphorylates histone H3 in the striatonigral medium spiny neurons of hemiparkinsonian mice. *Journal of neurochemistry* 108(3):621-633.
51. Pittenger C*, et al.* (2006) Impaired bidirectional synaptic plasticity and procedural memory formation in striatum-specific cAMP response element-binding protein-deficient mice. *J Neurosci* 26(10):2808-2813.
52. Calabresi P*, et al.* (2000) Dopamine and cAMP-regulated phosphoprotein 32 kDa controls both striatal long-term depression and long-term potentiation, opposing forms of synaptic plasticity. *J Neurosci* 20(22):8443-8451.
53. Di Filippo M*, et al.* (2009) Short-term and long-term plasticity at corticostriatal synapses: implications for learning and memory. *Behavioural brain research* 199(1):108-118.

**Figure legends**

**Fig. 1. Characterization of synaptic responses and long term plasticity in striatal slices treated with the MEK inhibitor U0126 (extracellular recordings).** (A) Application of 5μM U0126 had no effect on the basal transmission measured as input/output response (DMSO, n=7; U0126, n=7). (B) LTD induced with HFS of corticostriatal synapses in the presence of physiological concentration of $Mg^{+2}$ was not significantly affected by pre-incubation (20min) with U0126 (5μM) in the bath solution (DMSO, n=6; U0126, n=6). (C) Field amplitudes as % of baseline 60 min after LTD induction were not affected by the U0126 treatment. (D) HFS-LTP

induction was blocked by the pre-treatment with 5μM U0126 (DMSO, n=7; U0126, n=7; post hoc Bonferroni, **p<0.001, ***p<0.0001). (E) Field amplitudes as % of baseline 60 min after LTP induction indicate a significant effect of U0126 treatment, ***p<0.0001. (F) U0126 (5μM) does not affect the LTP maintenance when applied 20 min after the HFS induction (n=4).

**Fig. 2. Electrophysiological analysis of the corticostriatal synaptic plasticity recorded from WT and Ras-GRF1 KO mice (intracellular recordings)** (A) High frequency stimulation protocol induced a normal long term depression (LTD) in both WT and mutant mice (WT n=8; Ras-GRF1 KO n=9; pre HFS vs. 40 min after HFS, Student's t test, p<0.05). (B) The histogram shows the EPSPs amplitude as % of control, measured at 40 min after tetanus, both in WT and mutant mice (C) A long-lasting potentiation (LTP) was induced only in half of the striatal spiny neurons (MSNs) recorded from Ras-GRF1 KO mice (WT, n=5; Ras-GRF1 KO first MSNs population, n=8; Ras-GRF1 KO second MSNs population, n=9; Ras-GRF1 KO first MSNs population vs. Ras-GRF1 KO second MSNs population, post hoc Bonferroni, ***p<0.001; WT vs. Ras-GRF1 KO second MSNs, ##p<0.01, ###p<0.001). (D) The histogram shows the means of EPSP amplitude as % of control, for all three cell populations, Student's t test, **p<0.01, ***p<0.001.

**Fig. 3. HFS-LTP is absent in the direct pathway MSNs from Ras-GRF1 KO (whole cell recordings).** (A) Representative example of MSN filled with Alexa fluor 594 in the post processed slices from M4 –EGFP and (B) A2A-EGFP mice (scale bar 20 μm). (C) HFS stimulating protocol induced LTP in fluorescent (n=5) and non fluorescent cells (n=5) from M4-EGFP mice. (D) EPSPs amplitudes 40 min after HFS as % of baseline. (E) Time course of HSF-LTP in fluorescent (n=4) and non fluorescent (n=5) cells from A2A-EGFP mice. (F) Histogram representing the EPSP amplitude as % of baseline 40 min after HFS (G) In M4-EGFP/Ras-GRF1 KO LTP was blocked in the direct pathway (direct pathway MSNs vs. indirect pathway MSNs, post hoc Bonferroni, **p<0.001, ***p<0.0001) (H) EPSP amplitudes 40 min after HFS as % of baseline (direct pathway MSN, n=5, vs indirect pathway MSN, n=5, ***p<0.0001). (I) HFS-LTP was blocked in the direct pathway MSNs from A2A-EGFP/Ras-GRF1 KO (direct pathway MSNs vs. indirect pathway MSNs, post hoc Bonferroni, ***p<0.0001). (J) EPSP amplitudes 40 min after HFS as % of baseline (direct pathway MSNs, n=6 vs. indirect pathway MSNs, n=4, ***p<0.0001)

**Fig. 4. Analysis of LTP in Parkinsonian and dyskinetic Ras-GRF1 KO and WT mice (intracellular recordings).** (A) The MSNs recorded from both WT and Ras-GRF1 KO mice lesioned with 6-OHDA lose the capability to show LTP. (B) The histogram shows the mean EPSP

amplitude as % of control, both in WT and lesioned mutant mice. (C) L-DOPA treated Ras-GRF1 KO mice presented a normal LTP after HFS. The subsequent LFS protocol induced a significant depotentiation for all (pre vs post LFS Dys Ras-GRF1 KO, Student's t-test, #$p<0.05$; Dys WT (n=4) vs. Dys Ras-GRF1 KO (n=4), post hoc Bonferroni *$p<0.05$, **$p<0.01$, ***$p<0.001$).

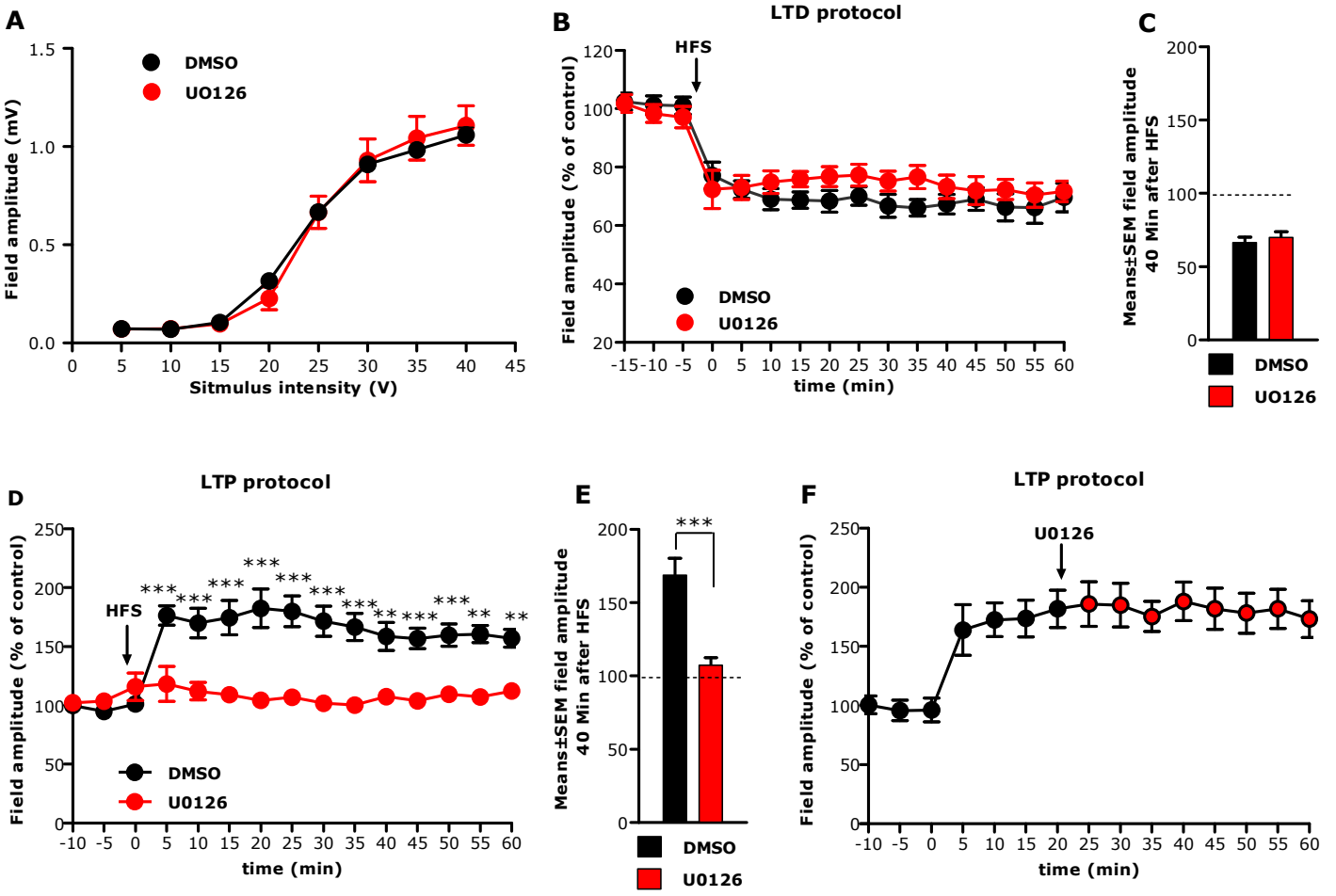


**Fig 1 Cerovic et al.**

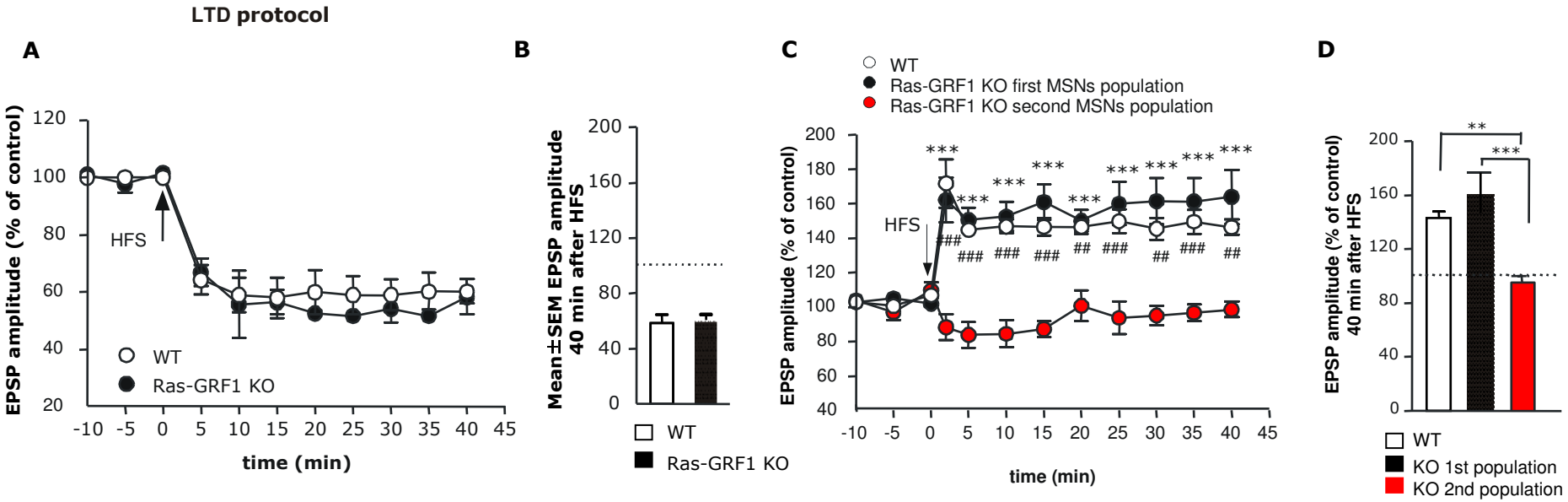


**Fig 2 Cerovic et al.**

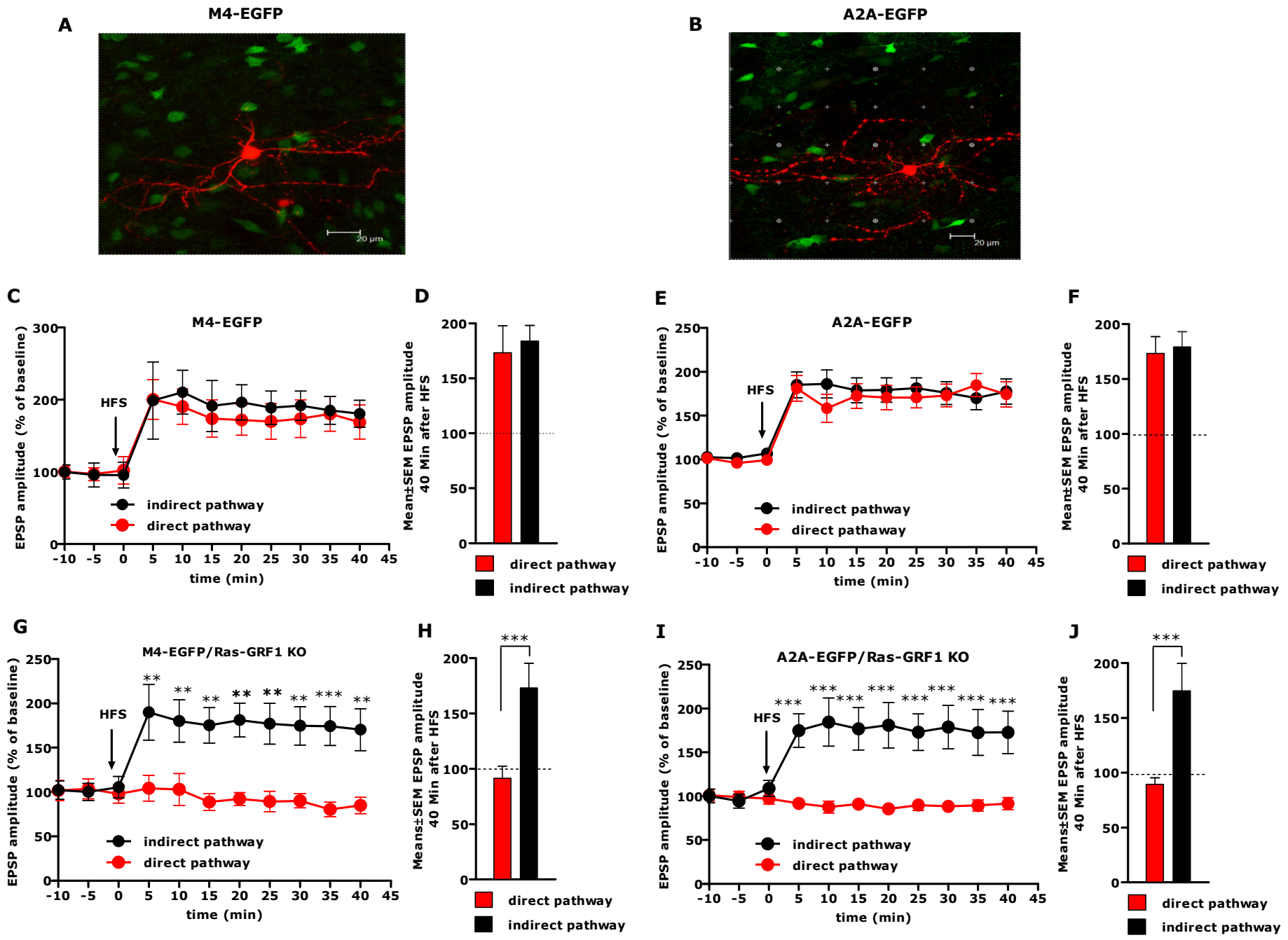


**Fig 3 Cerovic et al.**

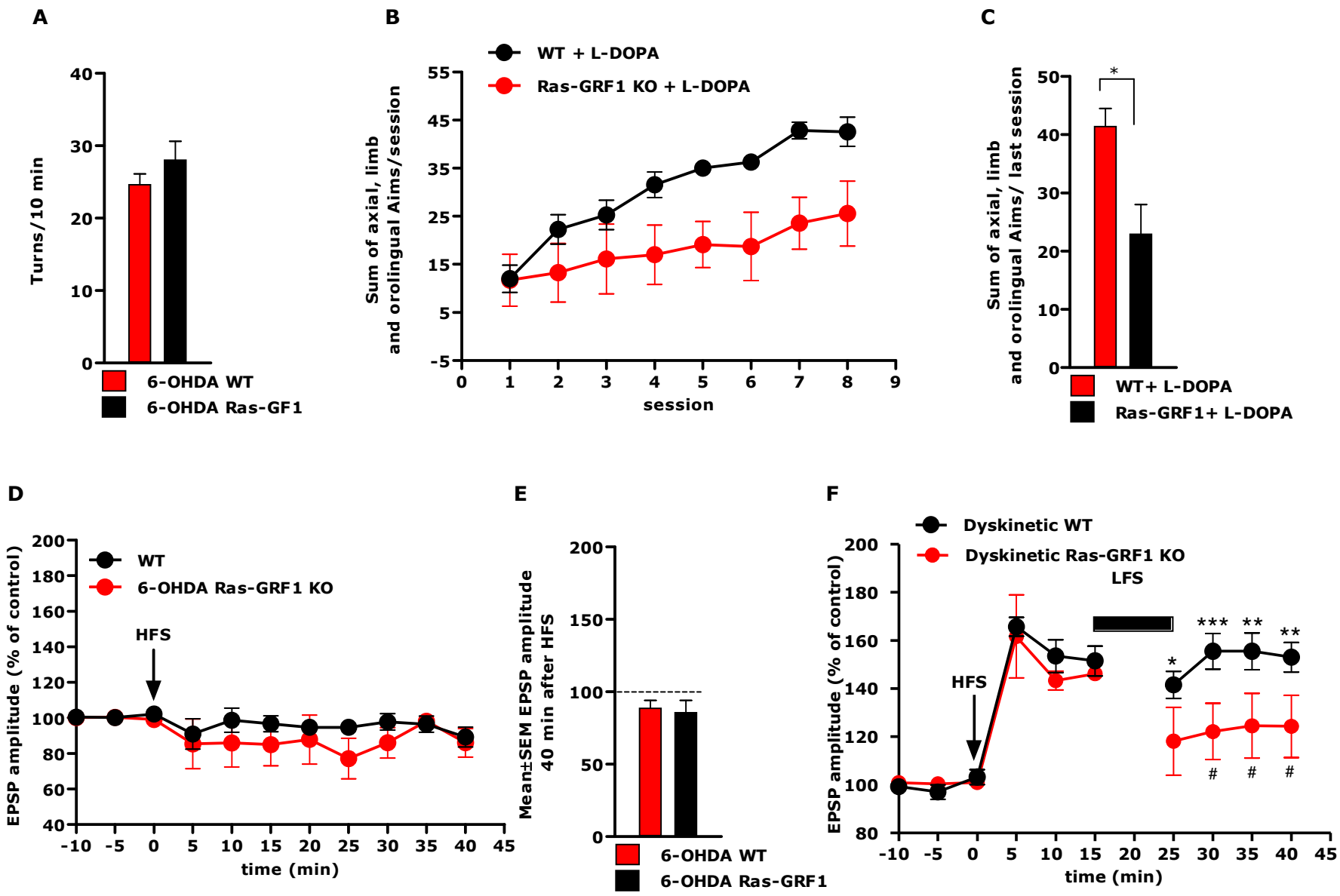


Fig 4 Cerovic et al.

**Supplementary Information**

## Methods

**Immunofluorescence *ex-vivo*.** Acute slices (250µm thick) from M4-EGFP, A2A-EGFP or M4-EGFP-GRF1KO mice, were cut and incubated for one hour in the way described in the extracellular filed recordings methods section. Using extracellular recordings, LTP was induced in the $Mg^{+2}$ free ACSF, using HFS protocol. After the LTP induction (10 min) slices were fixed in ice cold 4% PFA for 20 min and stored in 30% sucrose overnight. Controlateral slices were fixed after 20 min perfusion with $Mg^{+2}$ free ACSF and used as controls. The following day slices were re-sliced into thinner sections (18µm) using the cryostat. These sections were incubated overnight with primary antibodies (NeuN 1:500 MAB-377, Chemicon, anti-phosphoS6 1:300, Cell Signaling or anti-phospho (Ser10)-acetyl (Lys14)-histone H3, 1:1000, Upstate) and then 1h with the secondary antibody (cy3 goat anti rabbit, Jackson Immuno Research 1:200, Alexa 406 1:200 ). Images were acquired with a Leica TCS SP2 laser scanning confocal microscope. We acquired 3 different fields in the proximity of the stimulation, and 3 fields in the same position in the control, non stimulated slice. Fluorescent cells were counted using Image J software.

**Immunohistochemistry.** Brains were perfused with 4% PFA in PBS, post-fixed and 35 µm thick sections were cut and kept in cryoprotective solution at -20°C. Free-floating sections were incubated overnight at 4°C with primary antibody Phospho-p44/42 Map Kinase (1:200, Cell Signalling) and then incubated with biotinylated secondary antibody Goat anti-rabbit IgG BA-1000 (1:200, Vector Labs) for 2 hours. Tissue sections were further processed using Vectastain ABC kit (1:200, Vector Labs) and DAB detection. Quantification of p-ERK positive neurons was performed from dorsolateral striatum, in 4 sections per mouse, bilaterally, using the Image J software. All visible positive nuclei or cell bodies within a field were counted and expressed as number of cells per square millimeter.

**Immunofluorescence post-mortem.** Sections from M4- and A2A-EGFP mice were mounted on slides and incubated overnight with antibodies NeuN (1:1000 Chemicon) and

anti-phosphoS6 ribosomal protein (Ser235/236) (1:200, Cell Signaling). Following 1 hour incubation with appropriate secondary antibodies cy3 goat anti rabbit (1:200, Jackson Immuno Research) and Pacific Blue $F(ab)_2$ fragment of goat anti-mouse (1:200, Invitrogen) slides were rinsed and incubated again with primary antibody anti GFP Alexa fluor 488 conjugated (1:200, Invitrogen) for 5 hours at 4°C in order to visualize EGFP-labeled neurons. Slides were then coverslipped with Dako fluorescent mounting medium (Dako) and kept at 4°C. Images were acquired with a Leica TCS SP2 laser scanning confocal microscope.

**Figure legends**

**Supplementary fig. 1. MEK inhibitor U0126 abolishes LTP in striatal slices (intracellular recordings) (A)** LTP was abolished in all tested cells when recordings were performed in presence of 5μM U0126 (n=5). **(B)** The histogram shows that EPSPs amplitude is not significantly different measured before and 30 min after tetanus p=0.89. (EPSPs amplitude is expressed as % of control).

**Supplementary fig. 2. Ribosomal protein S6 phosphorylation is increased 10 min after LTP inducing stimulus.** In all images immunofluorescence of p-S6 is represented in red, EGFP in green and neuronal nuclear labeling NeuN in blue. **(A)** Representative images of non-stimulated, control slices (upper panels) and HFS stimulated slices (lower panels) from M4-EGFP, **(B)** A2A-EGFP and **(C)** M4-EGFP/ Ras-GRF1 KO mice. **(D)** No increase in p-S6 levels was observed in slices pre-treated with 5μM U0126. Scale bars 20 μm. **(E)** Graph showing the percentage of p-S6 positive neurons over the total number of NeuN-positive cells in M4-EGFP, A2A-EGFP and M4-EGFP/Ras-GRF1 KO, in non-stimulated and HFS stimulated slices (M4-EGFP, A2A-EGFP control (n=13) vs. HFS stimulation (n=15) **P<0.001; M4-EGFP/Ras-GRF1 KO control n=8 vs. HFS stimulation n=8, Student's t test *p<0.01). Graph also shows that the increase in p-S6 levels 10 min after HFS protocol is prevented by application of 5 μM U0126 in the bath solution (n=3). **(F)** Percentage of p-S6 positive cells over the number of cells in direct pathway in control and HFS stimulated slices from M4-EGFP (control n=7, HFS n=8;

Student's t test $p<0.05$*) and M4-EGFP/Ras-GRF1 KO mice (control n=9 vs. HFS n=8, Student's t test *$p>0.05$). **(G)** Percentage of p-S6 positive cells over the number of cells in indirect pathway, in control and HFS stimulated slices from A2A-EGFP mice (control n=6 vs. HFS n=7, Student's t test *$p<0.01$) and M4-EGFP/Ras-GRF1 KO mice (control n=8 vs. HFS n=8, Student's t test *$p<0.01$). Data are means ± SEM.

**Supplementary fig. 3. Attenuated Abnormal Involuntary Movements (AIMs) after L-dopa treatment in Ras-GRF1 KO mice** (A) Spontaneous turning evaluation after 6-OHDA denervation in Ras GRF1 KO and wt mice. (B) Chronic L-DOPA treatment induces mild abnormal involuntary movements (AIMs) in Ras GRF1 KO mice (n=7) compared to WT (n=7) animals. Genotype effect, two way ANOVA, $p<0.001$. (C) The histogram shows the AIMs amplitude in Ras GRF1 KO compared to WT L-DOPA-treated groups measured in the last session test, Student's t-test, *$p<0.05$.

**Supplementary fig 4**

**(A)** Representative photomicrographs of phospho-ERK1/2 immunoreactive cells in the dorsolateral part of the striatum after 9 days of L-dopa treatment. An aberrant phospho-ERK activation was observed in dyskinetic WT animals while a severe reduction was seen in Ras-GRF1 KO animals. **(B)** Quantification of p-ERK1/2 positive cells (mean±sem) in the striatum of Ras-GRF1 mutants and control animals. Two–way ANOVA revealed a significant reduction in the number of pERK positive cells in lesioned striatum of Ras-GRF1 mutants (n=8) in comparison to littermate controls (n=8) (Tukey's HSD test, *$p<.001$ genotype effect). **(C)** Immunofluorescence of citoplasmatic p-S6 (red), and neuronal nuclear labeling NeuN (blu) of MSNs of dyskinetic Ras-GRF1 mutants and control animals. The graph provided quantitative data of the percentage number of p-S6 positive cells over the total NeuN-positive neurons.

**(D)** Immunofluorescence of nuclear p-H3 (red), and nuclear NeuN (blu) of MSNs of Ras-GRF1 mutants and control animals. (WT n=7 vs. Ras-GRF1 KO n=9, Student's t test *$p<0.05$).

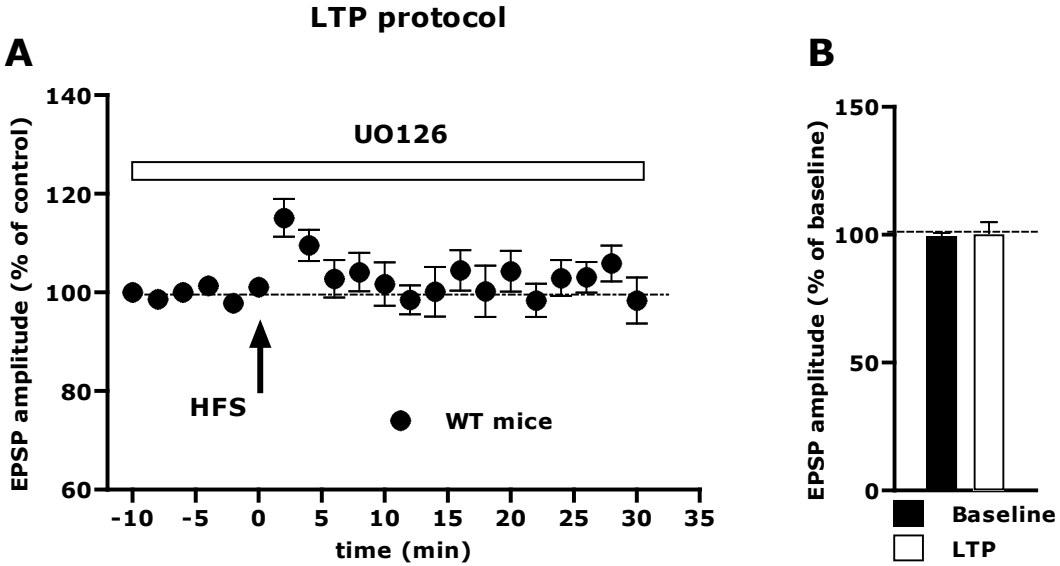


Cerovic et al. Supplementary Fig 1

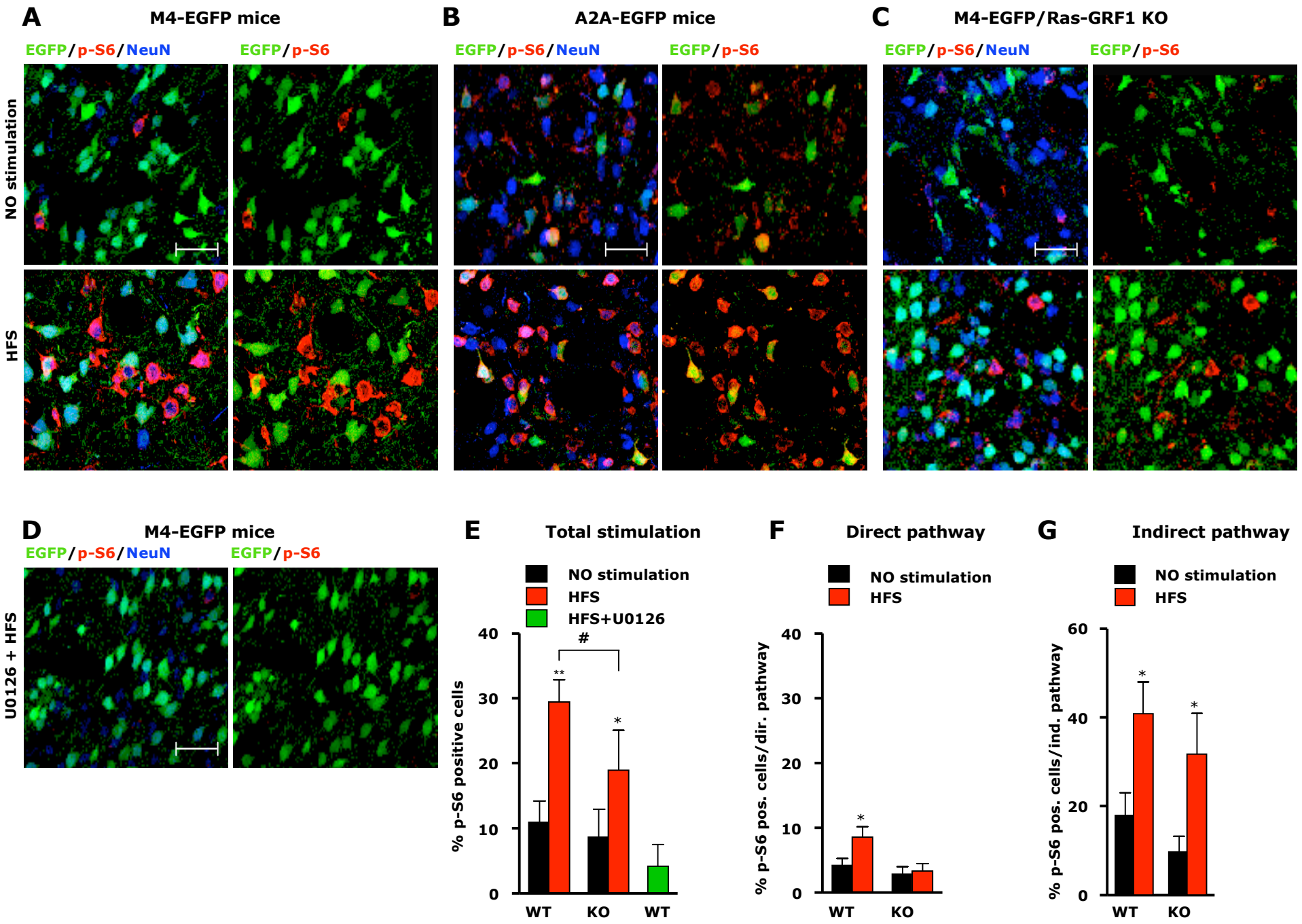


Cerovic et al. Supplementary Fig.2

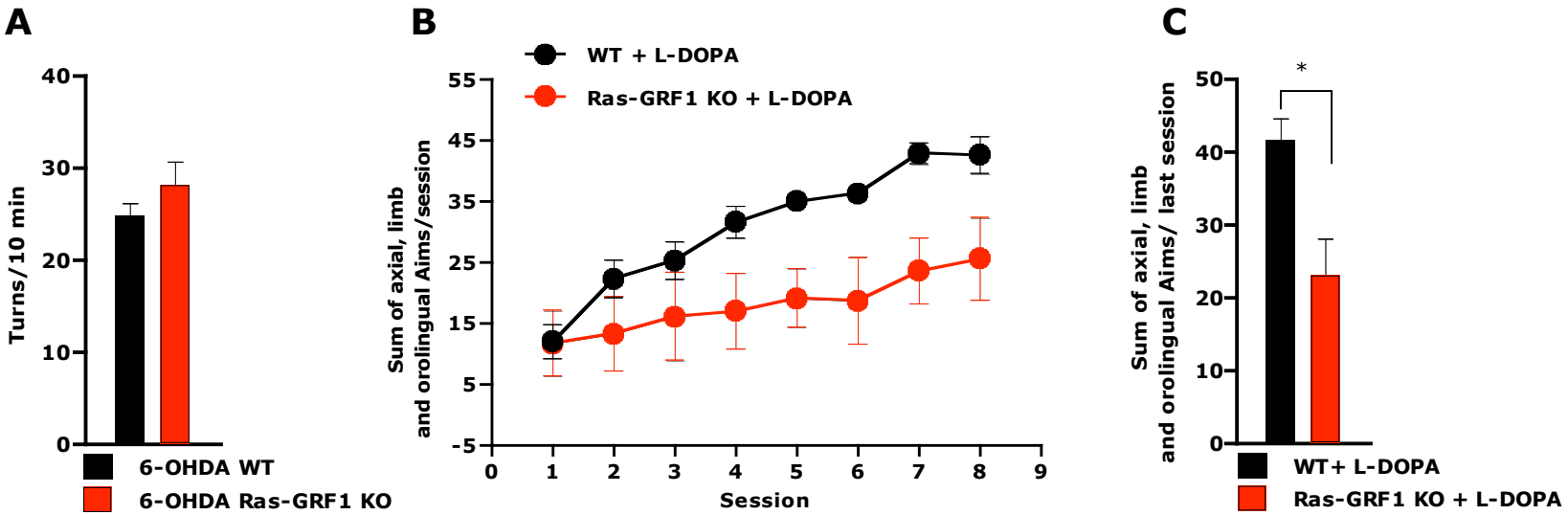


**Cerovic et al. Supplementary Fig. 3**

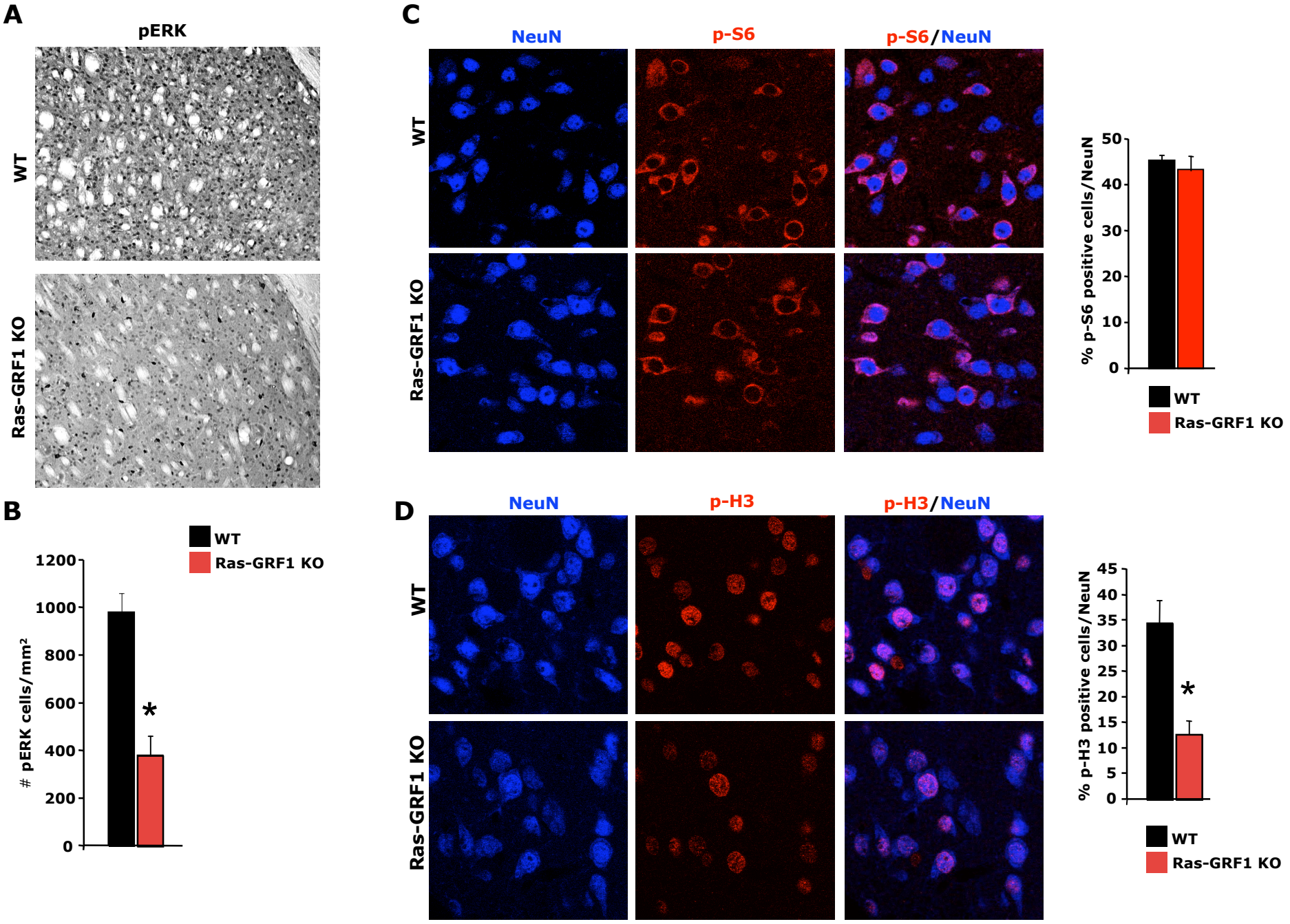


Cerovic et al. Supplementary Fig 4